

Site U1407¹

R.D. Norris, P.A. Wilson, P. Blum, A. Fehr, C. Agnini, A. Bornemann, S. Boulila, P.R. Bown, C. Cournede, O. Friedrich, A.K. Ghosh, C.J. Hollis, P.M. Hull, K. Jo, C.K. Junium, M. Kaneko, D. Liebrand, P.C. Lippert, Z. Liu, H. Matsui, K. Moriya, H. Nishi, B.N. Opdyke, D. Penman, B. Romans, H.D. Scher, P. Sexton, H. Takagi, S.K. Turner, J.H. Whiteside, T. Yamaguchi, and Y. Yamamoto²

Chapter contents

Background and objectives	1
Operations	2
Lithostratigraphy	4
Biostratigraphy	8
Paleomagnetism	12
Age-depth model and mass accumulation rates	14
Age-depth model	14
Geochemistry	15
Physical properties	17
Stratigraphic correlation	18
References	21
Figures	23
Tables	72

Background and objectives

Integrated Ocean Drilling Program (IODP) Site U1407 (proposed Site SENR-20A; 41°25.5'N, 49°48.8'W; 3073 m water depth) is a mid-depth site (~2600 meters below sea level [mbsl] paleodepth at 50 Ma) (Tucholke and Vogt, 1979) in the upper end of the Expedition 342 Paleogene Newfoundland sediment drifts depth transect (Fig. F1). The site is positioned to capture a record of sedimentation ~1.9 km shallower than the largely sub-carbonate compensation depth (CCD) record drilled at Site U1403 (Figs. F2, F3). The location above the average late Paleogene CCD should be sensitive to both increases and decreases in carbonate burial, whether these reflect variations in dissolution related to changes in the CCD, changes in carbonate production, or variations in background noncarbonate sedimentation. Our primary scientific objectives for drilling Site U1407 were

- To reconstruct the mid-depth CCD in a primarily carbonate-dominated record for the early and middle Eocene;
- To obtain records of the Eocene and Paleocene in carbonate-rich sediment that host abundant foraminifers suitable to the construction of geochemical climate records;
- To evaluate the history of deep water on sediment chemistry, grain size, and provenance; and
- To evaluate biological evolution during Paleogene climate transitions.

The secondary objective included dating acoustic horizons to better constrain regional sedimentation during the Paleogene and Cretaceous and allow us to anticipate the likely age of the sedimentary sequence at the remaining Expedition 342 sites.

The primarily calcareous sequence expected at Site U1407 should record changes in ocean alkalinity and carbonate production. Sites U1403 and U1404 were mainly positioned to capture large-amplitude CCD deepening events such as the carbonate budget “overshoots” that are thought to be associated with the most extreme climate perturbations of the Cenozoic such as those involved with the Cretaceous/Paleogene (K/Pg) boundary, the Paleocene/Eocene Thermal Maximum (PETM) and the Eocene-Oligocene transition (EOT) (see the “Site U1403” and “Site U1404” chapters [Norris et al., 2014c, 2014d]). Those events are recorded at deepwater sites as stratigraphically thin intervals of calcareous sediment in otherwise noncalcareous sediment. In contrast, transient shoaling of the CCD in generally carbonate

¹Norris, R.D., Wilson, P.A., Blum, P., Fehr, A., Agnini, C., Bornemann, A., Boulila, S., Bown, P.R., Cournede, C., Friedrich, O., Ghosh, A.K., Hollis, C.J., Hull, P.M., Jo, K., Junium, C.K., Kaneko, M., Liebrand, D., Lippert, P.C., Liu, Z., Matsui, H., Moriya, K., Nishi, H., Opdyke, B.N., Penman, D., Romans, B., Scher, H.D., Sexton, P., Takagi, H., Turner, S.K., Whiteside, J.H., Yamaguchi, T., and Yamamoto, Y., 2014. Site U1407. In Norris, R.D., Wilson, P.A., Blum, P., and the Expedition 342 Scientists, *Proc. IODP, 342: College Station, TX (Integrated Ocean Drilling Program)* doi:10.2204/iodp.proc.342.108.2014

²Expedition 342 Scientists’ addresses.



rich sequences should be recorded at Site U1407 by decreases in carbonate preservation and decreasing carbonate content relative to clay or biosiliceous sediment, as we have already observed at Site U1406. As an upper to mid-depth site on the Newfoundland ridges depth transect, Site U1407 should have a few intervals in which the sediment is 100% carbonate but also intervals where carbonate content decreases in the record. Carbonate content is expected to be generally higher at sites in shallower water depth, such as the majority of the sites located on Southeast Newfoundland Ridge, including Site U1407.

The high carbonate contents anticipated in sediment at Site U1407 should permit the construction of detailed stable isotope records and calcareous microfossil biostratigraphy that can be tied by physical property records and magnetochronology to Sites U1403–U1406 further downslope. Ties between sites on Southeast Newfoundland Ridge and those on J-Anomaly Ridge will allow the isotope stratigraphy and biochronology developed for Sites U1406 and U1407 to be extended to the entire lower half of the depth transect. Site U1407 assumes greater importance in the depth transect because the lower and middle Eocene sedimentary sequence at Site U1406 was relatively condensed and incompletely recovered.

Ultimately, the goal is to use the combination of the lower and middle Eocene record at Site U1407 and the younger Paleogene record at Site U1406 to produce composite records of stable isotope and carbonate content and mass accumulation rate (MAR) variability that can be tied to the more intermittent geochemical records at Sites U1403–U1405. Our aim is to match carbonate-rich intervals across all of the J-Anomaly Ridge sites with the sites on Southeast Newfoundland Ridge to create an orbital-resolution record of fluctuations in ocean chemistry and deep-water origins.

Site U1407 was proposed in response to our discovery that there is a subtle but recognizable internal stratigraphy to the acoustically transparent sequence on J-Anomaly Ridge. Seismic data show an intermittent fuzzy reflector near the middle of the J-Anomaly Drift as well as a zone of fuzzy, slightly less transparent reflections in the lower half of the drift. Drilling on J-Anomaly Ridge showed that these two fuzzy reflector packages correspond to the Eocene/Oligocene boundary and lower and middle Eocene sediment. We used those interpretations of the seismic stratigraphy to propose sites that would preferentially target the lower half of the acoustically transparent seismic package. Site U1407 and its upslope companion, Site U1408, were designed to recover advanced pis-

ton corer (APC) records of the lower and middle Eocene sequence.

The seismic stratigraphy of Site U1407 shows a complex array of reflectors below the presumed Eocene sedimentary sequence. We proposed to drill into this reflector-rich section in order to help bridge our seismic stratigraphic interpretations from J-Anomaly Ridge across Southeast Newfoundland Ridge. As at Site U1403, the primary goal was to date the reflector package and to recover intervals of calcareous sediment that could be useful for paleoceanographic studies of Paleogene and, potentially, Cretaceous events. Targets of particular interest included the early Paleogene hyperthermals, the K/Pg boundary, and an Upper Cretaceous sequence that could be matched in a depth transect with the Maastrichtian–Campanian sequence at Site U1403. We also expected that the sequence at Site U1407 includes, at depth, shallow-marine reef carbonates and possibly overlying black shale of various oceanic anoxic events such as those cored in the deep Newfoundland Basin during Ocean Drilling Program (ODP) Leg 210.

We hypothesized that Site U1407 should provide a record of primarily calcareous ooze and chalk of rough age-equivalence to sites in deeper water on J-Anomaly Ridge. In particular, Site U1407 should provide a carbonate-rich record through the early and middle Eocene as a counterpart to the largely sub-CCD record drilled through this interval at Sites U1403 and U1404 and thereby improve age and water depth control on the behavior of the CCD in the North Atlantic during this key interval of the Cenozoic when the CCD in the equatorial Pacific was at its most dynamic (Lyle, Wilson, Janecek, et al., 2002; Pälike et al., 2012).

Operations

All times are local ship time (UTC – 2.5 h). See Table **T1** for coring summary.

Hole U1407A summary

Latitude: 41°25.4993'N

Longitude: 49°48.7987'W

Water depth below sea level (m): 3073.13

Date started: 0800 h, 7 July 2012

Date finished: 1005 h, 9 July 2012

Time on hole (days): 2.1

Seafloor depth (m drilling depth below rig floor [DRF]): 3084.7

Seafloor depth estimation method: mudline core

Rig floor to sea level (m): 11.57



Penetration depth (m drilling depth below seafloor [DSF]): 308.7
 Cored interval (m): 308.7
 Recovered length (m): 205.64
 Recovery (%): 67
 Total cores (number): 35
 APC cores (number): 15
 Extended core barrel (XCB) cores (number): 20
 Drilling system: 11 $\frac{1}{16}$ inch APC/XCB bit with 136.00 m bottom-hole assembly (BHA)
 Objective: core from seafloor to ~250 m DSF or until science objectives are met
 Result: target exceeded; objectives met

Hole U1407B summary

Latitude: 41°25.4990'N
 Longitude: 9°48.7840'W
 Water depth below sea level (m): 3073.5
 Date started: 1005 h, 9 July 2012
 Date finished: 1340 h, 10 July 2012
 Time on hole (days): 1.1
 Seafloor depth (m DRF): 3085.1
 Seafloor depth estimation method: mudline core
 Rig floor to sea level (m): 11.63
 Penetration depth (m DSF): 276.3
 Cored interval (m): 241.3
 Recovered length (m): 234.54
 Recovery (%): 97
 Drilled interval (m): 35
 Drilled interval (number): 2
 Total cores (number): 26
 APC cores (number): 10
 XCB cores (number): 16
 Drilling system: 11 $\frac{1}{16}$ inch APC/XCB bit with 136.00 m BHA
 Objective: core from seafloor to ~270 m DSF
 Result: target reached; objectives met

Hole U1407C summary

Latitude: 41°25.5000'N
 Longitude: 49°48.8137'W
 Water depth below sea level (m): 3075.2
 Date started: 1340 h, 10 July 2012
 Date finished: 1915 h, 12 July 2012
 Time on hole (days): 1.2
 Seafloor depth (m DRF): 3086.8
 Seafloor depth estimation method: mudline core
 Rig floor to sea level (m): 11.64
 Penetration depth (m DSF): 261.6
 Cored interval (m): 237.6
 Recovered length (m): 244.36
 Recovery (%): 103
 Drilled interval (m): 24
 Drilled interval (number): 2
 Total cores (number): 27

APC cores (number): 10
 XCB cores (number): 17
 Drilling system: 11 $\frac{1}{16}$ inch APC/XCB bit with 136.00 m BHA
 Objective: repeat cored sequence from Hole U1407B
 Result: target reached; objectives met

Description

After a 120 nmi, 11 h transit from Site U1406 at a speed of 10.9 kt, the vessel arrived at Site U1407 at 0800 h on 7 July 2012. The plan for Site U1407 called for drilling three holes to a depth of ~250 m DSF. Holes U1407A, U1407B, and U1407C were successfully cored to 308.7, 276.3, and 261.6 m DSF, respectively, without any significant problems. Recovery was mediocre in the first hole because of weather but improved in the second and third holes. Overall recovery for Site U1407 was 86.9%. The total time spent at Site U1407 was 107.25 h (4.5 days).

Hole U1407A coring

The second attempt at a mudline core recovered 6.81 m, establishing Hole U1407A at 1655 h on 7 July at a seafloor depth of 3084.7 m DRF (3073.1 mbsl). Cores 342-U1407A-1H through 15H were retrieved using nonmagnetic core barrels and the FlexIT core orientation tool. The first partial stroke was experienced with Core 11H, and the APC was advanced by recovery to Core 15H (121.9 m DSF). The XCB was deployed for Cores 16X through 35X to a final depth of 308.7 m DSF. The seafloor was cleared at 1005 h on 9 July, ending Hole U1407A. Overall core recovery for Hole U1407A was 205.64 m for the 308.7 m cored (66.6% recovery). This relatively low APC recovery can most likely be attributed to the high heave and large pitch and roll of the vessel during coring operations as well as low recovery in cherts and reef sediment. The total time spent on Hole U1407A was 50.00 h.

Hole U1407B coring

The vessel was offset 20 m east. Hole U1407B was spudded at 1200 h on 9 July, and an 8.4 m mudline core established the seafloor at 3085.1 m DRF (3073.5 mbsl). Cores 342-U1407B-1H through 11H were recovered using nonmagnetic core barrels and the FlexIT core orientation tool. A 3 m interval (27.4–30.4 m DSF) was drilled without coring in an attempt to cover a coring gap in Hole U1407A. Based on the poor recovery of an interval of chert layers in Hole U1407A, the interval from 95 to 127 m DSF was drilled without coring using the XCB. Cores 13X through 28X were then recovered to a final depth of 276.3 m DSF. The seafloor was cleared at 1340 h on



10 July, ending Hole U1407B. The recovery for Hole U1407B was 234.54 m over the 241.3 m cored (97% recovery). The total time spent on Hole U1407B was 27.75 h.

Hole U1407C coring

The vessel was offset 40 m west. Hole U1407C was spudded at 1510 h on 10 July, and a 7.7 m mudline core established the seafloor at 3086.8 m DRF (3075.2 mbsl). Cores 342-U1407C-1H through 11H (0–93.0 m DSF) were recovered using nonmagnetic core barrels. No core orientation was performed in Hole U1407C. A 3 m interval was drilled without coring to optimize core overlap in multiple holes. Once again, a 21 m interval (96–117 m DSF) was drilled without coring through the chert layers using the XCB. Cores 13X through 29X were then recovered to a final depth of 261.6 m DSF. The seafloor was cleared at 1805 h on 11 July. The drill string was pulled up to 2792 m DRF, and the rig was secured for a dynamic positioning move to the next site at 1915 h on 11 July, ending Hole U1407C. Overall recovery for Hole U1407C was 244.4 m from the 237.6 m interval cored (103% recovery). The total time spent on Hole U1407C was 29.5 h.

Lithostratigraphy

The sedimentary sequence recovered from Holes U1407A–U1407C presents a diverse collection of deep-sea pelagic to shallow-marine (including reefal) sediment of Pleistocene to Early Cretaceous (late Albian) age and comprising six lithostratigraphic units (Figs. F4, F5; Table T2). Unit I is ~8 m thick and composed of grayish brown to pale brown Pleistocene foraminiferal nannofossil ooze interbedded at the decimeter scale with foraminiferal sand and clay with nannofossils (Fig. F5A). Rock fragments of pebble to cobble size and coarse silt- to sand-sized quartz and amphibole are pervasive. Unit II is a ~10 m thick sequence of early Oligocene age composed of pale brown clay with nannofossils with disseminated manganese nodules, sulfide patches, and intercalated millimeter- to centimeter-sized sulfide layers (Fig. F5B). Unit III consists of ~65 m of middle Eocene pale brown to greenish gray nannofossil ooze with foraminifers. Sulfide patches and layers are also present (Fig. F5C). An abrupt downhole change in color from light greenish gray (5GY 7/1) into white (N8) is associated with a significant shift in physical proxies and carbonate content that marks the contact between Units III and IV. Unit IV is a ~20 m thick sequence of lower Eocene nannofossil ooze with foraminifers (Fig. F5D). Unit V is composed of Paleocene to Albian nannofossil chalk and is divided

into two subunits (Va and Vb; Fig. F5E, F5F). Subunit Va consists of ~60 m of Paleocene nannofossil chalk with foraminifers and radiolarians. Subunit Vb is ~95 m thick and composed of mainly nannofossil chalk, or nannofossil chalk with foraminifers, of Albian to Paleocene age. Subunit Vb also contains black shale of the Cenomanian/Turonian boundary Oceanic Anoxic Event (OAE) 2 (93.5 Ma). The top of Unit VI is a laminated, partially silicified, and dolomitized calcareous sandstone of late Albian age (Fig. F5G). The remainder of Unit VI was extremely poorly recovered but consists of fossiliferous backreef and lagoonal moldic limestones of Albian age (Fig. F5H). Representative smear slide photographs of all of these lithostratigraphic units are shown in Figures F6 and F7.

Lithostratigraphic units and boundaries are defined by changes in lithology (as identified by visual core description and smear slide observations), physical properties including color reflectance (L^* , a^* , and b^*), and biogenic content (calcium carbonate and silica). The lithologic differences observed between units are primarily attributable to varying abundances of nannofossils, diatoms, radiolarians, and foraminifers (Figs. F8, F9, F10). Lithologic descriptions are based on sediment recovered in Hole U1407A and supplemented with observations from Holes U1407B and U1407C.

Unit I

Intervals: 342-U1407A-1H-1, 0 cm, to 2H-1, 95 cm; 342-U1407B-1H-1, 0 cm, to 1H-6, 64 cm; 342-U1407C-1H-1, 0 cm, to 1H-CC, 11 cm

Depths: Hole U1407A = 0.00–7.75 meters below seafloor (mbsf); Hole U1407B = 0.00–8.14 mbsf; Hole U1407C = 0.00–7.70 mbsf

Age: Pleistocene

Lithologies: foraminiferal nannofossil ooze, foraminiferal sand, and clay with nannofossils

Unit I is 7.75–8.14 m thick and consists of multicolored sediment of mainly grayish brown (10YR 5/2), light gray (10YR 7/2), and pale brown (10YR 6/3) foraminiferal nannofossil ooze and secondary reddish brown (5YR 5/3) clay with nannofossils present in decimeter-thick beds (Fig. F5A). Sand-sized foraminifers are locally concentrated into patches or in continuous to semicontinuous beds. Pebble- to cobble-sized rock fragments, coarse silt- to sand-sized quartz, and amphibole are also present. Unit I is distinguished from the underlying nannofossil-rich clay of Unit II by the presence of foraminiferal sand beds and the abundance of foraminifers (Figs. F5A, F5B, F6, F7, F8, F9, F10). The contact between Unit I (Pleistocene) and Unit II (early Oligocene) is characterized by a ~30–40 cm thick yellowish to rusty



brown clay rich in disseminated sulfides and manganese oxides.

Unit II

Intervals: 342-U1407A-2H-1, 95 cm, to 2H-CC, 17 cm; 342-U1407B-1H-6, 64 cm, to 2H-CC, 14 cm; 342-U1407C-3H-1, 0 cm, to 3H-3, 93 cm

Depths: Hole U1407A = 7.75–15.89 mbsf; Hole U1407B = 8.14–18.04 mbsf; Hole U1407C = 10.70–14.63 mbsf

Age: early Oligocene

Lithology: clay with nannofossils

Unit II is 3.93–9.90 m thick and consists of very pale brown (10YR 7/3) clay with nannofossils of early Oligocene age. Discrete manganese nodules of varying size (1–5 cm) and patches of disseminated sulfides as thick as 10 cm are present as secondary components within the ochre to black clay (7.5YR 5/8) (Fig. F5B). Unit II is distinguished from underlying Unit III by its relatively minor abundance of carbonate (<25 wt% compared to ~50 wt%; Fig. F4), nannofossils, and foraminifers (Figs. F6, F7, F8, F9, F10).

Unit III

Intervals: 342-U1407A-3H-1, 0 cm, to 9H-CC, 25 cm; 342-U1407B-3H-1, 0 cm, to 10H-6, 10 cm; 342-U1407C-3H-3, 93 cm, to 9H-6, 66 cm

Depths: Hole U1407A = 16.30–83.18 mbsf; Hole U1407B = 17.90–85.50 mbsf; Hole U1407C = 14.63–75.86 mbsf

Age: middle Eocene

Lithology: nannofossil ooze with foraminifers

Unit III consists of ~65 m of very pale brown (10YR 8/2) to light greenish gray (5GY 6/1) nannofossil ooze with foraminifers of middle Eocene age (Figs. F5C, F6C). A notable gradational change in color from very pale brown (10YR 8/2) into light greenish gray (5GY 7/1) occurs between 43.2 and 43.5 mbsf (Fig. F4). Greenish gray (5GY 6/1) mottling and layering and subtle color banding of light greenish gray (5GY 7/1) occur within host greenish gray (5GY 7/1) nannofossil ooze (Fig. F5C). Millimeter-scale clay layers with ochre Fe oxide stain and altered glauconite are also commonly observed. Black sulfide patches and layers are occasionally present throughout the unit. Bioturbation is moderate to heavy with discrete *Planolites* and *Zoophycos* burrows. Unit III is distinguished from underlying Unit IV by an abrupt downhole change in color from the distinctive light greenish gray (5GY 7/1) sediment to white (N8) sediment (Fig. F4). Additionally, Unit IV is characterized by an increase in the abundance of biosiliceous components compared to Unit III, in which these com-

ponents are absent or only rarely present (Figs. F8, F9, F10).

Unit IV

Intervals: 342-U1407A-10H-1, 0 cm, to 12H-1, 100 cm; 342-U1407B-10H-6, 10 cm, to 11H-CC, 6 cm; 342-U1407C-9H-6, 66 cm, to 11H-CC, 10 cm

Depths: Hole U1407A = 82.80–102.80 mbsf; Hole U1407B = 85.50–95.01 mbsf; Hole U1407C = 75.86–96.05 mbsf

Age: early Eocene

Lithologies: nannofossil ooze with foraminifers and nannofossil ooze with radiolarians

Unit IV is ~20 m thick and consists of white (N8) nannofossil ooze with foraminifers of early Eocene age. The prominent change in color from overlying Unit III to the white of Unit IV is associated with a significant increase in carbonate content, from ~40 wt% in Unit III to >80 wt% in Unit IV (Figs. F4, F11). Other physical properties such as magnetic susceptibility and natural gamma radiation (NGR) also noticeably shift across the Unit III/IV boundary (Fig. F11). The lower part of Unit IV is composed of very pale brown (10YR 8/2) nannofossil ooze with radiolarians to pink (7.5YR 8/3) radiolarian nannofossil ooze with brown (10YR 5/3) mottling. The poorly recovered interval between the base of this lithostratigraphic unit and the upper boundary of Unit V (Fig. F4) contains chert in all three holes. The thickness and number of individual chert layers as well as the nature of interbedded sediment is unknown as a result of poor recovery in this interval.

Unit V

Intervals: 342-U1407A-16X-1, 0 cm, to 31X-5, 60 cm; 342-U1407B-13X-1, 0 cm, to 28X-2, 46 cm; 342-U1407C-13X-1, 0 cm, to 29X-CC, 38 cm

Depths: Hole U1407A = 121.90–267.30 mbsf; Hole U1407B = 127.00–268.66 mbsf; Hole U1407C = 117.00–261.79 mbsf

Age: Paleocene to Albian

Lithologies: nannofossil chalk, nannofossil chalk with foraminifers, and nannofossil chalk with foraminifers and radiolarians

Unit V and its two Subunits, Va and Vb, comprise an ~155 m thick succession of nannofossil chalk and nannofossil chalk with foraminifers of Paleocene to Albian age (Fig. F4). The boundary between Subunits Va and Vb is defined by the rarity or the absence of radiolarians in Subunit Vb (Figs. F8, F9, F10). Sub-unit Vb includes a prominent interval of zeolitic claystones with organic matter (black shale) that are described in detail in “Cenomanian/Turonian



boundary interval and Oceanic Anoxic Event 2.” Unit V is distinguished from underlying Unit VI by a change from pelagic sediment to neritic, laminated, and partially silicified and dolomitized calcareous sandstone (grainstone and framestone).

Subunit Va

Intervals: 342-U1405A-16X-1, 0 cm, to 22X-1, 30 cm; 342-U1405B-13X-1, 0 cm, to 17X-6, 74 cm; 342-U1405C-13X-1, 0 cm, to 19X-CC, 46 cm

Depths: Hole U1407A = 121.90–174.60 mbsf; Hole U1407B = 127.00–173.59 mbsf; Hole U1407C = 117.00–176.01 mbsf

Age: Paleocene

Lithologies: nannofossil chalk with foraminifers and radiolarians and nannofossil chalk with radiolarians

Subunit Va is an ~45–60 m thick sequence of white (N8) to pinkish white (7.5YR 8/2) nannofossil chalk with foraminifers and radiolarians and nannofossil chalk with radiolarians of Paleocene age. Chert fragments and black patches of sulfides are present occasionally. Bioturbation is moderate to heavy with some well-preserved *Zoophycos* burrows. Secondary lithologies within Subunit Va include laminated siltstone beds, one of which displays a 3 cm thick basal division of an inversely graded bed overlain by normally graded sediment (Fig. F12). This graded bed is overlain by an 11 cm thick siltstone layer with horizontal to inclined laminations. The comparably minor bioturbation and the sedimentary structures in this bed suggest that it is an event bed, potentially from a current-resuspended density flow. Physical proxies (color reflectance parameters, NGR, and magnetic susceptibility) show low variability in Subunit Va compared to the underlying Subunit Vb (Fig. F4). Carbonate content within Subunit Va is lower than in Subunit Vb (see “Geochemistry”). The rarity or absence of radiolarians in Subunit Vb marks the transition from Subunit Va to Vb (Figs. F8, F9, F10).

Subunit Vb

Intervals: 342-U1405A-22X-1, 30 cm, to 31X-5, 60 cm; 342-U1405B-17X-6, 74 cm, to 28X-2, 46 cm; 342-U1405C-20X-1, 0 cm, to 29X-CC, 38 cm

Depths: Hole U1407A = 174.60–267.30 mbsf; Hole U1407B = 173.59–268.66 mbsf; Hole U1407C = 175.00–261.79 mbsf

Age: early Paleocene to Albian

Lithologies: nannofossil chalk and nannofossil chalk with foraminifers

Subunit Vb is predominantly greenish white (10Y 8/1) and white (N 8) to pinkish white (7.5YR 8/2) nannofossil chalk and nannofossil chalk with foraminifers with disseminated patches and layers of sulfides and

spans a 86.79–95.07 m thick sequence from the Albian to Paleocene. Secondary lithologies within Subunit Vb include laminated claystone with nannofossils, laminated to massive zeolitic claystone with organic matter, and chert and radiolarian sand (Fig. F7). Two dark gray to black sequences of nannofossil- and organic-rich claystone with black to dark green color alternations (Figs. F13, F14, F15) are associated with the Cenomanian–Turonian OAE 2 (~93 Ma). A detailed description of this interval in all three holes drilled is provided in “Cenomanian/Turonian boundary interval and Oceanic Anoxic Event 2.” Macroscopic fossils include an aptychus, inoceramid shell fragments, and belemnites in Cores 342-U1407A-28X and 29X. In Section 342-U1407B-27X-CC, Subunit Vb is distinguished from underlying Unit VI by a change from calcareous chalk to laminated and partially silicified and dolomitized calcareous sandstone (grainstone and framestone).

Unit VI

Intervals: 342-U1407A-31X-5, 107 cm, to 35X-CC, 8 cm; 342-U1407B-28X-2, 46 cm, to 28X-CC, 49 cm

Depths: Hole U1407A = 267.77–299.18 mbsf; Hole U1407B = 268.66–269.82 mbsf

Age: late Albian

Lithologies: grainstone, pelletal packstone, and framestone

Unit VI is composed of ~32 m of very poorly recovered carbonate reef lithologies from Holes U1407A and U1407B. The top of Unit VI is laminated sandstone that contains fine sand-sized clasts of carbonate, quartz, dolomite, and occasional belemnites (Fig. F5G). Slightly deeper in Unit VI is coarse sand cemented by Fe-Mn oxides (interval 342-U1407A-31X-CC, 17–18 cm; Fig. F16A, F16B). The sediment recovered in Sample 342-U1407A-32X-CC, 0–3 cm, is a pelleted carbonate mudstone (Fig. F16C, F16D). Large benthic orbitolinid foraminifers were found in Section 342-U1407A-33X-CC, allowing a late Albian age assignment (Fig. F16E, F16F). Section 35X-CC contains molds of gastropods, bivalves, corals, and echinoderm spines. This section also includes a packstone that thin section analysis revealed to be a pel-bio-micrite in the Folk classification (Folk, 1959) (Fig. F16C, F16D). A reef platform facies for these lithologies is consistent with the surface geometry indicated by seismic data.

Lithostratigraphic unit summary

The lithostratigraphy of Site U1407 comprises a pelagic to neritic sedimentary sequence of Pleistocene to Early Cretaceous (late Albian) age. Pleistocene sediment is ~8 m thick and includes foraminiferal nan-

nofossil ooze intercalated with decimeter-thick beds of foraminiferal sand (Unit I). This unit overlies ~10 m of early Oligocene clay with nannofossils (Unit II). Units III and IV are of early to middle Eocene age and comprise an ~85 m thick sequence of nannofossil ooze with foraminifers. An abrupt downhole increase in calcium carbonate from ~43 to ~93 wt%, together with prominent shifts in other physical properties (color reflectance L*, magnetic susceptibility, and NGR) mark the boundary between these two units. A correlative increase in carbonate content is also seen at Sites U1403–U1406. Unit V is composed of 155 m of nannofossil chalk of late Paleocene to Albian age. A prominent black shale horizon (zeolitic claystone with organic matter) associated with the Cenomanian/Turonian boundary OAE 2 (~93 Ma) was recovered from all three holes drilled at Site U1407 and is described in detail below. Finally, Unit VI is ~32 m thick and composed of nannofossil chalk capped by belemnite-bearing, fine-grained sandstone with horizontal laminations. Below, coarse-grained Fe-Mn oxide-coated sand is found in a sequence with poorly recovered shallow-water carbonates. This reef sediment is of Albian age, as inferred from the occurrence of the large benthic foraminifer *Orbitolina*. Directly above this sandy succession at Section 342-U1407A-31X-6, 35 cm (and above), thermocline-dwelling foraminifers like *Rotalipora* are observed, suggesting at least an upper bathyal water depth at this level.

Cenomanian/Turonian boundary interval and Oceanic Anoxic Event 2

The geologic record of the Cenomanian/Turonian boundary transition is characterized by widely distributed organic matter-rich black shale deposition and $\delta^{13}\text{C}$ enrichment in carbonate and organic carbon that together define OAE 2 (e.g., Sageman et al., 2006; Jenkyns, 2010). Drilling operations at Site U1407 recovered an OAE sequence in all three holes, defined on the basis of lithology (organic matter-rich zeolitic claystones or black shale) and calcareous nannofossil biostratigraphy (see “[Biostratigraphy](#)”). Significant differences in the lithostratigraphic sequence and thickness of beds exists between Holes U1407A, U1407B, and U1407C (Fig. F13), partly because of drilling disturbances and mass wasting indicated by slump features (Fig. F15). Thicknesses of beds in all of the OAE descriptions that follow will represent the maximum bed thickness observed.

The downhole OAE 2 lithostratigraphy (Fig. F13) comprises a 9.95 m thick sequence that includes a greenish white nannofossil chalk with foraminifers interbedded with dark gray nannofossil claystone

bands (maximum thickness in Hole U1407C is from 231.45 to 241.45 mbsf) that transitions to a 0.95 m thick interval of white to light gray nannofossil chalk and dark gray to black claystone bands (maximum thickness in Hole U1407C is from 230.30 to 231.25 mbsf). The greenish white and white nannofossil chalk is overlain by organic matter-rich, submillimeter-scale laminated to massive black shale with interbedded dark gray claystone with disseminated submillimeter pyrite framboids. The black shale ranges in thickness from 15 cm in Hole U1407C to 44 cm in Hole U1407A. Estimates of the true thickness of the OAE 2 black shale at Site U1407 are complicated by significant drilling disturbance. The black shale is overlain by 26 cm of laminated greenish gray nannofossil claystone and dark gray radiolarian sand (best expressed in Hole U1407B at 231.92–232.18 mbsf) and 107 cm of greenish white nannofossil chalk with interbedded chert and silicified limestone with radiolarians (best expressed in Hole U1407A at 229.56–230.64 mbsf) (Figs. F13, F14). In Holes U1407A and U1407B, a striking transition to 3.6 m of pink to pinkish gray foraminiferal nannofossil chalk occurs. The overlying pinkish brown clayey nannofossil chalk is likely to be of middle Turonian age on the basis of the first occurrence of *Lithastrinus septenarius* (Fig. F13).

Shipboard nannofossil stratigraphy from Holes U1407A and U1407B (see “[Biostratigraphy](#); Fig. F4) indicate a relatively complete yet highly condensed OAE 2 sequence. Elsewhere, the last occurrence of *Corollithion kennedyi*, present at 232.6 and 232.8 mbsf in Holes U1407A and U1407B, respectively, occurs after the initial rise in marine $\delta^{13}\text{C}$ that defines the initiation of OAE 2 (Sageman et al., 2006). This placement suggests that the OAE 2 interval begins in the underlying nannofossil chalks and that black shale deposition at Site U1407 lags onset of the global increase in the fractional burial of organic carbon. The first occurrence of *Quadrum intermedium* occurs in the greenish white nannofossil chalk ~80 cm above the black shale (Fig. F13) and is within the $\delta^{13}\text{C}$ excursion plateau that defines the heart of OAE 2. The termination of OAE 2 elsewhere (Sageman et al., 2006) occurs between the first occurrence of *Q. intermedium* and the first occurrence of *Quadrum gartneri* in the early Turonian and is tentatively placed between *Q. intermedium* and *Q. gartneri* datums at the transition from greenish white to pink chalk at 229.60 mbsf in Hole U1407A (Fig. F4). The lack of a well-developed pink chalk in Hole U1407B suggests the presence of a hiatus or slumping at 230.64 mbsf.

The color transitions and lithologies seen at Site U1407 are very similar to Cenomanian/Turonian



boundary sequences from the Umbria-Marche Basin of Italy. The greenish white to pink nannofossil chalk is reminiscent of the Scaglia Bianca and Scaglia Rossa limestones that bound the Bonarelli horizon (Arthur and Premoli Silva, 1982). The black shale in Holes U1407A and U1407B comprises a “doublet” separated by dark gray claystone (Fig. F14). The presence of radiolarian sand, chert, and silicified limestone with radiolarians at Site U1407 is also very similar to Italian sequences. However, the position of the black shale relative to *C. kennedyi* suggests that the black shale deposition at Southeast Newfoundland Ridge occurred later than in the Tethys Ocean.

Early Paleocene to early Campanian stratigraphic inversions and unconformities

Drilling at Site U1407 recovered a biostratigraphically complete upper to lower Paleocene sequence (nannofossil Subzone NP9a to Zone NP4). The Paleocene sequence is truncated by a series of unconformities and stratigraphic inversions beginning with a chert layer separating the Danian (Zone NP4) from the Campanian (Zone UC16) (see Danian–Campanian unconformity in interval 342-U1407A-22X-CC, 5–30 cm, in Fig. F17). This unconformity is underlain by younger Danian strata (Zone NP2) that are in turn terminated by an abrupt contact between the Danian and the upper Maastrichtian (Zone UC20) in Section 342-U1407A-23X-3. Nannofossils in Section 23X-CC are indicative of the lower Campanian (Sub-zone UC14d/UC15a boundary). We did not date the relative ages of lithostratigraphic contacts observed between Sections 342-U1407A-23X-3 and 23X-CC. Litho- and biostratigraphic evidence from Holes U1407B and U1407C suggest a comparable number of unconformities and hiatuses between holes, although variation clearly exists with regard to the thickness and presence of some intervals. In Hole U1407C, we identified a third unconformity between the upper Maastrichtian and lower Campanian in Section 342-U1407C-20X-1. The stratigraphically complex interval spanning the Danian to lower Campanian is likely not fully resolved by shipboard biostratigraphy, given a number of undated lithostratigraphic contacts observed in all three holes. The presence of deformational structures in Hole U1407B (Figs. F15, F17) suggests local slumping as the cause of the observed stratigraphic complexities.

Biostratigraphy

Coring at Site U1407 recovered a 300 m thick sequence of Pleistocene to upper Albian nannofossil ooze with varying amounts of clay and foraminifers.

Minor black shale, calcareous sandstone, and limestone lithologies are present in the mid-Cretaceous section. Nannofossils, planktonic foraminifers, and smaller benthic foraminifers are present in all but the mid-Cretaceous black shale, sandstone, and limestone lithologies, which contain larger benthic foraminifers and macrofossils. Radiolarians are only present in the middle Eocene, lower Eocene, and Paleocene. Thin Pleistocene and lower Oligocene intervals overlie a middle Eocene through upper Albian succession, with significant hiatuses between the lower Eocene and uppermost Paleocene, the lowermost Paleocene and uppermost Maastrichtian, and the uppermost Maastrichtian and Campanian. Sedimentation rates are relatively high (~0.4–1.5 cm/k.y.) through the Paleogene and mid-Cretaceous but low (~0.1–0.5 cm/k.y.) through the Maastrichtian to Turonian.

The uppermost brown foraminifer sandy clay and nannofossil ooze (Core 342-U1407A-1H; 0–6.81 mbsf) contains nannofossils and planktonic foraminifers that indicate Pleistocene ages (nannofossil Zones NN21–NN19). Below this (Sample 342-U1407A-1H-CC; 6.78 mbsf), nannofossils and planktonic foraminifers provide a well-defined biostratigraphy indicating a lower Oligocene to upper Albian succession. Benthic foraminifers are generally rare (the “present” category) but increase in abundance during short intervals of the Paleocene and Cretaceous. Benthic foraminifer preservation is good to very good through most of the recovered sequence, although poor to moderate preservation is seen in the Oligocene interval and occasionally in the Cretaceous succession.

An integrated calcareous and siliceous microfossil biozonation is shown in Figure F18. Datum and zonal determinations from nannofossils, planktonic foraminifers, and radiolarians are in close agreement. An age-depth plot including biostratigraphic and paleomagnetic datums is shown in Figure F19. A summary of calcareous and siliceous microfossil abundances and preservation is given in Figure F20.

Calcareous nannofossils

Calcareous nannofossil biostratigraphy is based on analysis of core catcher and additional working section half samples from Holes U1407A–U1407C. Depth positions and age estimates of biostratigraphic marker events are shown in Table T3. Calcareous nannofossil occurrence data are shown in Table T4. Note that the distribution chart is based on shipboard study only and is therefore biased toward age-diagnostic species.

At Site U1407, the preservation of calcareous nannofossils is generally moderate and good. The upper-

most sediment in Hole U1407A contains abundant nannofossils of Pleistocene Zones NN21–NN19, as indicated by the presence of abundant *Emiliania huxleyi* in Sample 342-U1407A-1H-1, 37 cm (0.37 mbsf), and the top of *Pseudoemiliania lacunosa* in Sample 1H-4, 20 cm (4.70 mbsf).

The short interval from Sample 342-U1407A-2H-5, 60 cm, to 3H-1, 110 cm (12.28–17.41 mbsf), can be assigned to lower Oligocene Zones NP23–NP21 based on the top of *Reticulofenestra umbilicus* and the top of *Coccilithus formosus*. The identification of Zone NP21 in Sample 342-U1407A-3H-1, 110 cm (17.41 mbsf), and Subzone NP15a in Sample 3H-2, 110 cm (18.91 mbsf), indicates the presence of a hiatus of ~11 m.y., representing the upper middle Eocene to lowermost Oligocene.

The interval from Sample 342-U1407A-3H-2, 110 cm, to 15H-CC (18.91–121.82 mbsf) is assigned to middle to lower Eocene nannofossil Subzone NP15c to Zone NP11. All primary zonal marker species are present and listed in Table T3.

The identification of Zone NP11 in Sample 342-U1407A-15H-CC (121.82 mbsf) and Subzone NP9a in Sample 16X-1, 8 cm (121.98 mbsf), indicates the presence of a hiatus of ~2 m.y., incorporating the lowermost Eocene and uppermost Paleocene, including the PETM.

The interval from Sample 342-U1407A-16X-1, 8 cm, to 23X-2, 125 cm (121.98–186.65 mbsf), is assigned to nannofossil Zones NP9–NP2, with all primary marker species present apart from *Heliolithus riedelii*, which prevents the formal differentiation of Zone NP8. The intra-Zone NP8 event, base of *Discoaster backmani*, confirms the presence of Zone NP8, with equivalent sediment in Samples 342-U1407A-18X-2, 113 cm, through 18X-CC (138.53–142.90 mbsf) (Table T3).

The identification of Zone NP2 in Sample 342-U1407A-23X-2, 125 cm (186.65 mbsf), and Subzone UC20c in Sample 23X-2, 135 cm (186.75 mbsf), indicates the presence of a hiatus of ~2.5 m.y., incorporating the lowermost Paleocene and uppermost Maastrichtian, including the K/Pg boundary. The presence of Campanian sediment assigned to Zone UC16 in Section 342-U1407A-22H-CC indicates that a short interval of older sediment has been incorporated into the lowermost Paleocene section, possibly by drilling disturbance. The identification of Subzone UC20c in Sample 342-U1407A-23X-3, 74 cm (187.64 mbsf), and the Subzone UC14d/UC15b boundary in Sample 23X-6, 97 cm (192.37 mbsf), indicates the presence of a hiatus of ~10 m.y., incorporating the lower Maastrichtian and upper Campanian.

The interval from Sample 342-U1407A-23X-6, 97 cm, to 31X-CC (192.37–268.60 mbsf) is assigned to Cretaceous nannofossil Zone UC20–Subzone UC0a based on the following biohorizons: base of *Nephrolithus frequens*, base of *Ceratolithoides kamptneri*, top of *Reinhardtites levis*, base of *Brownsonia parca constricta*, base of *Lithastrinus grillii*, base of *Micula staurophora*, base of *L. septenarius*, base of *Q. gartneri*, top of *Helenea chiastia*, base of *Lithraphidites acutus*, base of *C. kennedyi*, top of *Hayesites*, and presence of *Eiffellithus turrieseiffelii* in the lowermost nannofossiliferous sediment (Table T3). Core 342-U1407A-28X contains a striking black shale lithology, and the presence of Turonian nannofossil Zone UC6 above and Cenomanian Zone UC5/UC4 below is strong evidence that this lithology is equivalent to OAE 2 black shale, such as the Italian Bonarelli level. Further high-resolution sampling is required to establish the succession of nannofossil extinction events across this interval.

The lowermost Cores 342-U1407A-32X through 35X (270.35–299.13 mbsf) are composed of calcareous sandstone and limestone lithologies that contain no nannofossils, most likely because of shallow water depths indicated by the presence of larger benthic foraminifers, corals, and molluscan shell fragments.

Radiolarians

Radiolarian biostratigraphy is based on analysis of all core catcher samples from Hole U1407A and selected section samples from Cores 342-U1407A-21X and 22X. No samples from Hole U1407B or U1407C were examined. Radiolarians are abundant and well preserved in the lower middle Eocene and the Paleocene but are either absent or indeterminate in both the upper Pleistocene–upper middle Eocene and lowermost Paleocene–Cretaceous intervals in Hole U1407A. Strong faunal affinities are noted with co-eval assemblages described from Blake Nose ODP Site 1051 (Sanfilippo and Blome, 2001) and J-Anomaly Ridge Deep Sea Drilling Project Site 384 (Nishimura 1992). Depth positions and age estimates of biostratigraphic marker events are shown in Table T5, and the radiolarian distribution is shown in Table T6. Note that the distribution chart is based on shipboard study only and is therefore biased toward age-diagnostic species.

Samples 342-U1407A-1H-CC through 6H-CC (6.78–54.7 mbsf) are barren of radiolarians. Samples 7H-CC through 9H-CC (64.16–83.16 mbsf) contain only poorly preserved spumellarian radiolarians that cannot be assigned to species.

Samples 342-U1407A-10H-CC through 11H-CC (92.32–102.04 mbsf) contain abundant and well-pre-



served middle Eocene radiolarians. This interval is correlated to radiolarian Zone RP11 based on the presence of primary index species *Dictyopora mongolfieri* and the absence of the primary index for Zone RP12, *Eusyringium lagena*. Correlation with Zone RP11 is supported by three additional bio-events that are known to occur with the zone; the tops of *Buryella clinata*, *Calocyctomma castum*, and *Lamptonium fabaeforme fabaeforme* occur within Sample 342-U1407A-11H-CC (102.04 mbsf).

Samples 342-U1407A-12H-CC through 15H-CC (102.84–121.82 mbsf) contain rare, poorly preserved radiolarians of likely Eocene age based on the presence of probable *Podocyrtis papalis* s.s.

Interval 342-U1407A-16X-CC through 22X-1, 24–25 cm (124.61–174.55 mbsf), contains abundant, well-preserved Paleocene radiolarians. Samples 342-U1407A-16X-CC through 18X-CC (124.61–142.90 mbsf) are correlated to Zone RP7 based on the common occurrence of primary index species *Bekoma bidartensis*. As at Site U1406, this interval would be assigned to the lowermost Eocene part of Zone RP7 based on the presence of *P. papalis*, *Theocorys? physzella*, and *Theocorys? aff. physzella* (sensu Sanfilippo and Blome, 2001). However, nannofossils indicate that Samples 342-U1407A-16X-1, 8 cm, through 19X-2, 32 cm (121.98–147.45 mbsf), are late Paleocene in age (nannofossil Subzone NP9a to Zone NP7/NP8). The faunal crossover from *Bekoma campechensis* to *B. bidartensis* occurs abruptly between Samples 18X-CC and 19X-CC (142.9–149.25 mbsf). A short hiatus of ~1 m.y. may occur between these two samples because uppermost Subzone RP6c has not been identified. This is a well-defined subzone at nearby Site 384, where the gradual faunal crossover between *B. campechensis* and *B. bidartensis* is observed. Only Subzones RP6b and RP6a are present in Hole U1407A. Sample 342-U1407A-19X-CC (149.25 mbsf) is assigned to Subzone RP6b based on the occurrence of *Stichocampe? caia*, a distinctive species restricted to this subzone. The subzone is also bracketed by the bases of *B. bidartensis* and *Pterocodon? poculum* in overlying Sample 342-U1407A-18X-CC (142.90 mbsf) and the top of *Orbula comitatas* in underlying Sample 20X-CC (164.85 mbsf). Interval 342-U1407A-20X-CC through 22X-1, 24–25 cm (164.85–174.55 mbsf), is the lowermost interval that contains age-diagnostic radiolarians in Hole U1407A and is assigned to Subzone RP6a based on the co-occurrence of *B. campechensis* and *O. comitatas*. The lowermost sample is inferred to be low in this subzone, as it contains the top of *Anthocyrtis mespilus*, a species with a range that extends no higher than nannofossil Zone NP4 at Site 384 (Nishimura, 1992). We estimate an age of 62 Ma for this last occurrence datum.

Radiolarians are absent from all samples examined from Sample 342-U1407A-22X-CC through 35X-CC (182.27–299.11 mbsf). A dark claystone in Sample 342-U1407A-28X-1, 18–20 cm (232.09 mbsf) within the Cenomanian/Turonian boundary interval was examined for radiolarians and benthic foraminifers but proved to be barren of microfossils. Radiolarians were observed in thin sections from three chert layers above the Cenomanian/Turonian boundary in Core 342-U1407B-24X (Fig. F21). All radiolarian tests are infilled or replaced by microcrystalline quartz, but in some specimens the test outline is preserved. This suggests that these cherts may be suitable for processing for radiolarians using the hydrofluouric acid method.

Planktonic foraminifers

Core catchers and additional samples from working section halves were examined in Hole U1407A. Samples contain diverse and well-preserved assemblages of planktonic foraminifers from the Pleistocene to the mid-Cretaceous. Depth positions and age estimates of biostratigraphic marker events are shown in Table T7. The stratigraphic distribution of planktonic foraminifers is shown in Table T8.

The uppermost interval from Samples 342-U1407A-1H-CC through 2H-1, 50–52 cm (6.78–7.31 mbsf), contains *Globorotalia truncatulinoides*, indicative of Pleistocene age. Samples 2H-2, 70–72 cm, through 2H-4, 50–52 cm (9.01–11.61 mbsf), contain poorly preserved assemblages containing no index markers except *Globorotalia inflata* and *Neogloboquadrina pachyderma*, suggesting an age of Pliocene–Pleistocene. A poorly preserved Oligocene assemblage (mainly comprising *Catapsydrax* spp. and *Dentoglobigerina galavis*) was recovered from Samples 342-U1407A-2H-5, 60–62 cm, through 2H-CC (12.28–15.95 mbsf). Samples 2H-7, 40–42 cm, through 3H-1, 110–112 cm (15.07–17.42 mbsf) contain poorly preserved specimens of *Acarinina bullbrookii*, *Globigerinatheka index*, and *Globigerinatheka mexicana*, suggesting a middle Eocene age.

Well-preserved and taxonomically diverse planktonic foraminifers of Eocene age are found in Samples 342-U1407A-3H-2, 110–112 cm, through 15H-CC (18.91–121.84 mbsf). Sample 3H-2, 110–112 cm (18.91 mbsf), contains *Guembelitrioides nuttalli* but lacks *Morozovella aragonensis* and *Morozovella crater*, indicating Zone E10. The top of *M. aragonensis* (the base of Zone E10), base of *G. nuttalli* (base of Zone E8), top of *Morozovella subbotinae* (base of Zone E6), and base of *M. aragonensis* (base of Zone E5) are found in Samples 342-U1407A-4H-1, 100–102 cm (26.81 mbsf), 10H-2, 110–112 cm (85.41 mbsf), 12H-1,



25–27 cm (102.11 mbsf), and 15H-CC (121.82 mbsf), respectively.

The interval from Sample 342-U1407A-16X-1, 35–37 cm, to 22X-CC, 10–12 cm (122.29–181.92 mbsf), contains planktonic foraminifers spanning upper to middle Paleocene Zones P5–P3. The top and base of *Globanomalina pseudomenardii* mark the respective top and base of Zone P4. The Paleocene/Eocene boundary is not recognized because of the absence of “excursion taxa” such as *Acarinina sibaiyaensis* and *Morozovella allisonensis*. Planktonic foraminifers of early Paleocene (Zone P1) age occur from Sample 342-U1407A-23X-2, 33–35 cm, to 23X-2, 126–127 cm (185.74–186.67 mbsf). An apparent inconsistency between the planktonic foraminiferal Zone P3/P4 boundary and the identification of nannofossil Zone NP2 is likely explained by the coarser resolution of the planktonic foraminiferal sampling in this particular interval.

Relatively diverse assemblages of Cretaceous planktonic foraminifers occur from Samples 342-U1407A-22H-CC, 30–32 cm, through 31X-CC (182.12–268.60 mbsf), in which preservation varies from good to occasionally poor. The base of the Campanian *Radotruncana calcarata* Zone occurs in Sample 23X-6, 12–15 cm (191.54 mbsf). The top and base of the lowermost Campanian to Santonian *Dicarinella asymmetrica* Zone are found in Samples 342-U1407A-24X-CC (199.40 mbsf) and 25X-CC (206.61 mbsf). The base of *Dicarinella concavata*, denoting the upper Turonian, occurs in Sample 27X-1, 33–35 cm (222.64 mbsf). The Cretaceous sequence at Site U1407 may thus contain the Campanian/Santonian, Santonian/Coniacian, and Coniacian/Turonian boundaries. The top and base of *Helvetoglobotruncana helvetica* (lower to upper Turonian) occurs in Samples 342-U1407A-27X-3, 29–30 cm (225.60 mbsf), and 27X-4, 65–67 cm (227.46 mbsf), respectively. Samples 28X-2, 14–15 cm, through 29X-3, 85–86 cm (233.53–245.00 mbsf), contain *Rotalipora cushmani*, marking the upper Cenomanian. The short *Thalmanninella reicheli* Zone occurs in Sample 342-U1407A29X-4, 85–86 cm (246.86 mbsf). The base of *Thalmanninella globotruncanoides*, indicating the lowermost Cenomanian, occurs in Sample 342-U1407A-31X-5, 70–71 cm (267.41 mbsf), and the upper Albian marker species *Planomalina buxtorfi* is found in Samples 31X-6, 36–37 cm, through 31X-CC (268.17–268.60 mbsf). An apparent inconsistency between the base of the *D. asymmetrica* Zone with the identification of nannofossil Zone UC9 is likely explained by the coarser resolution of the planktonic foraminiferal sampling in this particular interval.

Benthic foraminifers

Benthic foraminifers were examined semiquantitatively in core catcher samples from Hole U1407A. Additional working section half samples taken from Cores 342-U1407A-2H through 31X and 342-U1407B-21X through 24X were examined for preservation and relative abundance of benthic foraminifers. Benthic foraminifers at this site are rare (the “present” category) relative to total sediment particles >150 µm in the Oligocene–Paleocene and slightly more abundant in parts of the Cretaceous (Fig. F20; Table T9).

Although preservation of benthic foraminifer tests is generally good to very good in the Eocene to Cretaceous, the Oligocene and parts of the Cretaceous succession contain some moderately or poorly preserved samples (Fig. F20). The occurrences of benthic foraminifers at this site are shown in Tables T9 and T10.

Sample 342-U1407A-1H-CC yields a well-preserved Pleistocene fauna containing mainly *Bolivina* sp., *Cassidulina subglobosa*, *Cibicidoides* spp., and *Pullenia* spp.

Samples 342-U1407A-2H-CC through 15H-CC (15.95–121.82 mbsf) are dominated by an Eocene assemblage of the calcareous taxa *Bulimina* spp., *C. subglobosa*, *Dentalina* sp., *Gyroidinoides* spp., *Nuttallides truempyi*, *Oridorsalis umbonatus*, and stiliostomellids (including *Stilostomella gracillima*, *Stilostomella lepidula*, *Stilostomella subspinosa*, and *Stilostomella* sp.). Agglutinated benthic foraminifers are minor constituents only. Overall, the Eocene assemblages show fluctuations between intervals of high abundance of infaunal taxa, indicating a high organic matter flux to the seafloor and intervals of dominantly epifaunal species.

Samples 342-U1407A-16X-CC through 22X-CC (124.61–182.27 mbsf) contain diagnostic Paleocene assemblages. Abundant calcareous taxa include *Bulimina* sp., *Dentalina* sp., gavelinellids (*Gavelinella beccariiformis*, *Gavelinella hyphalus*, and *Gavelinella* sp.), *Gyroidinoides* spp., *Lenticulina* cf. *adenalensis*, *N. truempyi*, and *Pullenia coryelli*. The agglutinated benthic foraminifer *Gaudryina pyramidata* occurs frequently to abundantly in these samples.

Benthic foraminifer assemblages of the Upper Cretaceous sediment from Samples 342-U1407A-23X-CC through 25X-CC (193.13–206.61 mbsf) are almost comparable to the overlying Paleocene assemblages, with additional species such as *Lenticulina rotulata*, *Marssonella oxycona*, and *Reussella* sp. occurring frequently to abundantly.



Sample 342-U1407A-27X-CC (230.88 mbsf) shows an assemblage that is typical of the black shale facies associated with OAE 2 (e.g., Holbourn and Kuhnt, 2002; Friedrich, 2010). The assemblage is dominated by the agglutinated species *Spiroplectinata annectens*. Abundant calcareous taxa are *Bolivina anambra*, *Pleurostomella reussi*, and *Tappanina laciniosa*, indicating low oxygen concentrations at the seafloor.

Underlying Cores 342-U1407A-28X through 31X show a lower Cenomanian to upper Albian benthic foraminifer assemblage characterized by *Astacolus* sp., gavelinellids (including *Gavelinella cenomanica*, *Gavelinella intermedia*, and *Gavelinella* sp.), *Gyroidinoides* spp., *L. rotulata*, *Osangularia schloenbachi*, and *S. annectens*.

The sandstone facies of Sample 342-U1407A-33X-CC (280.00 mbsf) contains few specimens of the larger benthic foraminifer genus *Orbitulina* (probably *Orbitulina concava* and *Orbitulina texana*), indicative of an Albian age (Fig. F22).

Macrofossils

Macrofossil remains such as algae, bivalves, cephalopods, corals, and gastropods are found in lithostratigraphic Unit VI (Fig. F23). Although calcareous hard parts of most specimens are not preserved, outer molds are found in the limestone.

Sample 342-U1407A-31X-CC (268.54 mbsf) yields two belemnites (possibly *Neohibolites*) (Fig. F23A). Well-preserved rostrums were horizontally embedded within this core catcher. Those two individuals are aligned side-by-side with adapical ends pointing in the same direction indicative of relatively strong bottom water current.

Although mostly preserved as outer molds, diverse shallow-marine macrofossil fauna were observed in Sample 342-U1407A-35X-CC (299.10 mbsf). Hermatypic corals, bivalves, and gastropods (Fig. F23D, F23E, F23F) are predominant, and coralline algae are subordinate (Fig. F23B).

Paleomagnetism

We completed a paleomagnetism study of APC and XCB cores from Holes U1407A–U1407C with the primary objective of establishing a magnetostratigraphic age model for the site. The natural remanent magnetization (NRM) of each archive section half was measured at 2.5 cm intervals before and after demagnetization treatment in a peak alternating field (AF) of 20 mT for cores from Holes U1407A and U1407B. For cores from Hole U1407C, we only measured NRM after 20 mT demagnetization. Archive section half measurement data were pro-

cessed by removing measurements made within 7.5 cm of section ends and from disturbed intervals described in the Laboratory Information Management System database. Cores 342-U1407A-1H through 15H and 342-U1407B-1H through 11H were azimuthally oriented using the FlexIT orientation tool (Table T11). All other cores were not oriented.

We also collected 142 discrete samples from working section halves to verify the archive-half measurement data and to measure anisotropy of magnetic susceptibility (AMS) and bulk susceptibility of Site U1407 sediment. Discrete samples were collected and stored in 7 cm³ plastic cubes and were typically taken from the least disturbed region closest to the center of each section in Hole U1407A. Selected samples were subjected to measurements of AMS, including bulk susceptibility, and NRM measurements after 20 mT AF demagnetization. Twenty-six samples were selected for additional step-wise demagnetization at 30, 40, and 60 mT. All discrete sample data are volume corrected to 7 cm³.

Results

Downhole paleomagnetism data after 20 mT demagnetization are presented for Holes U1407A, U1407B, and U1407C in Figures F24, F25, and F26, respectively. Similar to paleomagnetism results from Sites U1403–U1406 (see “Paleomagnetism” in the “Site U1403,” “Site U1404,” “Site U1405,” and “Site U1406” chapters [Norris et al., 2014c, 2014d, 2014e, 2014f]), section-half measurement data from XCB cores are difficult to interpret because of biscuiting and substantial core disturbance. We chose to interpret only results obtained from APC cores except for a few cases in which XCB core disturbance is remarkably low.

We report two principal features in the paleomagnetism data at Site U1407. First, we observed five discrete zones of different levels of magnetic intensity. Second, inclination values cluster at ~45° and -30°, a trend that is associated with clustering of declination values at ~0° and 180°, respectively. These features are discussed in detail below.

Magnetic intensity zonation

Magnetic intensity values can be divided into five intervals (Figs. F24, F25, F26):

1. $\sim 10^{-3}$ to 10^{-2} A/m at 0–30 mbsf,
2. $\sim 10^{-5}$ to 10^{-4} A/m at ~30–100 mbsf,
3. $\sim 10^{-4}$ A/m at ~130–180 mbsf,
4. $\sim 10^{-3}$ to 10^{-2} A/m at ~180–230 mbsf, and
5. $\sim 10^{-4}$ to 10^{-3} A/m at ~240–270 mbsf.

This behavior is most evident in Holes U1407B and U1407C. Exceptions to this zonation occur in two



intervals. At ~80–100 mbsf, magnetization intensity is high and inclination values are close to 90°. We conclude that this interval is affected by a strong drilling overprint. Magnetic intensity is especially low (~ 10^{-6} A/m) from ~230 to 240 mbsf. This interval corresponds to OAE 2 (Cenomanian/Turonian boundary), and the strong reducing conditions associated with this event have probably dissolved most of the primary magnetic material from this interval.

These magnetic trends generally correspond with lithostratigraphy. Sediment at Site U1407 changes from pale brown lower Oligocene clay with nannofossils (lithostratigraphic Unit II) to greenish gray nannofossil ooze with foraminifers (Unit III) at ~16 mbsf. The third magnetic intensity zone corresponds to Subunit Va, which is composed of nannofossil chalk with radiolarians and foraminifers. The fourth magnetic intensity zone is restricted to the upper ~50 m of Subunit Vb, a nannofossil chalk with occasional radiolarians. The lowest magnetic intensity zone occurs in the lowermost ~30 m of Subunit Vb.

Inclination and declination clustering

Inclination values following 20 mT AF demagnetization often cluster around 45° and -30°. Inclination clustering is usually associated with declination clustering at ~0° and 180°, respectively. The approximately -30° inclination is shallow with respect to the reversed polarity value expected at the ~40°N latitude of Site U1407. This shallow bias is readily attributed to a small normal polarity drilling overprint that remains after 20 mT AF demagnetization. AF demagnetization at 20 mT removes most of the drilling overprint in most APC-recovered intervals and some XCB-recovered intervals, so we can utilize the positive and negative polarity clustering behavior to readily identify magnetozones in Site U1407 sediment.

Comparison between pass-through and discrete sample data

AF demagnetization results for 95 discrete samples are summarized in Table T12. Of the 26 samples treated with a peak AF demagnetization field of 60 mT, 12 reveal reasonably stable components of magnetization (e.g., Fig. F27A, F27B). These samples have remanent magnetizations that are strong enough to be measured by the onboard JR-6A spinner magnetometer. The remaining samples typically display NRM intensities that decrease by an order of magnitude following AF demagnetization in a 20 mT field. This behavior indicates that a drilling overprint probably obscures the primary magnetic signal. Nevertheless, these results are useful for veri-

fying the 20 mT pass-through paleomagnetism data from the archive section halves.

In general, paleomagnetism data from archive section halves and discrete samples from oriented APC core intervals agree well. In contrast, some discrete samples from XCB cores show single stable components that are consistent with the archive-half measurement data (e.g., Fig. F27B), but others show stable components that do not decay toward the origin and are not consistent with the section-half measurement data (e.g., Fig. F27C). These results suggest that section-half measurement data from XCB core intervals should be interpreted with care, similar to our conclusions regarding paleomagnetism data at Sites U1403 and U1406.

Magnetostratigraphy

The shipboard downhole results reveal a series of normal and reversed magnetozones between Cores 342-U1407A-6H and 10H (~47–91 mbsf), between Cores 342-U1407B-6H and 11H (~48–91 mbsf), and between Cores 342-U1407C-6H and 10H (~43–84 mbsf). These magnetostratigraphies can be unambiguously correlated between all three holes. Downhole plots indicate that additional series of magnetozones are recorded lower in the recovered interval in all three holes, but shore-based studies are necessary to identify and fully characterize magnetozones in these intervals, and for Holes U1407B and U1407C, provide independent age control to correlate them to the geomagnetic polarity timescale (GPTS).

By utilizing radiolarian, foraminifer, and nannofossil biostratigraphic datums from Hole U1407A (see “[Biostratigraphy](#)”), we can correlate magnetozones to the GPTS. The shipboard magnetostratigraphic age model is based on Hole U1407A, for which we have the most biostratigraphic datums. Extension of this age model to the magnetozonation observed in Holes U1407B and U1407C is contingent on the accuracy of the stratigraphic correlation between holes, which is corroborated by lithologic marker horizons, biostratigraphic datums, and physical property features (see “[Stratigraphic correlation](#)”). Our correlation is presented in Table T13 and is shown in Figures F24, F25, F26, and F28.

In Hole U1407A, we correlated the magnetostratigraphy in Cores 342-U1407A-6H through 10H to lower Chron C20r (~43.4 Ma) through upper Chron C22r (~49.4 Ma). With the aid of nannofossil datums, we correlated a reversed to normal downhole polarity transition in Section 342-U1407A-19X-2 to the Chron C25r/C26n boundary (58.959 Ma). We attribute the difficulty in correlating magnetozones observed in Cores 342-U1407A-11H through 18X to



the GPTS to the two long hiatuses implied by the biostratigraphic datums (see “[Biostratigraphy](#)”). Magnetozone correlations for Holes U1407B and U1407C are similar to Hole U1407A, with the exception that we did not observe the Chron C25r–C26n transition in the former holes.

The correlations described above provide a shipboard chronostratigraphic framework for interpreting the early to middle Eocene sediment record at Site U1407. The most salient implication of this age model is that sedimentation rates along Southeast Newfoundland Ridge at the paleowater depth of Site U1407 varied between ~2.0 and 8.7 cm/k.y. during the middle Eocene (Fig. [F19](#)).

Magnetic susceptibility and anisotropy of magnetic susceptibility

Bulk magnetic susceptibility measured on 78 discrete samples is summarized in Table [T14](#). Downhole variation in whole-round magnetic susceptibility (WRMS) and discrete sample magnetic susceptibility (DSMS) for Hole U1407A are shown in Figure [F24](#). The WRMS data for Hole U1407A are shown in raw form; they have not been trimmed at section ends or filtered for obvious outliers, so noise in the data probably reflects edge effects or spurious measurements. We multiplied the WRMS data, which are in instrument units, by a factor of 0.577×10^{-5} to convert to approximate SI volume susceptibilities (see “[Paleomagnetism](#)” in the “Methods” chapter [Norris et al., 2014b]). WRMS and DSMS data agree very well after this conversion, and we attribute small absolute differences to the fact that the conversion factor applied to the WRMS data is not constant downhole because of changes in core diameter and density; only discrete samples provide calibrated susceptibility values in SI units. Both magnetic susceptibility data sets show the same first- and second-order cyclic trends, indicating that these trends are robust features of Site U1407 sediment. Although discrete samples were collected from each core section for the entire depth of Hole U1407A, we chose to measure only odd-numbered samples.

AMS results for the discrete samples are also summarized in Table [T14](#) and are shown in Figure [F29](#). The eigenvalues associated with the maximum (τ_1), intermediate (τ_2), and minimum (τ_3) magnetic susceptibilities at Site U1407 show prominent downhole variation. Eigenvalues are consistently divergent from the top of Hole U1407A to ~82 mbsf. The exceptional divergence observed from ~82 to ~102 mbsf is probably spurious. The soupy consistency of the white nannofossil ooze that characterizes lithostratigraphic Unit IV also has extremely low

magnetic susceptibility values. Similarly, the large divergence between eigenvalues from ~122 to 175 mbsf may be an artifact of the very weak magnetic susceptibility in Subunit Va. The modest and more variable divergence observed below ~175 mbsf is similar to downhole magnetic anisotropy trends observed in the lowest intervals of holes at previous Expedition 342 sites. The degree of anisotropy is modest with respect to sites at J-Anomaly Ridge. In general, the shape anisotropy is triaxial. We do not observe a strong depth-dependence in the inclination of the minimum eigenvector (V_3), suggesting that there is not a preferred fabric orientation of oblate particles.

Age-depth model and mass accumulation rates

At Site U1407, we recovered a 300 m thick sequence of Pleistocene to upper Albian nannofossil ooze with varying amounts of clay and foraminifers. Sedimentation rates are relatively high (~1.0–8.7 cm/k.y.) through the Paleogene and a short interval in the mid-Cretaceous (Albian/Cenomanian boundary interval) but low through the Maastrichtian to Turonian (~0.1–0.5 cm/k.y.). Thin Pleistocene and lower Oligocene intervals overlie a middle Eocene through upper Albian succession with significant hiatuses between the lower Eocene and uppermost Paleocene, the lowermost Paleocene and uppermost Maastrichtian, and the uppermost Maastrichtian and Campanian (see “[Biostratigraphy](#)”).

Biostratigraphic and magnetostratigraphic datums from Hole U1407A (Table [T15](#)) were compiled to construct an age-depth model for this site (Fig. [F19](#)). A selected set of datums (Table [T16](#)) was used to create an age-depth correlation and calculate linear sedimentation rates (LSRs). Total MAR, carbonate MAR (CAR), and noncarbonate MAR (nCAR) were calculated at 0.2 m.y. intervals using a preliminary shipboard splice rather than the sampling splice described in this volume (Table [T17](#); Fig. [F30](#)).

Age-depth model

The age-depth model is tied to Pleistocene to upper Eocene nannofossil datums in the upper 18 m of Hole U1407A. Through the middle Eocene, paleomagnetic datums are used as the primary tie points. Apart from a single radiolarian datum, the age-depth model is tied to nannofossil datums for the remainder of Hole U1407A, which ranges from lower Eocene to Albian. Good agreement exists between nannofossil datums and other datums over this interval.



Clusters of nannofossil datums at two horizons in the lower Eocene served to identify two short hiatuses (49.5–51.5 and 54.4–55.6 Ma). The Maastrichtian and upper Campanian is also inferred to be extremely condensed from a series of closely spaced nannofossil datums between 186.65 and 206.57 mbsf.

Linear sedimentation rates

Below the condensed Pleistocene–Miocene interval in the upper 20 mbsf, LSRs in Hole U1407A are high in the middle Eocene (~2 cm/k.y.); moderately high in the Paleocene (1 cm/k.y.); and low in the uppermost Cretaceous and Miocene, Eocene, and Paleocene (0.2–0.9 cm/k.y.).

Mass accumulation rates

MARs range from <0.1 g/cm²/k.y. in the Oligocene to Pleistocene to peak values of ~4 and 9 g/cm²/k.y. in the Cenomanian/Turonian boundary interval (~93 Ma) and during the early Eocene (~50 Ma), respectively. Carbonate contents dominate the sediment accumulation until the lower/middle Eocene boundary. After this time, carbonate and noncarbonate constituents accumulate at roughly equal rates. Peaks in MAR occur during the Turonian (~1 g/cm²/k.y.), the middle to late Paleocene (1–1.5 g/cm²/k.y.), and the middle Eocene (2.0 g/cm²/k.y.).

Geochemistry

The geochemistry program carried out routine shipboard analyses for Site U1407, including

- Analysis of interstitial gas compounds on headspace samples;
- Measurement of minor and trace element concentrations in interstitial water squeezed from whole-round samples from Hole U1407A;
- Inorganic carbon, total carbon, and total nitrogen determinations of solid sediment samples from multiple holes; and
- Characterization of organic matter by source-rock pyrolysis.

Headspace gas samples

Headspace gas samples for standard safety monitoring were collected at a frequency of one sample per core in Hole U1407A (Table T18), generally in the bottom half of each core (i.e., Sections 4, 5, or 6). Methane increases very slightly downhole, with values between 1.4 and 4.12 ppmv. Higher molecular weight hydrocarbons were not detected in measurable amounts.

Interstitial water samples

Twenty interstitial water samples were collected from Hole U1407A, covering a depth range from close to the sediment/seawater interface to ~270 mbsf. Samples were collected at a typical frequency of one per core (Table T19). In some cases, disturbed cores or low recovery prohibited collection of whole-round samples for interstitial water analysis, as was the case with Cores 342-U1407A-13H through 15H, which had no recovery. In other instances, systematic whole-round sampling was temporarily suspended because of the suspected presence of critical lithologies or chronostratigraphic boundaries in the core. For example, we did not sample Core 342-U1407A-28X, which contains a black shale sequence deposited during OAE 2 (see “[Biostratigraphy](#)”; see also “[Ocean Anoxic Event 2](#)” in the “Expedition 342 summary” chapter [Norris et al., 2014a]). Results of the chemical analyses are presented in Table T19 and Figure F31. Depletion of shipboard supplies of the laboratory strontium standard prompted a mission to collect seawater for preparation as a replacement standard. We were ultimately unable to confirm the calibration range, therefore strontium values for Sites U1407–U1411 are not reported.

Interstitial water profiles show evidence of compartmentalization, with prominent abrupt downhole shifts in magnesium, manganese, and potassium at ~100–120 mbsf, suggesting that the unrecovered sequence of cherts acts as an aquiclude (Fig. F31) with strong physical control on the transport of dissolved chemical constituents within interstitial water.

The downhole decrease in interstitial water Mg concentration is gradual from the sediment/water interface to 110 mbsf, where concentrations reach a minimum of 51 mM just above the chert-rich interval. Below the chert-rich interval, the downhole profile for Mg shows a reversed gradient to the base of the sediment column suggestive of a source of Mg within the highly porous underlying reefal carbonate sediment of lithostratigraphic Unit VI (see “[Lithostratigraphy](#)”). Superimposed on these general trends, the transient increases at 60, 140, 190, and 270 mbsf observed in Hole U1407A (Fig. F31) indicate a local net magnesium source within the sediment column. Possible sources include weathering of igneous minerals (Gieskes and Lawrence, 1981) and the release of magnesium absorbed to sediment-particle surfaces by ion exchange with interstitial fluid ammonium (von Breymann and Suess, 1990). Support for the first interpretation is the presence of an ash layer at 140 mbsf (see “[Lithostratigraphy](#)”). Support for the latter interpretation is corroborated by broadly correlative increases in ammonium concentrations. The calcium concentration of interstitial



fluid shows a relatively subtle depth increase to the top of the chert-rich interval. Below the chert, Ca shows a slightly reversed gradient (downhole decrease). This reversed gradient in calcium corresponds to a downhole decrease in alkalinity and increased lithification (~180 and ~270 mbsf, respectively; see “[Lithostratigraphy](#)”), suggesting that alkalinity and Ca are partially controlled by carbonate diagenesis. Within this stratigraphic interval, preservation of foraminifers varies from good to occasionally poor, including calcareous nannofossils at ~270 mbsf (see “[Biostratigraphy](#)”).

Overall, potassium interstitial water concentrations decrease downhole from maximum values of 12–13 mM above the chert-rich layer to minimum values of 10–12 mM below the chert-rich layer. Prominent superimposed inflections to higher values occur at 200 and 250 mbsf and may reflect enhanced sorption onto clay minerals (e.g., Arthur, 1979), particularly illite, which is found in greater abundance in lithostratigraphic Subunit Vb (see “[Lithostratigraphy](#)”).

In contrast to Sites U1403–U1406, changes in the chemical composition of interstitial water at Site U1407 do not show a strong influence of the respiration of organic carbon.

The interstitial water profiles of the redox-sensitive metals Mn and Fe exhibit low to below detection limit concentrations. Manganese concentrations are 0–4.9 µM above the chert layer, with a large, broad peak extending from 180 to 200 mbsf below the chert layer, close to the deposition of the organic matter-rich black shale sequences (up to 16.7 wt% organic matter) in lithostratigraphic Unit IV. The peak is very modest compared to previous sites and is possibly a function of the age of the black shale. Under conditions in which reducible Mn oxides are not abundant, continuing anaerobic microbial activity would shift to reduction of sulfate, and lower sulfate concentrations and increased alkalinity would be expected (e.g., Gieskes, 1981). However, whereas alkalinity increases slightly downhole to the chert-rich layer, the sulfate interstitial water profile is characterized by relative stability, with values between 30 and 28 mM over the entire interval, suggesting the modest manganese peak may not be associated with anaerobic microbial activity. Instead, it is possible that the Mn enrichment is the result of inorganic sedimentary diagenesis. Shipboard-based X-ray diffraction measurements did not detect the presence of manganese carbonate phases (e.g., rhodochrosite or ankerite), which are common in organic matter-rich sediment. Interstitial water squeeze cakes were sampled for further shore-based chemical analysis.

Sediment samples

Sediment plugs (5 cm³) for downhole analysis of sediment elemental geochemistry were taken from Cores 342-U1407A-1H through 31X at an average resolution of one sample per section, adjacent to the moisture and density samples (Table [T20](#)). Additional samples were taken from Cores 342-U1407B-7H and 10H at 40 cm intervals to resolve high-amplitude features in carbonate contents captured in Hole U1407A.

Results

Concentrations of inorganic carbon vary from 0.05 to 11.06 wt% in sediment at Site U1407. These concentrations are equivalent to 0% to 93% CaCO₃, assuming that all of the carbonate is calcite. Total organic carbon (TOC) values are typically 0.1–0.5 wt% over the entire interval. The 0 wt% carbonate values at 10 mbsf are recorded in the Oligocene clay beneath the Pleistocene veneer at Site U1407. The most prominent change in carbonate content at this site is a downhole step increase associated with the downhole transition from middle Eocene to lower Eocene sediment (from 59 to 82.5 wt%; ~80 mbsf); this step correlates with shifts in several proxies (e.g., color reflectance, magnetic susceptibility, NGR, TOC, and total nitrogen values; Fig. [F32](#)). This decrease in carbonate is linked to a change in production, preservation, or dilution by other sedimentary components. Although this interval corresponds to an increase in TOC, it does not correspond to high productivity, as inferred by increased siliceous tests.

A sedimentary sequence of zeolitic claystone (black shale) and chalk representing the Cenomanian-Turonian OAE 2 was recovered at ~220 mbsf in Hole U1407A. Two comparable OAE 2 successions, but with different lithostratigraphic expressions, were recovered in Holes U1407B and U1407C. Homogeneous to laminated organic-rich black shale from Hole U1407A has pyrolysis-derived TOC content of 4–16.7 wt% and variable carbonate content (1.2–4.4 wt%), reflecting the calcite-rich laminae in the black shale. Organic matter is Type II kerogen, derived from algal and microbial primary production. Hydrogen indexes (~600–620 mg hydrocarbons per g organic carbon) and T_{max} values (<415°C) indicate that the organic matter is thermally immature and relatively well preserved (Fig. [F33](#)). In addition, improved organic matter preservation is implied by C/N ratios that increase as organic carbon concentrations increase, suggesting that nitrogen-rich components were more readily degraded than other organic matter components during sinking of organic matter through a strongly developed oxygen-minimum



zone, elevating C/N ratios of surviving organic matter (cf. Twitchell et al., 2002).

The downhole TOC profile (Fig. F33) shows a sharp increase near the onset of black shale deposition followed by a trend of ever-decreasing amounts of TOC to near-zero levels toward the top of the bed. The TOC profile suggests that the environment of deposition in the black shale initially produced a high degree of preservation in the kerogen, but with time the degree of preservation decreased to the point at which little TOC was preserved and carbonate deposition once again became dominant (85 wt% carbonate at 230 mbsf; Figs. F13, F32).

Physical properties

Physical property measurements were made on whole-round sections, section halves, and discrete samples from section halves. Gamma ray attenuation (GRA) bulk density, magnetic susceptibility, *P*-wave velocity, and NGR measurements were made on the whole-round sections using the Whole-Round Multisensor Logger (WRMSL). Thermal conductivity measurements could not be performed at Site U1407 because of technical problems. Compressional wave velocity on section halves was also measured at a frequency of two in each section (at ~50 and 100 cm) using a *P*-wave caliper (PWC). For moisture and density (MAD) analyses, one discrete sample was collected in each section (typically at ~35 cm from the top of a section). The Section Half Multisensor Logger (SHMSL) was used to measure spectral reflectance and magnetic susceptibility on archive section halves.

Magnetic susceptibility

Overall, whole-round magnetic susceptibility ranges from -3 to 185 instrument units (IU) (Fig. F34). In lithostratigraphic Unit I, magnetic susceptibility displays high and variable values (30–185 IU) followed by an abrupt decrease at the boundary with Unit II. Throughout Units II–IV, the values become more uniform (5–30 IU). In Subunit Va (~120–175 mbsf), magnetic susceptibility values are low (-1–7 IU), but display a few distinct peaks >50 IU at 147 and 162 mbsf in Hole U1407A, at 140 and 164 mbsf in Hole U1407B, and at 143 and 166 mbsf in Hole U1407C. In the middle of Subunit Vb (~190–230 mbsf), magnetic susceptibility is relatively high (10–60 IU) and shows prominent and superimposed peaks. The interval of high magnetic susceptibility can be traced among all three holes (see “**Stratigraphic correlation**”). Magnetic susceptibility is low (1–5 IU) below 230 mbsf in Subunit Vb and Unit VI.

Density and porosity

Two methods were used to measure bulk density at Site U1407. The GRA density method provides an estimate from whole-round sections. The MAD method, applied to 144 discrete samples in Hole U1407A, provides an independent measure of bulk density as well as dry bulk density, grain density, water content, and porosity.

At Site U1407, bulk density ranges from 1.5 to 2.1 g/cm³ and, overall, gradually increases downhole. MAD bulk density is, in general, consistent with GRA bulk density (Fig. F34). The average offset between MAD and GRA bulk density is small (0.03 g/cm³), but a larger offset is seen in the lower intervals of lithostratigraphic Subunit Vb (250–270 mbsf in Hole U1407A), where the reduced diameter and fracturing of XCB cores affected the GRA density measurements. From the top of the holes at Site U1407 to the base of Unit I, density increases from ~1.5 to >1.8 g/cm³. Throughout Units II–IV, bulk density gradually increases again from 1.5 to 1.8 g/cm³. From the top of Unit V to 150 mbsf, density is lower than in Unit IV, which is likely related to the change in coring methods from APC to XCB. MAD bulk density in Unit V increases downhole from 1.5 to 2.1 g/cm³. At the bottom of Subunit Vb, bulk density is ~2.0 g/cm³.

Sediment water content at Site U1407 ranges from 5 to 19 wt%, and porosity varies from 39 to 74 vol%. Water content and porosity generally decrease downhole. In lithostratigraphic Unit I, both properties display low values (30–47 wt% and 55–70 vol%), which we interpret as an artifact of measuring foraminiferal sand with a method designed for saturated fine-grained sediment (see “**Physical properties**” in the “Methods” chapter [Norris et al., 2014b]); therefore, these values do not represent accurate measurements of water content and porosity. From Unit II to IV, water content and porosity gradually decrease downhole, falling from 45 to 30 wt% for water content and from 60 to 50 vol% for porosity. These trends are expected as a result of increased sediment compaction with depth. Water content and porosity are more variable in Unit V (19–48 wt% and 39–70 vol%, respectively).

Grain density ranges from 2.5 to 2.9 g/cm³ at Site U1407. Grain density decreases from 2.8 g/cm³ at the top of the sediment column to 2.6 g/cm³ at 100 mbsf. In the interval from 130 to 210 mbsf, grain density is more variable, ranging from 2.5 to 2.9 g/cm³. In sediment below 220 mbsf, grain density is relatively invariant and varies from 2.7 to 2.9 g/cm³.



P-wave velocity

P-wave velocity was measured using the *P*-wave logger (PWL) on all whole-round sections and using the PWC on undisturbed section halves from Holes U1407A–U1407C.

P-wave velocity varies from 1450 to 1670 m/s for PWL data and from 1480 to 3310 m/s for PWC data in all three holes. *P*-wave velocity measured with the PWL is slightly higher than that measured by the PWC in the APC-cored interval and slightly lower in the XCB-cored interval, with the offsets averaging ~20 m/s (Fig. F35). *P*-wave velocity exhibits a gradual increase toward the bottom of all three holes. In sediment below 120 mbsf, *P*-wave velocities both increase as a result of lithification and become more variable downhole (from 1650 to ~2000 m/s), possibly caused by the change from APC to XCB drilling. In the upper part of Subunit Vb, *P*-wave velocity data show abrupt increases at ~180 and 206 mbsf.

Natural gamma radiation

NGR was measured on whole-round sections in Holes U1407A–U1407C and ranges from 2 to 56 cps (Fig. F35). In lithostratigraphic Units I–III, NGR values average 20 cps, with prominent peaks in all three holes at ~9 mbsf (to ~50 cps; Unit I/II boundary) and at ~25 mbsf (> 30 cps) within Unit II. NGR values drop to 2 cps at the boundary between Units III and IV (82 mbsf in Hole U1407A, 85 mbsf in Hole U1407B, and 76 mbsf in Hole U1407C). The decrease in NGR counts at the Unit III/IV boundary corresponds to a large increase in carbonate content. From Unit IV to V, NGR displays low values (2–5 cps), with notable peaks of >20 cps. In Subunit Va, NGR data show a peak at ~140 mbsf that occurs only in Holes U1407B and U1407C. Other prominent events were observed lower in all three holes: at the Subunit Va/Vb boundary (~175 mbsf) and at 200, 232 (>50 cps), and 238 mbsf. These last three peaks correspond to the black shale associated with OAE 2 (see “[Lithostratigraphy](#)” and “[Geochemistry](#)”).

Color reflectance

Reflectance values were measured on archive section halves in all three holes. For Hole U1407C, the resolution of measurements decreased from 2.5 to 5.0 cm to speed up core processing. Changes in color reflectance a^* and b^* are consistent among all three holes except for an interval of poor data quality between 130 and 210 mbsf in Hole U1407A caused by a technical problem with the SHMSL (Fig. F36). For all three holes, a^* and b^* range from -3 to 21 and -25 to 29, respectively.

Both a^* and b^* decrease from ~10 to ~5 from the top of the sediment column to ~40 mbsf. In lithostratigraphic Unit III, a^* and b^* display high values at the top of the unit and then decrease to near-zero values at ~42 mbsf. This decrease in Unit III is caused by a change in sediment color from light brown to greenish (see “[Lithostratigraphy](#)”). Reflectance parameter a^* increases through Unit IV. In Subunit Va, both a^* and b^* have high values, ranging from 4 to 11. Both reflectance parameters decrease between ~170 and ~180 mbsf in Hole U1407B and U1407C and between 230 and 240 mbsf in all three holes. These fluctuations correspond to alternations of light and dark brown sediment. Correlative minima in the a^* records are observed at ~230 mbsf in Hole U1407B (-3.5) and in Hole U1407C (-4.8); this interval corresponds to the greenish white chalk layer just above the black shale of OAE 2 (see “[Lithostratigraphy](#)”).

Color parameter L^* exhibits the same trends in all three holes, and values range from 13 to 95. From the top of the sediment column to the upper part of lithostratigraphic Unit III, L^* increases from ~50 to ~75. At the top of Unit IV, L^* increases sharply from 75 to 90, corresponding to a downhole transition to white sediment and a notable increase in carbonate content (see “[Lithostratigraphy](#)” and “[Geochemistry](#)”). In Subunits Va and Vb, L^* averages ~75, whereas in the interval from 180 to 200 mbsf, L^* shows substantial fluctuations and a peak to ~90 at 190 mbsf in Holes U1407A and U1407B and at 185 mbsf in Hole U1407C. A minimum was observed at ~232 mbsf in all three holes; this interval is associated with the black shale of OAE 2.

The sharp, high-amplitude expression of the Unit III/IV boundary in color reflectance as well as in NGR and other high-amplitude correlative features in Unit Vb lead us to speculate that an error occurred on the rig floor with the pipe tally. Most likely, at the time the 7.7–10.7 mbsf interval was drilled without coring in Hole U1407C, a 9.5 m pipe was added but not accounted for (a human error possible because no core was taken), leading to sample depth registrations that are too shallow by that amount between 10.7 and 96.0 mbsf. After another interval was drilled without coring from 96 to 117 mbsf, the error apparently corrected itself.

Stratigraphic correlation

Sampling splice

We constructed a splice for Site U1407 that is stratigraphically continuous from ~28 to ~116 m core composite depth below seafloor (CCSF) and from



~156 to 317 m CCSF (Fig. F37). A thick unrecovered interval from ~116 to 137 m CCSF is associated with a drilling advance through unrecoverable chert. Large differences in the thickness of distinctive lithostratigraphic units in the lower portion of the sediment column complicate the choice of tie points from ~156 to 317 m CCSF, where it is impossible to align all distinctive features in physical property records. We based our correlation and splice construction primarily on NGR and magnetic susceptibility measured on whole-round sections. Line-scan core images of section halves were particularly useful for correlation from ~260 to 312 m CCSF. Our correlation yields a growth rate of 17% for Holes U1407A and U1407B and 18% for Hole U1407C (Fig. F38), which represents the average increase of the CCSF depth scale relative to each hole's mbsf depth scale. We interpret these large growth rates to be a function of thickness variations in stratigraphy across the site at the base of the sediment column (~156–317 m CCSF), which require the application of relatively large differential offsets. The affine table (Table T21) summarizes the individual offsets for each core drilled.

Correlation during drilling operations

To aid real-time correlation at Site U1407, we assessed magnetic susceptibility and GRA bulk density data collected at 2.5 cm resolution on the Special Task Multisensor Logger before allowing cores to equilibrate to room temperature. Distinct changes in lithology and physical properties aided real-time correlation in the upper ~91 m CCSF of the drilled sediment column at Site U1407. As a result, we were able to offset our coring gaps in this interval. In particular, three step changes in magnetic susceptibility associated with color changes provided reliable ties between the three holes. These occur at the transition from the Pleistocene in lithostratigraphic Unit I to the Oligocene in Unit II at ~8 m CCSF (Fig. F39), the color change from tan to green in Unit III at ~46 m CCSF, and the color change from green to white at the boundary between Units III and IV at ~94 m CCSF. The tan to green color transition occurs at similar mbsf depths in all three holes. In contrast, the distinct green-to-white color change occurs ~10 m shallower in mbsf depth in Hole U1407C compared to Holes U1407A and U1407B. Based on correlation using physical property data between the two ties provided by the color changes, it appears that there is a gap approximately equal to the length of one core between Cores 342-U1407C-6H and 7H. No obvious justification is evident for such a large lateral discontinuity in the sediment column penetrated at Hole U1407C compared to Holes U1407A and

U1407B, so we consider an unrecorded drilling advance the most likely explanation for the large mbsf depth difference in Hole U1407C.

After a partial stroke for Core 342-U1407A-12H (~116 m CCSF), Cores 13H and 14H had zero recovery and Core 15H was a 0.1 m advance. As a result, drilling operations switched to XCB coring for Core 16X. In general, recovery in the XCB interval of Hole U1407A was poor, with a low recovery of 14% for Core 17X and only Core 20X achieving 100% nominal recovery.

As a result of poor recovery, the strategy for Holes U1407B and U1407C was to advance without recovery through the chert interval from ~112 to ~136 m CCSF. In Holes U1407B and U1407C, we directed drilling operations to advance without recovery until the drillers detected that they had broken through the chert-rich interval. In Hole U1407C, we began successfully recovering XCB cores at a shallower depth, corresponding to Core 342-U1407A-16H. XCB coring yielded better recovery in Holes U1407B and U1407C compared to Hole U1407A; many cores had >100% nominal recovery.

Hole U1407A spans the thickest sediment column recovered at this site, with a maximum depth for the bottom of Core 342-U1407A-35X of 308.7 mbsf (355.7 m CCSF). However, Cores 32X through 35X, corresponding to the interval below ~317 m CCSF, all had <2% recovery. The recovered material indicated drilling had reached Albian reef deposits. For this reason, drilling of Holes U1407B and U1407C ended at 276.3 mbsf (323.01 m CCSF) and 261.6 mbsf (309.69 m CCSF), respectively.

Correlation and splice construction

For stratigraphic correlation and splice construction, we used NGR and magnetic susceptibility data. These two data series showed clear, correlatable features throughout the sediment column (see “Physical properties”). NGR was the most useful data set for correlation from 0 to ~116 m CCSF, and magnetic susceptibility was most useful from ~137 to 200 m CCSF. Both data series showed distinctive features from ~200 to 317 m CCSF (Figs. F37, F40). We also considered additional data to ensure that there were no large discrepancies between data sets, including GRA bulk density collected on the whole-round sections after cores equilibrated to room temperature and color reflectance (see “Physical properties”). From ~200 to 312 m CCSF, line-scan core images of section halves aided interpretation of the physical property data. Our correlation is consistent with both biostratigraphic and paleomagnetism results (see “Biostratigraphy” and “Paleomagnetism”).



We defined Core 342-U1407A-1H as the anchor in our splice, though there was a clear agreement between the mudline cores recovered in Holes U1407A and U1407B. As a result of the large degree of overlap between Cores 342-U1407A-2H, 342-U1407B-2H, and 342-U1407C-3H and between Cores 342-U1407A-3H, 342-U1407B-3H, and 342-U1407C-4H, Cores 342-U1407C-4H and 342-U1407A-4H are appended. In the upper ~30 m, a number of tentative offsets are associated with these appended cores. We applied a very large offset (12.39 m) to Core 342-U1407C-7H because this core follows the hypothesized unrecorded advance between Cores 6H and 7H. Consistent with this large offset, Cores 342-U1407A-6H and 342-U1407B-7H both contain a distinctive, sawtooth-shaped peak in magnetic susceptibility that does not appear in any of the cores in Hole U1407C (Fig. F37B). We also evaluated line-scan core images, which support our correlation of Core 342-U1407C-7H with 342-U1407A-7H and 8H and 342-U1407B-8H. This offset also aligns the green-to-white color change associated with the boundary between lithostratigraphic Units III and IV between the three holes. Finally, paleomagnetism chron identifications also show a large, ~10 m discrepancy in Hole U1407C at ~75 mbsf compared to Holes U1407A and U1407B (Table T20).

We applied another very large offset (14.98 m) to Core 342-U1407B-13X, the first recovered core in Hole U1407B following the drilled advance through the chert layer. The top of Core 13X belongs to nanofossil Subzone NP9a and the core catcher to Zone NP8, whereas the first cores below the chert-rich interval in Holes U1407A and U1407C are entirely within Zone NP9. Cores 342-U1407A-18X, 342-U1407B-13X, and 342-U1407C-15X all show distinctive magnetic susceptibility peaks. Another reliable tie occurs between Cores 342-U1407B-14X and 342-U1407C-16X associated with a prominent NGR peak. We interpret the large offset for Core 342-U1407B-13X as indicative of differences in the thickness of the chert interval between the holes. Lithostratigraphic Unit IV, which terminates at the top of the chert (defined operationally by the first partial APC stroke), was ~8 m thinner in Hole U1407B compared to Holes U1407A and U1407C, indicating variations in the top depth of the chert between holes, as well.

Below ~190 m CCSF, splice construction was more difficult than in the upper sediment column above the chert-rich interval because of clear variations in stratigraphic thickness of similar units in the different holes. The first example occurs in Cores 342-

U1407A-24X, 342-U1407B-20X, and 342-U1407C-21X and 22X, in which it is impossible to align all features in both NGR and magnetic susceptibility without large overlaps between successive cores at the same hole and/or squeezing and stretching of individual cores. Our correlation represents a compromise between these two data sets, but we cannot align all distinctive features.

A second example of variations in the thickness of similar stratigraphic units between holes is associated with the interval recording OAE 2 from ~265 to 275 m CCSF. In Cores 342-U1407A-28X, 342-U1407B-24X, and 342-U1407C-26X, the thickest black shale corresponds to a prominent NGR peak. Using this NGR peak as a correlation tie point means that it is impossible to align features in either NGR or magnetic susceptibility below the peak from ~270 to 275 m CCSF. These differences in physical properties between the three holes are also obvious in a bed-by-bed comparison of the lithostratigraphy (Fig. F13). Next, from the black shale to the bottom of the recovered sediment column in each hole, a series of distinctive color changes of varying thickness exists between holes. In this interval, from ~275 to 317 m CCSF, we used line-scan core images of section halves to interpret the possible overlap among cores from each hole. For instance, we applied a large offset (10.43 m) to the top of Core 342-U1407C-28X based on the very different colors of sediment between Cores 342-U1407B-25X (whitish gray to grayish pink) and 342-U1407C-28X (tan). Similarly, we do not allow a greater overlap between Core 342-U1407A-29X and 342-U1407B-25X because Core 342-U1407A-29X is grayish pink to tan, with none of the overlying whitish gray sediment present in Core 342-U1407B-25X. We suggest that these large offsets do not imply large coring gaps; rather, they are indicative of the varying thickness of sedimentary units in the infill over the Albian reefal sediment below the sediment column recovered at Site U1407.

The Site U1407 splice can be used as a sampling guide, but we suggest using caution when using the splice for sampling below ~225 m CCSF, where clear variations in the stratigraphy exist between the three holes. In the splice table (Table T22), we labeled tie points as tentative if they occur near the top or bottom ~50 cm of a core and/or are not associated with a prominent feature in physical properties. We recommend overlapping splice intervals at the tie points by a few decimeters (or more, where splice ties are labeled as tentative) to accommodate anticipated development of the depth scale.



References

- Arthur, M.A., 1979. Origin of Upper Cretaceous multicolored claystones of the Western Atlantic. In Tucholke, B.E., Vogt, P.R., et al., *Init. Repts. DSDP*, 43: Washington, DC (U.S. Govt. Printing Office), 417–420. doi:[10.2973/dsdp.proc.43.111.1979](https://doi.org/10.2973/dsdp.proc.43.111.1979)
- Arthur, M.A., and Premoli-Silva, I., 1982. Development of widespread organic carbon-rich strata in the Mediterranean Tethys. In Schlanger, S.O., and Cita, M.B. (Eds.), *Nature and Origin of Cretaceous Carbon-Rich Facies*: London (Academic Press), 7–54.
- Folk, R.L., 1959. Practical petrographical classification of limestones. *AAPG Bull.*, 43(1):1–38. <http://aapg-bull.geoscienceworld.org/content/43/1/1.abstract>
- Friedrich, O., 2010. Benthic foraminifera and their role to decipher paleoenvironment during mid-Cretaceous oceanic anoxic events—the “anoxic benthic foraminifera” paradox. *Rev. Micropaleontol.*, 53(3):175–192. doi:[10.1016/j.revmic.2009.06.001](https://doi.org/10.1016/j.revmic.2009.06.001)
- Gieskes, J.M., 1981. Deep-sea drilling interstitial water studies: implications for chemical alteration of the oceanic crust, Layers I and II. In Warme, J.E., Douglas, R.G., and Winterer, E.L. (Eds.), *The Deep Sea Drilling Project: A Decade of Progress*. Spec. Publ.—Soc. Econ. Paleontol. Mineral., 32:149–167. http://archives.datapages.com/data/sepm_sp/SP32/Deep_Sea_Drilling_Interstitial_Water_Studies.html
- Gieskes, J.M., and Lawrence, J.R., 1981. Alteration of volcanic matter in deep-sea sediments: evidence from the chemical composition of interstitial waters from deep sea drilling cores. *Geochim. Cosmochim. Acta*, 45(10):1687–1703. doi:[10.1016/0016-7037\(81\)90004-1](https://doi.org/10.1016/0016-7037(81)90004-1)
- Gradstein, F.M., Ogg, J.G., Schmitz, M.D., and Ogg, G.M. (Eds.), 2012. *The Geological Time Scale 2012*: Amsterdam (Elsevier).
- Holbourn, A., and Kuhnt, W., 2002. Cenomanian-Turonian paleoceanographic change on the Kerguelen Plateau: a comparison with Northern Hemisphere records. *Cretaceous Res.*, 23(3):333–349. doi:[10.1006/cres.2002.1008](https://doi.org/10.1006/cres.2002.1008)
- Jenkyns, H.C., 2010. Geochemistry of oceanic anoxic events. *Geochem., Geophys., Geosyst.*, 11(3):Q03004. doi:[10.1029/2009GC002788](https://doi.org/10.1029/2009GC002788)
- Kirschvink, J.L., 1980. The least-squares line and plane and the analysis of palaeomagnetic data. *Geophys. J. R. Astron. Soc.*, 62(3):699–718. doi:[10.1111/j.1365-246X.1980.tb02601.x](https://doi.org/10.1111/j.1365-246X.1980.tb02601.x)
- Lyle, M., Wilson, P.A., Janecek, T.R., et al., 2002. *Proc. ODP Init. Repts.*, 199: College Station, TX (Ocean Drilling Program). doi:[10.2973/odp.proc.ir.199.2002](https://doi.org/10.2973/odp.proc.ir.199.2002)
- Nishimura, A., 1992. Paleocene radiolarian biostratigraphy in the northwest Atlantic at Site 384, Leg 43, of the Deep Sea Drilling Project. *Micropaleontology*, 38(4):317–362. doi:[10.2307/1485764](https://doi.org/10.2307/1485764)
- Norris, R.D., Wilson, P.A., Blum, P., Fehr, A., Agnini, C., Bornemann, A., Boulila, S., Bown, P.R., Cournede, C., Friedrich, O., Ghosh, A.K., Hollis, C.J., Hull, P.M., Jo, K., Junium, C.K., Kaneko, M., Liebrand, D., Lippert, P.C., Liu, Z., Matsui, H., Moriya, K., Nishi, H., Opdyke, B.N., Penman, D., Romans, B., Scher, H.D., Sexton, P., Takagi, H., Turner, S.K., Whiteside, J.H., Yamaguchi, T., and Yamamoto, Y., 2014a. Expedition 342 summary. In Norris, R.D., Wilson, P.A., Blum, P., and the Expedition 342 Scientists, *Proc. IODP*, 342: College Station, TX (Integrated Ocean Drilling Program). doi:[10.2204/iodp.proc.342.101.2014](https://doi.org/10.2204/iodp.proc.342.101.2014)
- Norris, R.D., Wilson, P.A., Blum, P., Fehr, A., Agnini, C., Bornemann, A., Boulila, S., Bown, P.R., Cournede, C., Friedrich, O., Ghosh, A.K., Hollis, C.J., Hull, P.M., Jo, K., Junium, C.K., Kaneko, M., Liebrand, D., Lippert, P.C., Liu, Z., Matsui, H., Moriya, K., Nishi, H., Opdyke, B.N., Penman, D., Romans, B., Scher, H.D., Sexton, P., Takagi, H., Turner, S.K., Whiteside, J.H., Yamaguchi, T., and Yamamoto, Y., 2014b. Methods. In Norris, R.D., Wilson, P.A., Blum, P., and the Expedition 342 Scientists, *Proc. IODP*, 342: College Station, TX (Integrated Ocean Drilling Program). doi:[10.2204/iodp.proc.342.102.2014](https://doi.org/10.2204/iodp.proc.342.102.2014)
- Norris, R.D., Wilson, P.A., Blum, P., Fehr, A., Agnini, C., Bornemann, A., Boulila, S., Bown, P.R., Cournede, C., Friedrich, O., Ghosh, A.K., Hollis, C.J., Hull, P.M., Jo, K., Junium, C.K., Kaneko, M., Liebrand, D., Lippert, P.C., Liu, Z., Matsui, H., Moriya, K., Nishi, H., Opdyke, B.N., Penman, D., Romans, B., Scher, H.D., Sexton, P., Takagi, H., Turner, S.K., Whiteside, J.H., Yamaguchi, T., and Yamamoto, Y., 2014c. Site U1403. In Norris, R.D., Wilson, P.A., Blum, P., and the Expedition 342 Scientists, *Proc. IODP*, 342: College Station, TX (Integrated Ocean Drilling Program). doi:[10.2204/iodp.proc.342.104.2014](https://doi.org/10.2204/iodp.proc.342.104.2014)
- Norris, R.D., Wilson, P.A., Blum, P., Fehr, A., Agnini, C., Bornemann, A., Boulila, S., Bown, P.R., Cournede, C., Friedrich, O., Ghosh, A.K., Hollis, C.J., Hull, P.M., Jo, K., Junium, C.K., Kaneko, M., Liebrand, D., Lippert, P.C., Liu, Z., Matsui, H., Moriya, K., Nishi, H., Opdyke, B.N., Penman, D., Romans, B., Scher, H.D., Sexton, P., Takagi, H., Turner, S.K., Whiteside, J.H., Yamaguchi, T., and Yamamoto, Y., 2014d. Site U1404. In Norris, R.D., Wilson, P.A., Blum, P., and the Expedition 342 Scientists, *Proc. IODP*, 342: College Station, TX (Integrated Ocean Drilling Program). doi:[10.2204/iodp.proc.342.105.2014](https://doi.org/10.2204/iodp.proc.342.105.2014)
- Norris, R.D., Wilson, P.A., Blum, P., Fehr, A., Agnini, C., Bornemann, A., Boulila, S., Bown, P.R., Cournede, C., Friedrich, O., Ghosh, A.K., Hollis, C.J., Hull, P.M., Jo, K., Junium, C.K., Kaneko, M., Liebrand, D., Lippert, P.C., Liu, Z., Matsui, H., Moriya, K., Nishi, H., Opdyke, B.N., Penman, D., Romans, B., Scher, H.D., Sexton, P., Takagi, H., Turner, S.K., Whiteside, J.H., Yamaguchi, T., and Yamamoto, Y., 2014e Site U1405. In Norris, R.D., Wilson, P.A., Blum, P., and the Expedition 342 Scientists, *Proc. IODP*, 342: College Station, TX (Integrated Ocean Drilling Program). doi:[10.2204/iodp.proc.342.106.2014](https://doi.org/10.2204/iodp.proc.342.106.2014)
- Norris, R.D., Wilson, P.A., Blum, P., Fehr, A., Agnini, C., Bornemann, A., Boulila, S., Bown, P.R., Cournede, C., Friedrich, O., Ghosh, A.K., Hollis, C.J., Hull, P.M., Jo, K., Junium, C.K., Kaneko, M., Liebrand, D., Lippert, P.C., Liu, Z., Matsui, H., Moriya, K., Nishi, H., Opdyke, B.N.,

- Penman, D., Romans, B., Scher, H.D., Sexton, P., Takagi, H., Turner, S.K., Whiteside, J.H., Yamaguchi, T., and Yamamoto, Y., 2014f. Site U1406. In Norris, R.D., Wilson, P.A., Blum, P., and the Expedition 342 Scientists, *Proc. IODP*, 342: College Station, TX (Integrated Ocean Drilling Program). doi:[10.2204/iodp.proc.342.107.2014](https://doi.org/10.2204/iodp.proc.342.107.2014)
- Pälike, H., Lyle, M.W., Nishi, H., Raffi, I., Ridgwell, A., Gamage, K., Klaus, A., Acton, G., Anderson, L., Backman, J., Baldauf, J., Beltran, C., Bohaty, S.M., Bown, P., Busch, W., Channell, J.E.T., Chun, C.O.J., Delaney, M., Dewangan, P., Dunkley Jones, T., Edgar, K.M., Evans, H., Fitch, P., Foster, G.L., Gussone, N., Hasegawa, H., Hathorne, E.C., Hayashi, H., Herrle, J.O., Holbourn, A., Hovan, S., Hyeong, K., Iijima, K., Ito, T., Kamikuri, S., Kimoto, K., Kuroda, J., Leon-Rodriguez, L., Malinverno, A., Moore, T.C., Jr., Murphy, B.H., Murphy, D.P., Nakamura, H., Ogane, K., Ohneiser, C., Richter, C., Robinson, R., Rohling, E.J., Romero, O., Sawada, K., Scher, H., Schneider, L., Sluijs, A., Takata, H., Tian, J., Tsujimoto, A., Wade, B.S., Westerhold, T., Wilkens, R., Williams, T., Wilson, P.A., Yamamoto, Y., Yamamoto, S., Yamazaki, T., and Zeebe, R.E., 2012. A Cenozoic record of the equatorial Pacific carbonate compensation depth. *Nature (London, U. K.)*, 488(7409):609–614. doi:[10.1038/nature11360](https://doi.org/10.1038/nature11360)
- Sageman, B.B., Meyers, S.R., and Arthur, M.A., 2006. Orbital time scale and new C isotope record for Ceno-
- manian/Turonian boundary stratotype. *Geology*, 34(2):125–128. doi:[10.1130/G22074.1](https://doi.org/10.1130/G22074.1)
- Sanfilippo, A., and Blome, C.D., 2001. Biostratigraphic implications of mid-latitude Paleocene–Eocene radiolarian faunas from Hole 1051A, ODP Leg 171B, Blake Nose, western North Atlantic. In Kroon, D., Norris, R.D., and Klaus, A. (Eds.), *Western North Atlantic Palaeogene and Cretaceous Palaeoceanography*. Geol. Soc. Spec. Publ., 183(1):185–224. doi:[10.1144/GSL.SP.2001.183.01.10](https://doi.org/10.1144/GSL.SP.2001.183.01.10)
- Tucholke, B.E., and Vogt, P.R., 1979. Western North Atlantic: sedimentary evolution and aspects of tectonic history. In Tucholke, B.E., Vogt, P.R., et al., *Init. Repts. DSDP*, 43: Washington, DC (U.S. Govt. Printing Office), 791–825. doi:[10.2973/dsdp.proc.43.140.1979](https://doi.org/10.2973/dsdp.proc.43.140.1979)
- Twichell, S.C., Meyers, P.A., and Diester-Haass, L., 2002. Significance of high C/N ratios in organic-carbon-rich Neogene sediments under the Benguela Current upwelling system. *Org. Geochem.*, 33(7):715–722. doi:[10.1016/S0146-6380\(02\)00042-6](https://doi.org/10.1016/S0146-6380(02)00042-6)
- von Breymann, M.T., Collier, R., and Suess, E., 1990. Magnesium adsorption and ion exchange in marine sediments: a multicomponent model. *Geochim. Cosmochim. Acta*, 54(12):3295–3313. doi:[10.1016/0016-7037\(90\)90286-T](https://doi.org/10.1016/0016-7037(90)90286-T)

Publication: 3 March 2014
MS 342-108



Figure F1. Bathymetric map of northwestern Southeast Newfoundland Ridge, northeast of J-Anomaly Ridge, Expedition 342. Data are based on multibeam mapping by the KNR179-1 site survey. Track lines, shotpoints, and line numbers are indicated for the single-channel seismic reflection profiles in Figures F2 and F3.

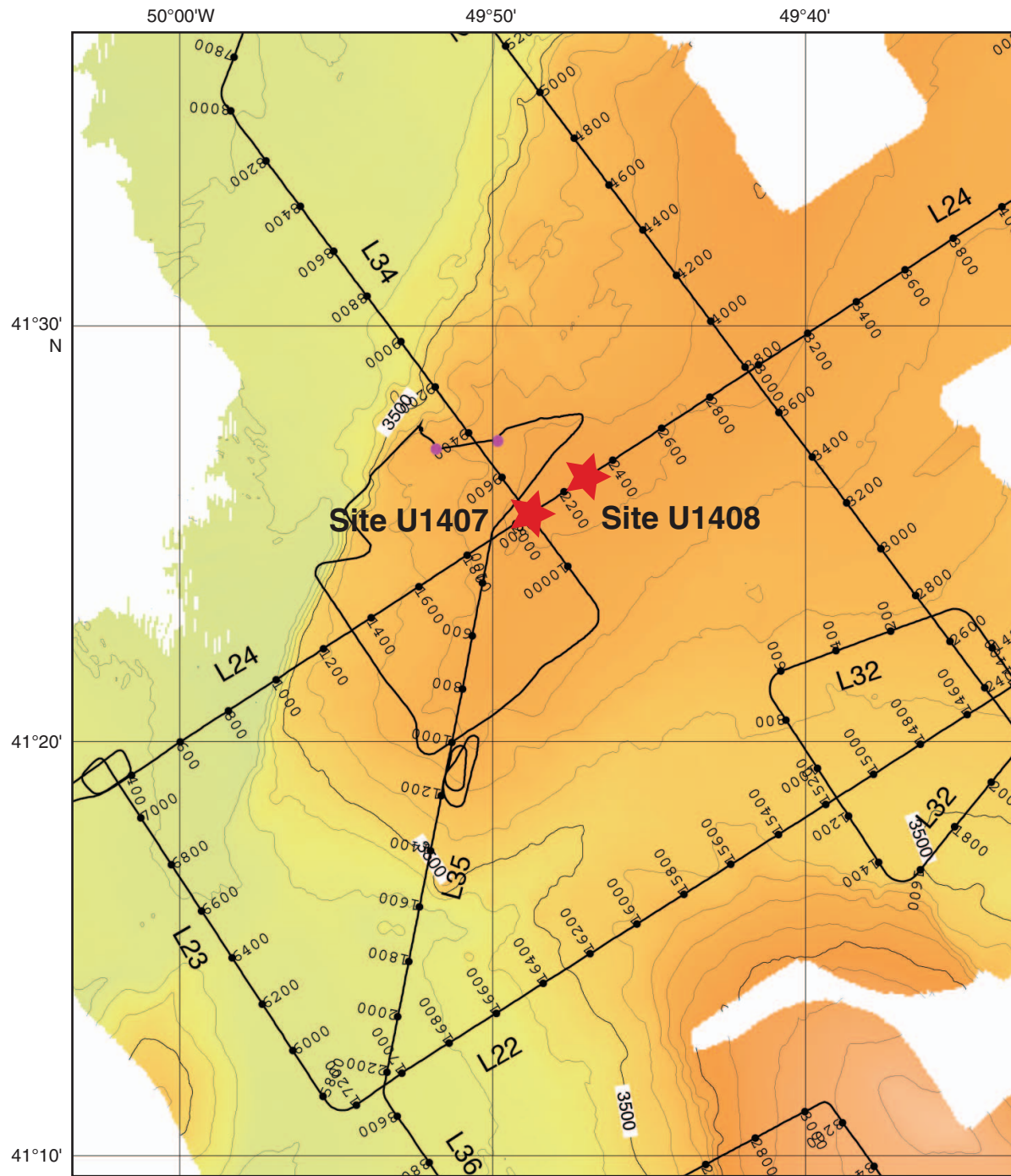


Figure F2. Single-channel seismic KNR179-1 Line 24. This is the southwest–northeast line crossing Site U1407 (at shotpoint [SP] 2060). White bars represent approximate depths of penetration for Sites U1407 and U1408.

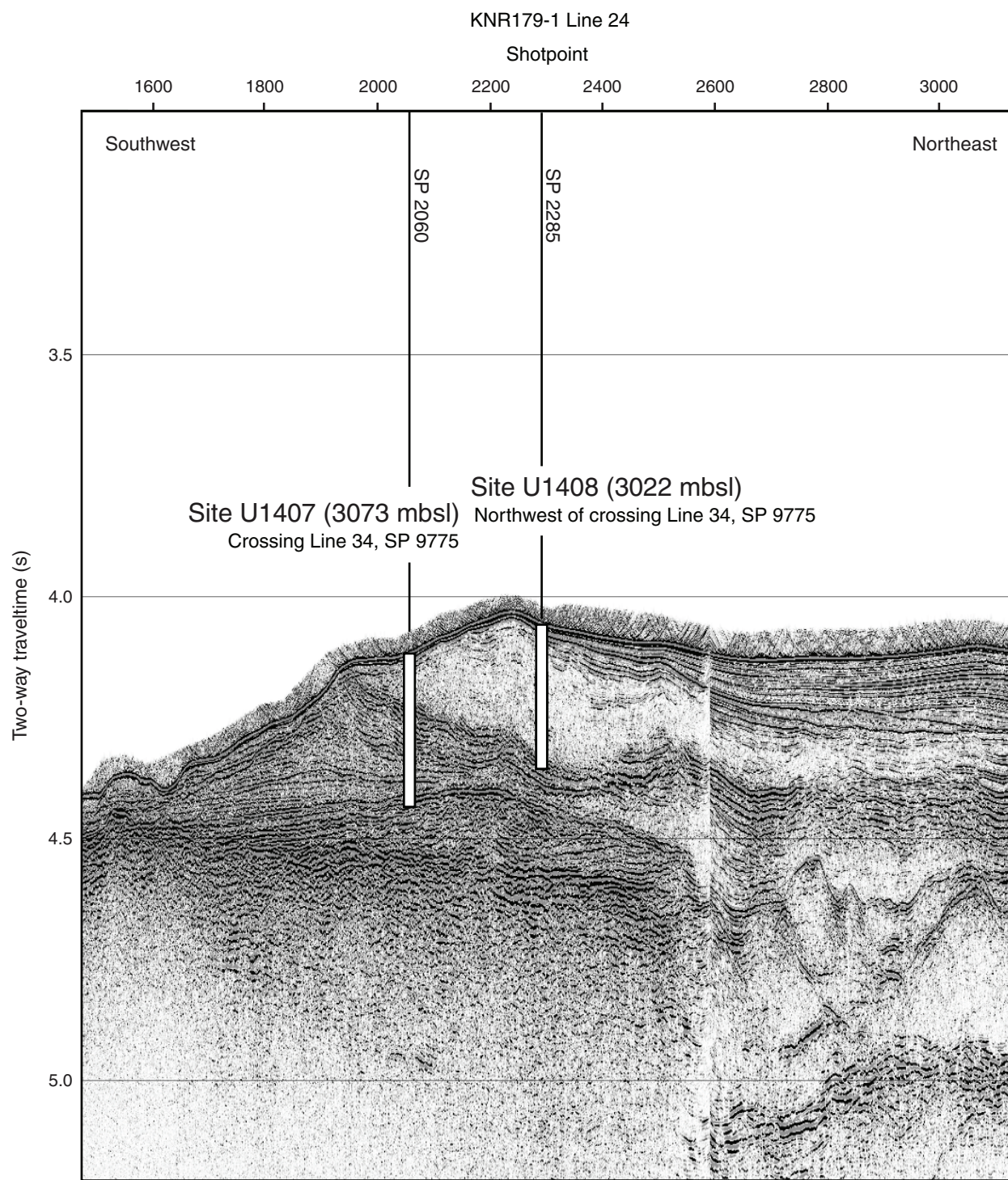


Figure F3. Single-channel seismic KNR179-1 Line 34. This is the northwest–southeast line crossing Site U1407 (at shotpoint [SP] 9775).

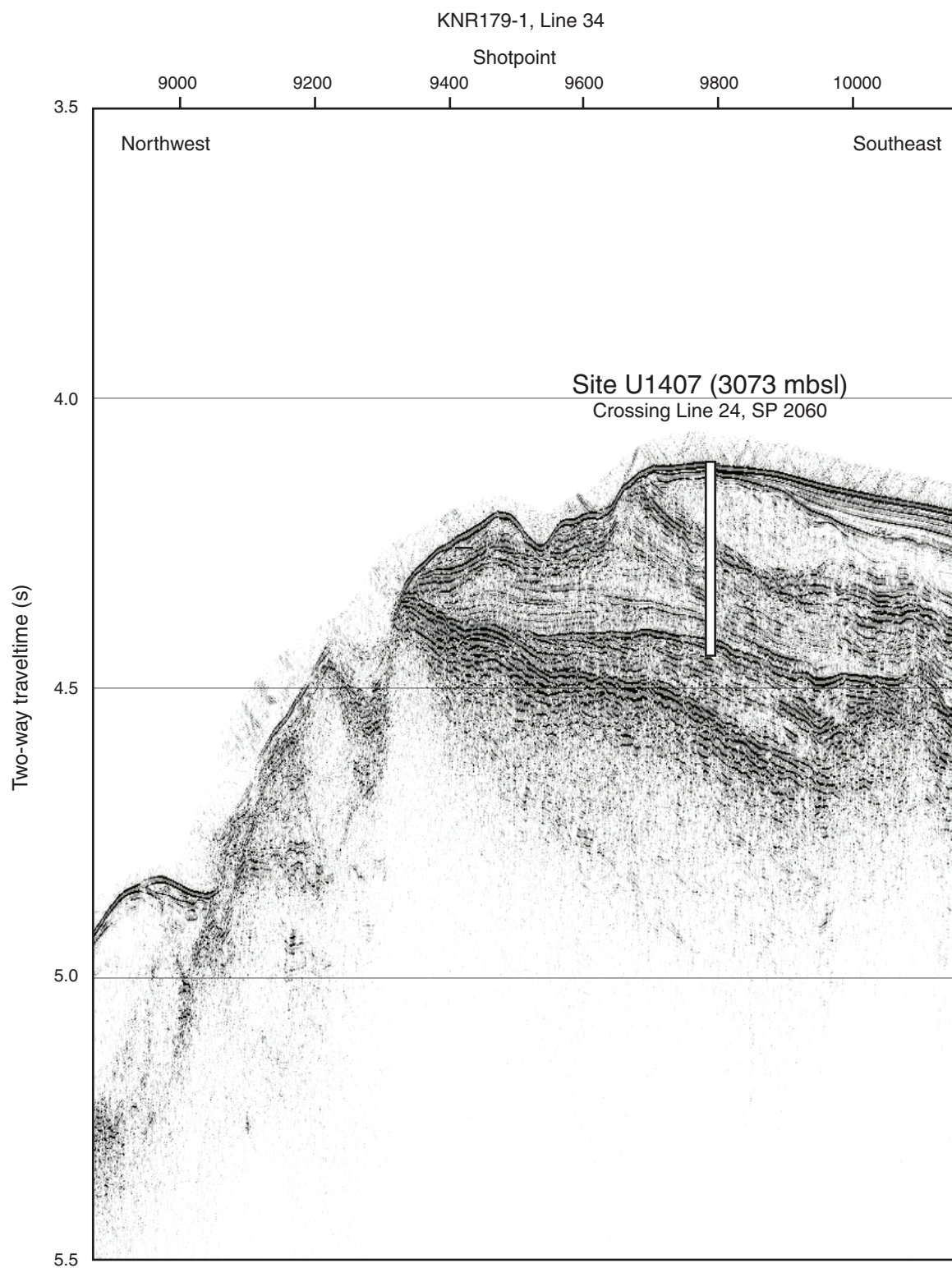


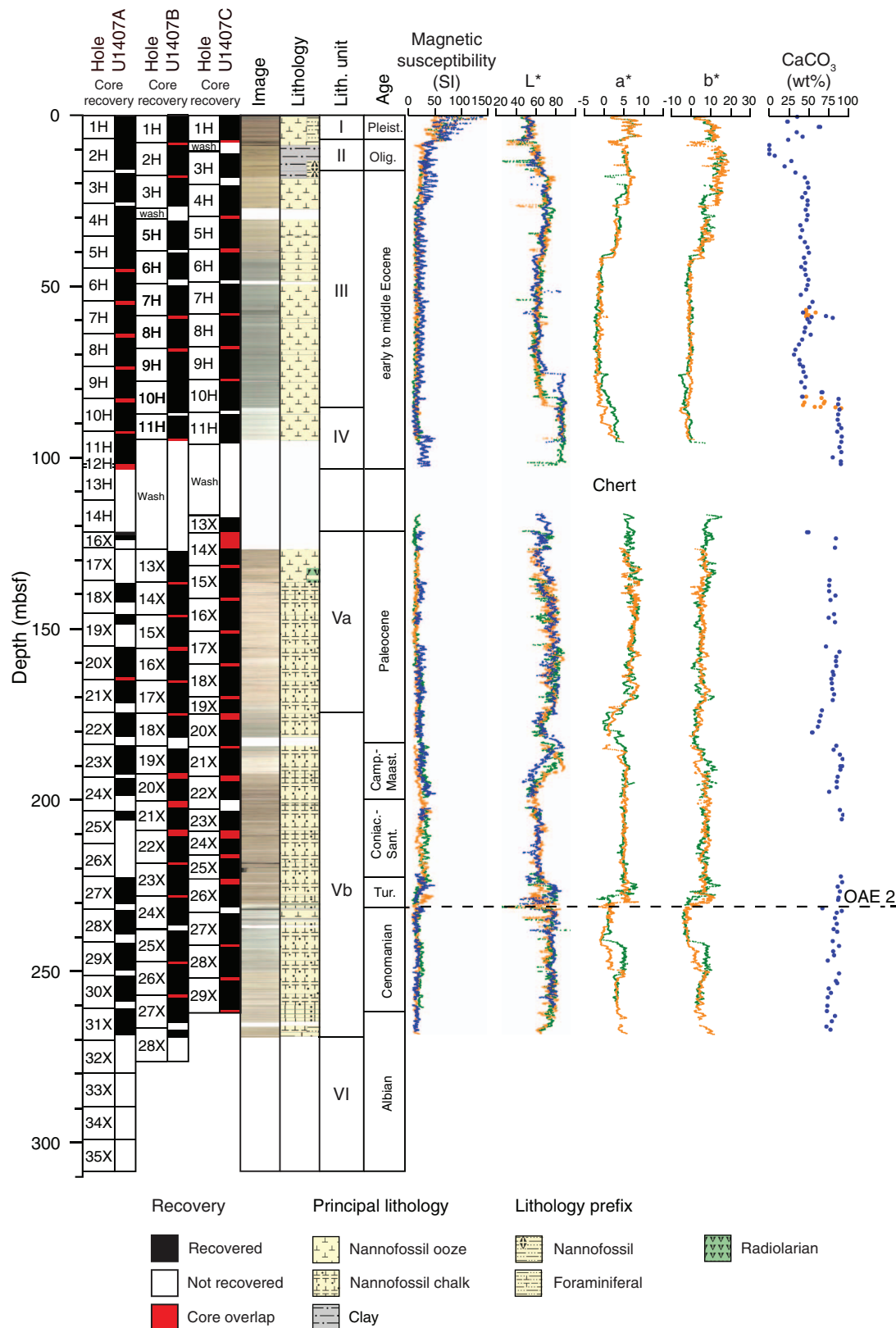
Figure F4. Lithostratigraphic summary, Site U1407. OAE 2 = Oceanic Anoxic Event 2.

Figure F5. Line-scan images of most common lithologies, Site U1407. A. Pleistocene foraminiferal sand within foraminiferal nannofossil ooze, Unit I. B. Early Oligocene clay with nannofossils, Unit II. C. Middle Eocene nannofossil ooze with foraminifers, Unit III. D. Early middle Eocene nannofossil ooze with foraminifers and radiolarians, Unit IV. E. Paleocene nannofossil chalk with foraminifers and radiolarians, Subunit Va. F. Cenomanian to Campanian nannofossil chalk with foraminifers, Subunit Vb. G. Late Albian fine-sized sandstone with horizontal laminations, Unit VI. H. Coral reef, Unit VI.

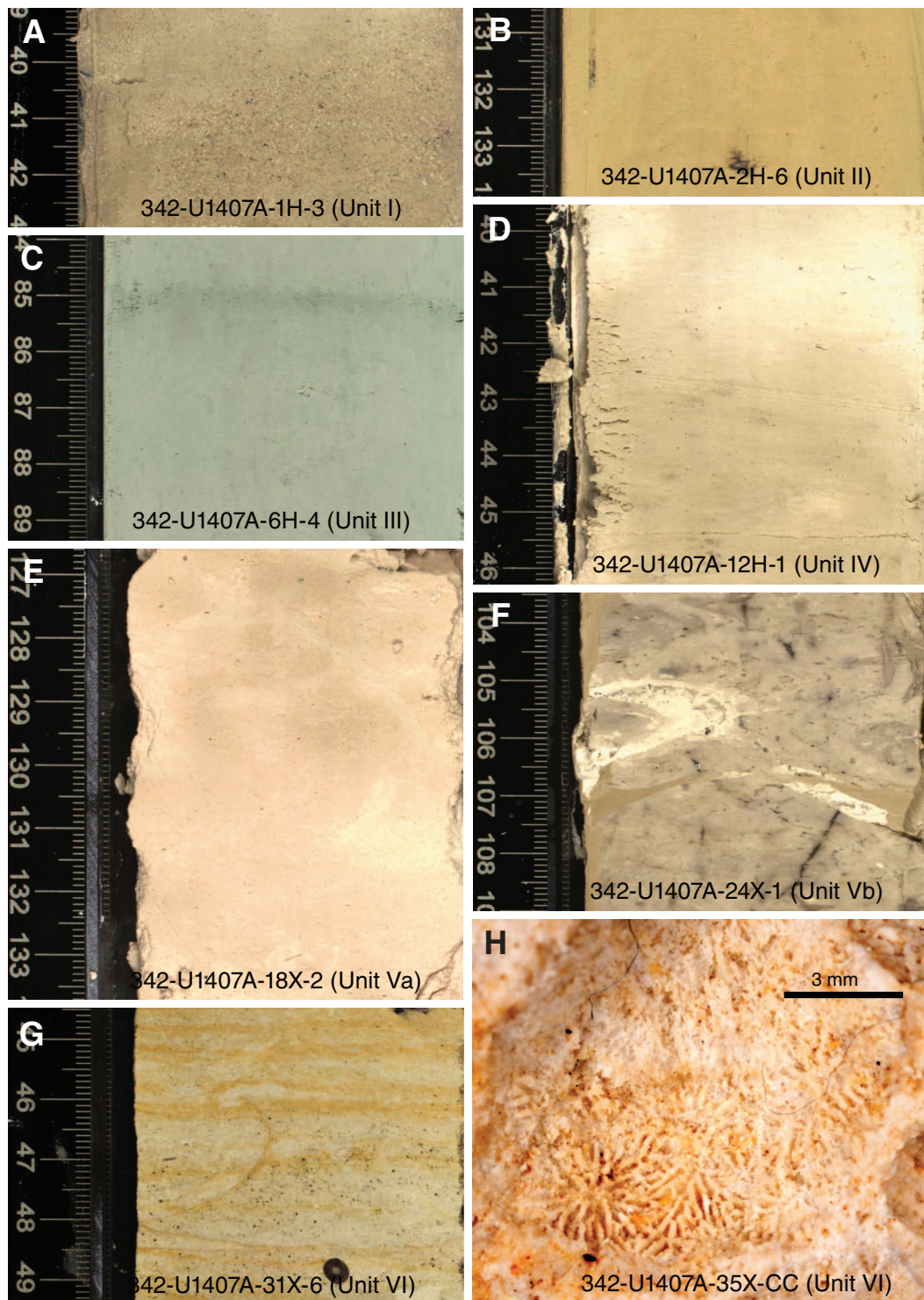


Figure F6. Photomicrographs of smear slides indicating the dominant lithologies of lithostratigraphic Units I–IV, Site U1407. A. Foraminiferal nannofossil ooze, Unit I. B. Clay with nannofossils, Unit II. C. Nannofossil ooze with foraminifers, Unit III. D. Nannofossil ooze with foraminifers, Unit IV.

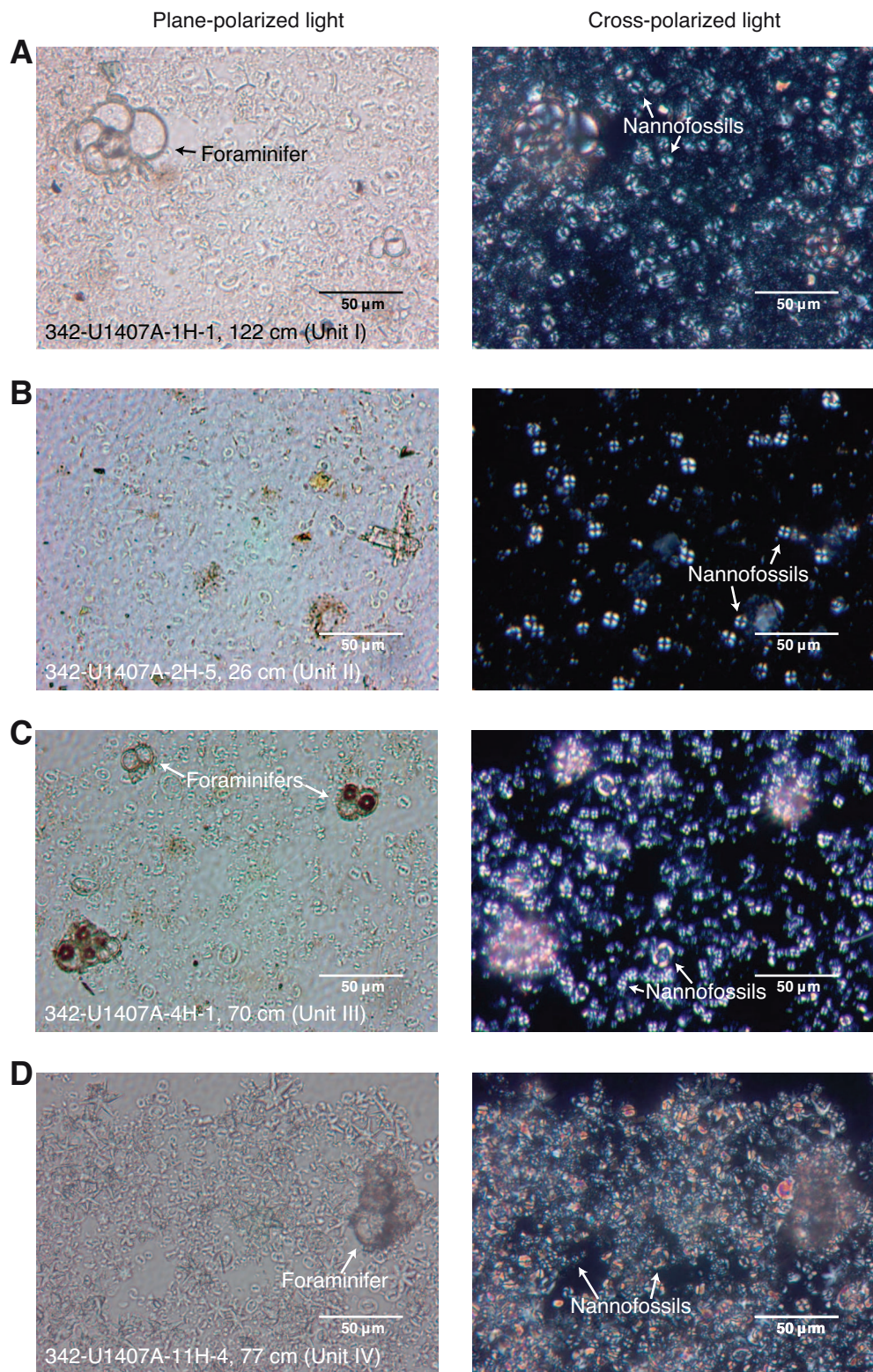


Figure F7. Photomicrographs of smear slides indicating the dominant lithologies of Unit V, Site U1407. A. Nannofossil chalk with radiolarians, Subunit Va. B. Nannofossil chalk with zeolites, Subunit Va. C. Nannofossil chalk, Subunit Vb. D. Zeolitic clay, Subunit Vb.

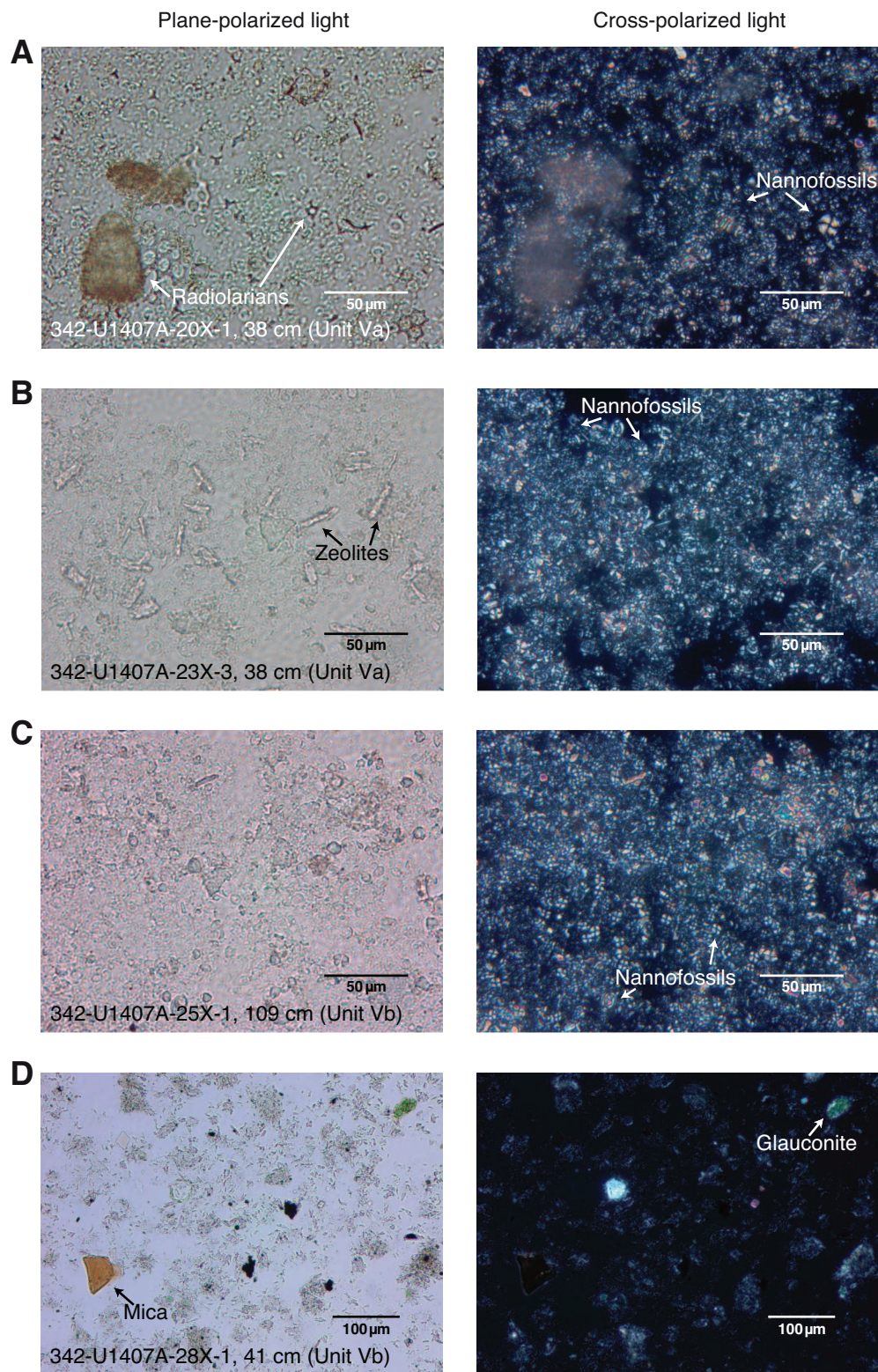


Figure F8. Plots of smear slide results of major biogenic and lithologic components and their relative abundance, Hole U1407A. Gray line represents black shale of the Cenomanian/Turonian Oceanic Anoxic Event 2. VA = very abundant, A = abundant, C = common, F = few, P = present.

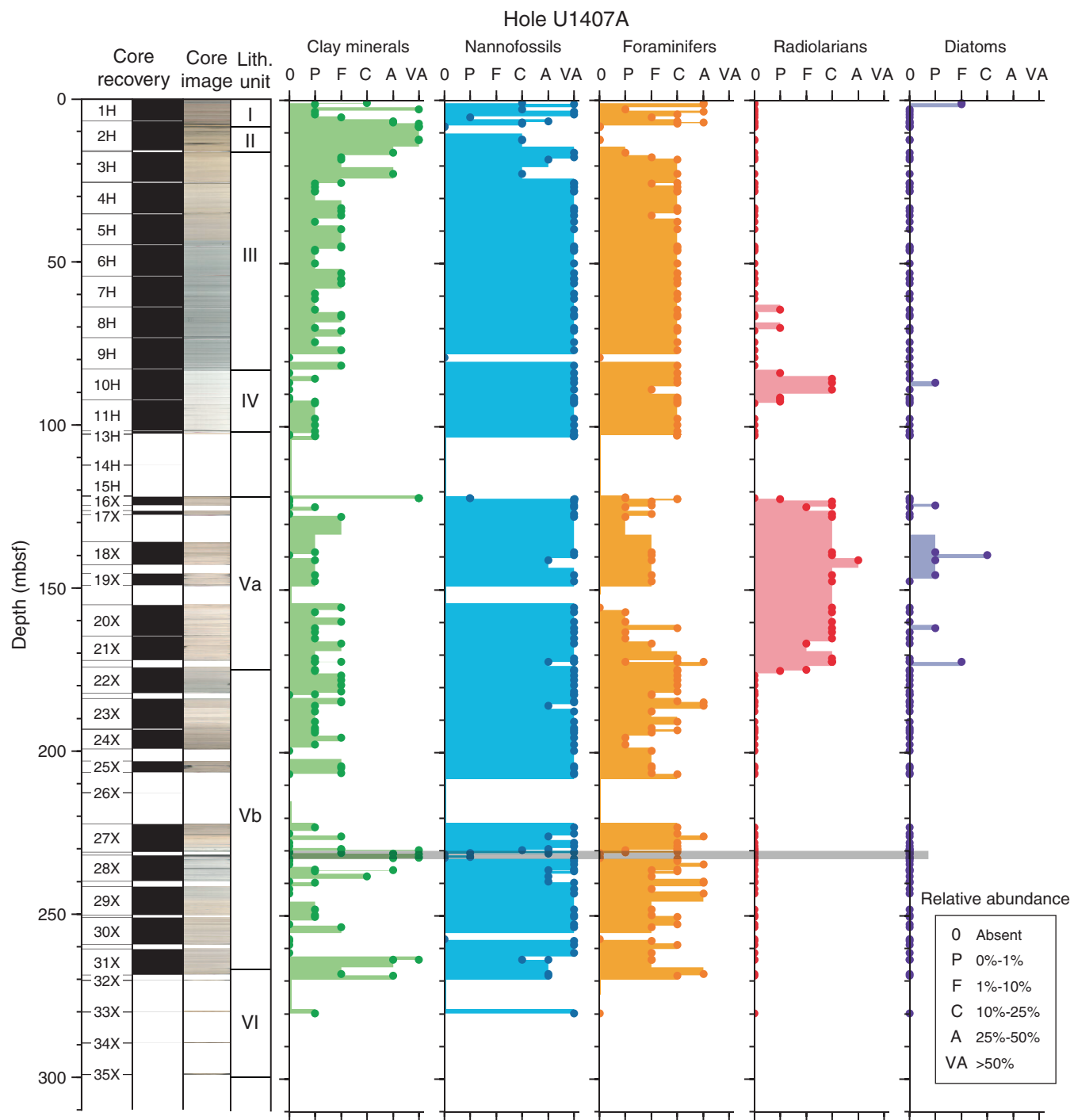


Figure F9. Plots of smear slide results of major biogenic and lithologic components and their relative abundance, Hole U1407B. Gray line represents black shale of the Cenomanian/Turonian Oceanic Anoxic Event 2. VA = very abundant, A = abundant, C = common, F = few, P = present.

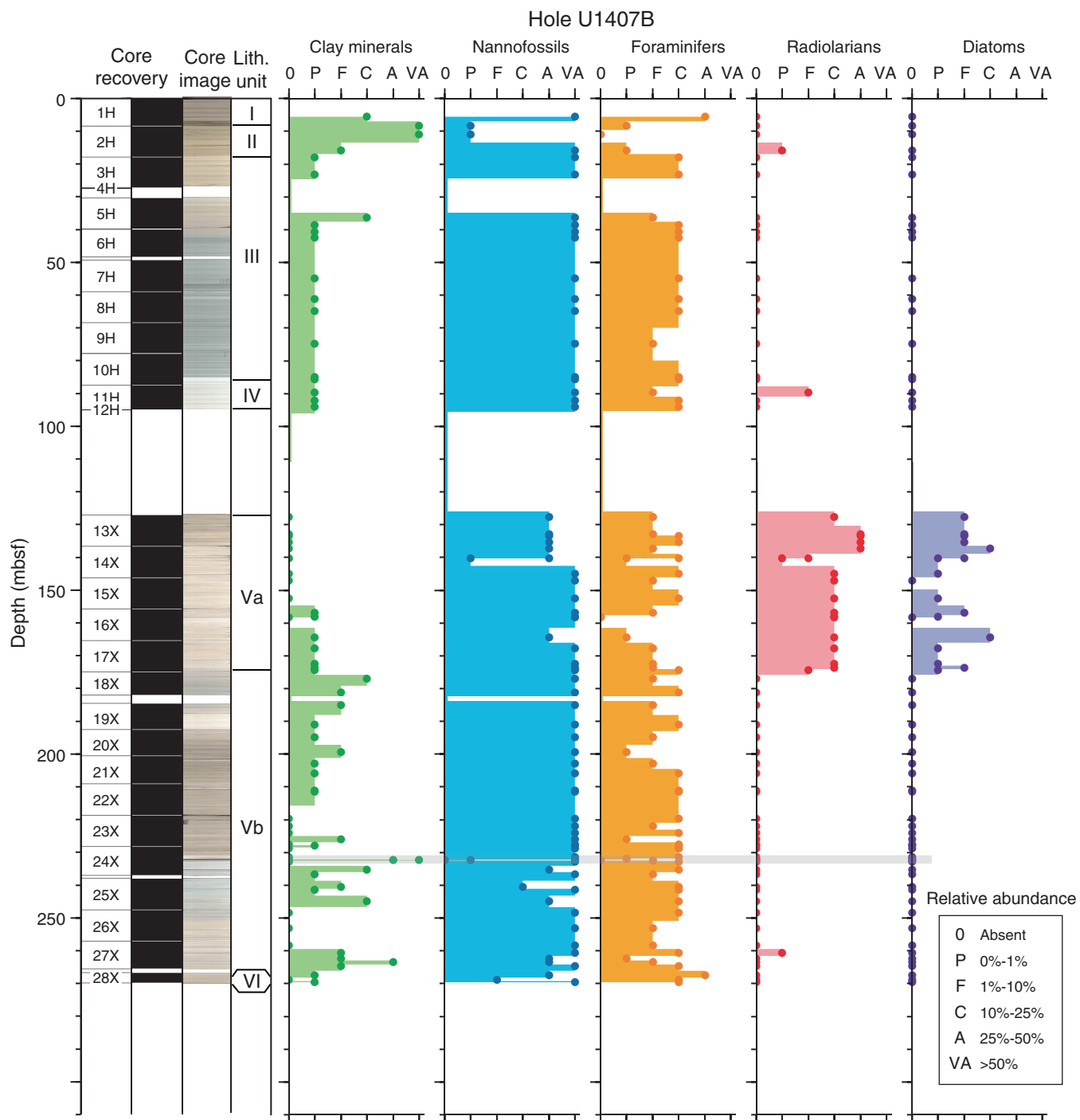


Figure F10. Plots of smear slide results of major biogenic and lithologic components and their relative abundance, Hole U1407C. Gray line represents black shale of the Cenomanian/Turonian Oceanic Anoxic Event 2. VA = very abundant, A = abundant, C = common, F = few, P = present.

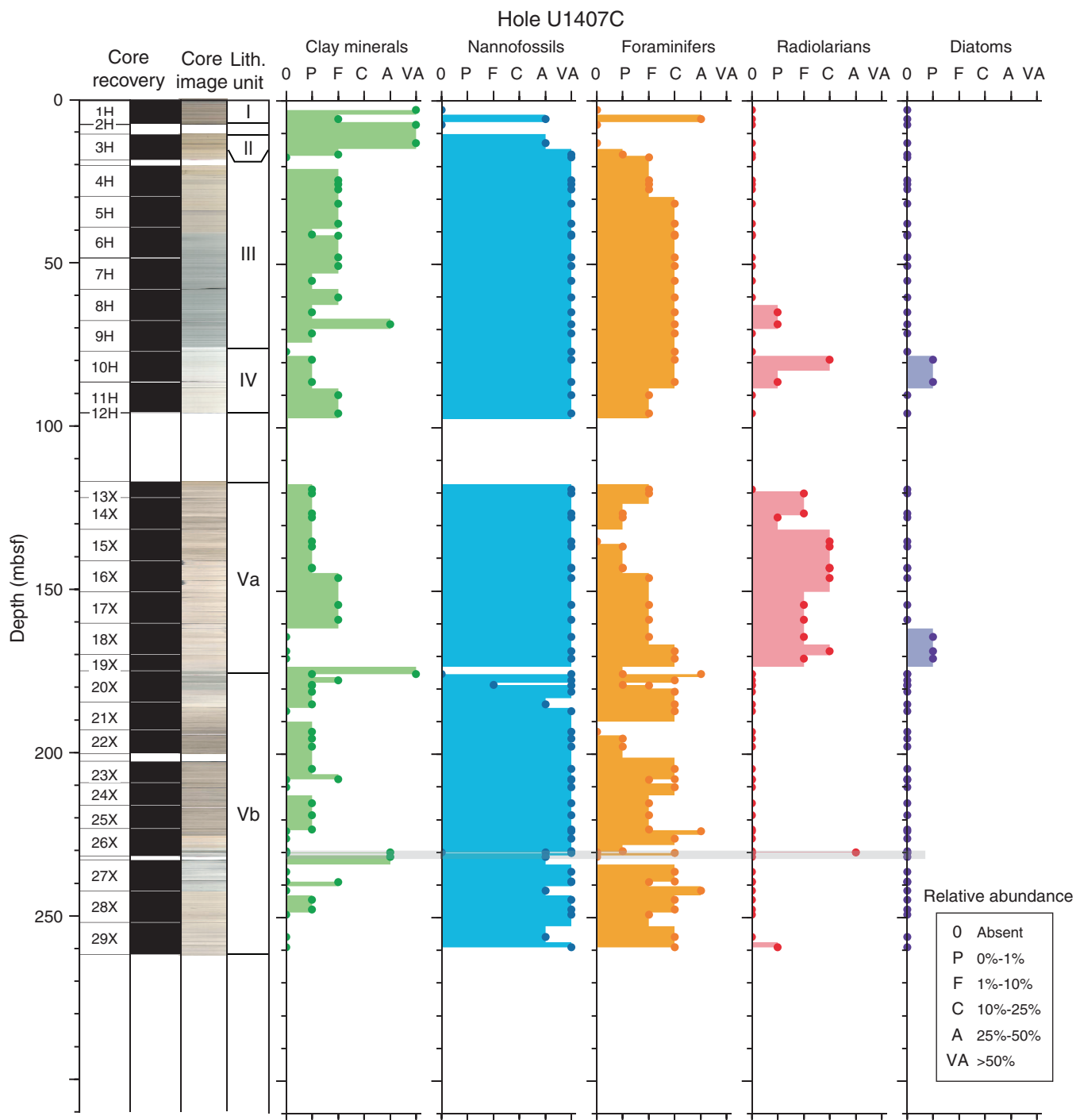


Figure F11. Core image of lithostratigraphic Unit III/ IV boundary, Hole U1407A. White (N 8) nannofossil ooze (Unit IV) forms a sharp contact with overlying greenish gray (5GY 6/1) clayey nannofossil ooze (Unit III). This is accompanied by a decline in carbonate content from ~85 to ~40 wt% and increases in magnetic susceptibility and natural gamma radiation (NGR). All three holes at Site U1407 feature several lighter intervals in the 5 m immediately above the boundary, characterized by higher nannofossil abundance and carbonate content of ~70 wt%.

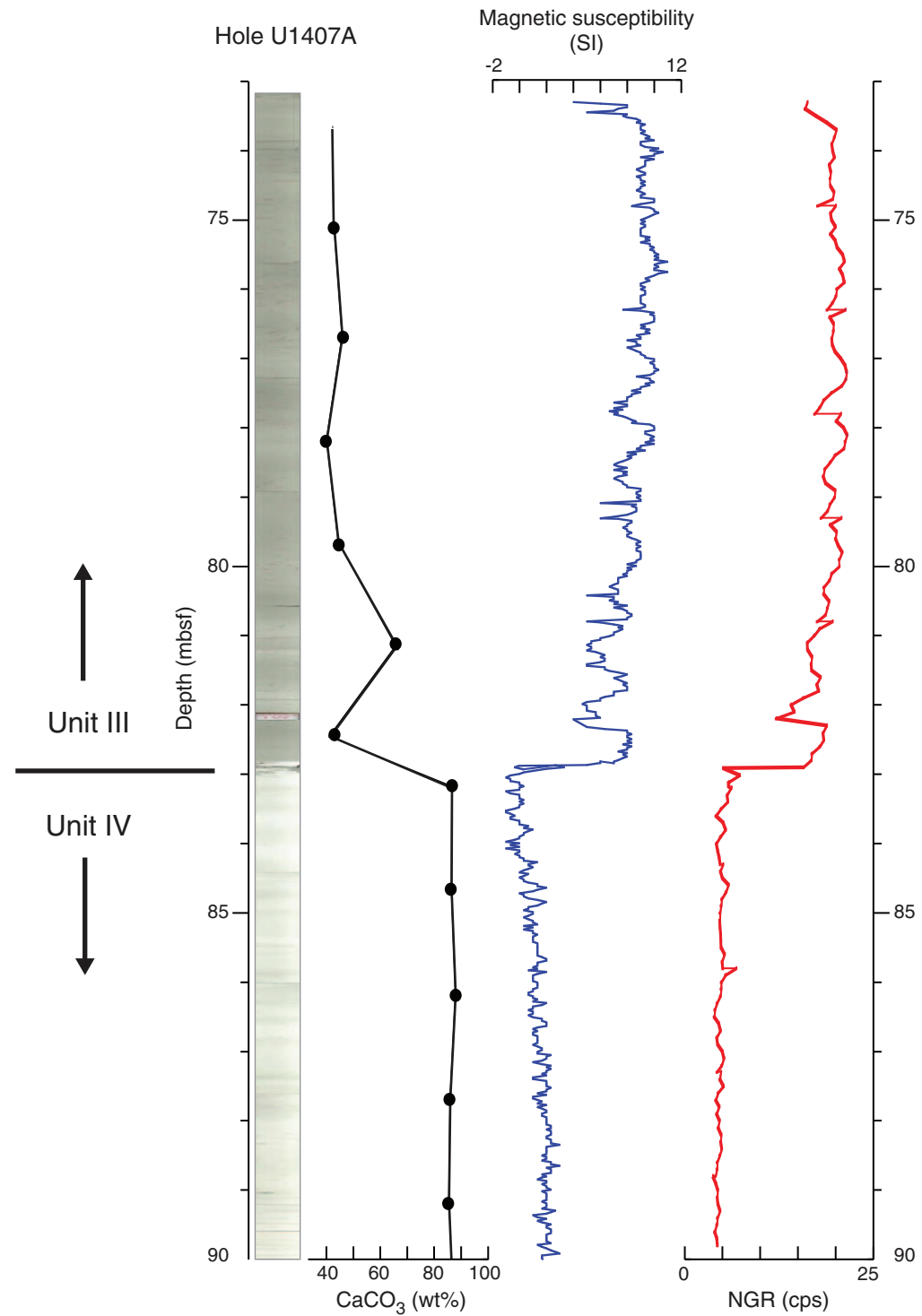


Figure F12. Core image of siltstone bed with basal-graded division overlain by horizontal to inclined laminations and possible ripple cross-lamination, Hole U1407A. This assemblage of physical sedimentary structures combined with comparably minor bioturbation suggests this might be a current-resuspended density flow deposit.

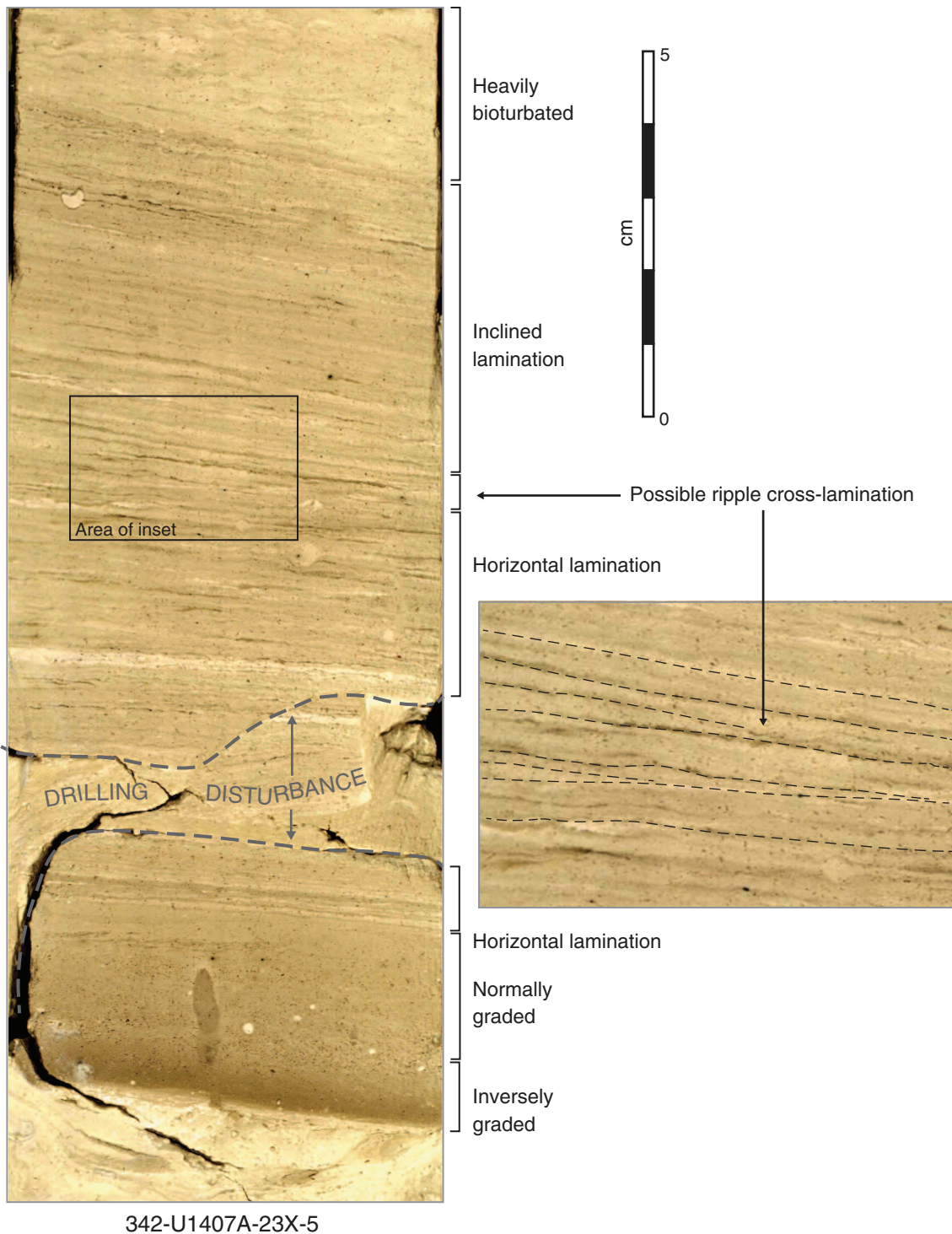


Figure F13. Stratigraphic logs, calcareous nannofossil datums, and total organic carbon (TOC) data, Site U1407. The interval includes the late Cenomanian through early Turonian and the Oceanic Anoxic Event 2 interval. The stratigraphic log accompanying the core scan photograph has a stylized weathering profile that denotes the relative resistance of the chalks to the more friable black shale and claystone.

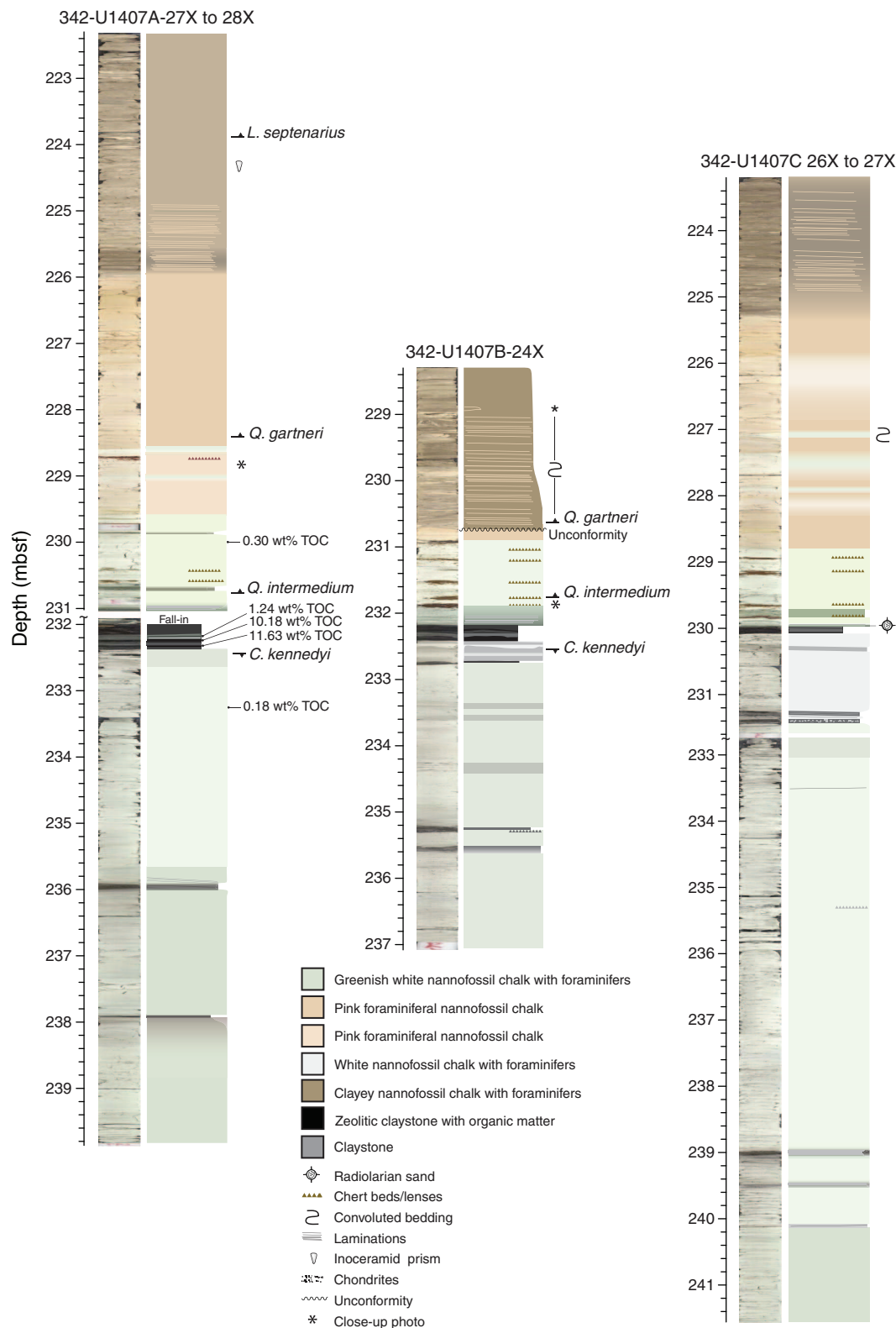


Figure F14. Core images of the Oceanic Anoxic Event 2 black shale horizons, Holes U1407A–U1407C. Gaps in Hole U1407A are the result of coring disturbance.

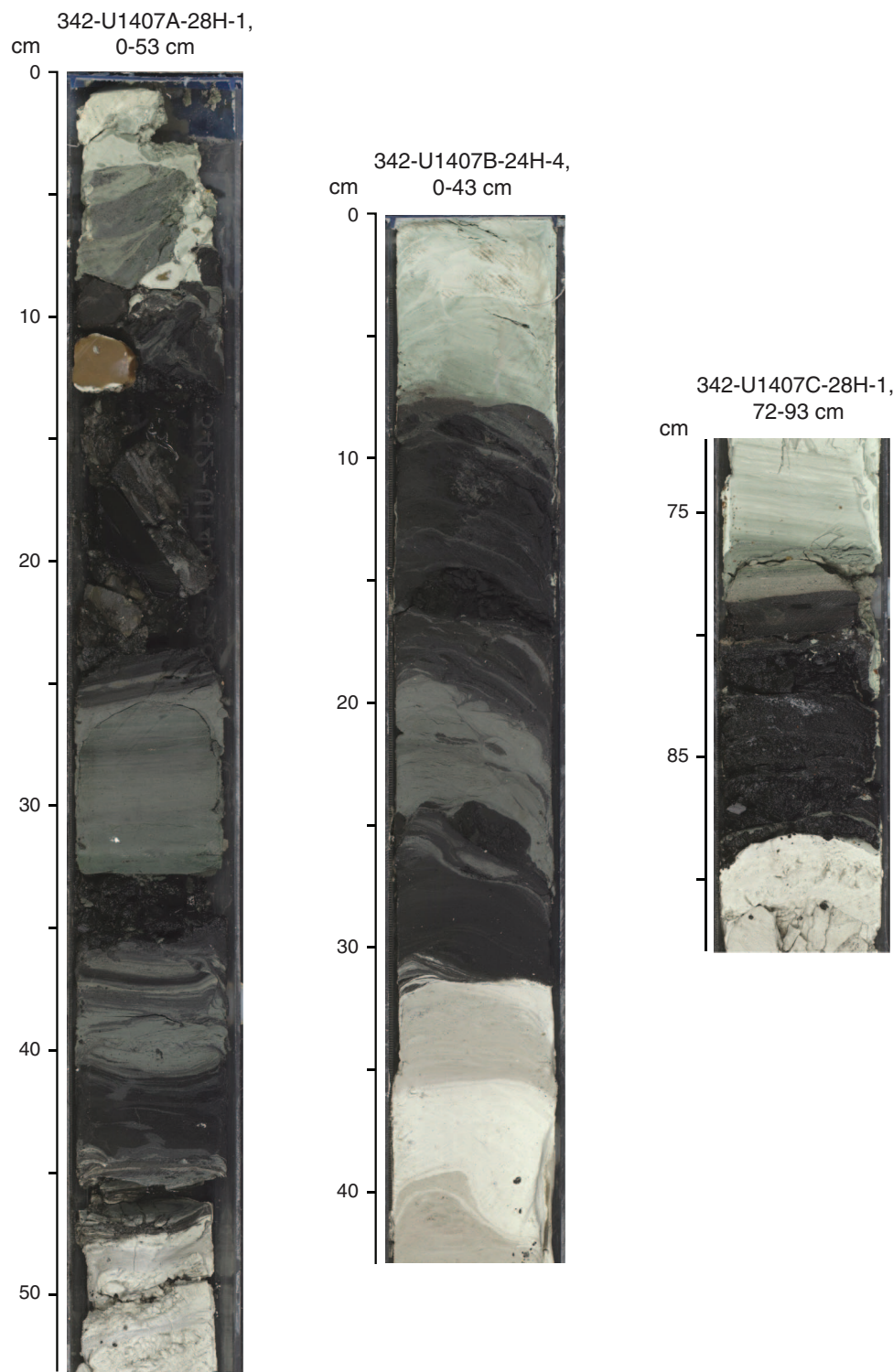


Figure F15. Core image close-ups of characteristic lithologies from the Oceanic Anoxic Event 2 interval, Site U1407. See Figure F13. A. Example of a pre-Oceanic Anoxic Event (OAE) 2 laminated claystone with well-developed *Chondrites* burrowing at the top of the interval. The wedge shape of this bed is the result of core rotation during extended core barrel drilling. B. Example of reddish brown chert with mottles that are accompanied by significant magnetic susceptibility peaks. Surrounding lithology is nannofossil chalk with clay (light green below chert) and nannofossil chalk (greenish white above chert). C. Mid-Turonian laminated clayey nannofossil chalk with well-preserved, slump-induced overturning. D. Red radiolarian chert hosted in pinkish white nannofossil chalk overlying the OAE. E. Laminated nannofossil claystone with radiolarians that directly overlie the black shale.

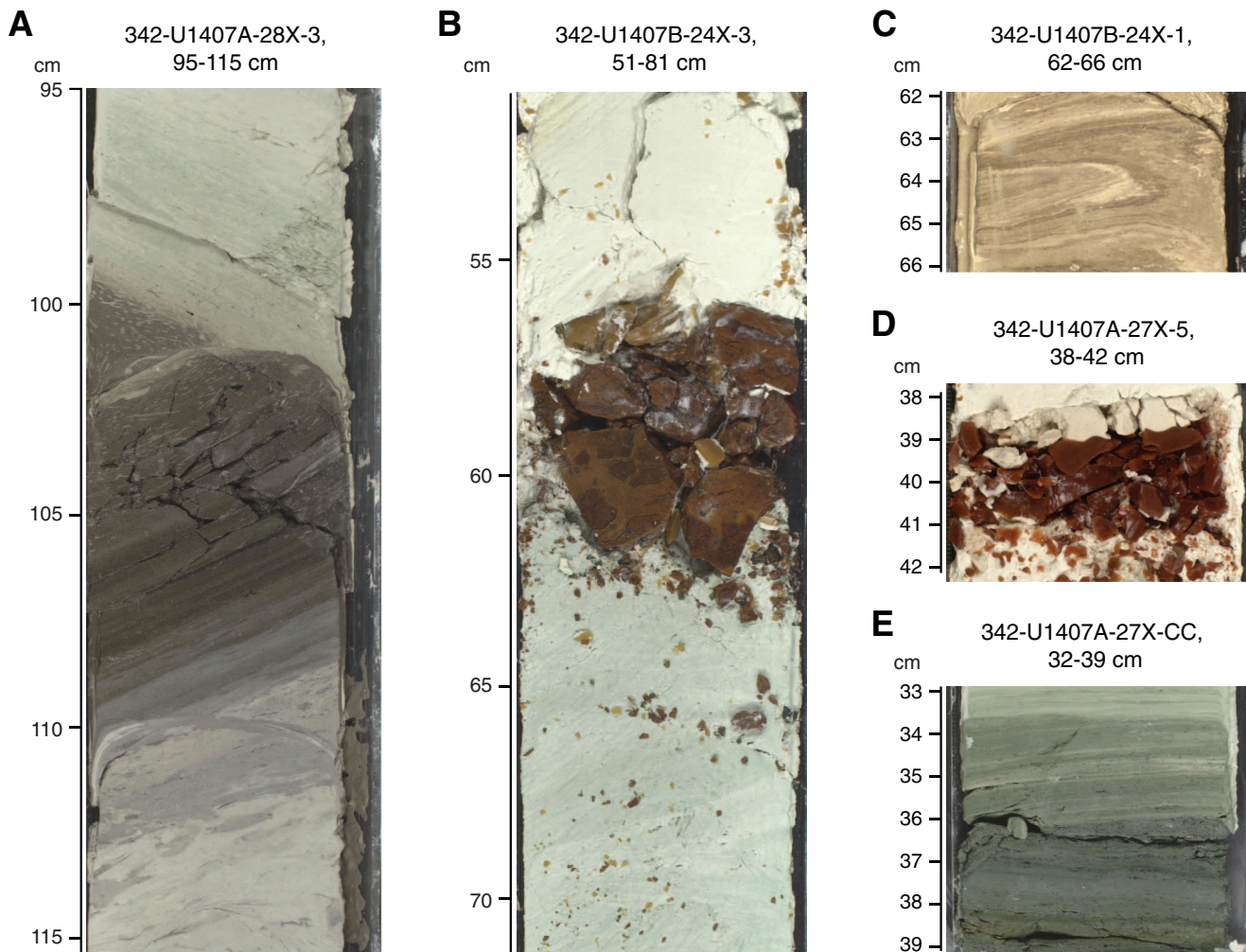


Figure F16. A, B. Thin section photomicrographs of a mixed carbonate clastic grainstone that has been lightly dolomitized and heavily cemented Fe-Mn crusts (Thin Section 3; Sample 342-U1407A-31X-CC, 17–18 cm). C, D. Thin section photomicrographs of a pel-bio-micrite (Thin Section 9; Sample 342-U1407A-35X-CC, 0–2 cm). E, F. Photographs of large benthic foraminifer *Orbitolina* (Sample 342-U1407A-33X-CC, 10–17 cm). For A–D, left images are under plane-polarized light and right images are under cross-polarized light.

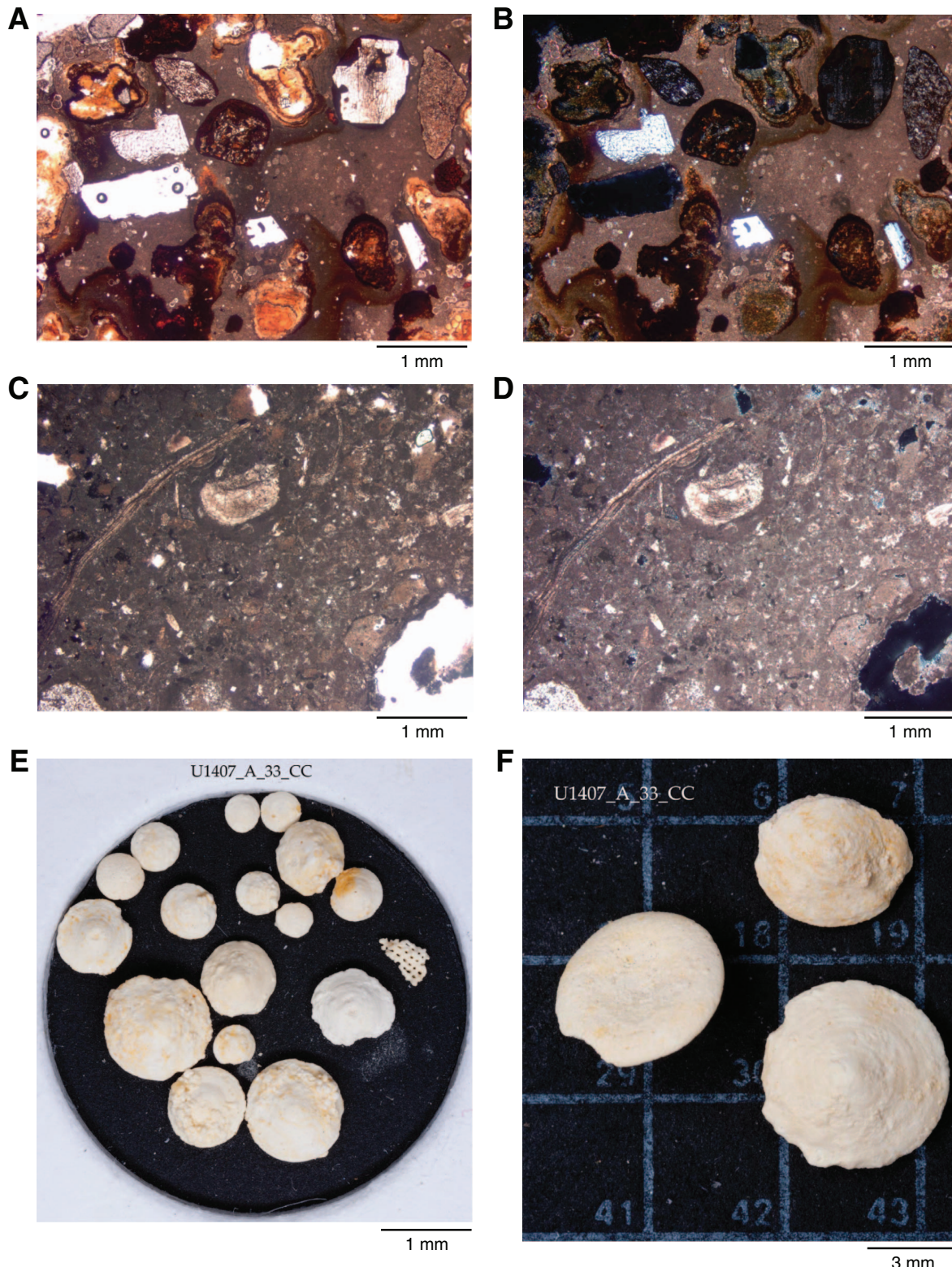


Figure F17. Core images of stratigraphic inversions from the upper Danian to Campanian, Site U1407. A relatively complete upper Paleocene to Danian sequence (see “[Biostratigraphy](#)”) is truncated by a series of unconformities and stratigraphic inversions spanning the upper Danian to lower Campanian (nannofossil Zone NP4 to Subzone UC14d/UC15a). The Maastrichtian unconformity (nannofossil Zones UC20–UC16) is only identified in Hole U1407C and may be attributed to either the biostratigraphic resolution over that interval or local variation in postdepositional processes.

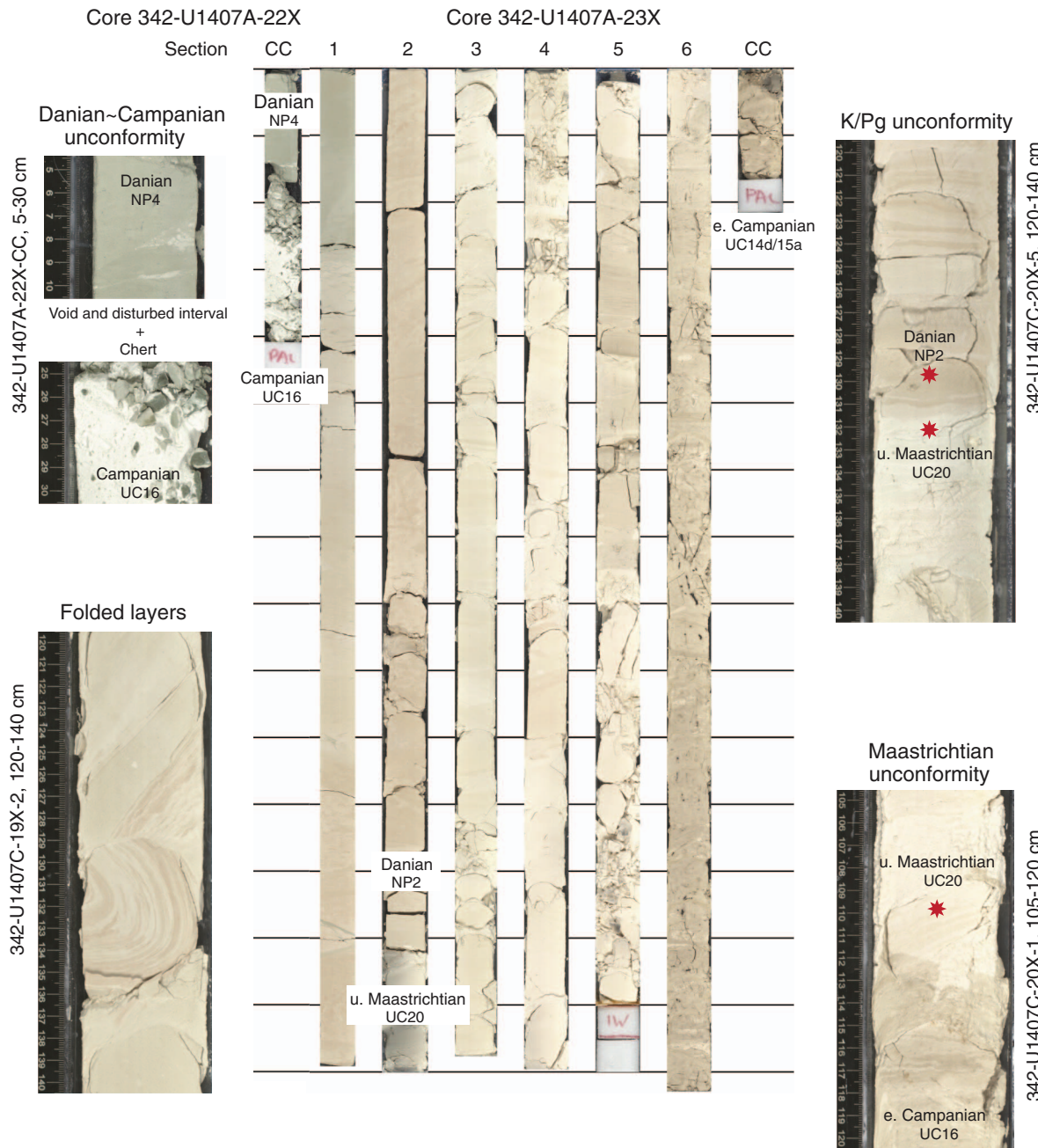


Figure F18. Integrated calcareous and siliceous microfossil biozonation, Site U1407.

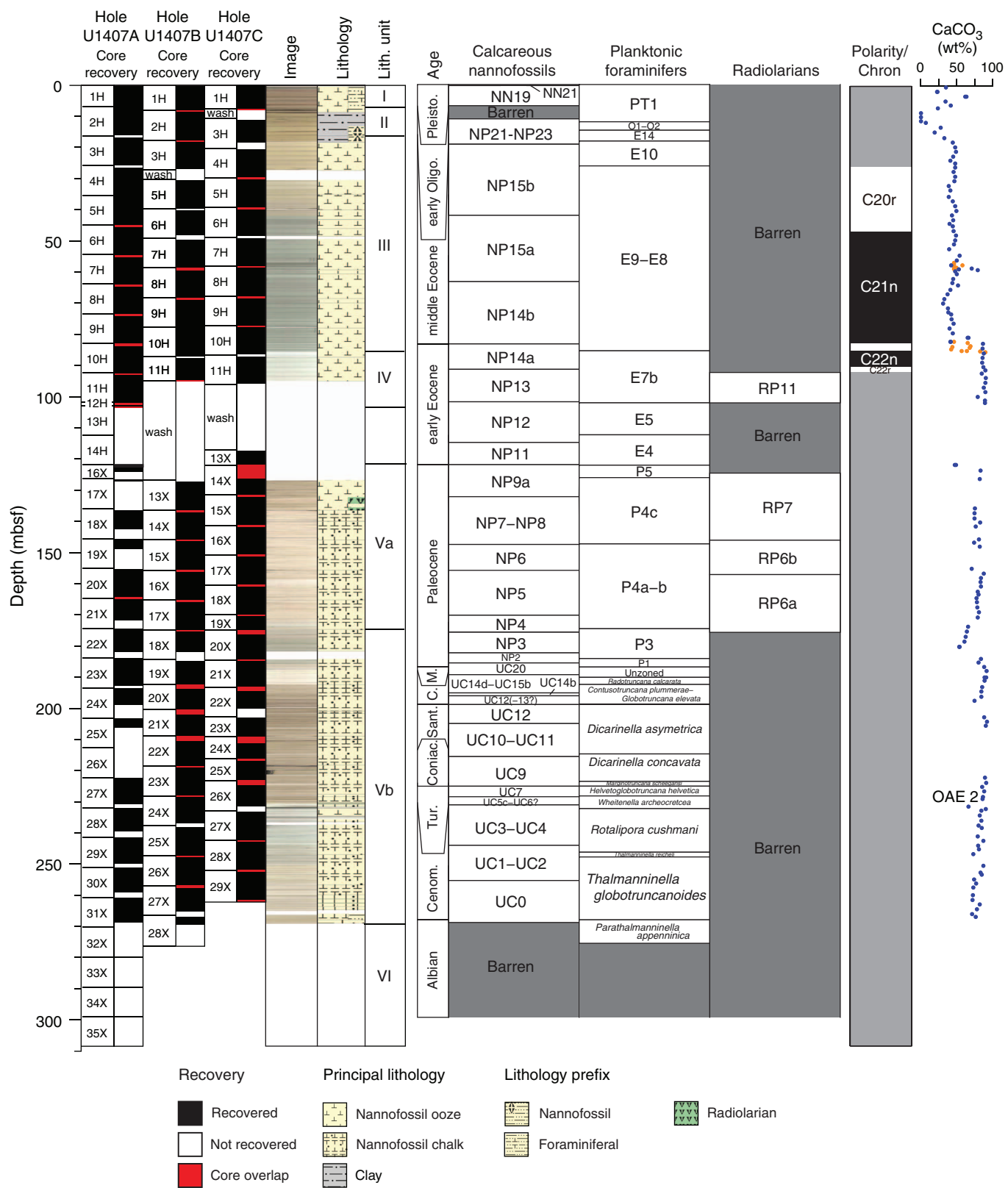


Figure F19. Age-depth model for Site U1407 showing biostratigraphic and magnetostratigraphic datums.

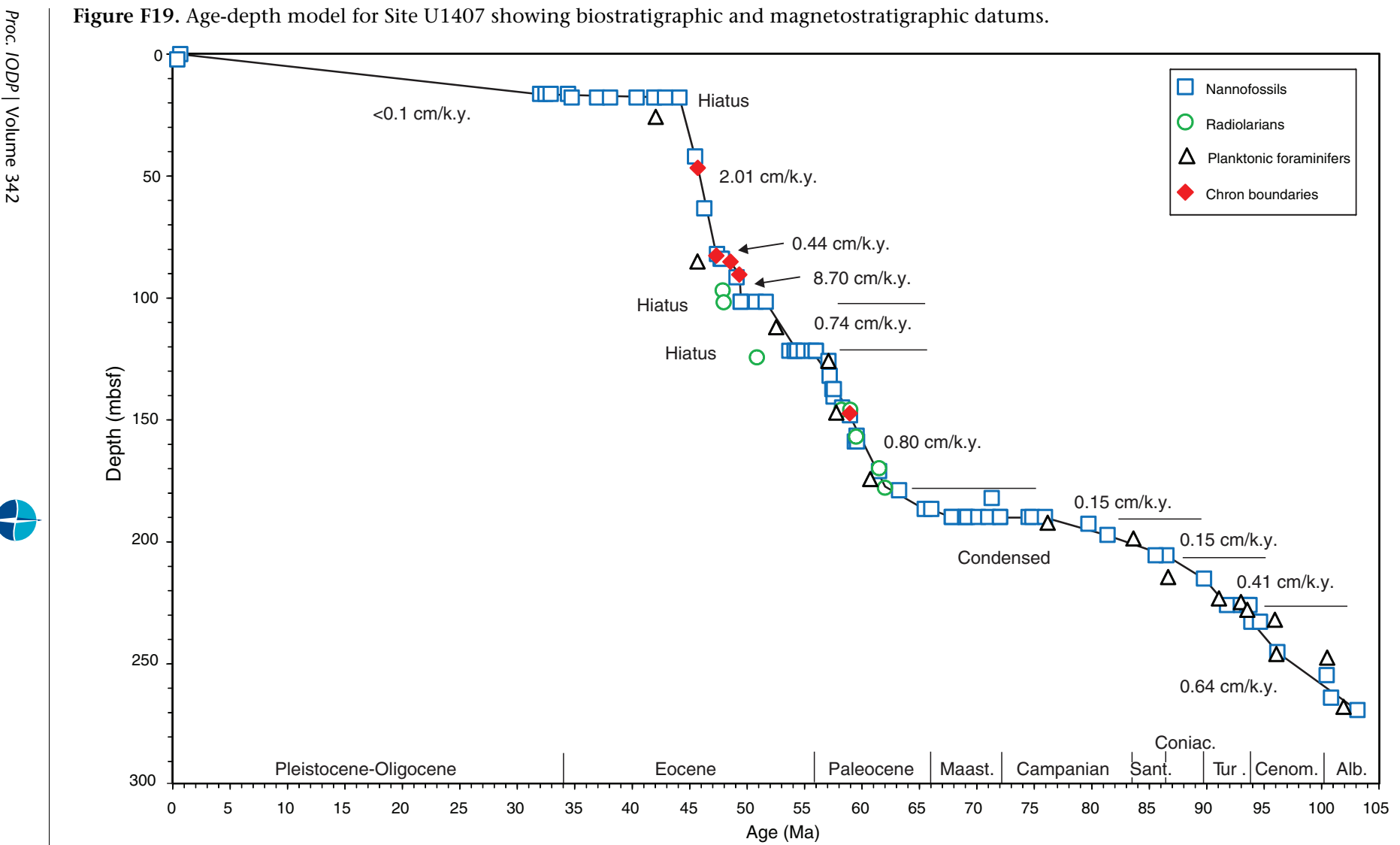


Figure F20. Group abundance and preservation of calcareous and siliceous microfossils, Site U1407. Solid and open symbols represent Holes U1407A and U1407B, respectively. Abundance: B = barren, P = present, R = rare, F = few, C = common, A = abundant, D = dominant. Preservation: P = poor, M = moderate, G = good, VG = very good.

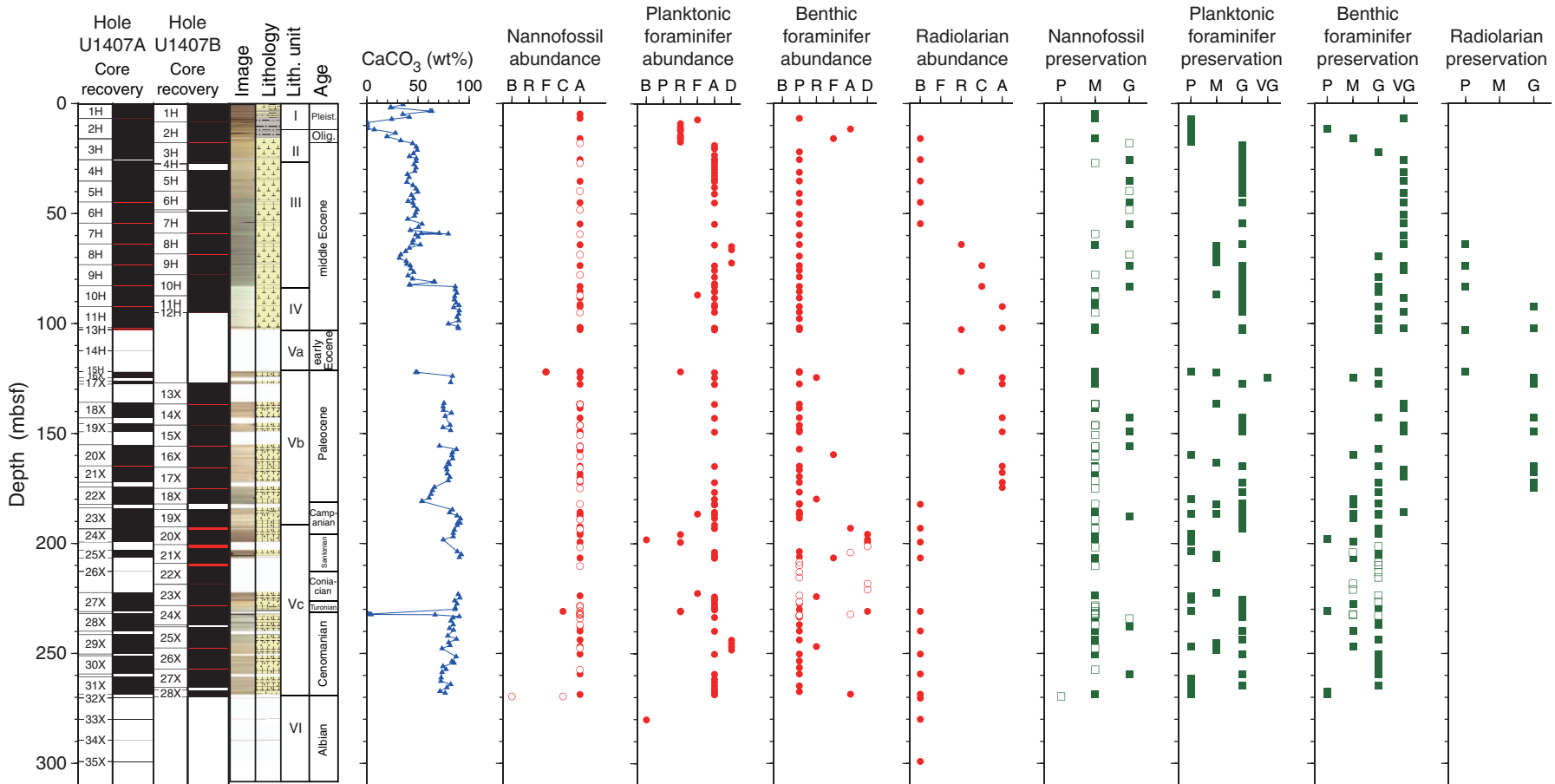


Figure F21. Photomicrographs of radiolarians preserved in chert within middle to lower Turonian sediment, Core 342-U1407B-24X. Left images taken under plane-polarized light and right images taken under cross-polarized light. A. Chert fragment showing circular outlines of radiolarians infilled with microcrystalline quartz and occurring in both darker and lighter laminae (Sample 342-U1407B-24X-1, 69–71 cm; 228.99 mbsf). B. Chert fragment showing numerous indistinct outlines of radiolarians, including a multirayed form (Sample 342-U1407B-24X-3, 22–24 cm; 231.74 mbsf). C. Chert fragment showing circular outlines of radiolarians infilled with microcrystalline quartz and a prominent quartz vein (Sample 342-U1407B-24X-3, 55–57 cm; 231.86 mbsf).

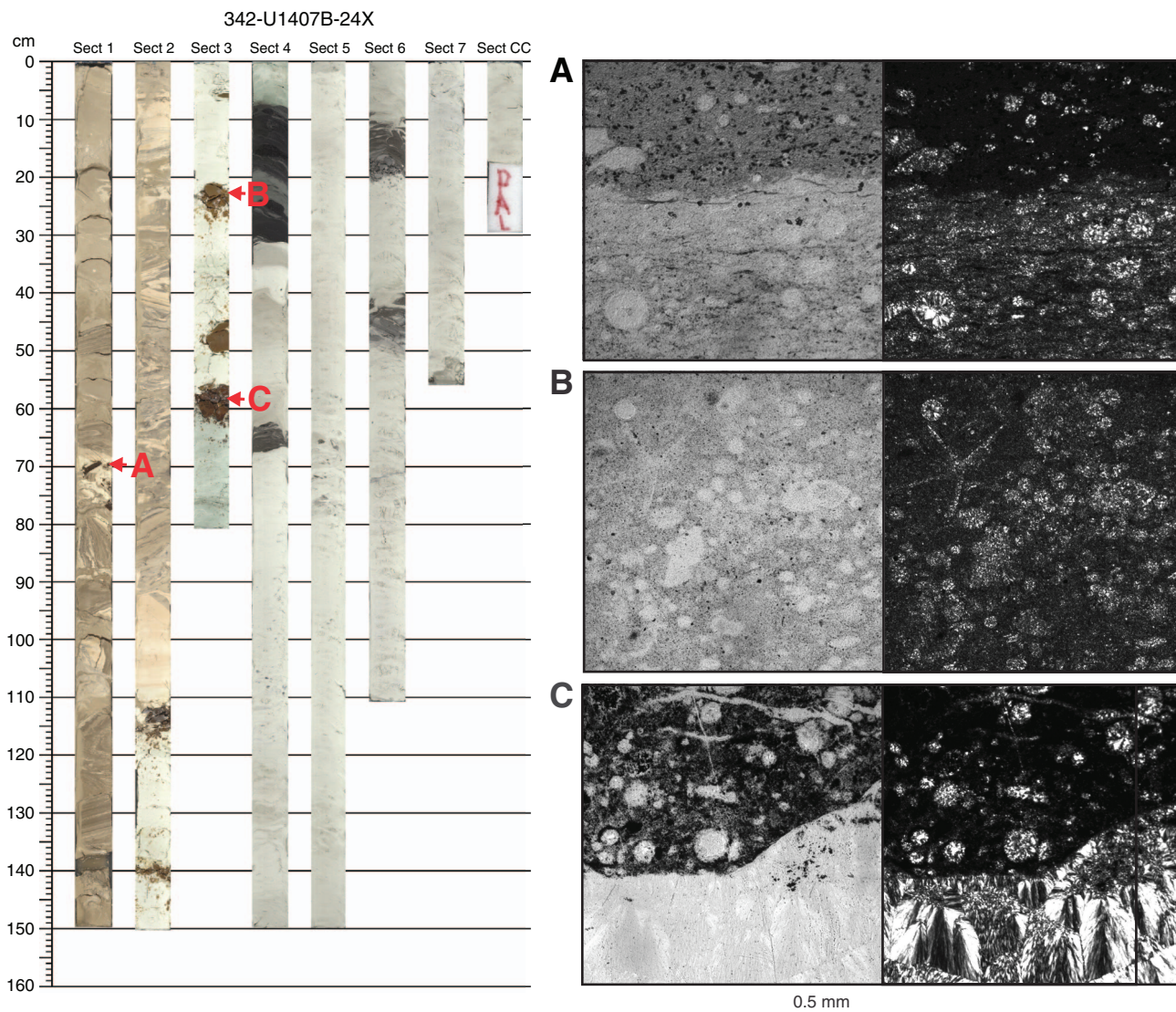


Figure F22. Close-up photograph of *Orbitolina texana?* (Sample 342-U1407A-33X-CC).



Figure F23. Close-up photographs of macrofossils. A. *Neohibolites*? (Sample 342-U1407A-31X-CC). B. Coralline algae (Sample 342-U1407A-35X-CC). C. Ahermatypic coral (Sample 342-U1407A-33X-CC). D. Turritellid gastropod (Sample 342-U1407A-35X-CC). E, F. Hermatypic coral (Sample 342-U1407A-35X-CC).

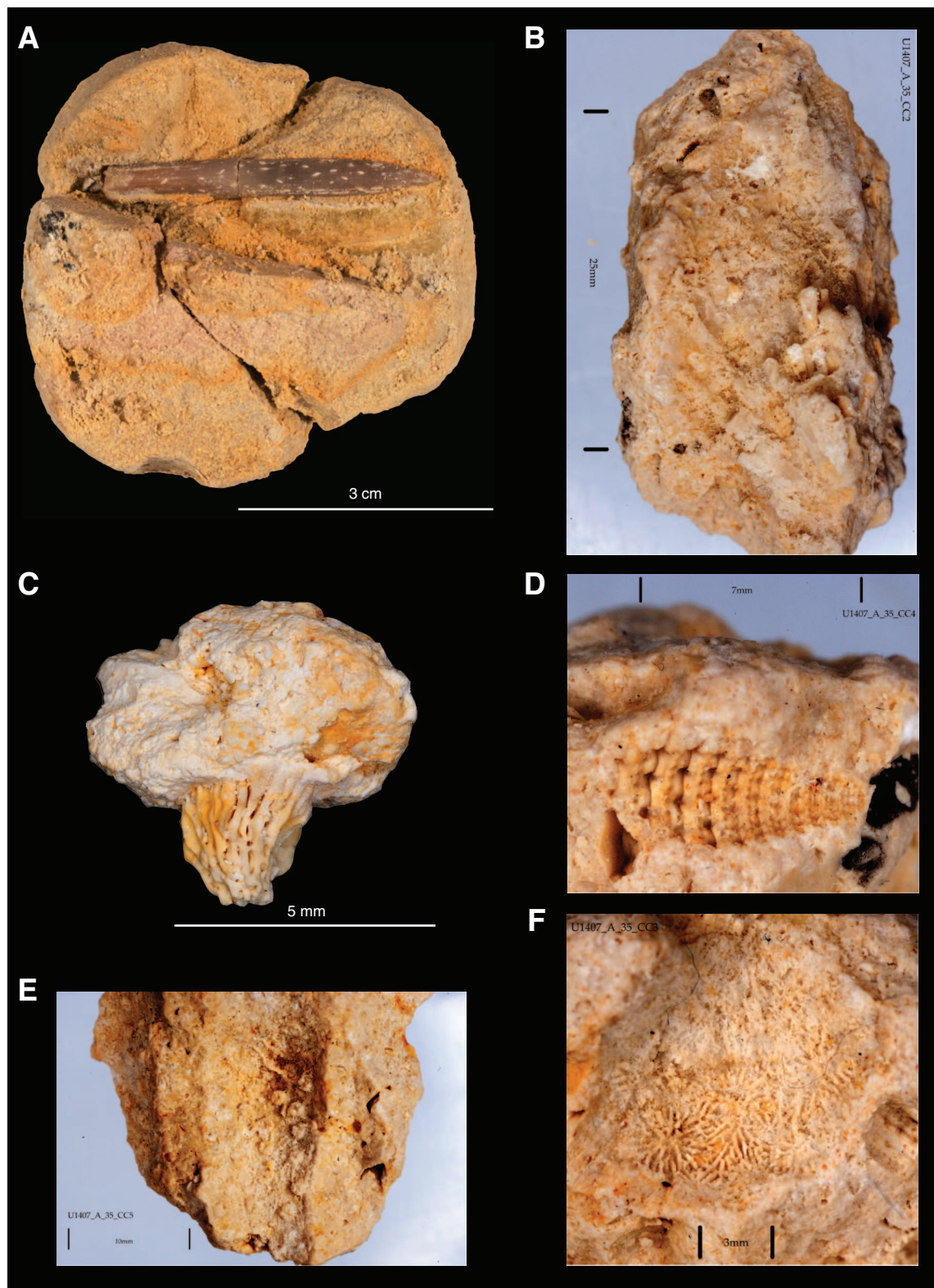


Figure F24. Plots of downhole variation of magnetic susceptibility and paleomagnetism data, Hole U1407A. Magnetization intensity, inclination, and declination are after 20 mT demagnetization. Only oriented advanced piston corer (APC) intervals show directions in geographic coordinates. Directions from all other intervals are shown in sample coordinates. For discrete sample data, if the samples were analyzed by principal component analysis (PCA; Kirschvink, 1980), then directions are shown according to PCA declination and inclination. Otherwise, directions following 20 mT demagnetization are shown. XCB = extended core barrel. Polarity: black = normal chron, white = reversed chron, gray = unidentified interval.

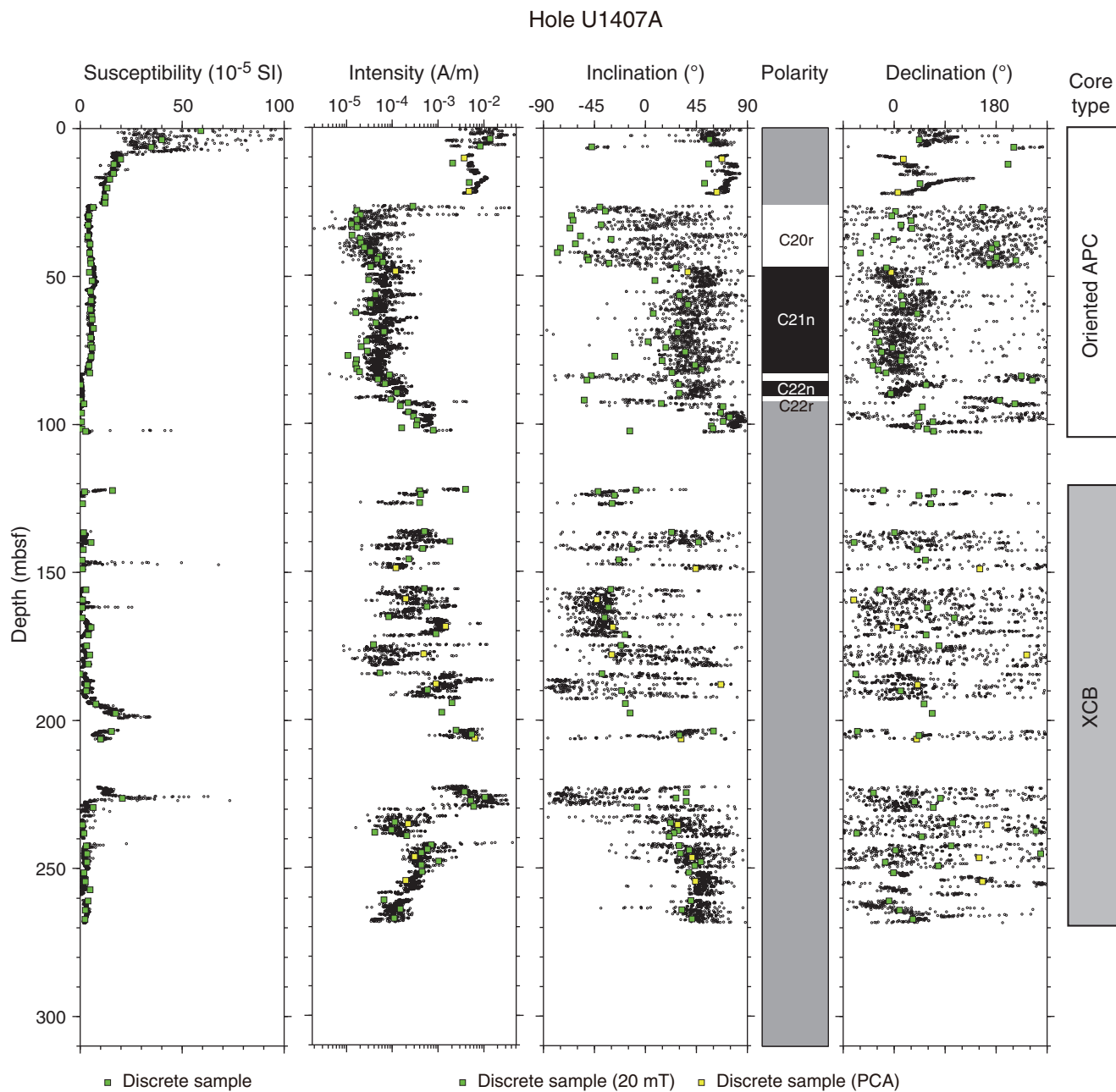


Figure F25. Plots of downhole variation of magnetic susceptibility and paleomagnetism data, Hole U1407B. Magnetization intensity, inclination, and declination are after 20 mT demagnetization. Only oriented advanced piston corer (APC) intervals show directions in geographic coordinates. Directions from all other intervals are shown in sample coordinates. XCB = extended core barrel. Polarity: black = normal chron, white = reversed chron, gray = unidentified interval.

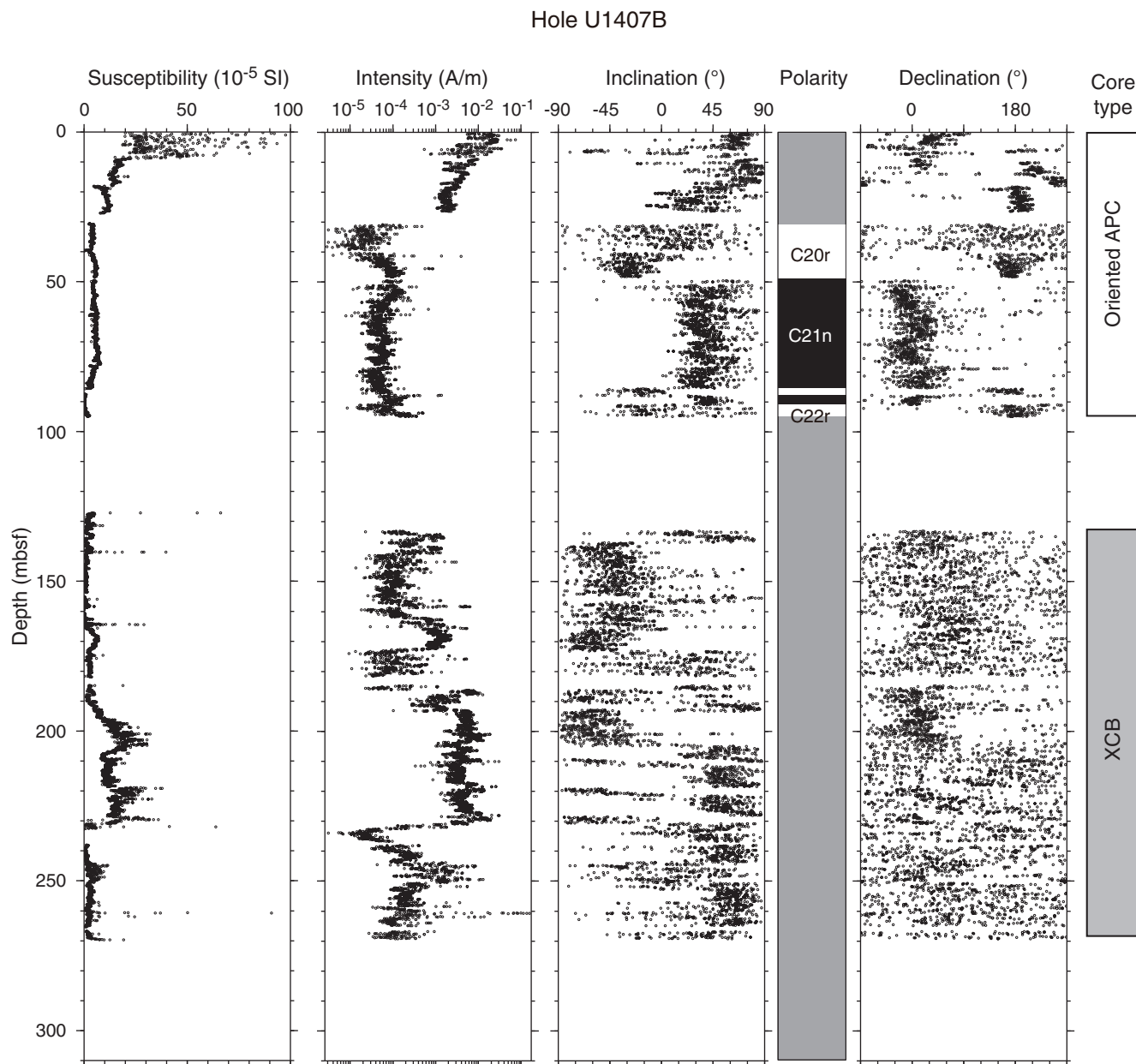


Figure F26. Plots of downhole variation of magnetic susceptibility and paleomagnetism data, Hole U1407C. Magnetization intensity, inclination, and declination are after 20 mT demagnetization. Directions are shown in sample coordinates. APC = advanced piston corer, XCB = extended core barrel. Polarity: black = normal chron, white = reversed chron, gray = unidentified interval.

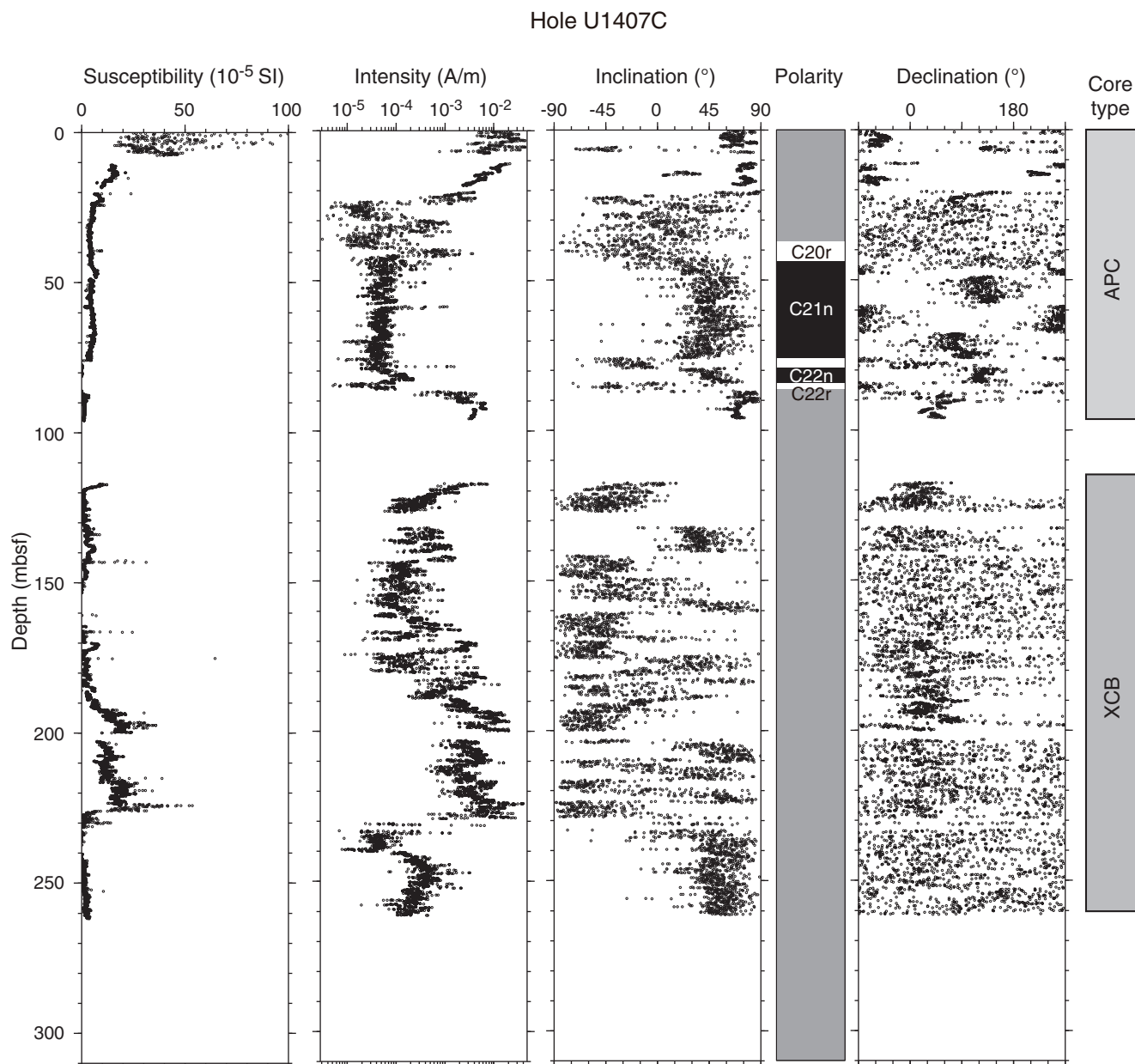


Figure F27. Plots of representative alternating field (AF) demagnetization results for discrete paleomagnetism samples, Site U1407. Upper plots show intensity variation with progressive demagnetization, and lower plots show vector endpoints of paleomagnetism directions on orthogonal vector diagrams (i.e., Zijderveld plots). Vector diagrams indicate well-resolved characteristic remanent magnetization (ChRM) directions from the (A) advanced piston corer and (B) extended core barrel (XCB) intervals, whereas (C) some samples from the XCB intervals do not show stable components. Solid circles = horizontal projections, open circles = vertical projections, gray circles = data not used to calculate ChRM direction, black dashed line = ChRM direction. Inc = inclination, Dec = declination, MAD = maximum angle of deviation.

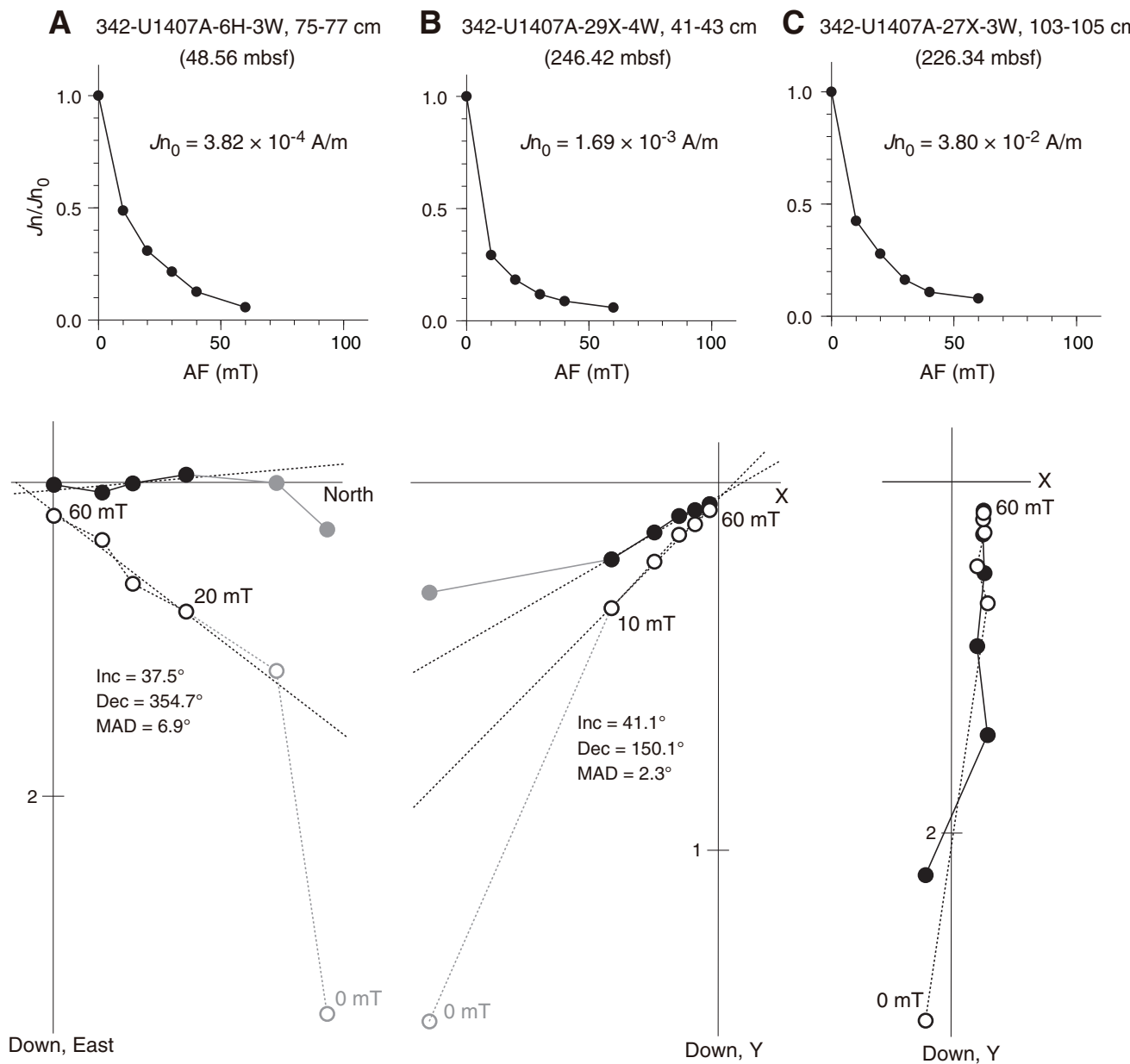


Figure F28. Illustration of magnetostratigraphy, Site U1407. Core recovery: black = recovered, white = not recovered, red = core overlap.

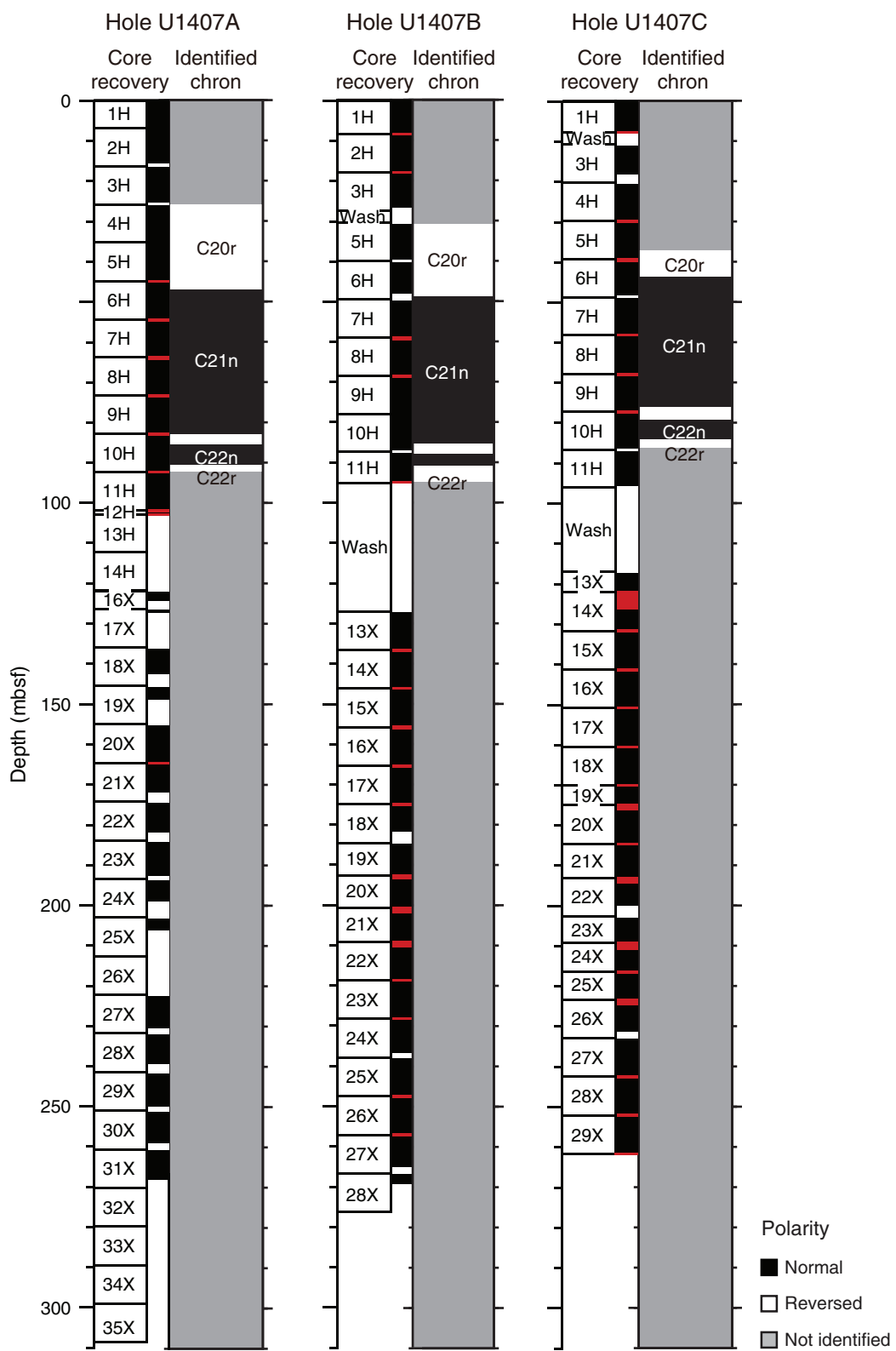


Figure F29. Plots of anisotropy of magnetic susceptibility vs. depth, Hole U1407A. Separation of eigenvalues is related to the shape and degree of the magnetic fabric (see “[Paleomagnetism](#)” in the “Methods” chapter [Norris et al., 2014b]). For example, if τ_1 and τ_2 are close or indistinguishable but distinct from τ_3 , then the bulk fabric is oblate. The absence of P (degree of anisotropy; τ_1/τ_3) data points in lithostratigraphic Unit IV indicates that values are off-scale and considered spurious; see text for details. Lithostratigraphic units are described in “[Lithostratigraphy](#).” Eigenvalues: τ_1 = maximum, τ_2 = intermediate, τ_3 = minimum. V_3 = minimum eigenvector. APC = advanced piston corer, XCB = extended core barrel.

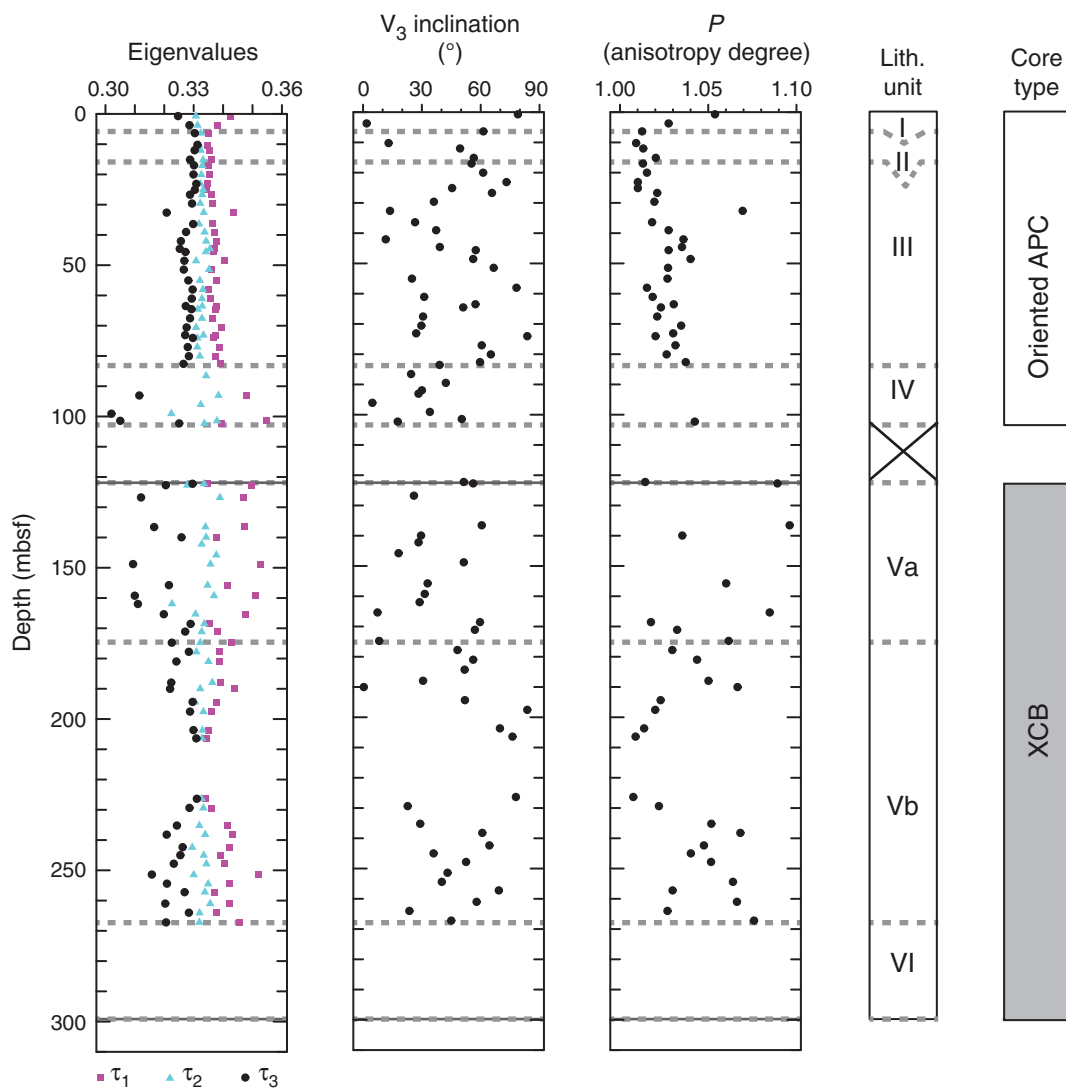


Figure F30. Plots of linear sedimentation rate (LSR), dry bulk density (DBD), carbonate content, and mass accumulation rate (MAR) at a 200 k.y. time step, Hole U1403A. Solid black diamonds are the inflection points in estimated LSR, DBD, and carbonate content. Geologic ages are shown on the GTS2012 timescale (Gradstein et al., 2012). CAR = carbonate mass accumulation rate, nCAR = noncarbonate mass accumulation rate.

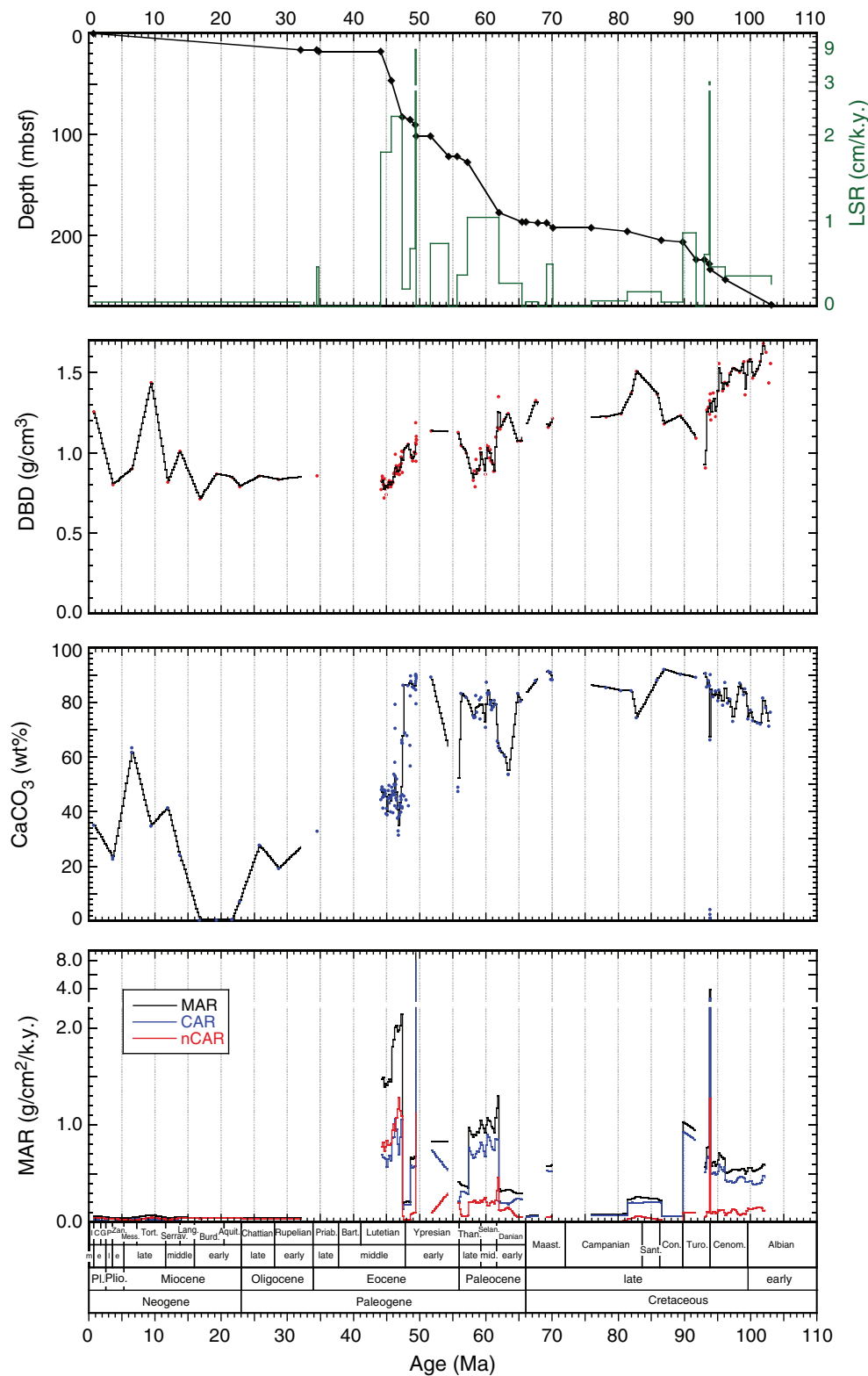


Figure F31. Plots of interstitial water constituent concentrations, Hole U1407A. See “[Lithostratigraphy](#)” for description of lithostratigraphic units.

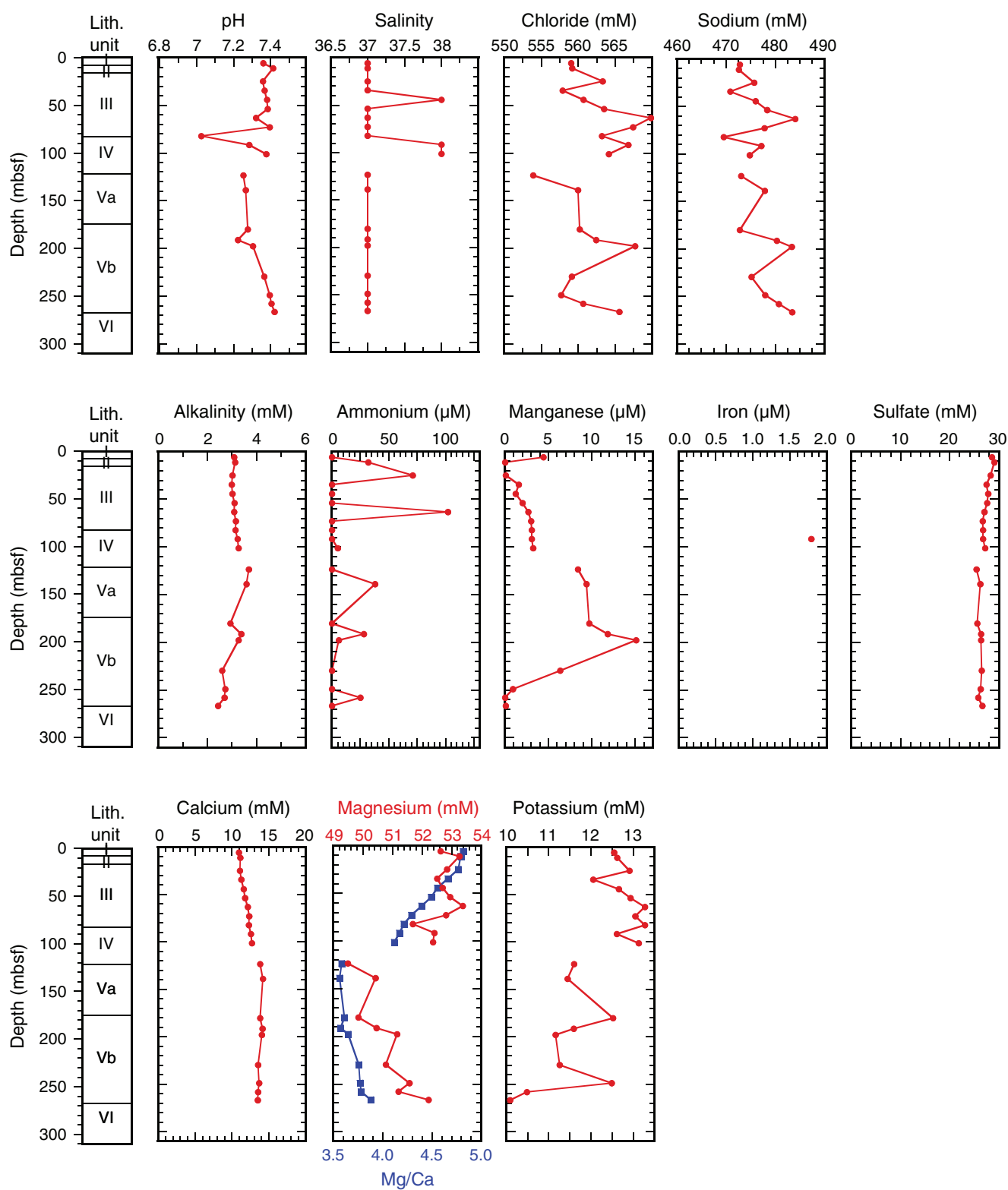


Figure F32. Plot of sedimentary carbonate contents, Holes U1407A (red) and U1407B (blue). Core recovery: black = recovered, white = not recovered, red = core overlap. TOC = total organic carbon.

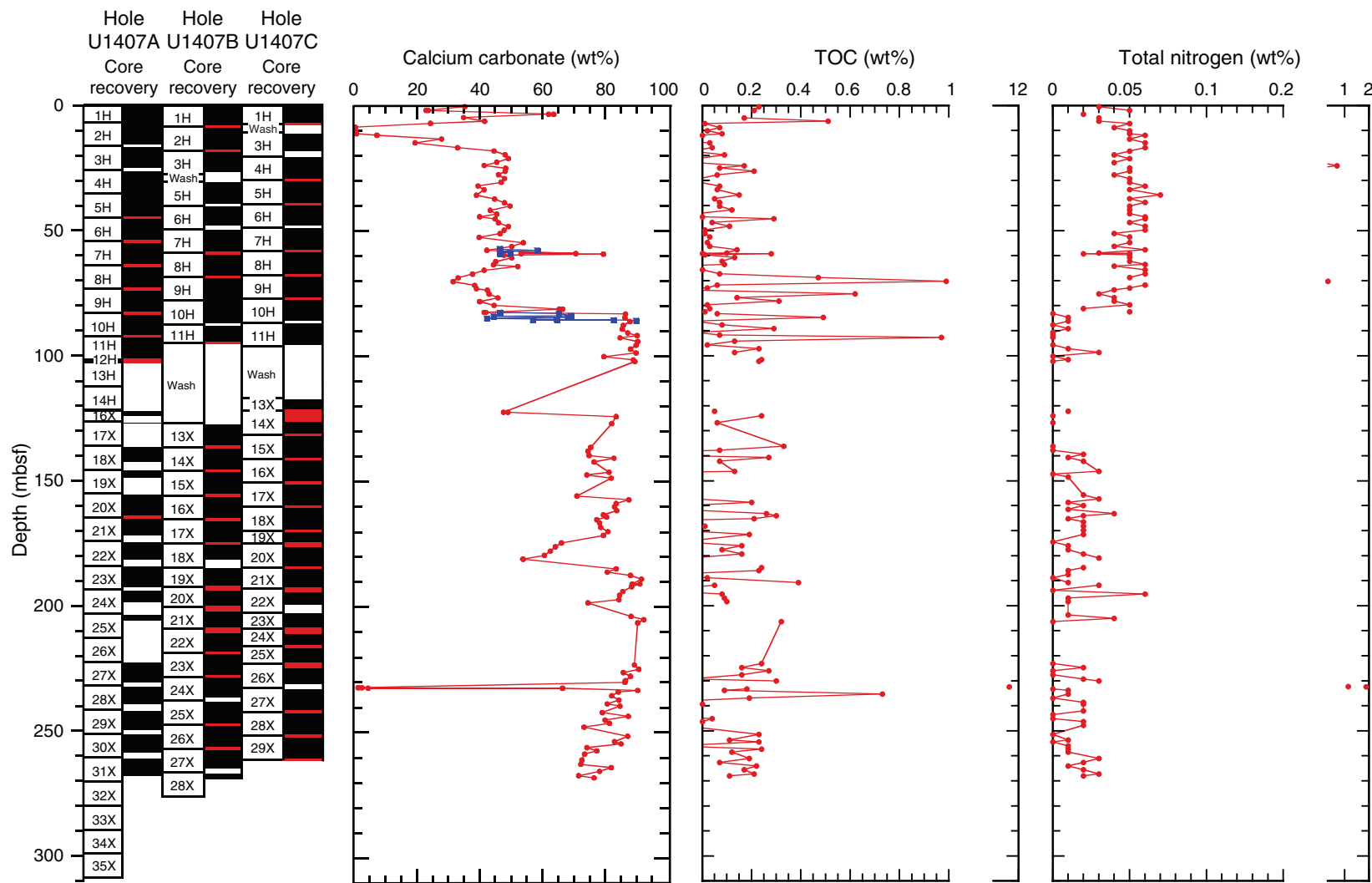


Figure F33. Core image, source-rock van Krevelen–type diagram, and plot of total organic carbon (TOC) for the late Cenomanian–early Turonian and Oceanic Anoxic Event 2 interval, Hole U1407A.

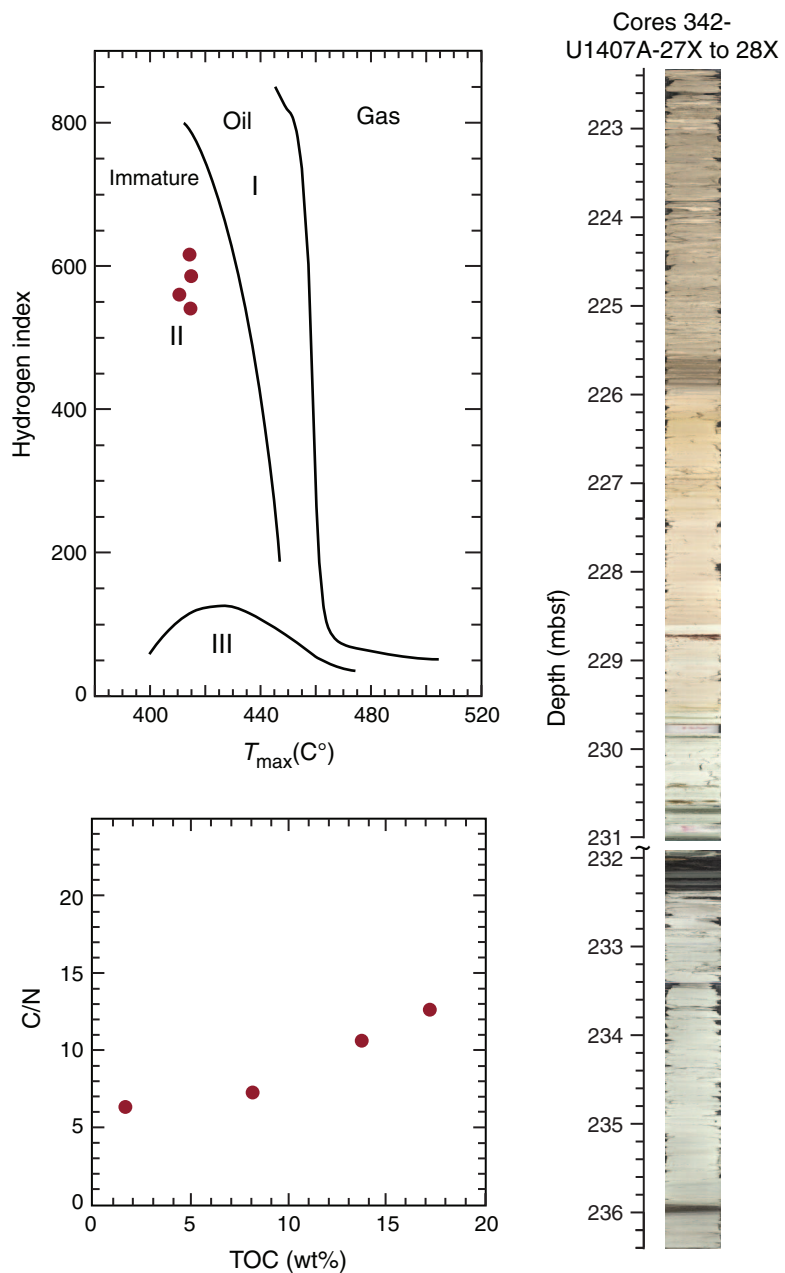


Figure F34. Plots of magnetic susceptibility (MS; truncated at 160 IU), bulk density (gray line = gamma ray attenuation density from Whole-Round Multisensor Logger, black circles = moisture and density analysis from discrete samples), porosity, water content, and grain density, Site U1407. Core recovery: black = recovered, white = not recovered, red = core overlap. Horizontal gray lines indicate lithostratigraphic unit boundaries (see “[Lithostratigraphy](#)”). APC = advanced piston corer, DI = drilled interval, XCB = extended core barrel.

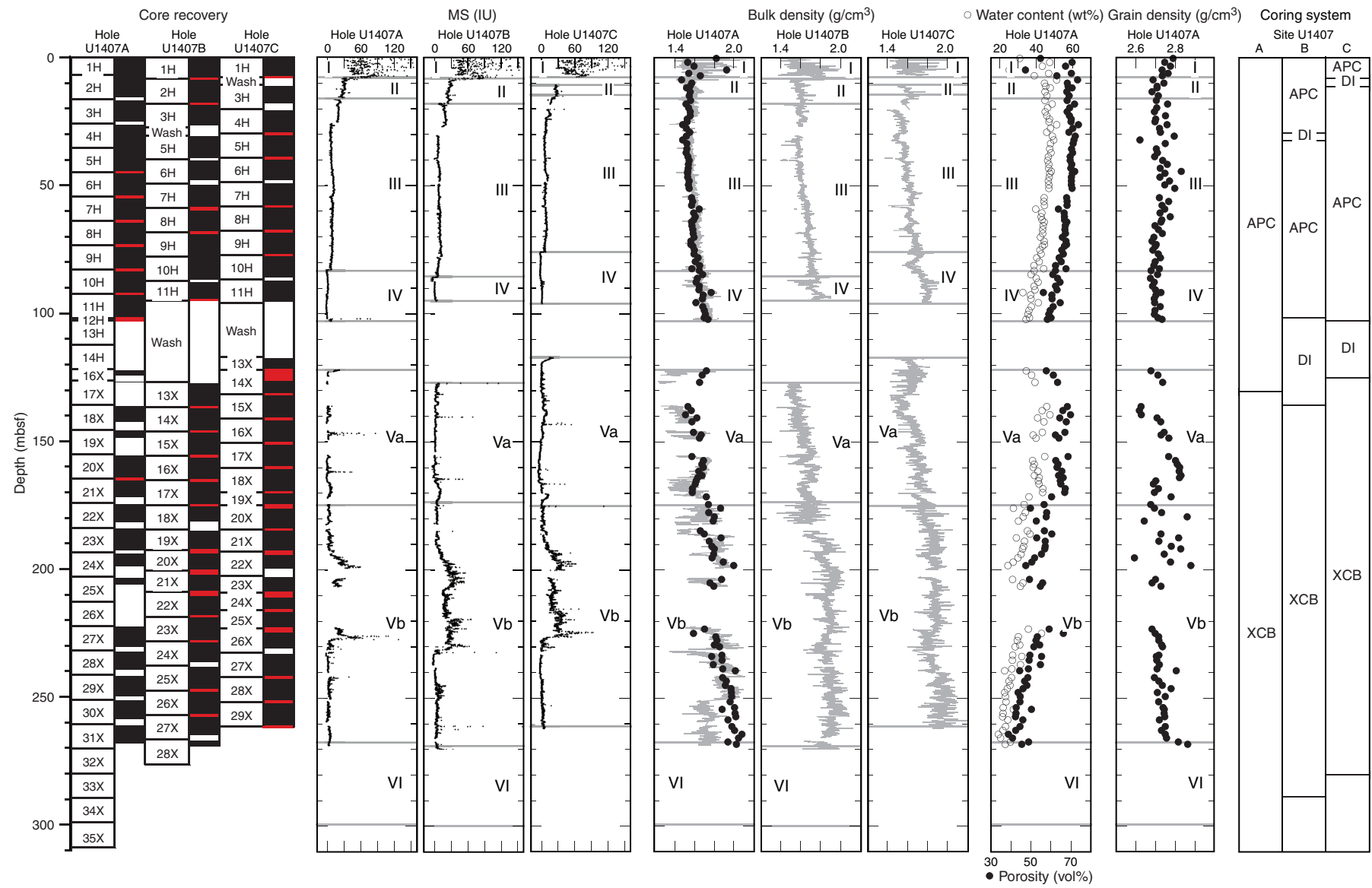


Figure F35. Plots of magnetic susceptibility (MS), P-wave velocity (gray line = P-wave logger data from Whole-Round Multisensor Logger, black circles = P-wave caliper probe data from working section halves), and natural gamma radiation (NGR), Site U1407. Core recovery: black = recovered, white = not recovered, red = core overlap. Horizontal gray lines indicate lithostratigraphic unit boundaries (see “[Lithostratigraphy](#)”). APC = advanced piston corer, DI = drilled interval, XCB = extended core barrel.

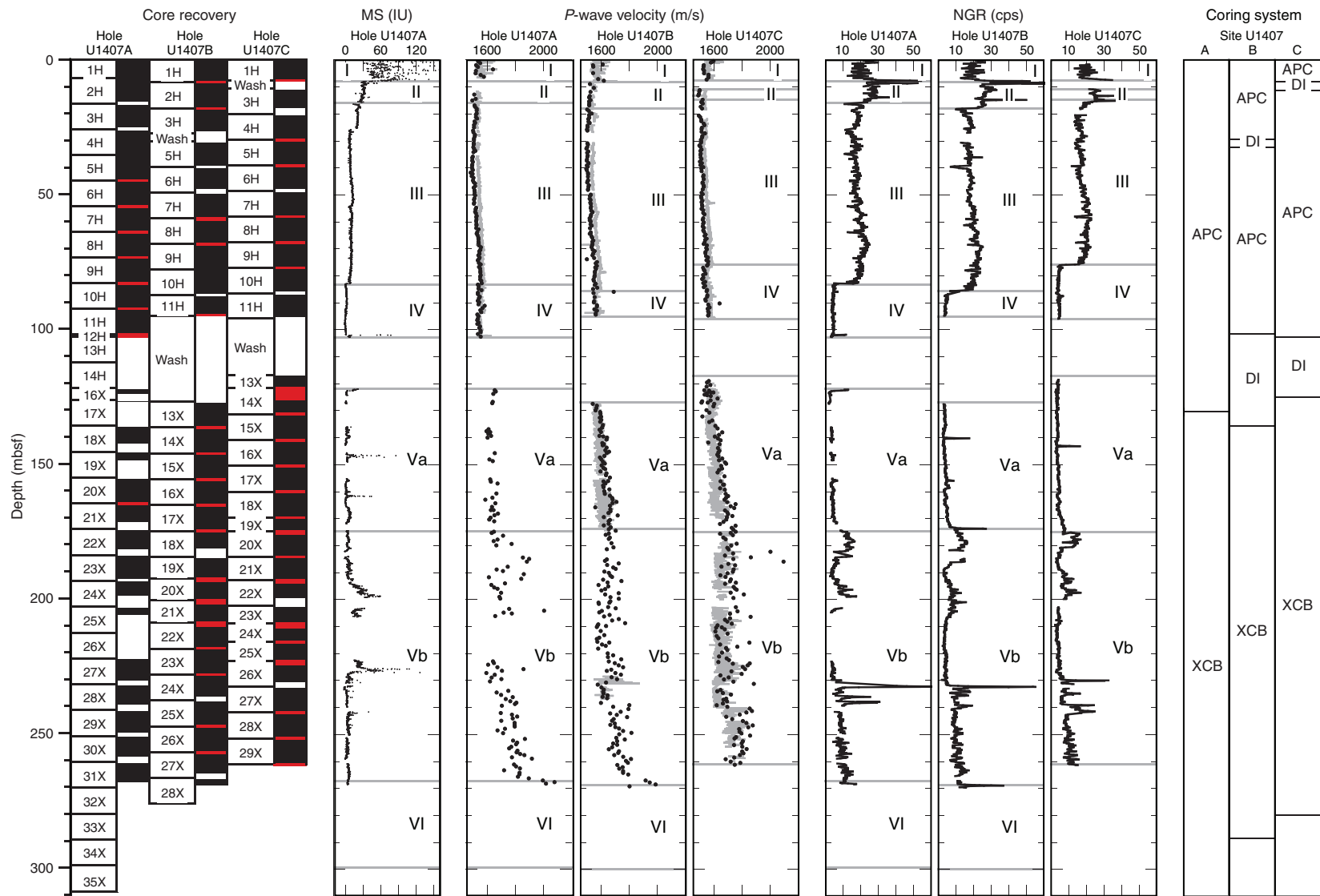


Figure F36. Plots of magnetic susceptibility (MS) and color reflectance (a^* , b^* , and L^*), Site U1407. Core recovery: black = recovered, white = not recovered, red = core overlap. Horizontal gray lines indicate lithostratigraphic unit boundaries (see “[Lithostratigraphy](#)”). APC = advanced piston corer, DI = drilled interval, XCB = extended core barrel.

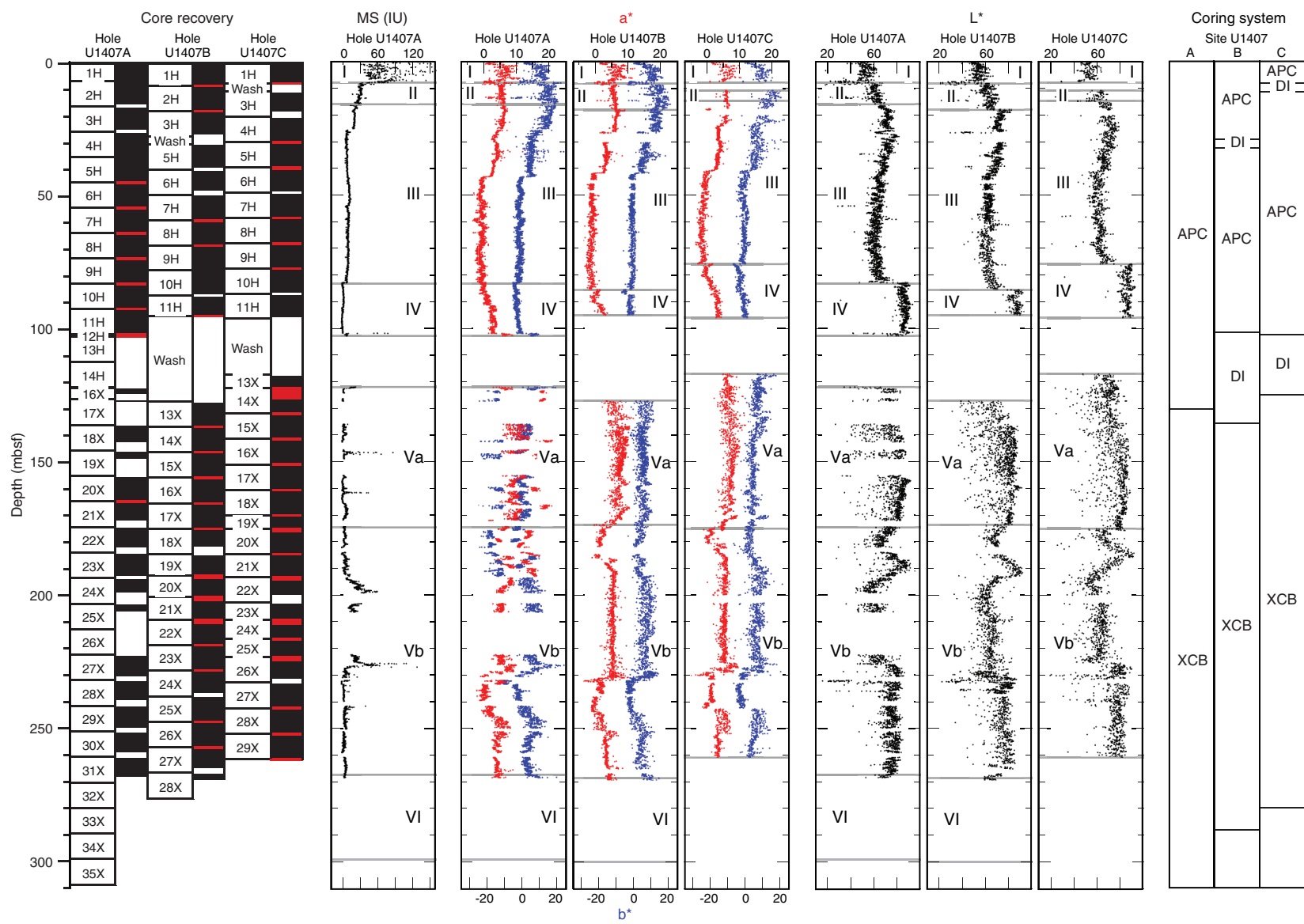


Figure F37. Plots of magnetic susceptibility data, Site U1407. Top panels show the spliced section for each interval of the splice. Bottom panels show all complete magnetic susceptibility records. Data from Holes U1407B and U1407C are offset by 10 and 20 IU, respectively, to aid visualization. Open circles indicate core tops. A. 0–50 m CCSF. (Continued on next six pages.)

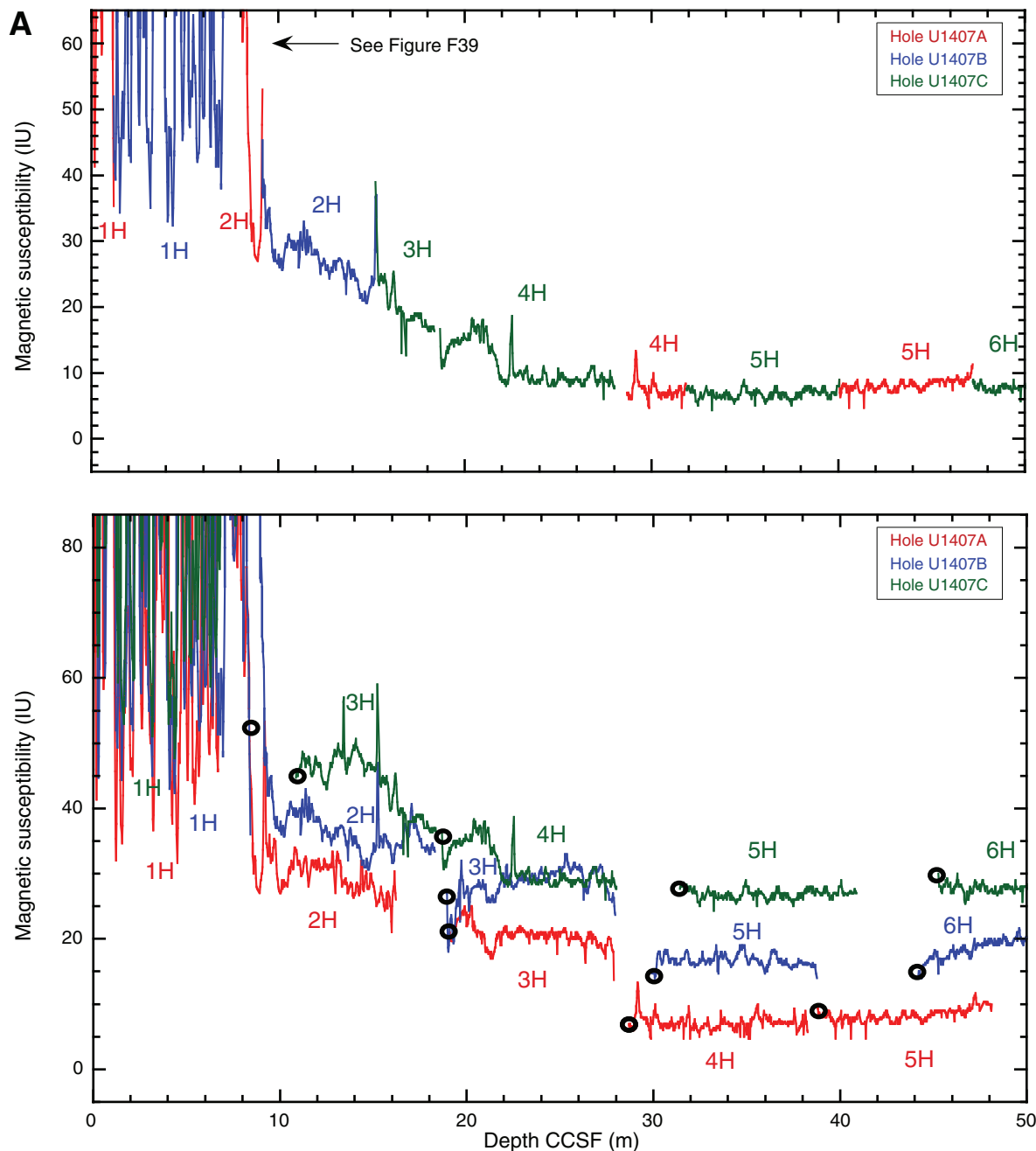


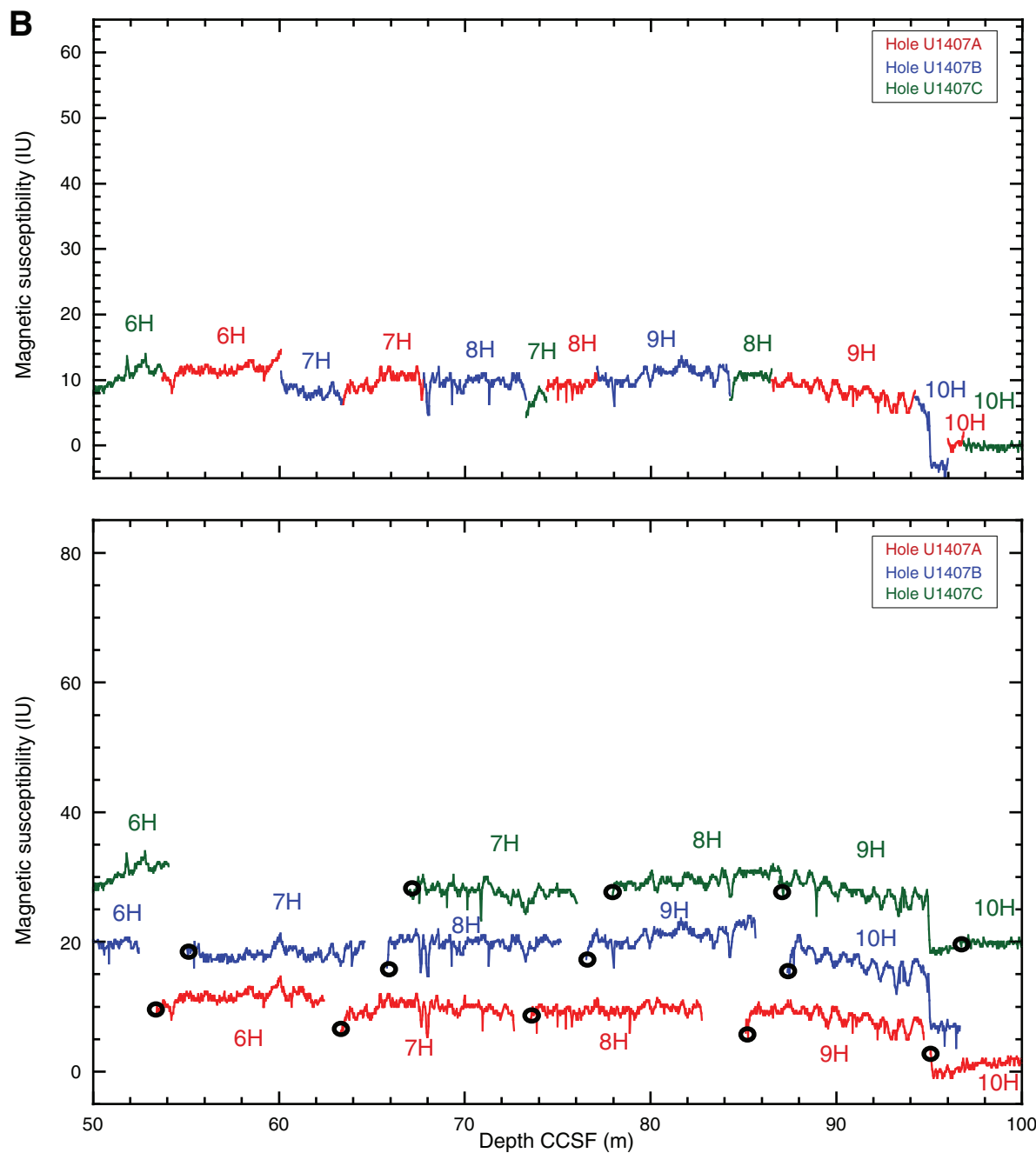
Figure F37 (continued). B. 50–100 m CCSF. (Continued on next page.)

Figure F37 (continued). C. 100–150 m CCSF. (Continued on next page.)

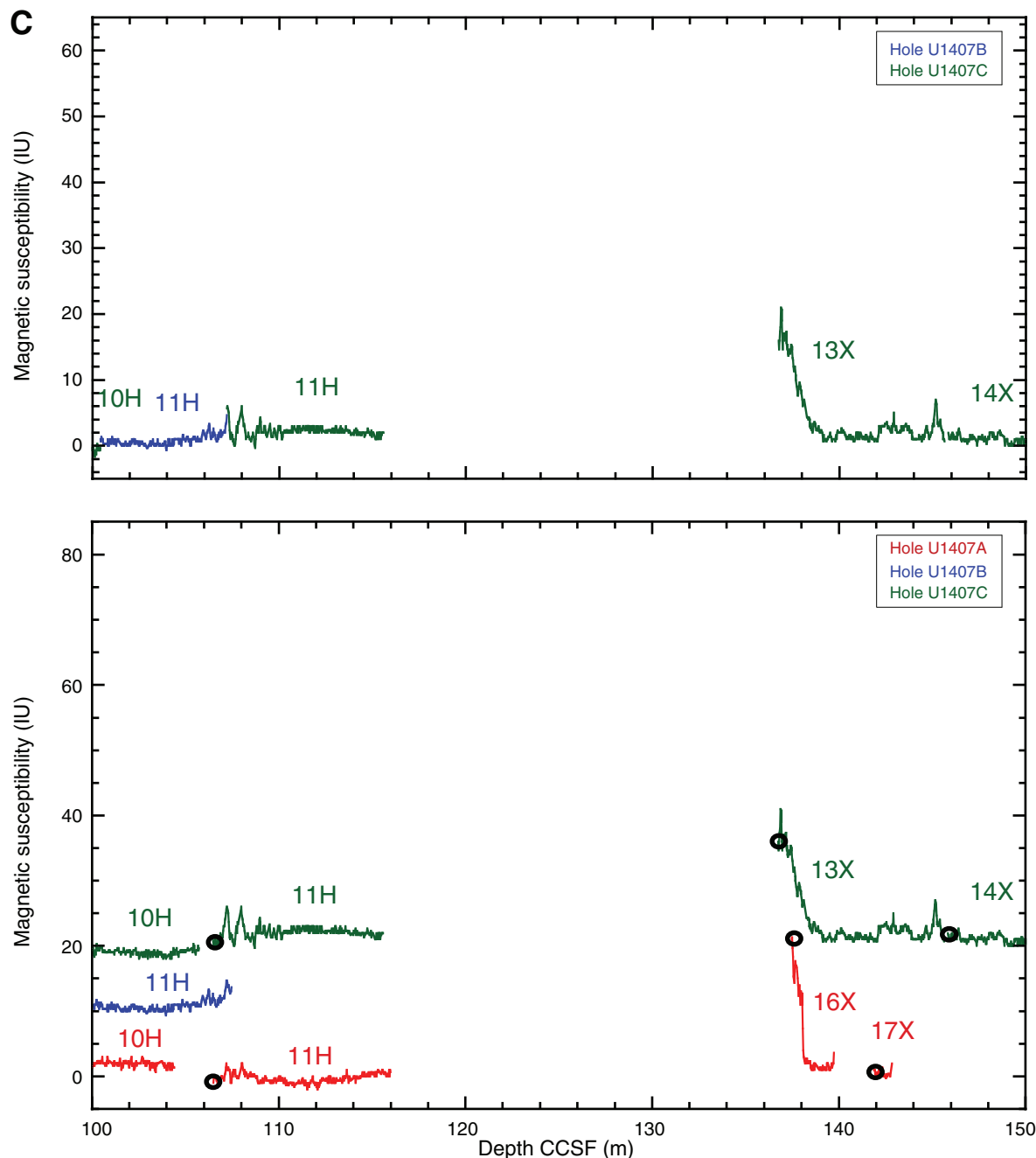


Figure F37 (continued). D. 150–200 m CCSF. (Continued on next page.)

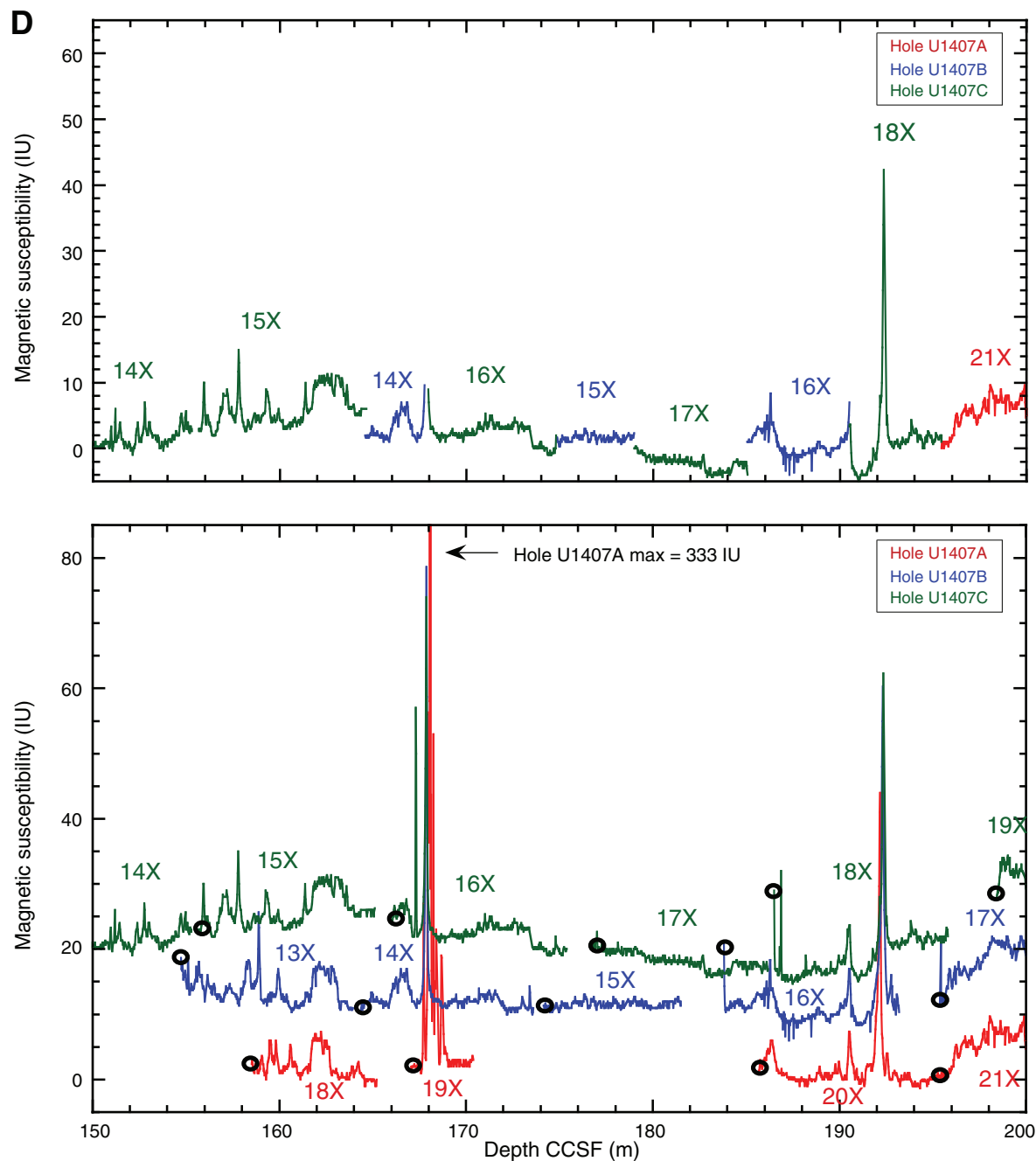


Figure F37 (continued). E. 200–250 m CCSF. (Continued on next page.)

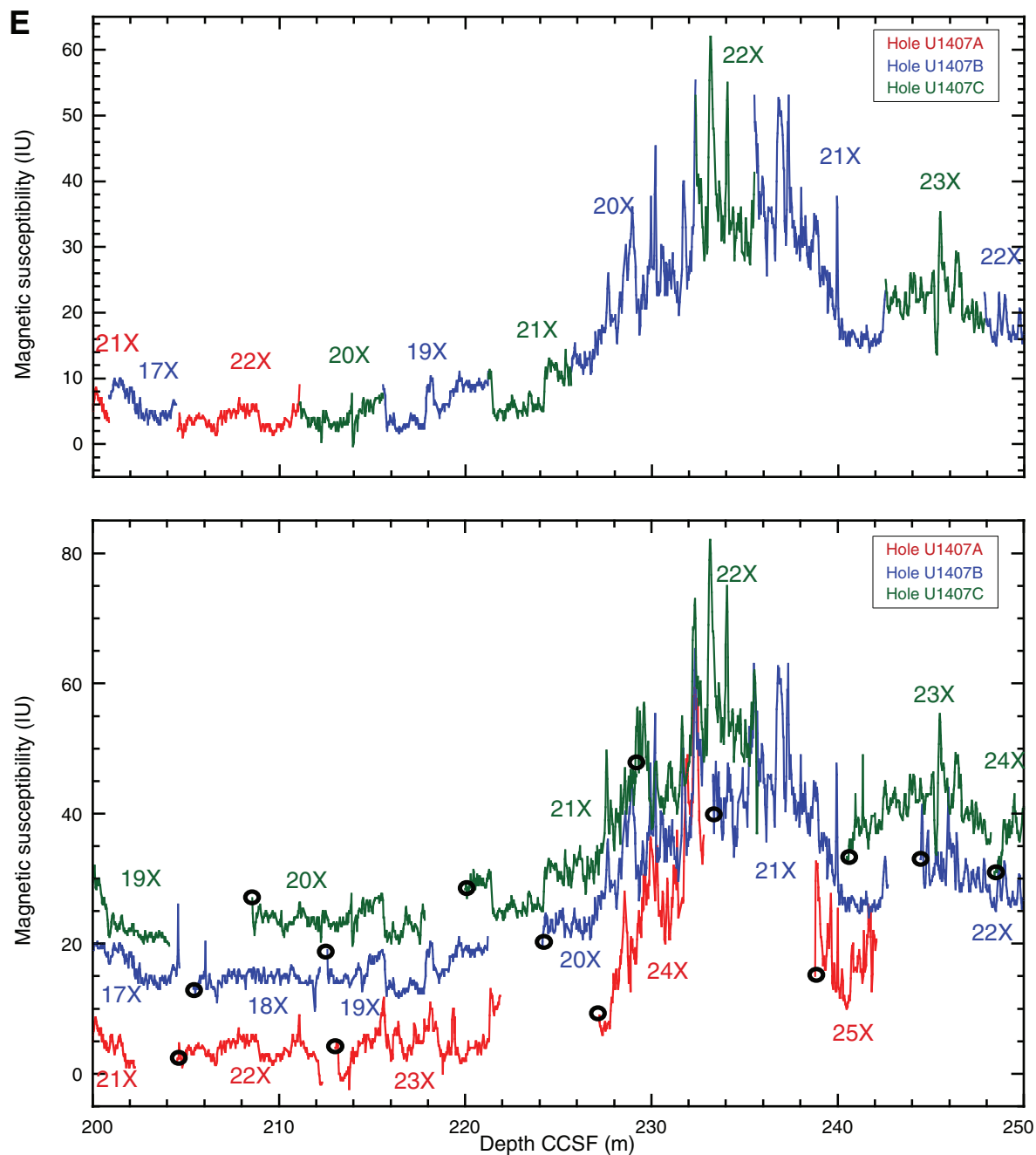


Figure F37 (continued). F. 250–300 m CCSF. (Continued on next page.)

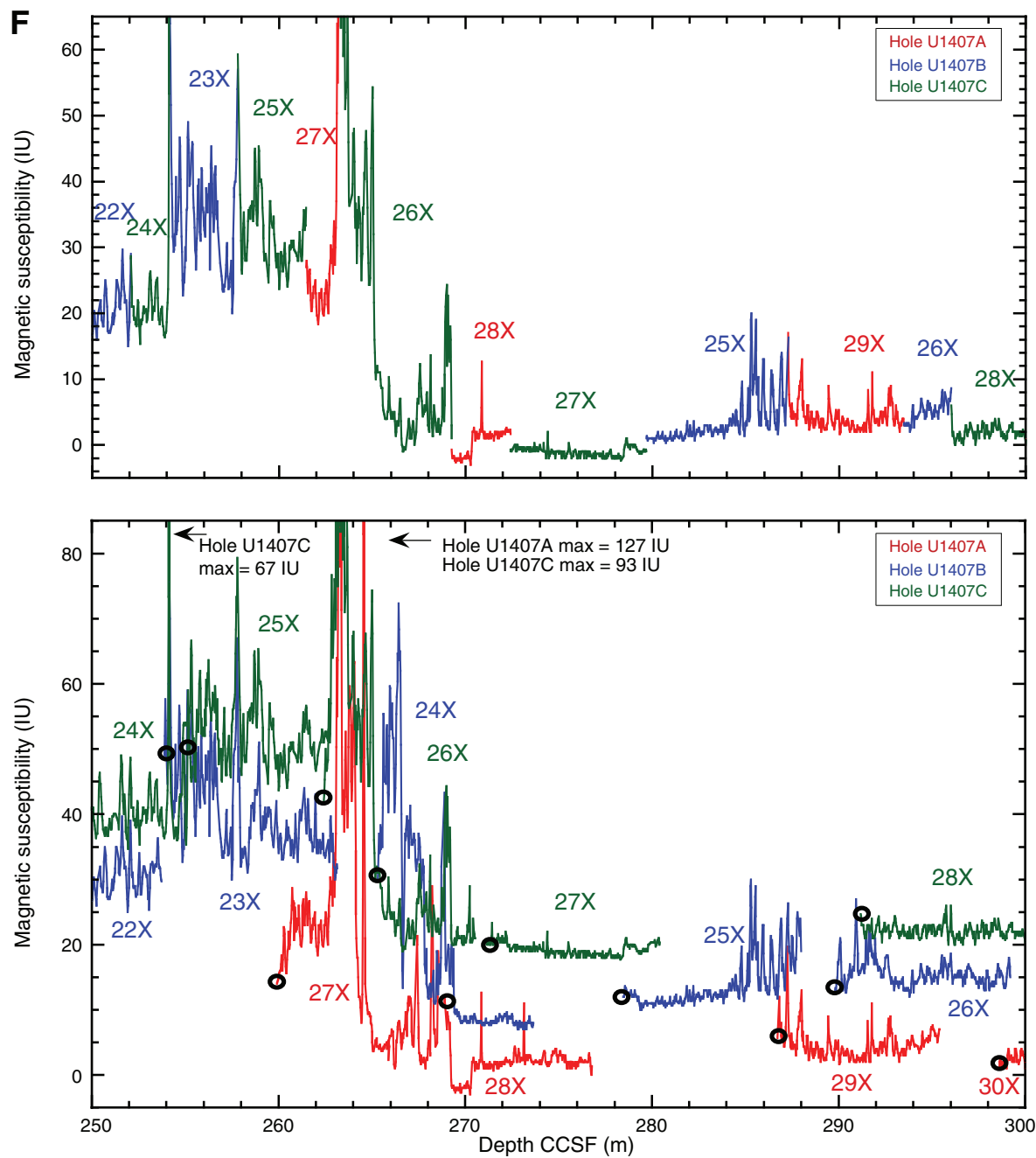


Figure F37 (continued). G. 300–350 m CCSF.

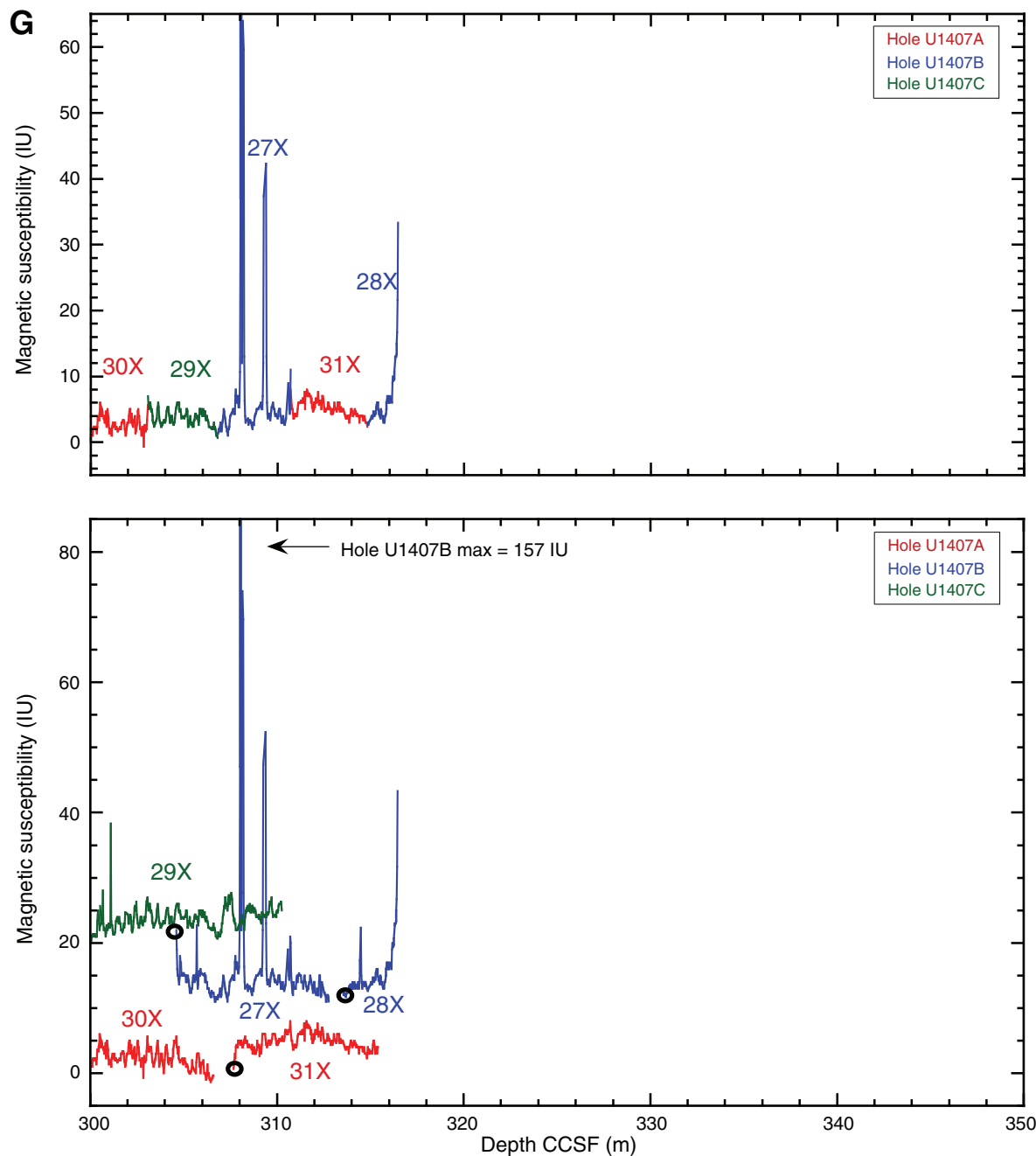


Figure F38. Plot of mbsf depth vs. CCSF depth, Site U1407. The growth factor is equal to the slope of the regression line.

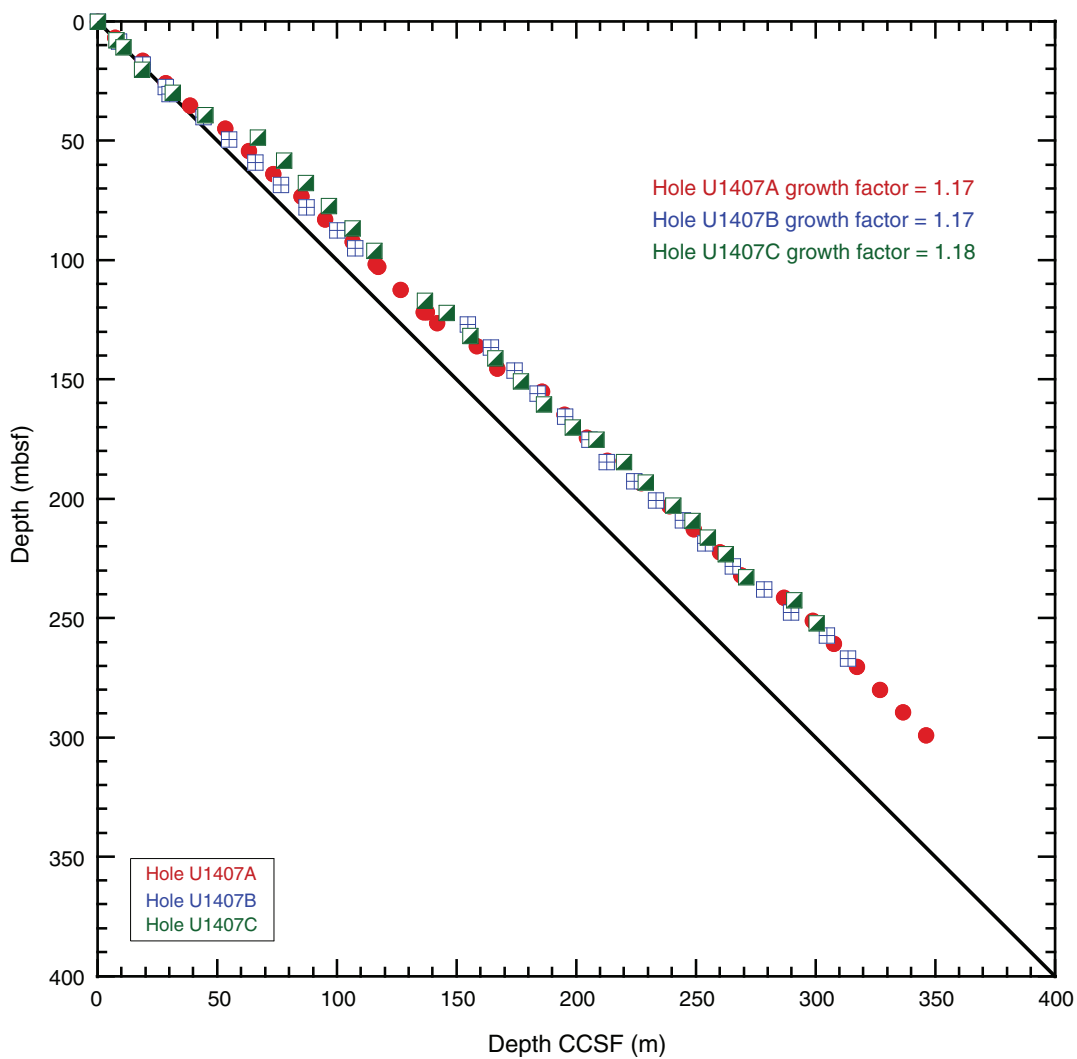


Figure F39. Plot of magnetic susceptibility data from 0–10 m CCSF, Site U1407. Note the large-amplitude cycles in magnetic susceptibility in Pleistocene lithostratigraphic Unit I.

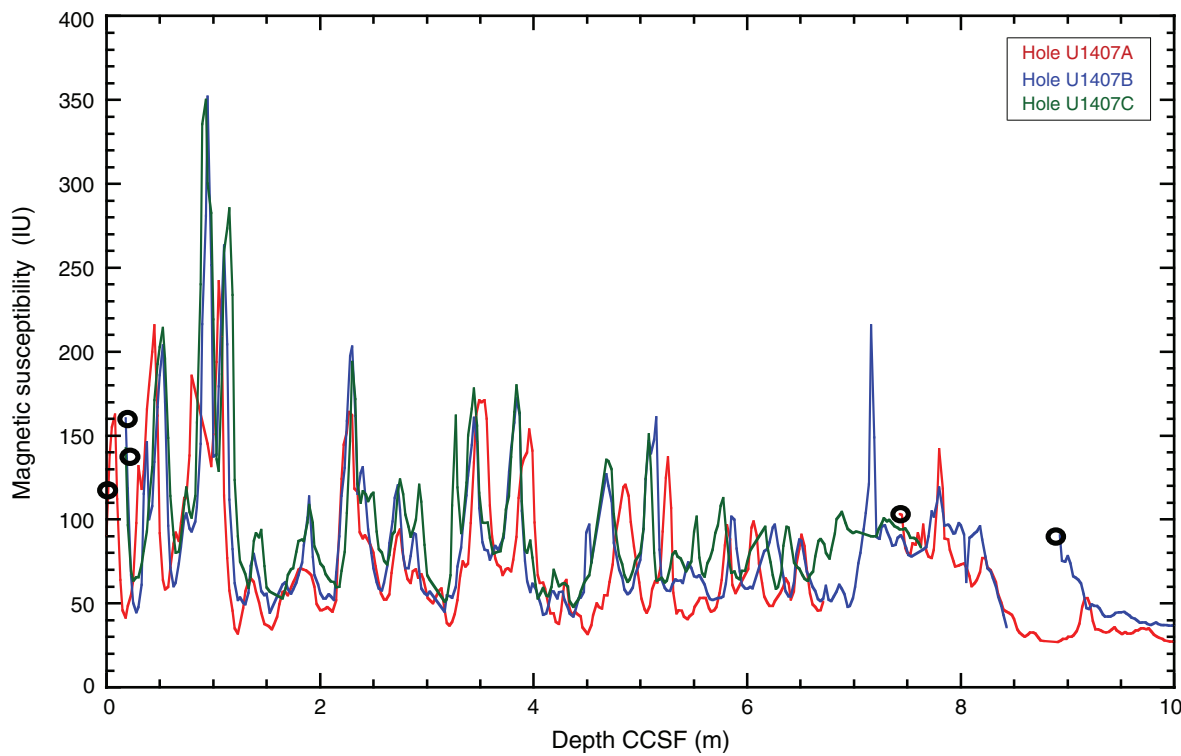


Figure F40. Plots of natural gamma radiation (NGR) data, Site U1407. Data from Holes U1407B and U1407C are offset by 10 and 20 cps, respectively, to aid visualization. Open circles indicate core tops. A. 0–50 m CCSF. B. 50–100 m CCSF. (Continued on next three pages.)

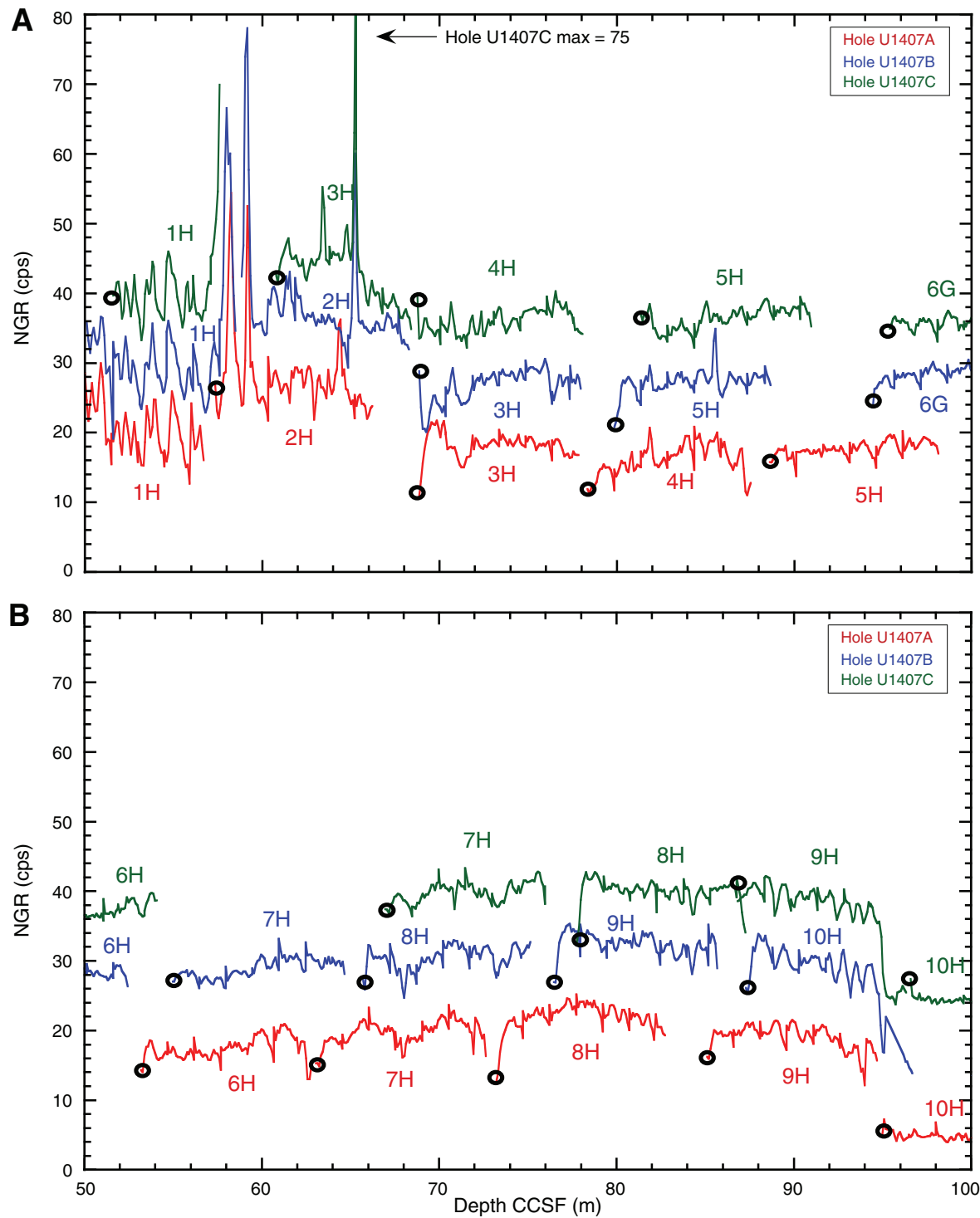


Figure F40 (continued). C. 100–150 m CCSF. D. 150–200 m CCSF. (Continued on next page.)

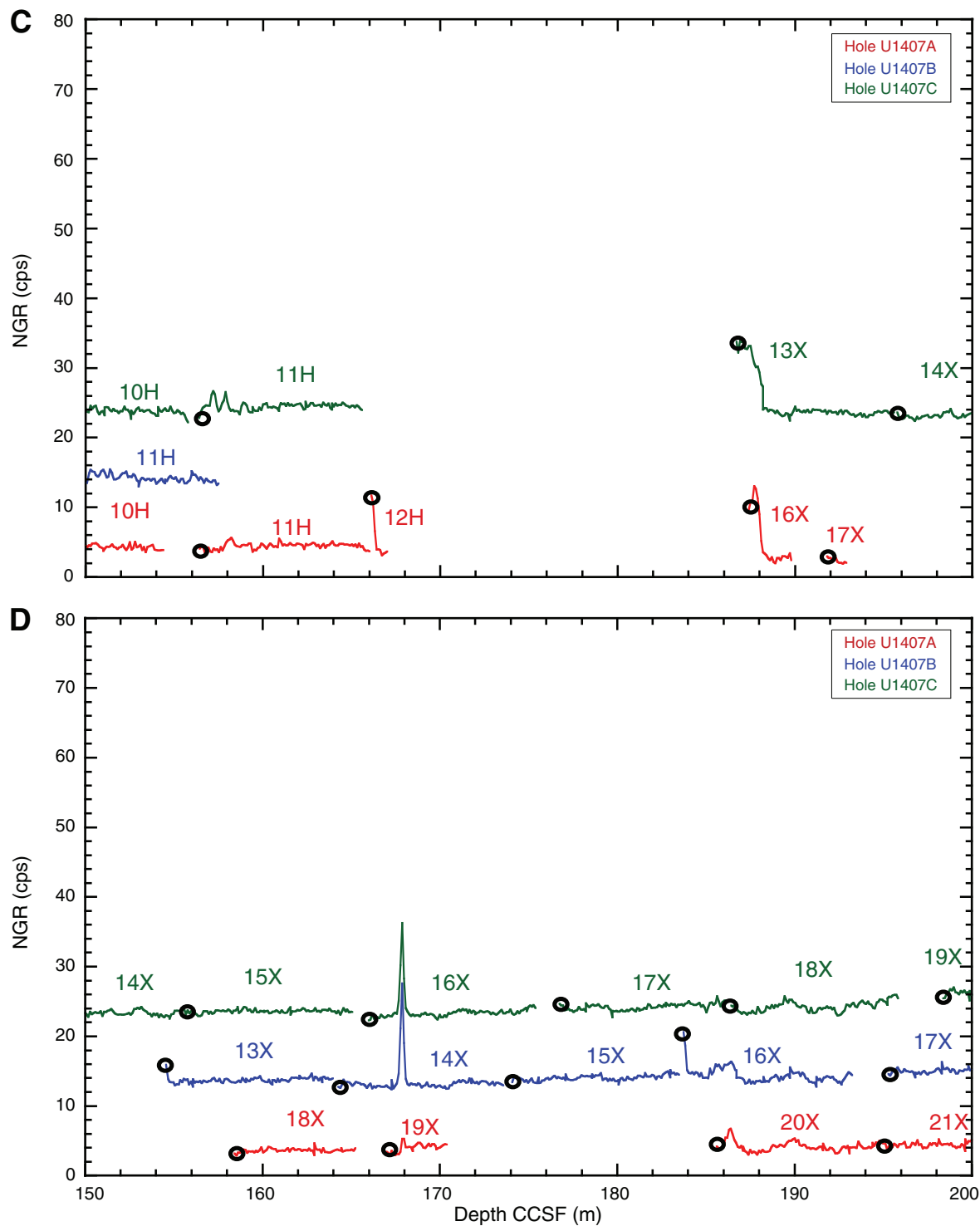


Figure F40 (continued). E. 200–250 m CCSF. F. 250–300 m CCSF. (Continued on next page.)

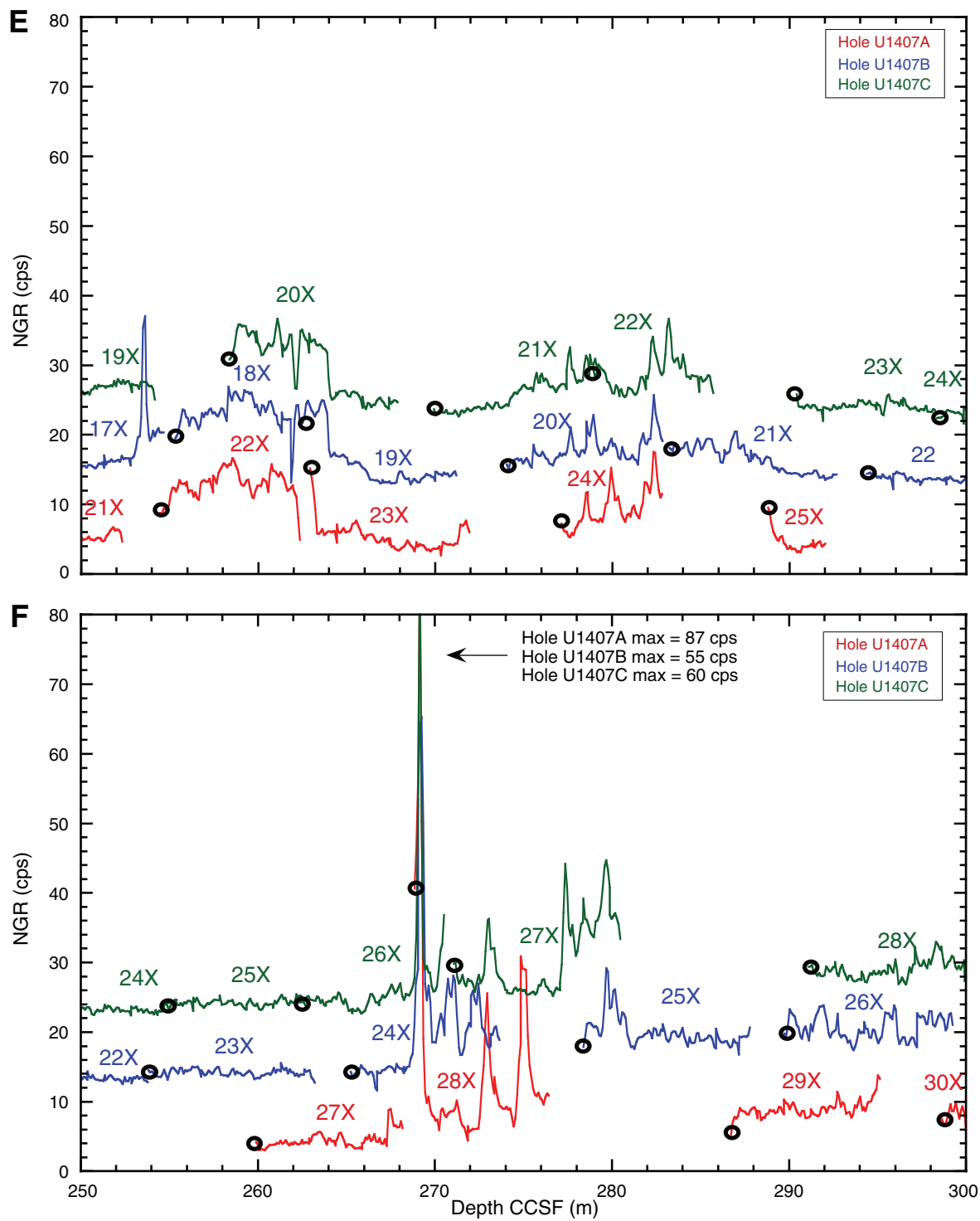


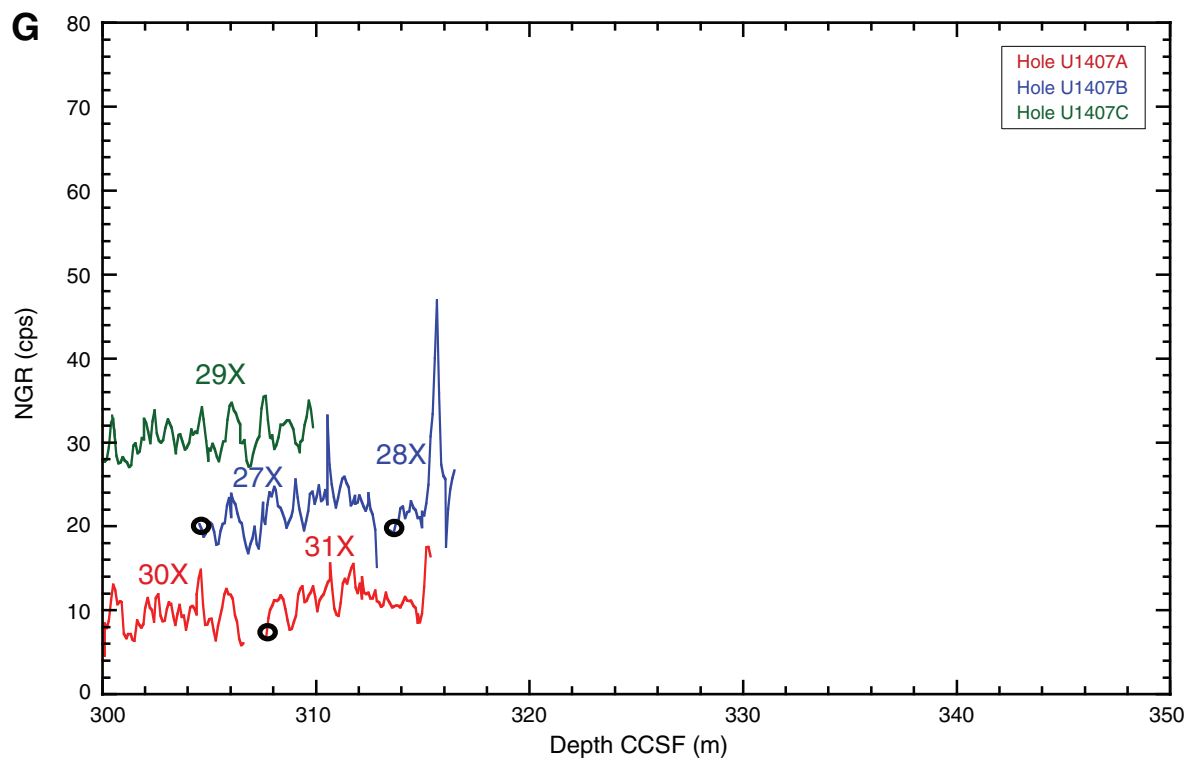
Figure F40 (continued). G. 300–350 m CCSF.

Table T1. Coring summary, Site U1407. (Continued on next page.)

Core, section	Date (2012)	Time UTC (h)	Depth DSF (m)			Depth CSF-A (m)				
			Top of cored interval	Bottom of cored interval	Interval cored (m)	Curated length (m)	Top of core	Bottom of core	Recovery (%)	Sections (N)
342-U1407A-										
1H	7 Jul	1945	0.0	6.8	6.8	6.81	0.00	6.81	100	6
2H	7 Jul	2040	6.8	16.3	9.5	9.17	6.80	15.97	97	8
3H	7 Jul	2125	16.3	25.8	9.5	9.25	16.30	25.55	97	8
4H	7 Jul	2205	25.8	35.3	9.5	9.50	25.80	35.30	100	8
5H	7 Jul	2245	35.3	44.8	9.5	9.79	35.30	45.09	103	8
6H	7 Jul	2330	44.8	54.3	9.5	9.92	44.80	54.72	104	8
7H	8 Jul	0015	54.3	63.8	9.5	9.89	54.30	64.19	104	8
8H	8 Jul	0100	63.8	73.3	9.5	9.85	63.80	73.65	104	8
9H	8 Jul	0150	73.3	82.8	9.5	9.88	73.30	83.18	104	8
10H	8 Jul	0235	82.8	92.3	9.5	9.57	82.80	92.37	101	8
11H	8 Jul	0320	92.3	101.8	9.5	9.79	92.30	102.09	103	8
12H	8 Jul	0455	101.8	102.8	1.0	1.08	101.80	102.88	108	2
13H	8 Jul	0550	102.8	112.3	9.5	0.00	102.80	102.80	0	0
14H	8 Jul	0635	112.3	121.8	9.5	0.01	112.30	112.31	0	1
15H	8 Jul	0730	121.8	121.9	0.1	0.03	121.80	121.83	30	1
16X	8 Jul	0930	121.9	126.3	4.4	2.76	121.90	124.66	63	3
17X	8 Jul	1055	126.3	135.9	9.6	1.32	126.30	127.62	14	2
18X	8 Jul	1155	135.9	145.5	9.6	7.05	135.90	142.95	73	6
19X	8 Jul	1345	145.5	155.1	9.6	3.80	145.50	149.30	40	4
20X	8 Jul	1445	155.1	164.7	9.6	9.77	155.10	164.87	102	8
21X	8 Jul	1545	164.7	174.3	9.6	7.56	164.70	172.26	79	6
22X	8 Jul	1705	174.3	183.9	9.6	7.99	174.30	182.29	83	6
23X	8 Jul	1755	183.9	193.5	9.6	9.25	183.90	193.15	96	7
24X	8 Jul	1900	193.5	203.1	9.6	5.93	193.50	199.43	62	5
25X	8 Jul	2000	203.1	212.7	9.6	3.55	203.10	206.65	37	4
26X	8 Jul	2040	212.7	222.3	9.6	0.00	212.70	212.70	0	0
27X	8 Jul	2125	222.3	231.9	9.6	8.72	222.30	231.02	91	7
28X	8 Jul	2225	231.9	241.5	9.6	7.96	231.90	239.86	83	7
29X	8 Jul	2335	241.5	251.1	9.6	8.78	241.50	250.28	91	7
30X	9 Jul	0110	251.1	260.7	9.6	8.27	251.10	259.37	86	7
31X	9 Jul	0255	260.7	270.3	9.6	7.96	260.70	268.66	83	7
32X	9 Jul	0435	270.3	279.9	9.6	0.06	270.30	270.36	1	1
33X	9 Jul	0610	279.9	289.5	9.6	0.17	279.90	280.07	2	1
34X	9 Jul	0825	289.5	299.1	9.6	0.09	289.50	289.59	1	1
35X	9 Jul	1045	299.1	308.7	9.6	0.11	299.10	299.21	1	1
			Totals:	308.7	205.64			67	180	
342-U1407B-										
1H	9 Jul	1445	0.0	8.4	8.4	8.49	0.00	8.49	101	7
2H	9 Jul	1530	8.4	17.9	9.5	9.64	8.40	18.04	101	8
3H	9 Jul	1615	17.9	27.4	9.5	9.24	17.90	27.14	97	7
4H	9 Jul	1630					****Drilled from 27.4 to 30.4 m DSF****			
5H	9 Jul	1655	30.4	39.9	9.5	9.43	30.40	39.83	99	7
6H	9 Jul	1740	39.9	49.4	9.5	8.45	39.90	48.35	89	6
7H	9 Jul	1830	49.4	58.9	9.5	9.96	49.40	59.36	105	8
8H	9 Jul	1905	58.9	68.4	9.5	9.81	58.90	68.71	103	8
9H	9 Jul	1955	68.4	77.9	9.5	9.51	68.40	77.91	100	7
10H	9 Jul	2040	77.9	87.4	9.5	9.48	77.90	87.38	100	7
11H	9 Jul	2125	87.4	95.0	7.6	7.61	87.40	95.01	100	6
12H	9 Jul	2345	95.0	127.0	32.0	0.00	95.00	95.00	0	0
13X	10 Jul	0035	127.0	136.6	9.6	9.73	127.00	136.73	101	8
14X	10 Jul	0120	136.6	146.2	9.6	9.68	136.60	146.28	101	8
15X	10 Jul	0200	146.2	155.8	9.6	9.78	146.20	155.98	102	8
16X	10 Jul	0250	155.8	165.4	9.6	9.82	155.80	165.62	102	8
17X	10 Jul	0340	165.4	175.0	9.6	9.71	165.40	175.11	101	8
18X	10 Jul	0520	175.0	184.6	9.6	7.07	175.00	182.07	74	6
19X	10 Jul	0610	184.6	192.6	8.0	8.95	184.60	193.55	112	7
20X	10 Jul	0710	192.6	200.6	8.0	9.24	192.60	201.84	116	7
21X	10 Jul	0755	200.6	209.1	8.5	9.71	200.60	210.31	114	8
22X	10 Jul	0840	209.1	218.7	9.6	9.62	209.10	218.72	100	8
23X	10 Jul	0930	218.7	228.3	9.6	9.61	218.70	228.31	100	8
24X	10 Jul	1030	228.3	237.9	9.6	8.78	228.30	237.08	91	8
25X	10 Jul	1125	237.9	247.5	9.6	9.78	237.90	247.68	102	8
26X	10 Jul	1225	247.5	257.1	9.6	9.94	247.50	257.44	104	8
27X	10 Jul	1335	257.1	266.7	9.6	8.38	257.10	265.48	87	7
28X	10 Jul	1435	266.7	276.3	9.6	3.12	266.70	269.82	33	3
			Totals:	276.3	234.54			91	189	

Table T1 (continued).

Core, section	Date (2012)	Time UTC (h)	Depth DSF (m)				Depth CSF-A (m)			
			Top of cored interval	Bottom of cored interval	Interval cored (m)	Curated length (m)	Top of core	Bottom of core	Recovery (%)	Sections (N)
342-U1407C-										
1H	10 Jul	1800	0.0	7.7	7.7	7.78	0.00	7.78	101	7
21	10 Jul	1820			****Drilled from 7.7 to 10.7 m DSF****					
3H	10 Jul	1840	10.7	20.2	9.5	7.84	10.70	18.54	83	7
4H	10 Jul	1930	20.2	29.7	9.5	9.77	20.20	29.97	103	8
5H	10 Jul	2040	29.7	39.2	9.5	9.90	29.70	39.60	104	8
6H	10 Jul	2125	39.2	48.7	9.5	9.30	39.20	48.50	98	8
7H	10 Jul	2215	48.7	58.2	9.5	9.60	48.70	58.30	101	7
8H	10 Jul	2300	58.2	67.7	9.5	9.85	58.20	68.05	104	8
9H	10 Jul	2350	67.7	77.2	9.5	9.61	67.70	77.31	101	7
10H	11 Jul	0035	77.2	86.7	9.5	9.36	77.20	86.56	99	8
11H	11 Jul	0110	86.7	96.0	9.3	9.35	86.70	96.05	101	8
121	11 Jul	0305			****Drilled from 96.0 to 117.0 m DSF****					
13X	11 Jul	0355	117.0	122.0	5.0	9.06	117.00	126.06	181	7
14X	11 Jul	0440	122.0	131.6	9.6	9.80	122.00	131.80	102	8
15X	11 Jul	0525	131.6	141.2	9.6	9.88	131.60	141.48	103	8
16X	11 Jul	0630	141.2	150.8	9.6	9.75	141.20	150.95	102	8
17X	11 Jul	0715	150.8	160.4	9.6	9.71	150.80	160.51	101	8
18X	11 Jul	0800	160.4	170.0	9.6	9.71	160.40	170.11	101	8
19X	11 Jul	0845	170.0	175.0	5.0	6.09	170.00	176.09	122	5
20X	11 Jul	1000	175.0	184.6	9.6	9.70	175.00	184.70	101	8
21X	11 Jul	1050	184.6	193.1	8.5	9.61	184.60	194.21	113	8
22X	11 Jul	1145	193.1	202.7	9.6	7.15	193.10	200.25	74	6
23X	11 Jul	1315	202.7	209.2	6.5	8.06	202.70	210.76	124	7
24X	11 Jul	1400	209.2	216.2	7.0	7.38	209.20	216.58	105	6
25X	11 Jul	1440	216.2	223.2	7.0	8.21	216.20	224.41	117	7
26X	11 Jul	1530	223.2	232.8	9.6	8.46	223.20	231.66	88	7
27X	11 Jul	1615	232.8	242.4	9.6	9.71	232.80	242.51	101	8
28X	11 Jul	1720	242.4	252.0	9.6	9.87	242.40	252.27	103	8
29X	11 Jul	1900	252.0	261.6	9.6	9.85	252.00	261.85	103	8
Totals:			261.6	244.36			98	201		
Site U1407 totals:			846.6	684.54			85	570		

DSF = drilling depth below seafloor, CSF-A = core depth below seafloor, method A. H = advanced piston core, X = extended core barrel core, numeric core type = drilled interval.



Table T2. Lithostratigraphic unit intervals, Site U1407.

Lith. unit	Core, section, interval (cm)		Depth (mbsf)	
	Top	Bottom	Top	Bottom
342-U1407A-				
I	1H-1, 0	2H-1, 95	0.00	7.75
II	2H-1, 95	2H-CC, 17	7.75	15.89
III	3H-1, 0	9H-CC, 25	16.30	83.18
IV	10H-1, 0	12H-1, 100	82.80	102.80
Va	16X-1, 0	22X-1, 30	121.90	174.60
Vb	22X-1, 30	31X-5, 60	174.60	267.30
VI	31X-5, 107	35X-CC, 8	267.77	299.18
342-U1407B-				
I	1H-1, 0	1H-6, 64	0.00	8.14
II	1H-6, 64	2H-CC, 14	8.14	18.04
III	3H-1, 0	10H-6, 10	17.90	85.50
IV	10H-6, 10	11H-CC, 6	85.50	95.01
Va	13X-1, 0	17X-6, 74	127.00	173.59
Vb	17X-6, 74	28X-2, 46	173.59	268.66
VI	28X-2, 46	28X-CC, 49	268.66	269.82
342-U1407C-				
I	1H-1, 0	1H-CC, 11	0.00	7.70
II	3H-1, 0	3H-3, 93	10.70	14.63
III	3H-3, 93	9H-6, 66	14.63	75.86
IV	9H-6, 66	11H-CC, 10	75.86	96.05
Va	13X-1, 0	19X-CC, 46	117.00	176.01
Vb	20X-1, 0	29X-CC, 38	175.00	261.79
VI	Not drilled			

Table T3. Calcareous nannofossil datums, Site U1407. (Continued on next page.)

Hole, core, section, interval (cm)	Top	Bottom	Age	Zone/Subzone	Marker species	Age (Ma)	Depth (mbsf)			
							Top	Bottom	Mid-point	±
342-	342-									
				Pleistocene						
U1407A-1H-1, 37	U1407A-1H-1, 37		NN21	Ba <i>Emiliana huxleyi</i>	0.70	0.37	0.37	0.37	0.00	
U1407A-1H-1, 37	U1407A-1H-4, 20		NN20	T <i>Pseudoemiliana lacunosa</i>	0.44	0.37	4.70	2.54	2.17	
U1407A-2H-6, 110	U1407A-2H-CC		NP23	T <i>Reticulofenestra umbilicus</i> (>14 µm)	32.02	14.28	15.95	15.12	0.84	
U1407A-2H-CC	U1407A-3H-1, 110			T <i>Isthmolithus recurvus</i>	32.49	15.95	17.41	16.68	0.73	
U1407A-2H-CC	U1407A-3H-1, 110		NP22	T <i>Coccolithus formosus</i>	32.92	15.95	17.41	16.68	0.73	
U1407A-2H-CC	U1407A-3H-1, 110		NP21	T <i>Discoaster saipanensis</i>	34.44	15.95	17.41	16.68	0.73	
U1407A-3H-1, 110	U1407A-3H-2, 110			T <i>Discoaster barbadiensis</i>	34.76	17.41	18.91	18.16	0.75	
U1407A-3H-1, 110	U1407A-3H-2, 110		NP19/NP20	B <i>Isthmolithus recurvus</i>	36.97	17.41	18.91	18.16	0.75	
U1407A-3H-1, 110	U1407A-3H-2, 110		NP18	Bc <i>Chiasmolithus oamaruensis</i>	38.09	17.41	18.91	18.16	0.75	
U1407A-3H-1, 110	U1407A-3H-2, 110		NP17	T <i>Chiasmolithus solitus</i>	40.40	17.41	18.91	18.16	0.75	
U1407A-3H-1, 110	U1407A-3H-2, 110			B <i>Reticulofenestra umbilicus</i> (>14 µm)	41.94	17.41	18.91	18.16	0.75	
U1407A-3H-1, 110	U1407A-3H-2, 110			T <i>Nannotetraena fulgens</i>	42.87	17.41	18.91	18.16	0.75	
U1407A-3H-1, 110	U1407A-3H-2, 110		NP15c	T <i>Chiasmolithus gigas</i>	44.12	17.41	18.91	18.16	0.75	
U1407A-5H-4, 110	U1407A-5H-6, 96		NP15b	B <i>Chiasmolithus gigas</i>	45.49	40.91	43.77	42.34	1.43	
U1407A-7H-6, 110	U1407A-7H-CC		NP15a	B <i>Nannotetraena fulgens</i>	46.29	62.91	64.16	63.54	0.63	
U1407A-9H-CC	U1407A-10H-2, 100			B <i>Nannotetraena cristata</i>	47.73	83.16	85.31	84.24	1.08	
U1407A-9H-6, 57	U1407A-9H-CC			T <i>Discoaster lodoensis</i>	47.41	81.37	83.16	82.27	0.89	
U1407A-9H-CC	U1407A-10H-2, 100			B <i>Blackites inflatus</i>	47.84	83.16	85.31	84.24	1.08	
U1407A-10H-6, 100	U1407A-10H-CC		NP14	B <i>Discoaster sublodoensis</i>	49.11	91.31	92.32	91.82	0.50	
U1407A-11H-CC	U1407A-12H-1, 15			B <i>Dictyococcites/Reticulofenestra*</i>	49.47	101.75	101.95	101.85	0.10	
U1407A-11H-CC	U1407A-12H-1, 15		NP13	T <i>Tribrachiatus orthostylus</i> *	49.47	101.75	101.95	101.85	0.10	
U1407A-11H-CC	U1407A-12H-1, 15			T <i>Toweius</i> spp.*	50.78	101.75	101.95	101.85	0.10	
U1407A-11H-CC	U1407A-12H-1, 15			B <i>Coccolithus crassus</i> *	51.64	101.75	101.95	101.85	0.10	
U1407A-14H-CC	U1407A-15H-CC		NP12	B <i>Discoaster lodoensis</i>	53.70	112.31	121.82	121.90	0.08	
U1407A-15H-CC	U1407A-16X-1, 8		NP11	T <i>Tribrachiatus contortus</i>	54.17	121.82	121.98	121.90	0.08	
U1407A-15H-CC	U1407A-16X-1, 8			B <i>Sphenolithus radians</i>	54.17	121.82	121.98	121.90	0.08	
U1407A-15H-CC	U1407A-16X-1, 8			B <i>Tribrachiatus orthostylus</i>	54.37	121.82	121.98	121.90	0.08	
U1407A-15H-CC	U1407A-16X-1, 8			B <i>Discoaster diastypus</i>	54.95	121.82	121.98	121.90	0.08	
U1407A-15H-CC	U1407A-16X-1, 8			T <i>Fasciculithus</i> spp.	55.64	121.82	121.98	121.90	0.08	
			Paleocene							
U1407A-15H-CC	U1407A-16X-1, 8			<i>Fasciculithus</i> diversity decline†	56.00	121.82	121.98	121.90	0.08	
U1407A-15H-CC	U1407A-16X-1, 8			T <i>Fasciculithus alani</i> †	56.00	121.82	121.98	121.90	0.08	
U1407A-16X-CC	U1407A-17X-CC			T <i>Ericsonia robusta</i> (>9 µm)†	57.10	124.61	127.57	126.09	1.48	
U1407A-17X-CC	U1407A-18X-1, 88		NP9	B <i>Discoaster multiradiatus</i>	57.21	127.57	136.78	132.18	4.61	
U1407A-18X-1, 88	U1407A-18X-2, 113			B <i>Discoaster delicatus</i> †	57.45	136.78	138.53	137.66	0.88	
U1407A-18X-2, 113	U1407A-18X-CC			B <i>Ericsonia robusta</i> (>9 µm)†	57.54	138.53	142.90	140.72	2.19	
U1407A-18X-1, 88	U1407A-18X-2, 113			Tc <i>Discoaster backmani</i> †	57.57	136.78	138.53	137.66	0.88	
U1407A-18X-CC	U1407A-19X-2, 32			B <i>Discoaster backmani</i> †	58.28	142.90	147.45	145.18	2.27	
U1407A-19X-2, 32	U1407A-19X-CC		NP7	B <i>Discoaster mohleri</i>	58.97	147.45	149.25	148.35	0.90	
U1407A-20X-2, 100	U1407A-20X-4, 85			B <i>Sphenolithus anarrhopus</i> †	59.40	157.60	160.45	159.03	1.42	
U1407A-20X-1, 63	U1407A-20X-2, 100		NP6	B <i>Heliolithus kleinpellii</i>	59.54	155.73	157.60	156.67	0.94	
U1407A-20X-2, 100	U1407A-20X-4, 85			B <i>Heliolithus cantabriae</i>	59.60	157.60	160.45	159.03	1.42	
U1407A-21X-4, 92	U1407A-21X-CC		NP5	B <i>Fasciculithus tympaniformis</i>	61.51	170.12	172.24	171.18	1.06	
U1407A-21X-CC	U1407A-22X-4, 82		NP4	B <i>Ellipsolithus macellus</i>	63.25	172.24	179.62	175.93	3.69	
U1407A-23X-2, 125	U1407A-23X-2, 135			B <i>Cruciplacolithus intermedius</i>	65.47	186.65	186.75	186.70	0.05	
U1407A-23X-2, 125	U1407A-23X-2, 135			T <i>Micula murus</i> , other Cretaceous nannofossils	66.04	186.65	186.75	186.70	0.05	



Table T3 (continued).

Hole, core, section, interval (cm)		Age	Zone/ Subzone	Marker species	Age (Ma)	Depth (mbsf)			
Top	Bottom					Top	Bottom	Mid-point	±
Cretaceous									
U1407A-23X-3, 74	U1407A-23X-6, 97	UC20cT	B <i>Ceratolithoides kamptneri</i>	67.84	187.64	192.37	190.01	2.37	
U1407A-23X-3, 74	U1407A-23X-6, 97	UC20bB	B <i>Nephrolithus frequens</i>	67.84	187.64	192.37	190.01	2.37	
U1407A-23X-3, 74	U1407A-23X-6, 97	UC20bT	B <i>Micula murus</i>	69.00	187.64	192.37	190.01	2.37	
U1407A-23X-3, 74	U1407A-23X-6, 97		B <i>Cribrocorona gallica</i>	69.00	187.64	192.37	190.01	2.37	
U1407A-23X-3, 74	U1407A-23X-6, 97	UC20	B <i>Lithraphidites quadratus</i>	69.18	187.64	192.37	190.01	2.37	
U1407A-23X-3, 74	U1407A-23X-6, 97	UC19	T <i>Reinhardtites levius</i>	70.14	187.64	192.37	190.01	2.37	
U1407A-23X-3, 74	U1407A-23X-6, 97	UC18	T <i>Tranolithus orionatus</i>	71.01	187.64	192.37	190.01	2.37	
U1407A-22X-CC	U1407A-22X-CC	UC18T	T <i>Uniplanarius trifidus</i>	71.31	182.27	182.27	182.27	0.00	
U1407A-23X-3, 74	U1407A-23X-6, 97	UC17	T <i>Broinsonia parca constricta</i>	72.02	187.64	192.37	190.01	2.37	
Campanian/Maastrichtian boundary									
U1407A-23X-3, 74	U1407A-23X-6, 97		T <i>Broinsonia parca constricta</i>	72.02	187.64	192.37	190.01	2.37	
U1407A-24X-1, base	U1407A-24X-2, 95		T <i>Reinhardtites anthophorus</i>	74.51	187.64	192.37	190.01	2.37	
U1407A-23X-3, 74	U1407A-23X-6, 97		B <i>Reinhardtites levius</i>	74.84	187.64	192.37	190.01	2.37	
U1407A-23X-3, 74	U1407A-23X-6, 97		T <i>Eiffellithus eximius</i>	75.93	187.64	192.37	190.01	2.37	
U1407A-23X-6, 97	U1407A-23X-CC		T <i>Lithastrinus grillii</i>	79.73	192.37	193.13	192.75	0.38	
U1407A-24X-2, 95	U1407A-24X-4, 75		B <i>Broinsonia parca constricta</i>	81.38	195.95	198.75	197.35	1.40	
U1407A-25X-2, 47	U1407A-25X-CC		B <i>Lithastrinus grillii</i>	86.50	204.82	206.61	205.72	0.90	
U1407A-25X-2, 47	U1407A-25X-CC		T <i>Lithastrinus septenarius</i>	85.56	204.82	206.61	205.72	0.90	
U1407A-25X-CC	U1407A-27X-1, 150		B <i>Micula stauropora</i>	89.77	206.61	223.80	215.21	8.60	
U1407A-27X-1, 150	U1407A-27X-4, 150		B <i>Lithastrinus septenarius s.l.</i>	91.78	223.80	228.30	226.05	2.25	
U1407A-27X-1, 150	U1407A-27X-4, 150		B <i>Eiffellithus eximius</i>	92.99	223.80	228.30	226.05	2.25	
U1407A-27X-1, 150	U1407A-27X-4, 150		B <i>Quadrum gartneri</i>	93.55	223.80	228.30	226.05	2.25	
U1407A-27X-1, 150	U1407A-27X-4, 150		B <i>Eprolithus moratus</i>	93.73	223.80	228.30	226.05	2.25	
U1407A-28X-1, 47	U1407A-28X-1, 150		T <i>Helenea chiastra</i>	93.90	232.37	233.40	232.89	0.52	
U1407A-28X-1, 47	U1407A-28X-1, 150		T <i>Corollithion kennedyi</i>	94.64	232.37	233.40	232.89	0.52	
U1407A-29X-2, 85	U1407A-29X-4, 85		B <i>Lithraphidites acutus</i>	96.16	243.85	246.85	245.35	1.50	
U1407A-29X-CC	U1407A-30X-CC		B <i>Corollithion kennedyi</i>	100.45	250.26	259.35	254.80	4.55	
U1407A-30X-CC	U1407A-31X-CC		T <i>Hayesites</i>	100.84	259.35	268.60	263.97	4.63	
U1407A-31X-CC	U1407A-32X-CC		B <i>Eiffellithus turrisieiffelii</i>	103.13	268.60	269.60	269.10	0.50	

* = from Agnini et al. (2006) recalibrated to GTS2012. † = from Agnini et al. (2007) recalibrated to GTS2012. B = base, Bc = Base common, T = top, Tc = Top common.

Table T4. Calcareous nannofossils datums, Site U1407. This table is available in an [oversized format](#).

Table T5. Radiolarian datums, Site U1407.

Core, section, interval (cm)		Age	Zone/ Subzone	Marker species	Age (Ma)	Depth (mbsf)		
Top	Bottom					Top	Bottom	Mid-point
342-U1407A-	342-U1407A-							
11H-CC	11H-CC							
11H-CC	16X-CC							
		Eocene	RP11	T <i>Buryella clinata</i>	47.9	92.32	102.04	97.18
				B <i>Dictyoprora mongolfieri</i>	47.98	102.04	124.61	113.33
11H-CC	16X-CC		RP7	T <i>Buryella tetradiica</i>	50.87	102.04	124.61	113.33
18X-CC	19X-CC			X <i>Bekoma campechensis</i> – <i>Bekoma bidartensis</i>	58.23	142.90	149.25	146.07
18X-CC	19X-CC			T <i>Stichocampe caia</i>	59	142.90	149.25	146.07
19X-CC	20X-CC			T <i>Orbula comitata</i>	59.5	149.25	164.85	157.05
21X-3, 8–12	21X-CC			B <i>Phormocyrtis striata exquisita</i>	61.5	167.80	172.24	170.02
21X-CC	22-1, 24–25	RP6a	RP6a	T <i>Anthocyrtis mespilus</i>	62	172.24	182.27	177.25

B= base, T = top, X = faunal crossover.

**Table T6.** Radiolarian distribution, Site U1407.

	Core, section, interval (cm)	Depth (mbsf)	Age	Zone/Subzone	Preservation		Abundance	Diatoms	
					G	A			
342-U1407A-10H-CC 11H-CC	92.32 102.04	Eocene Eocene	RP11 RP11	G G	A A		x x		<i>Amphirospedum murrayanum</i> <i>Amphirospedum murrayanum</i> var. A <i>Amphirospedum prolifum</i> <i>Amphiternis alamedaensis</i> <i>Amphisphaera coronata</i> <i>Amphisphaera goruna</i> <i>Amphisphaera macrospheara</i> <i>Anthocrytis?</i> <i>mepilus</i> <i>Aspis velutochlamydosaurus</i> <i>Axonprunum pieriniae</i> <i>Bekoma bidartensis</i> <i>Bekoma campechensis</i> <i>Bekoma? demissa</i> <i>Bekoma divaricata</i> <i>Bekoma? oliva</i> <i>Bunyella clinata</i> <i>Bunyella pentadica</i> <i>Bunyella tetradica</i> <i>Bunyella tetradica</i> var. A <i>Calocyclus hispida</i> <i>Calocyctoma ampulla</i> <i>Calocyctoma castum</i> <i>Casidetus mariae</i> <i>Clathrocyctas capiteanum</i> <i>Clathropyrgus grandifrenestra</i> <i>Dictyopora amphora</i> <i>Dictyopora mongolfieri</i> <i>Dictyopora urceolus</i> <i>Dorcadospiris platyacantha</i> <i>Lamptonium? columbus</i> <i>Lamptonium fabaeforme</i> <i>Lamptonium pennatum</i> <i>Lipinella</i> sp. (Nishimura, 1992) <i>Lithospilus mendocia</i> <i>Lithotria doellii</i> <i>Lophocrytis? siliqua</i> <i>Lophocrytis lacchia</i> <i>Lophocrytis semipolita</i> gr.
16X-CC 17X-CC 18X-CC	124.61 127.57 142.90	Paleocene Paleocene Paleocene	RP7 RP7 RP7	G G G	A A A	R R R	x x x	x x x	
19X-CC	149.25	Paleocene	RP6b	G	A	C			
20X-CC 21X-3, 8-12 21X-CC 22X-1, 24-25	164.85 167.80 172.24 174.55	Paleocene Paleocene Paleocene Paleocene	RP6a RP6a RP6a RP6a	G G G P	A A A C	F R C C	x x x x	x x x x	

Preservation: G = good, P = poor. Abundance: A = abundant, C = common, F = few, R = rare. See “**Biostratigraphy**” in the “Methods” chapter (Norris et al., 2014b) for preservation and abundance definitions.

	Core, section, interval (cm)	Depth (mbsf)	Age	Zone/Subzone	Preservation		Abundance	Diatoms	
					G	A			
342-U1407A-10H-CC 11H-CC	92.32 102.04	Eocene Eocene	RP11 RP11	G G	A A		x ?	x x	<i>Lophocrytis pseudojacchia</i> <i>Lycocystis amphitrite</i> <i>Lycocystis anacolum</i> <i>Lycocystis auxilla</i> <i>Lycocystoma bellum</i> <i>Lychnocanomata carinatum</i> <i>Lychnocanomata elongata</i> <i>Lychnocanomata? pileus</i> <i>Middourium regularis</i> <i>Orbulia comitata</i> <i>Peripheraena decora</i> <i>Peripheraena helasteriscus</i> <i>Pentivitato? dummiticai</i> <i>Phacostaurus quadratus</i> <i>Phormocysts striata exquisita</i> <i>Phormocysts striata striata</i> <i>Phormocysts turrida</i> <i>Podocrytis apharma</i> <i>Podocrytis papalis</i> <i>Pterocodon poculum</i> <i>Pterocyrtidium? horisenkoi</i> <i>Pterocyrtidium genitetae</i> <i>Saturnalis circularis</i> <i>Sethochytis babylonis</i> <i>Spongatractus balbis</i> <i>Spongamelissa adunca</i> <i>Stichocampe caja</i> <i>Stichomitria cecena</i> <i>Stylosphaera minor</i> <i>Stylo trochus nitidus</i> <i>Thecoconys anapographa</i> <i>Thecoconys aff. physella</i> <i>Thecoctyle cryptocapsula</i> <i>Thecoctyle leptigaster</i> <i>Thecoctyle lissula</i> <i>Thrysoctyle annulae</i> <i>Thrysoctyle hirsuta</i> <i>Thrysoctyle hirsutoides</i> <i>Velutacillula paleacea</i> <i>Xiphospira circularis</i>
16X-CC 17X-CC 18X-CC	124.61 127.57 142.90	Paleocene Paleocene Paleocene	RP7 RP7 RP7	G G G	A A A	R R R	x x x	x x x	
19X-CC	149.25	Paleocene	RP6b	G	A	C	x	x x	
20X-CC 21X-3, 8-12 21X-CC 22X-1, 24-25	164.85 167.80 172.24 174.55	Paleocene Paleocene Paleocene Paleocene	RP6a RP6a RP6a RP6a	G G G P	A A A C	F R C C	x x x x	x x x x	

Table T7. Planktonic foraminifer datums, Site U1407.

Core, section, interval (cm)				Age	Zone/Subzone	Marker event	Age (Ma)	Depth (mbsf)			
Top	Bottom	Top	Bottom					Top	Bottom	Mid-point	±
342-U1407A-	342-U1407A-										
3H-CC	4H-1, 100–102	middle Eocene	E10/E9			T <i>Morozovella aragonensis</i>	43.26	25.43	26.80	26.12	0.69
10H-2, 100–102	10H-2, 110–112	middle Eocene	E8/E7			B <i>Guembelitrioides nuttalli</i>	45.70	85.30	85.40	85.35	0.05
12H-CC	15H-CC	middle Eocene	E5/E4			B <i>Morozovella aragonensis</i>	52.50	102.80	121.80	112.30	9.50
16X-CC	17X-CC	late Paleocene	P4/P5			T <i>Globanomalina pseudomenardii</i>	57.10	124.60	127.50	126.04	1.48
19X-1, 77–78	19X-3, 1–3	late Paleocene	P4c/P4b			B <i>Acarinina soldadoensis</i>	57.79	146.27	148.32	147.30	1.02
21X-CC	21X-CC	late Paleocene	P4a/P3			B <i>Globanomalina pseudomenardii</i>	60.73	172.21	176.65	174.43	2.22
23X-6, 12–15	23X-CC	Campanian	<i>Radotruncana calcarata/Contusotruncana aplummerae</i>			T <i>Radotruncana calcarata</i>	76.18	191.52	193.10	192.31	0.79
24X-4, 19–21	24X-CC	Campanian	<i>Globotruncanita elevata/Dicarinella asymetrica</i>			T <i>Dicarinella asymetrica</i>	83.64	198.19	199.37	198.78	0.59
25X-CC	27X-1, 33–35	Santonian	<i>Dicarinella asymetrica/Dicarinella concavata</i>			B <i>Dicarinella asymetrica</i>	86.66	206.57	222.63	214.60	8.03
27X-1, 33–35	27X-2, 39–41	Turonian	<i>Dicarinella concavata/Marginotruncana schneegansi</i>			B <i>Dicarinella concavata</i>	91.08	222.63	224.19	223.41	0.78
27X-2, 39–41	27X-3, 29–30	Turonian	<i>Marginotruncana schneegansi/Helvetoglobotruncana helvetica</i>			T <i>Helvetoglobotruncana helvetica</i>	92.99	224.19	225.59	224.89	0.70
27X-4, 65–67	27X-5, 30–31	Turonian	<i>Helvetoglobotruncana helvetica/Whiteinella archaeocretacea</i>			B <i>Helvetoglobotruncana helvetica</i>	93.53	227.45	228.60	228.03	0.58
27X-CC, 1–2	28X-2, 14–15	Cenomanian	<i>Whiteinella archaeocretacea/Rotalipora cushmanni</i>			T <i>Rotalipora cushmanni</i>	95.94	230.60	233.50	232.09	1.45
29X-3, 85–86	29X-4, 85–86	Cenomanian	<i>Thalmanninella reicheli/Thalmanninella globotruncanoides</i>			B <i>Thalmanninella reicheli</i>	96.08	245.35	246.85	246.10	0.75
29X-4, 85–86	29X-5, 85–86	Cenomanian	<i>Thalmanninella globotruncanoides/Parathalmanninella appenninica</i>			B <i>Thalmanninella globotruncanoides</i>	100.50	246.85	248.35	247.60	0.75
31X-5, 70–71	31X-6, 36–37	Albian	<i>Parathalmanninella appenninica</i>			T <i>Planomalina buxtorfi</i>	101.92	267.40	268.16	267.78	0.38

T = top, B = base.

Table T8. Planktonic foraminifer distribution, Site U1407. This table is available in an [oversized format](#).

Table T9. Abundance and preservation of benthic foraminifers, Site U1407.

Core, section, interval (cm)	Depth (mbsf)	Preservation	Abundance
342-U1407A-			
2H-4, 50–52	11.61	P	A
3H-4, 110–112	21.91	G	P
4H-4, 100–102	31.31	VG	P
5H-4, 110–112	40.91	VG	P
6H-4, 110–112	50.41	VG	P
7H-4, 110–112	59.91	VG	P
8H-4, 100–102	69.31	G	P
9H-2, 100–102	75.81	VG	P
9H-4, 100–102	78.81	G	P
10H-2, 110–112	85.41	G	P
10H-4, 100–102	88.31	VG	P
11H-2, 100–102	94.81	VG	P
11H-4, 100–102	97.81	G	P
12H-1, 25–27	102.06	VG	P
16X-1, 35–37	122.26	G	P
18X-1, 76–78	136.67	VG	P
18X-2, 106–108	138.47	VG	P
19X-1, 77–78	146.28	VG	P
19X-3, 1–3	148.33	VG	P
20X-2, 49–51	157.10	G	P
20X-4, 4–6	159.65	M	F
21X-2, 38–40	166.59	VG	P
21X-4, 32–34	169.53	VG	P
22X-2, 85–87	176.66	G	P
22X-4, 100–102	179.81	M	R
22X-CC, 10–12	181.92	G	P
22X-CC, 30–32	182.12	M	P
23X-2, 114–115	186.55	G	P
23X-2, 126–127	186.67	M	P
23X-2, 135–136	186.76	G	P
23X-2, 33–35	185.74	VG	P
23X-4, 13–15	188.54	M	P
24X-2, 81–85	195.83	G	D
24X-4, 19–21	198.20	P	D
25X-1, 66–68	203.77	G	P
25X-3, 38–40	206.05	G	P
27X-2, 39–41	224.20	G	R
27X-4, 65–67	227.46	M	P
27X-6, 26–27	230.07	G	P
28X-2, 14–15	233.55	G	P
28X-4, 44–45	236.85	G	P
29X-2, 85–86	243.86	G	P
29X-4, 85–86	246.86	M	R
30X-2, 90–91	253.51	G	P
30X-4, 90–91	256.51	G	P
31X-3, 106–107	264.77	G	P
31X-5, 70–71	267.41	P	P
342-U1407B-			
21X-1, 69–70	201.30	G	D
21X-3, 46–47	204.17	M	A
21X-6, 41–42	208.62	G	P
22X-1, 73–74	209.84	G	P
22X-3, 86–87	212.97	G	P
22X-5, 46–47	215.57	G	P
22X-7, 60–61	218.22	M	D
23X-2, 82–83	221.03	M	D
23X-4, 45–46	223.66	G	P
23X-6, 31–32	226.52	G	P
24X-4, 3–4	232.15	M	A
24X-4, 40–41	232.52	M	P
24X-4, 74–75	232.86	G	P

Preservation: VG = very good, G = good, M = moderate, P = poor. Abundance: D = dominant, A = abundant, F = few, R = rare, P = present. See “Biostratigraphy” in the “Methods” chapter (Norris et al., 2014b) for preservation and abundance definitions.



**Table T10.** Benthic foraminifer distribution, Site U1407. (Continued on next two pages.)

Core, section	Depth (mbfs)	Preservation	Abundance	<i>Aegialina quadrata</i>	<i>Alabamina dissimilata</i>	<i>Ammodiscus edentaceus</i>	<i>Ammodiscus tenuissima</i>	<i>Anomidiopsis seminibratus</i>	<i>Anomidiopsis sp.</i>	<i>Astacolus sp.</i>	<i>Buliminula parallelus</i>	<i>Buliminella sp.</i>	<i>Buliminella semibullosa</i>	<i>Calymene laevigata</i>	<i>Ciliatoides klenbergi</i>	<i>Ciliatoides mundulus</i>	<i>Ciliatoides pseudemarginatus</i>	<i>Ciliatoides spiratus</i>	<i>Chitina laevis</i>	<i>Dorothyia rotoides</i>	<i>Ellipsidoplintha macrocephala</i>	<i>Ellipsidoplintha unimbonifera?</i>	<i>Elongularia sp.</i>	<i>Foraminella sp.</i>	<i>Hypselodiscus sp.</i>	<i>Hypselodiscus tenuis</i>		
342-U1407A-																												
1H-CC	6.78	VG	P																									P
2H-CC	15.95	MP	F																									F
3H-CC	25.49	VG	P																									P
4H-CC	35.28	VG	P																									P
5H-CC	45.03	VG	P																									P
6H-CC	54.70	VG	P																									P
7H-CC	64.16	VG	P																									P
8H-CC	73.63	VG	P																									P
9H-CC	83.16	G	P																									F
10H-CC	92.32	G	P	P																								F
11H-CC	102.04	G	P	P																								F
12H-CC	102.84	G	P																									F
15H-CC	121.82	G	P																									F
16X-CC	124.61	M	R																									F
17X-CC	127.57	G	P		P																							F
18X-CC	142.90	G	P																									F
19X-CC	149.25	VG	P																									F
20X-CC	164.85	G	P																									P
21X-CC	172.24	G	P		P																							F
22X-CC	182.27	M	P																									F
23X-CC	193.13	G	A																									F
24X-CC	199.40	M	D																									F
25X-CC	206.61	M	F																									F
27X-CC	230.88	P	D																									F
28X-CC	239.84	M	P																									F
29X-CC	250.26	G	P																									F
30X-CC	259.35	G	P																									F
31X-CC	268.60	P	A																									F

Preservation: VG = very good, G = good, M = moderate, P = poor. Abundance: D = dominant, A = abundant, F = few, R = rare, P = present. See “[Biostratigraphy](#)” in the “Methods” chapter (Norris et al., 2014b) for preservation and abundance definitions.

Table T10 (continued). (Continued on next page.)

Core, section	Depth (mbsf)	Preservation	Abundance	<i>Fissurina</i> sp.	<i>Caudynia pyramidata</i>	<i>Caudynia beccariiformis</i>	<i>Cavolinella concomitans</i>	<i>Cavolinella cf. intermediata</i>	<i>Gyroidinoides globosus</i>	<i>Gyroidinoides</i> spp.	<i>Karrerella</i> sp.	<i>Lagidina</i> sp.	<i>Lenticulina cf. adenensis</i>	<i>Lenticulina rotula</i>	<i>Lenticulina</i> spp.	<i>Lingulogavelinella</i> sp.	<i>Marsupella oxycona</i>	<i>Neofabellina semireticulata</i>	<i>Neofabellina</i> sp. a.	<i>Nodularia</i> sp.	<i>Nuttallites truempyi</i>	<i>Obliquaria</i> sp.	<i>Ostrea</i> sp.	<i>Ostrosalis umbonatus</i>	<i>Ostrolammina sahybenbachii</i>	<i>Ostrolammina illecebundi</i>	<i>Pleurostomella tenuis</i>	<i>Pleurostomella russi</i>	<i>Pleurostomella</i> spp.	<i>Polygyra</i> sp.	<i>Pulicaria clavigeris</i>					
342-U1407A-1H-CC	6.78	VG	P	P									P	P	P													P	F	F	F	F	P	P		
2H-CC	15.95	M	F																										F	F	F	F	F	P	P	
3H-CC	25.49	VG	P	P																																
4H-CC	35.28	VG	P	P																																
5H-CC	45.03	VG	P	F	P																															
6H-CC	54.70	VG	P	F																																
7H-CC	64.16	VG	P	F																																
8H-CC	73.63	VG	P	F																																
9H-CC	83.16	G	P																																	
10H-CC	92.32	G	P																																	
11H-CC	102.04	G	P			P																														
12H-CC	102.84	G	P																																	
15H-CC	121.82	G	P																																	
16X-CC	124.61	M	R	A	P																															
17X-CC	127.57	G	P	A	A																															
18X-CC	142.90	G	P	F	A																															
19X-CC	149.25	VG	P	P	A	A																														
20X-CC	164.85	G	P	P	A	A																														
21X-CC	172.24	G	P		F	F																														
22X-CC	182.27	M	P	A	F																															
23X-CC	193.13	G	A	F	D																															
24X-CC	199.40	M	D	F	A																															
25X-CC	206.61	M	F	A	F																															
27X-CC	230.88	P	D		F																															
28X-CC	239.84	M	P	P	F	F																														
29X-CC	250.26	G	P	P	P	F																														
30X-CC	259.35	G	P		F																															
31X-CC	268.60	P	A																																	



Table T10 (continued).

Core, section	Depth (mbsf)	Preparation	Abundance	Pullate cavity	Pullate diaphanopelagic	Radiolaria sp.	Sarcodinia sp.	Spiroctenaria sp.	Spiralaminaria graciliformis	Spiralaminaria granularis	Spiralaminaria sp.	Stilosomella epedita	Stilosomella sp.	Streptosphaera saprosita	Tritaxis sp.	Trichomonads	Unguiculata sp.
342-U1407A-																	
1H-CC	6.78	VG	P	P												P	P
2H-CC	15.95	M	F	P													
3H-CC	25.49	VG	P	P													
4H-CC	35.28	VG	P	P													
5H-CC	45.03	VG	P	P													
6H-CC	54.70	VG	P	P													
7H-CC	64.16	VG	P	P													
8H-CC	73.63	VG	P	P													
9H-CC	83.16	G	P	P													
10H-CC	92.32	G	P	P													
11H-CC	102.04	G	P	P													
12H-CC	102.84	G	P	P													
15H-CC	121.82	G	P	P													P
16X-CC	124.61	M	R	P													
17X-CC	127.57	G	P	F													
18X-CC	142.90	G	P	P													P
19X-CC	149.25	VG	P	F													F
20X-CC	164.85	G	P	F													
21X-CC	172.24	G	P	A													
22X-CC	182.27	M	P	P													
23X-CC	193.13	G	A	F													
24X-CC	199.40	M	D	F													
25X-CC	206.61	M	F	P													
27X-CC	230.88	P	D														
28X-CC	239.84	M	P														
29X-CC	250.26	G	P														
30X-CC	259.35	G	P														
31X-CC	268.60	P	A														



Table T11. Core orientation data, Site U1407.

Hole U1407A		Hole U1407B	
Core	MTF (°)	Core	MTF (°)
1H	158	1H	212
2H	201	2H	108
3H	28	3H	44
4H	5	4H	—
5H	333	5H	353
6H	142	6H	6
7H	338	7H	251
8H	316	8H	332
9H	243	9H	338
10H	313	10H	348
11H	59	11H	273
12H	20		
13H	170		
14H	91		
15H	168		

MTF = magnetic tool face orientation from geomagnetic north. — = no tool data.

Table T12. Summary of AF demagnetization results for discrete samples, Hole U1407A. (Continued on next page.)

Core, section, interval (cm)	Depth (mbsf)	Declination 20 mT or PCA (°)	Inclination 20 mT or PCA (°)	PCA MAD (°)	PCA range (mT)	NRM 20 mT (A/m)	Measurement error (%)
342-U1407A-							
1H-3W, 73–75	3.74	44.6	56.6			1.36E-02	3.3
1H-5W, 34–36	6.35	211.0	-47.5			8.30E-03	3.2
2H-3W, 48–50	10.29	16.0	67.4	6.7	20–60	3.75E-03	3.9
2H-5W, 34–36	12.02	201.2	55.8			2.09E-03	4.3
3H-2W, 75–77	18.56	45.6	52.3			4.80E-03	3.8
3H-4W, 75–77	21.56	6.7	63.1	4.5	20–60	4.70E-03	4.3
4H-1W, 87–89	26.68	156.7	-40.3			2.82E-04	6.2
4H-2W, 75–77	28.06	2.5	-35.5			1.67E-05	22.3
4H-3W, 75–77	29.56	-4.5	-65.1			2.02E-05	8.9
4H-4W, 81–83	31.12	29.8	-64.0			1.68E-05	11.9
4H-5W, 75–77	32.56	12.0	-39.0			1.27E-05	26.0
4H-6W, 50–52	33.81	31.2	-66.5			1.70E-05	19.5
5H-1W, 105–107	36.36	-31.0	-57.2			1.33E-05	20.2
5H-2W, 75–77	37.56	-1.3	-30.3			2.00E-05	13.2
5H-3W, 75–77	39.06	180.4	-61.7			2.07E-05	5.2
5H-4W, 75–77	40.56	172.3	-74.9			2.43E-05	15.6
5H-5W, 75–77	42.06	-59.4	-77.8			3.35E-05	11.8
5H-6W, 75–77	43.56	180.4	-51.7			5.29E-05	4.2
5H-7W, 27–29	44.58	214.9	-50.3			4.65E-05	11.0
6H-1W, 75–77	45.56	167.8	-32.0			6.30E-05	7.4
6H-2W, 75–77	47.06	-14.1	27.1			3.38E-05	10.8
6H-3W, 75–77	48.56	-5.3	37.5	6.9	20–60	1.18E-04	3.0
6H-5W, 60–62	51.41	44.4	8.5			3.04E-05	18.2
7H-2W, 70–72	56.51	12.9	29.9			4.28E-05	17.3
7H-4W, 75–77	59.56	14.8	37.5			3.32E-05	6.9
7H-6W, 75–77	62.56	40.8	6.8			1.61E-05	31.7
8H-2W, 75–77	66.06	-30.9	29.3			4.36E-05	15.5
8H-4W, 75–77	69.06	-32.8	28.6			6.64E-05	9.8
8H-6W, 75–77	72.06	-26.4	2.5			2.77E-05	32.0
9H-1W, 74–76	74.05	-2.8	18.0			2.10E-05	8.1
9H-2W, 74–76	75.55	-22.3	35.2			2.86E-05	11.7
9H-3W, 74–76	77.05	13.3	-27.1			1.08E-05	7.8
9H-4W, 74–76	78.55	11.9	14.7			1.66E-05	11.9
9H-5W, 74–76	80.05	-36.9	43.8			1.60E-05	8.8
9H-6W, 74–76	81.55	-28.0	49.5			1.70E-05	33.1
9H-7W, 29–31	82.60	-14.7	23.4			1.94E-05	12.6
10H-1W, 74–76	83.55	224.3	-47.6			8.74E-05	8.9
10H-2W, 74–76	85.05	244.0	-51.5			4.84E-05	9.0



Table T12 (continued).

Core, section, interval (cm)	Depth (mbsf)	Declination 20 mT or PCA (°)	Inclination 20 mT or PCA (°)	PCA MAD (°)	PCA range (mT)	NRM 20 mT (A/m)	Measurement error (%)
10H-3W, 74–76	86.55	56.3	29.3			6.90E-05	6.5
10H-5W, 74–76	89.55	-6.2	30.1			1.27E-04	5.2
10H-7W, 39–41	91.90	186.2	-53.9			9.23E-05	5.8
11H-1W, 74–76	93.05	213.3	14.1			2.22E-04	6.3
11H-2W, 22–24	94.03	49.7	68.4			1.50E-04	5.4
11H-3W, 74–76	96.05	40.8	66.4			2.25E-04	4.5
11H-4W, 74–76	97.55	43.6	74.3			2.91E-04	3.8
11H-5W, 74–76	99.05	68.4	68.6			3.53E-04	4.2
11H-6W, 72–74	100.53	41.8	58.1			3.39E-04	4.3
11H-7W, 14–16	101.45	57.8	59.7			1.61E-04	7.0
12H-1W, 48–50	102.29	69.8	-13.9			7.82E-04	1.7
16X-1W, 34–36	122.25	-19.5	-8.2			4.00E-03	6.2
16X-1W, 81–83	122.72	70.3	-41.7			3.94E-04	3.9
16X-2W, 57–59	123.98	43.8	-27.4			4.20E-04	3.1
17X-1W, 49–51	126.80	64.0	-29.5			3.98E-04	1.7
18X-1W, 58–60	136.49	0.7	23.0			5.09E-04	5.3
18X-3W, 99–101	139.90	-70.6	46.9			1.83E-03	6.2
18X-5W, 29–31	142.20	40.7	-11.6			4.67E-04	2.4
19X-1W, 27–29	145.78	55.3	-23.5			2.30E-04	1.7
19X-3W, 48–50	148.80	151.0	44.5	13.2	20–60	1.20E-04	6.6
20X-1W, 67–69	155.78	-25.0	-30.5			5.03E-04	7.2
20X-3W, 113–115	159.24	-71.3	-42.9	11.7	30–60	1.96E-04	7.1
20X-5W, 80–82	161.91	58.6	-32.7			5.68E-04	3.1
21X-1W, 60–62	165.31	106.0	-36.0			8.33E-05	7.0
21X-3W, 80–82	168.51	5.6	-28.9	1.2	20–60	1.45E-03	4.7
21X-5W, 41–43	171.12	56.1	-18.1			9.02E-04	2.4
22X-1W, 40–42	174.71	78.9	-21.5			3.87E-05	9.0
22X-3W, 50–52	177.81	234.0	-29.8	9.4	20–60	4.91E-04	4.7
23X-1W, 37–39	184.28	-67.5	-38.3			5.37E-05	8.5
23X-3W, 101–103	187.92	41.1	66.6	15.0	30–60	9.04E-04	3.6
23X-5W, 6–8	189.97	11.4	-21.0			5.84E-04	6.1
24X-1W, 86–88	194.37	53.1	-17.8			2.01E-03	1.1
24X-3W, 106–108	197.57	67.2	-13.6			1.21E-03	2.8
25X-1W, 58–60	203.69	-65.1	60.0			2.47E-03	6.7
25X-2W, 67–69	205.03	43.8	30.0			5.42E-03	3.2
25X-3W, 69–71	206.36	39.7	31.4	2.7	20–60	6.39E-03	3.4
27X-2W, 65–67	224.46	-36.8	36.1			3.80E-03	6.8
27X-3W, 103–105	226.34	81.4	26.9			1.06E-02	4.6
27X-4W, 62–64	227.43	36.1	35.9			5.20E-03	3.9
27X-5W, 109–111	229.40	68.8	-7.5			6.02E-03	4.8
28X-2W, 126–128	234.67	103.4	22.3			1.14E-04	8.2
28X-3W, 29–31	235.20	164.0	28.4	2.3	10–60	2.20E-04	5.5
28X-4W, 91–93	237.32	250.0	28.7			9.61E-05	4.7
28X-5W, 26–28	238.17	-66.2	25.3			4.19E-05	6.2
28X-6W, 22–24	239.23	48.6	20.9			2.09E-04	2.5
29X-1W, 91–93	242.42	100.6	29.8			7.09E-04	5.6
29X-2W, 82–84	243.83	2.4	38.6			5.92E-04	5.1
29X-3W, 51–53	245.02	258.5	31.0			4.31E-04	6.4
29X-4W, 41–43	246.42	150.1	41.1	2.3	10–60	3.07E-04	6.0
29X-5W, 37–39	247.88	-15.4	48.8			1.03E-03	4.8
29X-6W, 17–19	249.18	78.2	43.4			4.29E-04	4.8
30X-1W, 35–37	251.46	-1.0	38.3			4.46E-04	4.7
30X-3W, 36–38	254.47	156.2	44.0	1.8	10–60	1.96E-04	5.3
30X-5W, 28–30	257.19	NA	NA			4.05E-04	4.5
31X-1W, 31–33	261.02	-9.0	40.2			6.62E-05	8.8
31X-3W, 35–37	264.06	9.9	32.0			1.50E-04	6.1
31X-5W, 48–50	267.19	33.2	41.0			1.10E-04	5.3

Declinations for Cores 1H to 12H are corrected to geographical coordinates using the FlexIT orientation data (Table T11). PCA = principal component analysis, MAD = maximum angle of deviation, NRM = natural remanent magnetism. NA = not available.



Table T13. Magnetostratigraphic tie points, Site U1407.

Chron boundary	Age (Ma)	Hole U1407A						Hole U1407B					
		Top		Bottom		Mid-point (mbsf)	Top		Bottom		Mid-point (mbsf)		
		Core, section, interval (cm)	Depth (mbsf)	Core, section, interval (cm)	Depth (mbsf)		Core, section, interval (cm)	Depth (mbsf)	Core, section, interval (cm)	Depth (mbsf)			
		342-U1407A-		342-U1407A-			342-U1407B-		342-U1407B-				
C20n/C20r	43.432	NI	NI	NI	NI	NI	NI	NI	NI	NI	NI		
C20r/C21n	45.724	6H-2, 52.5	46.83	6H-2, 82.5	47.13	46.98	6H-6, 77.5	48.18	7H-1, 10.0	49.50	48.84		
C21n/C21r	47.349	9H-7, 52.5	82.83	10H-1, 32.5	83.13	82.98	10H-5, 137.5	85.28	10H-6, 22.5	85.63	85.46		
C21r/C22n	48.566	10H-2, 95.0	85.20	10H-2, 140.0	85.7	85.45	11H-1, 52.5	87.93	11H-1, 60.0	88.00	87.97		
C22n/C22r	49.344	10H-6, 32.5	90.63	10H-6, 45.0	90.75	90.69	11H-3, 45.0	90.85	11H-3, 55.0	90.95	90.90		
C22r/C23n.1n	50.628	NI	NI	NI	NI	NI	NI	NI	NI	NI	NI		
C23n.1n/C23n.1r	50.835	NI	NI	NI	NI	NI	NI	NI	NI	NI	NI		
C23n.1r/C23n.2n	50.961	NI	NI	NI	NI	NI	NI	NI	NI	NI	NI		
C23n.2n/C23r	51.833	NI	NI	NI	NI	NI	NI	NI	NI	NI	NI		
C23r/C24n.1n	52.620	NI	NI	NI	NI	NI	NI	NI	NI	NI	NI		
C24n.1n/C24n.1r	53.074	NI	NI	NI	NI	NI	NI	NI	NI	NI	NI		
C24n.1r/C24n.2n	53.199	NI	NI	NI	NI	NI	NI	NI	NI	NI	NI		
C24n.2n/C24n.3n	53.274	NI	NI	NI	NI	NI	NI	NI	NI	NI	NI		
C24n.2r/C24n.3n	53.416	NI	NI	NI	NI	NI	NI	NI	NI	NI	NI		
C24n.3n/C24r	53.983	NI	NI	NI	NI	NI	NI	NI	NI	NI	NI		
C24r/C25n	57.101	NI	NI	NI	NI	NI	NI	NI	NI	NI	NI		
C25n/C25r	57.656	NI	NI	NI	NI	NI	NI	NI	NI	NI	NI		
C25r/C26n	58.959	19X-2, 40.0	147.40	19X-2, 72.5	147.73	147.57	NI	NI	NI	NI	NI		

Ages from Gradstein et al. (2012). NI = not identified.

Chron boundary	Age (Ma)	Hole U1407C					
		Top		Bottom		Mid-point (mbsf)	
		Core, section, interval (cm)	Depth (mbsf)	Core, section, interval (cm)	Depth (mbsf)		
		342-U1407C-		342-U1407C-			
C20n/C20r	43.432	NI	NI	NI	NI	NI	
C20r/C21n	45.724	6H-2, 140.0	42.10	6H-4, 10.0	43.80	42.95	
C21n/C21r	47.349	9H-6, 65.0	75.85	9H-6, 77.5	75.98	75.92	
C21r/C22n	48.566	10H-2, 47.5	79.18	10H-2, 62.5	79.33	79.26	
C22n/C22r	49.344	10H-5, 77.5	83.98	10H-5, 102.5	84.23	84.11	
C22r/C23n.1n	50.628	NI	NI	NI	NI	NI	
C23n.1n/C23n.1r	50.835	NI	NI	NI	NI	NI	
C23n.1r/C23n.2n	50.961	NI	NI	NI	NI	NI	
C23n.2n/C23r	51.833	NI	NI	NI	NI	NI	
C23r/C24n.1n	52.620	NI	NI	NI	NI	NI	
C24n.1n/C24n.1r	53.074	NI	NI	NI	NI	NI	
C24n.1r/C24n.2n	53.199	NI	NI	NI	NI	NI	
C24n.2n/C24n.3n	53.274	NI	NI	NI	NI	NI	
C24n.2r/C24n.3n	53.416	NI	NI	NI	NI	NI	
C24n.3n/C24r	53.983	NI	NI	NI	NI	NI	
C24r/C25n	57.101	NI	NI	NI	NI	NI	
C25n/C25r	57.656	NI	NI	NI	NI	NI	
C25r/C26n	58.959	NI	NI	NI	NI	NI	

Table T14. Summary of anisotropy of magnetic susceptibility of discrete samples, Hole U1407A. (Continued on next page.)

Core, section, interval (cm)	Depth (mbsf)	τ_3	V ₃ (°)		V ₂ (°)		τ_1	V ₁ (°)		Bulk susceptibility (SI)	Anisotropy (%)	P	L	F	
			Declination	Inclination	Declination	Inclination		Declination	Inclination	(SI)	(%)				
342-U1407A-															
1H-1W, 70–72	0.71	0.3253	16.4	80.3	0.3314	196.8	9.7	0.3433	106.8	0.1	5.92E-04	1.8	1.055	1.036	1.019
1H-3W, 73–75	3.74	0.3292	89.7	3.1	0.3320	180.7	19.0	0.3388	350.6	70.7	4.01E-04	1.0	1.029	1.020	1.008
1H-5W, 34–36	6.35	0.3311	143.3	62.8	0.3331	269.6	16.9	0.3358	6.2	20.6	3.48E-04	0.5	1.014	1.008	1.006
2H-3W, 48–50	10.29	0.3319	44.3	14.4	0.3326	255.6	73.3	0.3355	136.4	8.3	1.99E-04	0.4	1.011	1.009	1.002
2H-5W, 34–36	12.02	0.3310	230.5	50.9	0.3331	114.1	19.9	0.3359	11.0	32.1	1.66E-04	0.5	1.015	1.008	1.006
2H-7W, 50–52	15.18	0.3295	192.6	57.7	0.3339	81.2	13.0	0.3366	343.9	29.0	1.64E-04	0.7	1.022	1.008	1.014
3H-1W, 75–77	17.06	0.3308	11.9	56.7	0.3336	202.3	32.9	0.3356	109.2	4.8	1.45E-04	0.5	1.015	1.006	1.008
3H-3W, 75–77	20.06	0.3306	173.4	62.6	0.3333	320.0	23.4	0.3361	55.9	13.5	1.31E-04	0.6	1.017	1.008	1.008
3H-5W, 82–84	23.13	0.3316	163.4	74.5	0.3330	271.3	4.9	0.3355	2.5	14.7	1.23E-04	0.4	1.012	1.007	1.004
3H-7W, 28–30	25.09	0.3311	207.2	46.7	0.3339	35.8	42.9	0.3350	301.8	4.3	1.21E-04	0.4	1.012	1.003	1.008
4H-1W, 87–89	26.68	0.3295	81.0	67.0	0.3336	300.8	18.1	0.3369	206.2	13.8	6.34E-05	0.7	1.023	1.010	1.013
4H-3W, 75–77	29.56	0.3301	190.2	37.5	0.3329	92.9	9.3	0.3370	351.3	50.9	4.39E-05	0.7	1.021	1.012	1.009
4H-5W, 75–77	32.56	0.3215	135.6	15.2	0.3341	271.4	69.3	0.3443	41.8	13.8	3.82E-05	2.3	1.071	1.031	1.039
5H-1W, 105–107	36.36	0.3305	325.9	27.9	0.3325	105.9	55.3	0.3370	225.5	18.9	3.81E-05	0.6	1.020	1.014	1.006
5H-3W, 75–77	39.06	0.3281	265.8	38.6	0.3344	57.3	47.8	0.3376	163.8	14.5	4.77E-05	1.0	1.029	1.010	1.019
5H-5W, 75–77	42.06	0.3264	119.4	12.9	0.3349	303.7	77.0	0.3386	209.7	0.9	4.59E-05	1.2	1.037	1.011	1.026
5H-7W, 27–29	44.58	0.3259	241.0	40.5	0.3362	146.6	5.2	0.3379	50.5	49.1	5.08E-05	1.2	1.037	1.005	1.031
6H-1W, 75–77	45.56	0.3279	321.8	58.8	0.3348	201.3	17.1	0.3374	102.9	25.3	5.16E-05	0.9	1.029	1.008	1.021
6H-3W, 75–77	48.56	0.3275	138.7	57.6	0.3315	304.2	31.6	0.3411	38.2	6.6	4.58E-05	1.4	1.041	1.029	1.012
6H-5W, 60–62	51.41	0.3273	171.7	67.9	0.3359	323.8	19.8	0.3367	57.3	9.5	5.88E-05	0.9	1.029	1.002	1.026
7H-1W, 70–72	55.01	0.3289	282.3	26.3	0.3328	99.8	63.6	0.3383	191.8	1.0	5.08E-05	0.9	1.028	1.017	1.012
7H-3W, 75–77	58.06	0.3303	23.5	79.7	0.3338	186.9	9.8	0.3358	277.4	2.9	5.26E-05	0.6	1.017	1.006	1.011
7H-5W, 75–77	61.06	0.3300	313.4	32.5	0.3335	76.5	40.6	0.3365	199.5	32.4	5.02E-05	0.7	1.020	1.009	1.011
7H-7W, 20–22	63.51	0.3280	280.2	58.6	0.3336	126.7	28.7	0.3384	30.1	11.8	5.66E-05	1.0	1.032	1.015	1.017
8H-1W, 75–77	64.56	0.3299	188.6	52.4	0.3321	91.8	5.3	0.3380	357.8	37.1	5.75E-05	0.8	1.025	1.018	1.007
8H-3W, 75–77	67.56	0.3295	141.1	31.9	0.3335	317.0	58.1	0.3370	50.0	1.9	6.51E-05	0.7	1.023	1.010	1.012
8H-5W, 75–77	70.56	0.3283	129.0	31.1	0.3315	294.6	58.1	0.3402	35.1	6.5	5.09E-05	1.2	1.036	1.026	1.010
8H-7W, 30–32	73.11	0.3278	295.9	28.5	0.3340	172.8	45.1	0.3382	45.2	31.3	5.17E-05	1.0	1.032	1.013	1.019
9H-1W, 74–76	74.05	0.3304	139.0	85.2	0.3320	311.4	4.8	0.3375	41.5	0.6	5.84E-05	0.7	1.022	1.017	1.005
9H-3W, 74–76	77.05	0.3286	160.8	61.8	0.3319	51.3	10.2	0.3394	316.3	26.0	5.35E-05	1.1	1.033	1.023	1.010
9H-5W, 74–76	80.05	0.3290	155.1	66.5	0.3328	281.3	14.4	0.3382	16.1	18.1	4.32E-05	0.9	1.028	1.016	1.012
9H-7W, 29–31	82.60	0.3272	41.0	61.0	0.3330	293.1	9.7	0.3398	198.1	27.1	4.72E-05	1.3	1.039	1.020	1.018
10H-1W, 74–76	83.55	0.2279	319.3	40.3	0.3618	66.5	19.3	0.4103	175.9	43.5	-4.40E-06	18.2	1.800	1.134	1.587
10H-3W, 74–76	86.55	0.2190	233.2	25.9	0.3349	132.1	21.8	0.4461	7.2	55.0	2.33E-06	22.7	2.037	1.332	1.529
10H-5W, 74–76	89.55	0.0389	216.8	43.6	0.4407	12.5	43.8	0.5205	114.7	12.4	-1.13E-06	48.2	13.396	1.181	11.342
10H-7W, 29–31	91.90	-0.9262	240.7	31.4	0.6986	333.0	3.8	1.2276	69.2	58.3	2.33E-07	215.4	-1.325	1.757	-0.754
11H-1W, 74–76	93.05	0.3122	29.3	29.7	0.3391	278.7	31.7	0.3487	152.4	43.8	1.82E-05	3.6	1.117	1.028	1.086
11H-3W, 74–76	96.05	0.2931	136.0	6.0	0.3331	235.7	58.0	0.3739	42.3	31.3	6.74E-06	8.1	1.276	1.123	1.136
11H-5W, 74–76	99.05	0.3027	342.2	35.4	0.3231	110.0	40.8	0.3742	228.9	29.2	7.00E-06	7.1	1.236	1.158	1.068
11H-7W, 14–16	101.45	0.3057	52.3	51.7	0.3386	143.2	0.7	0.3556	233.7	38.3	8.37E-06	5.0	1.163	1.050	1.108
12H-1W, 48–50	102.29	0.3257	288.0	19.0	0.3343	190.9	19.9	0.3400	58.2	61.9	2.61E-05	1.4	1.044	1.017	1.026
16X-1W, 34–36	122.25	0.3303	52.5	52.7	0.3342	170.1	19.5	0.3355	272.1	30.4	1.58E-04	0.5	1.016	1.004	1.012
16X-1W, 81–83	122.72	0.3212	216.0	57.6	0.3285	325.8	12.1	0.3503	62.8	29.5	2.09E-05	2.9	1.091	1.066	1.023
17X-1W, 49–51	126.80	0.3127	300.7	27.4	0.3396	193.8	29.3	0.3477	65.4	47.8	1.19E-05	3.5	1.112	1.024	1.086
18X-1W, 58–60	136.49	0.3172	210.8	61.9	0.3347	301.9	0.6	0.3481	32.2	28.1	1.63E-05	3.1	1.098	1.040	1.055
18X-3W, 99–101	139.90	0.3265	291.9	30.9	0.3349	31.5	15.5	0.3386	144.4	54.6	5.30E-05	1.2	1.037	1.011	1.026
18X-5W, 29–31	142.20	0.3151	101.8	29.7	0.3334	350.2	32.8	0.3515	223.7	42.8	1.45E-05	3.6	1.116	1.054	1.058
19X-1W, 27–29	145.78	0.2987	354.9	19.5	0.3384	260.8	11.4	0.3628	142.2	67.2	9.30E-06	6.4	1.215	1.072	1.133
19X-3W, 48–50	148.80	0.3101	199.1	52.7	0.3364	66.1	27.5	0.3535	323.2	23.1	1.11E-05	4.3	1.140	1.051	1.085

Table T14 (continued).

Core, section, interval (cm)	Depth (mbsf)	τ_3	V_3 ($^{\circ}$)		V_2 ($^{\circ}$)		V_1 ($^{\circ}$)		Bulk susceptibility (SI)	Anisotropy (%)	P	L	F		
			Declination	Inclination	Declination	Inclination	Declination	Inclination							
20X-1W, 67–69	155.78	0.3223	47.6	34.3	0.3354	297.6	26.7	0.3422	178.6	43.9	2.77E–05	2.0	1.062	1.020	1.041
20X-3W, 113–115	159.24	0.3106	245.1	32.9	0.3376	144.1	16.5	0.3518	31.6	52.2	1.23E–05	4.1	1.133	1.042	1.087
20X-5W, 80–82	161.91	0.3117	355.9	30.1	0.3233	251.6	23.0	0.3649	130.6	50.5	1.02E–05	5.3	1.171	1.129	1.037
21X-1W, 60–62	165.31	0.3205	314.8	8.7	0.3313	69.4	69.8	0.3482	221.9	18.1	9.78E–06	2.8	1.086	1.051	1.034
21X-3W, 80–82	168.51	0.3297	137.3	61.0	0.3343	3.7	20.9	0.3360	266.1	19.2	5.37E–05	0.6	1.019	1.005	1.014
21X-5W, 41–43	171.12	0.3278	336.4	58.3	0.3334	69.9	2.2	0.3389	161.3	31.6	3.93E–05	1.1	1.034	1.016	1.017
22X-1W, 40–42	174.71	0.3233	310.4	9.6	0.3329	169.4	77.8	0.3437	41.7	7.6	3.11E–05	2.0	1.063	1.032	1.030
22X-3W, 50–52	177.81	0.3291	143.7	49.5	0.3316	348.4	37.8	0.3393	248.6	12.4	4.74E–05	1.0	1.031	1.023	1.008
22X-5W, 69–71	181.00	0.3248	277.5	57.5	0.3357	167.0	12.6	0.3395	69.8	29.5	3.92E–05	1.5	1.045	1.012	1.033
23X-1W, 37–39	184.28	–0.2766	29.2	53.2	–0.1572	121.1	1.4	1.4337	212.1	36.8	1.44E–07	171.0	–5.184	–9.123	0.568
23X-3W, 101–103	187.92	0.3231	199.9	31.9	0.3370	301.5	17.9	0.3398	56.2	52.3	3.34E–05	1.7	1.052	1.008	1.043
23X-5W, 6–8	189.97	0.3226	229.3	1.7	0.3329	133.9	72.6	0.3446	319.8	17.3	3.00E–05	2.2	1.068	1.035	1.032
24X-1W, 86–88	194.37	0.3303	254.4	53.3	0.3312	23.8	25.3	0.3384	126.3	24.7	7.66E–05	0.8	1.025	1.022	1.003
24X-3W, 106–108	197.57	0.3295	103.8	85.0	0.3340	322.2	3.9	0.3366	232.0	3.1	1.73E–04	0.7	1.021	1.008	1.014
25X-1W, 58–60	203.69	0.3306	110.6	71.1	0.3337	254.1	15.4	0.3357	347.1	10.7	1.53E–04	0.5	1.015	1.006	1.009
25X-3W, 69–71	206.36	0.3315	193.5	77.6	0.3335	313.8	6.3	0.3350	45.0	10.6	1.01E–04	0.3	1.010	1.004	1.006
27X-3W, 103–105	226.34	0.3318	90.6	79.2	0.3334	235.5	8.9	0.3348	326.5	6.1	2.06E–04	0.3	1.009	1.004	1.005
27X-5W, 109–111	229.40	0.3292	19.4	24.0	0.3340	285.6	8.6	0.3369	177.3	64.3	6.38E–05	0.8	1.023	1.009	1.015
28X-3W, 29–31	235.20	0.3250	191.9	30.6	0.3326	88.9	20.8	0.3423	330.2	51.6	1.15E–05	1.7	1.053	1.029	1.023
28X-5W, 26–28	238.17	0.3215	316.6	62.2	0.3346	118.2	26.6	0.3439	212.0	7.6	1.89E–05	2.2	1.070	1.028	1.041
29X-1W, 91–93	242.42	0.3269	282.9	65.8	0.3302	93.8	23.9	0.3429	185.3	3.4	3.02E–05	1.6	1.049	1.039	1.010
29X-3W, 51–53	245.02	0.3262	212.2	37.3	0.3341	67.2	47.0	0.3397	316.6	18.1	3.29E–05	1.4	1.042	1.017	1.024
29X-5W, 37–39	247.88	0.3239	189.5	53.9	0.3350	57.8	25.9	0.3411	315.7	23.4	3.28E–05	1.7	1.053	1.018	1.034
30X-1W, 35–37	251.46	0.3165	241.1	44.4	0.3307	339.3	8.3	0.3528	77.5	44.5	1.87E–05	3.6	1.115	1.067	1.045
30X-3W, 36–38	254.47	0.3216	105.7	41.6	0.3356	303.9	46.9	0.3427	204.0	9.2	2.56E–05	2.1	1.066	1.021	1.043
30X-5W, 28–30	257.19	0.3276	193.1	70.6	0.3345	311.2	9.5	0.3379	44.1	16.8	4.82E–05	1.0	1.031	1.010	1.021
31X-1W, 31–33	261.02	0.3210	186.6	59.2	0.3363	80.5	9.4	0.3427	345.2	29.1	3.88E–05	2.2	1.068	1.019	1.048
31X-3W, 35–37	264.06	0.3290	46.2	24.9	0.3327	171.2	51.0	0.3383	302.0	27.9	2.52E–05	0.9	1.028	1.017	1.011
31X-5W, 48–50	267.19	0.3213	30.3	46.3	0.3326	124.5	4.0	0.3462	218.4	43.4	2.41E–05	2.5	1.078	1.041	1.035

τ_1 , τ_2 , and τ_3 are eigenvalues, and V_3 , V_2 , and V_1 are eigenvectors associated with the minimum, intermediate, and maximum susceptibility, respectively. Measurement field = 300 A/m, sample volume = 7 cm³. P = anisotropy degree, L = lineation, F = foliation.



Table T15. Biostratigraphic and magnetostratigraphic datums, Hole U1407A. (Continued on next page.)

Datum tie point	Datum	Datum type	Zone/Subzone	Age (Ma)	Depth (mbsf)		
					Top	Bottom	Mid-point
D01	Ba <i>Emiliana huxleyi</i>	Calcareous nannofossil	NN21	0.70	0.37	0.37	0.37
	T <i>Pseudoemiliana lacunosa</i>	Calcareous nannofossil	NN20	0.44	0.37	4.70	2.54
D02	T <i>Reticulofenestra umbilicus</i> (>14 µm)	Calcareous nannofossil	NP23	32.02	14.28	15.95	15.12
	T <i>Isthmolithus recurvus</i>	Calcareous nannofossil		32.49	15.95	17.41	16.68
	T <i>Coccolithus formosus</i>	Calcareous nannofossil	NP22	32.92	15.95	17.41	16.68
D03	T <i>Discoaster saipanensis</i>	Calcareous nannofossil	NP21	34.44	15.95	17.41	16.68
D04	T <i>Discoaster barbadensis</i>	Calcareous nannofossil		34.76	17.41	18.91	18.16
	B <i>Isthmolithus recurvus</i>	Calcareous nannofossil	NP19/NP20	36.97	17.41	18.91	18.16
	Bc <i>Chiasmolithus oamaruensis</i>	Calcareous nannofossil	NP18	38.09	17.41	18.91	18.16
	T <i>Chiasmolithus solitus</i>	Calcareous nannofossil	NP17	40.40	17.41	18.91	18.16
	B <i>Reticulofenestra umbilicus</i> (>14 µm)	Calcareous nannofossil		41.94	17.41	18.91	18.16
	T <i>Nannotetraena fulgens</i>	Calcareous nannofossil		42.87	17.41	18.91	18.16
D05	T <i>Chiasmolithus gigas</i>	Calcareous nannofossil	NP15c	44.12	17.41	18.91	18.16
	B <i>Chiasmolithus gigas</i>	Calcareous nannofossil	NP15b	45.49	40.91	43.77	42.34
	B <i>Nannotetraena fulgens</i>	Calcareous nannofossil	NP15a	46.29	62.91	64.16	63.54
	B <i>Nannotetraena cristata</i>	Calcareous nannofossil		47.73	83.16	85.31	84.24
	T <i>Discoaster lodoensis</i>	Calcareous nannofossil		47.41	81.37	83.16	82.27
	B <i>Blackites inflatus</i>	Calcareous nannofossil		47.84	83.16	85.31	84.24
	B <i>Discoaster sublodoensis</i>	Calcareous nannofossil	NP14	49.11	91.31	92.32	91.82
D10	B <i>Dictyococcites/Reticulofenestra</i>	Calcareous nannofossil		49.47	101.75	101.95	101.85
	T <i>Tribrachiatus orthostylus</i>	Calcareous nannofossil	NP13	49.47	101.75	101.95	101.85
D11	T <i>Toweius</i> spp.	Calcareous nannofossil		50.78	101.75	101.95	101.85
	B <i>Coccolithus crassus</i>	Calcareous nannofossil		51.64	101.75	101.95	101.85
	B <i>Discoaster lodoensis</i>	Calcareous nannofossil	NP12	53.70	112.31	121.82	117.07
	T <i>Tribrachiatus contortus</i>	Calcareous nannofossil	NP11	54.17	121.82	121.98	121.90
	B <i>Sphenolithus radians</i>	Calcareous nannofossil		54.17	121.82	121.98	121.90
D12	B <i>Tribrachiatus orthostylus</i>	Calcareous nannofossil		54.37	121.82	121.98	121.90
	B <i>Discoaster diastypus</i>	Calcareous nannofossil		54.95	121.82	121.98	121.90
D13	T <i>Fasciculithus</i> spp.	Calcareous nannofossil		55.64	121.82	121.98	121.90
	<i>Fasciculithus</i> division decline	Calcareous nannofossil		56.00	121.82	121.98	121.90
	T <i>Fasciculithus alanii</i>	Calcareous nannofossil		56.00	121.82	121.98	121.90
	T <i>Ericsonia robusta</i> (>9 µm)	Calcareous nannofossil		57.10	124.61	127.57	126.09
D14	B <i>Discoaster multiradiatus</i>	Calcareous nannofossil	NP9	57.21	127.57	136.78	132.18
	B <i>Discoaster delicatus</i>	Calcareous nannofossil		57.45	136.78	138.53	137.66
	B <i>Ericsonia robusta</i> (>9 µm)	Calcareous nannofossil		57.54	138.53	142.90	140.72
	Tc <i>Discoaster backmanii</i>	Calcareous nannofossil		57.57	136.78	138.53	137.66
	B <i>Discoaster backmanii</i>	Calcareous nannofossil		58.28	142.90	147.45	145.18
	B <i>Discoaster mohleri</i>	Calcareous nannofossil	NP7	58.97	147.45	149.25	148.35
	B <i>Sphenolithus anarrhopus</i>	Calcareous nannofossil		59.40	157.60	160.45	159.03
	B <i>Heliolithus kleinpelli</i>	Calcareous nannofossil	NP6	59.54	155.73	157.60	156.67
	B <i>Heliolithus cantabriae</i>	Calcareous nannofossil		59.60	157.60	160.45	159.03
	B <i>Fasciculithus tympaniformis</i>	Calcareous nannofossil	NP5	61.51	170.12	172.24	171.18
	B <i>Ellipsolithus macellus</i>	Calcareous nannofossil	NP4	63.25	172.24	179.62	176.93
D16	B <i>Cruciplacolithus intermedius</i>	Calcareous nannofossil		65.47	186.65	186.75	186.70
D17	T <i>Micula murus</i> , other Cretaceous nannofossils	Calcareous nannofossil		66.04	186.65	186.75	186.70
D18	B <i>Ceratolithoides kamptneri</i>	Calcareous nannofossil	UC20cT	67.84	187.64	192.37	190.01
	B <i>Nephrolithus frequens</i>	Calcareous nannofossil	UC20bB	67.84	187.64	192.37	190.01
	B <i>Micula murus</i>	Calcareous nannofossil	UC20bT	69.00	187.64	192.37	190.01
	B <i>Cribrocorona gallica</i>	Calcareous nannofossil		69.00	187.64	192.37	190.01
D19	B <i>Lithraphidites quadratus</i>	Calcareous nannofossil	UC20	69.18	187.64	192.37	190.01
D20	T <i>Reinhardtites levius</i>	Calcareous nannofossil	UC19	70.14	187.64	192.37	190.01
	T <i>Tranolithus orionatus</i>	Calcareous nannofossil	UC18	71.01	187.64	192.37	190.01
	T <i>Uniplanarius trifidus</i>	Calcareous nannofossil	UC18T	71.31	182.27	182.27	182.27
	T <i>Broinsonia parca constricta</i>	Calcareous nannofossil	UC17	72.02	187.64	192.37	190.01
	T <i>Broinsonia parca constricta</i>	Calcareous nannofossil		72.02	187.64	192.37	190.01
	T <i>Reinhardtites anthophorus</i>	Calcareous nannofossil		74.51	187.64	192.37	190.01
	B <i>Reinhardtites levius</i>	Calcareous nannofossil		74.84	187.64	192.37	190.01
D21	T <i>Eiffellithus eximus</i>	Calcareous nannofossil		75.93	187.64	192.37	190.01
	T <i>Lithastrinus grillii</i>	Calcareous nannofossil		79.73	192.37	193.13	192.75
D22	B <i>Broinsonia parca constricta</i>	Calcareous nannofossil		81.38	195.95	198.75	197.35
D23	B <i>Lithastrinus grillii</i>	Calcareous nannofossil		86.50	204.82	206.61	205.72
	T <i>Lithastrinus septenarius</i>	Calcareous nannofossil		85.56	204.82	206.61	205.72
D24	B <i>Micula stauropora</i>	Calcareous nannofossil		89.77	206.61	223.80	215.21
D25	B <i>Lithastrinus septenarius</i> sensu lato	Calcareous nannofossil		91.78	223.80	228.30	226.05
D26	B <i>Eiffellithus eximus</i>	Calcareous nannofossil		92.99	223.80	228.30	226.05
	B <i>Quadrum gartneri</i>	Calcareous nannofossil		93.55	223.80	228.30	226.05
D27	B <i>Eprolithus moratus</i>	Calcareous nannofossil		93.73	223.80	228.30	226.05
D28	T <i>Helenea chiastia</i>	Calcareous nannofossil		93.90	232.37	233.40	232.89

Table T15 (continued).

Datum tie point	Datum	Datum type	Zone/Subzone	Age (Ma)	Depth (mbsf)			
					Top	Bottom	Mid-point	
D29	T <i>Corollithion kennedyi</i>	Calcareous nannofossil		94.64	232.37	233.40	232.89	
	B <i>Lithraphidites acutus</i>	Calcareous nannofossil		96.16	243.85	246.85	245.35	
	B <i>Corollithion kennedyi</i>	Calcareous nannofossil		100.45	250.26	259.35	254.80	
	T <i>Hayesites</i>	Calcareous nannofossil		100.84	259.35	268.60	263.97	
D30	B <i>Eiffellithus turriseiffelii</i>	Calcareous nannofossil		103.13	268.60	269.60	269.10	
D15	T <i>Buryella clinata</i>	Radiolarian		47.90	92.32	102.04	97.18	
	B <i>Dictyoprora mongolfieri</i>	Radiolarian		47.98	102.04	124.61	102.00	
	T <i>Buryella tetradaica</i>	Radiolarian		50.87	102.04	124.61	124.61	
	X <i>Bekoma campechensis</i> – <i>B. bidartensis</i>	Radiolarian		58.23	142.90	149.25	146.07	
	T <i>Stichocampe caia</i>	Radiolarian		59.00	142.90	149.25	146.07	
	T <i>Orbulus comitata</i>	Radiolarian		59.50	149.25	164.85	157.05	
	B <i>Phormocyrtis striata exquisita</i>	Radiolarian		61.50	167.80	172.24	170.02	
	T <i>Anthocystis mespilus</i>	Radiolarian		62.00	172.24	182.27	177.25	
	T <i>Morozovella aragonensis</i>	Planktonic foraminifer		E10/E9	43.26	25.43	26.80	26.12
	B <i>Guembelitrioides nuttalli</i>	Planktonic foraminifer		E8/E7	45.70	85.30	85.40	85.35
D06	B <i>Morozovella aragonensis</i>	Planktonic foraminifer		E5/E4	52.54	102.80	121.80	112.30
	T <i>Globanomalina pseudomenardii</i>	Planktonic foraminifer		P4/P5	57.10	124.56	127.51	126.04
	B <i>Acarinina soldadoensis</i>	Planktonic foraminifer		P4c/P4b	57.79	146.27	148.32	147.30
	B <i>Globanomalina pseudomenardii</i>	Planktonic foraminifer		P4a/P3	60.73	172.21	176.65	174.43
	T <i>Radotruncana calcarata</i>	Planktonic foraminifer			76.18	191.52	193.10	192.31
	T <i>Dicarinella asymetrica</i>	Planktonic foraminifer			83.64	198.19	199.37	198.78
	B <i>Dicarinella asymetrica</i>	Planktonic foraminifer			86.66	206.57	222.63	214.60
	B <i>Dicarinella concavata</i>	Planktonic foraminifer			91.08	222.63	224.19	223.41
	T <i>Helvetoglobotruncana helvetica</i>	Planktonic foraminifer			92.99	224.19	225.59	224.89
	B <i>Helvetoglobotruncana helvetica</i>	Planktonic foraminifer			93.53	227.45	228.60	228.03
D07	T <i>Rotalipora cushmani</i>	Planktonic foraminifer			95.94	230.63	233.54	232.09
D08	B <i>Thalmanninella reicheli</i>	Planktonic foraminifer			96.08	245.35	246.85	246.10
D09	B <i>Thalmanninella globotruncanoides</i>	Planktonic foraminifer			100.50	246.85	248.35	247.60
	T <i>Planomalina buxtorfi</i>	Planktonic foraminifer			101.92	267.40	268.16	267.78
D06	C20r/C21n	Chron boundary			45.72			46.98
D07	C21n/C21r	Chron boundary			47.35			82.98
D08	C21r/C22n	Chron boundary			48.57			85.45
D09	C22n/C22r	Chron boundary			49.34			90.69
	C25r/C26n	Chron boundary			58.96			147.57

T = top, Tc = top common, B = base, Ba = base acme, Bc = base common, X = faunal crossover.



Table T16. Datum tie points, Hole U1407A.

Datum tie point	Datum	Datum type	Zone/Subzone	Age (Ma)	Mid-point depth (mbsf)	Distance (m)	Duration (Ma)	LSR (cm/k.y.)	Notes
D01	Ba <i>Emiliana huxleyi</i>	Calcareous nannofossil	NN21	0.70	0.37				
D02	T <i>Reticulofenestra umbilicus</i> (>14 µm)	Calcareous nannofossil	NP23	32.02	15.12	15.12	31.32		
D03	T <i>Discoaster saipanensis</i>	Calcareous nannofossil	NP21	34.44	16.68	1.56	2.42	0.14	
D04	T <i>Discoaster barbadiensis</i>	Calcareous nannofossil		34.76	18.16	1.48	0.32	0.46	
D05	T <i>Chiasmolithus gigas</i>	Calcareous nannofossil	NP15c	44.12	18.16	0.00	9.36	0.00	Hiatus
D06	C20r/C21n	Chron boundary		45.72	46.98	28.82	1.60	1.80	Average rate = 2.01 cm/k.y.
D07	C21n/C21r	Chron boundary		47.35	82.98	36.00	1.62	2.22	
D08	C21r/C22n	Chron boundary		48.57	85.45	2.47	1.22	0.20	Average rate = 0.39 cm/k.y.
D09	C22n/C22r	Chron boundary		49.34	90.69	5.24	0.78	0.67	
D10	B <i>Dictyococcites/Reticulofenestra*</i>	Calcareous nannofossil		49.47	101.85	11.16	0.13	8.70	
D11	B <i>Coccolithus crassus*</i>	Calcareous nannofossil		51.64	101.85	0.00	2.17	0.00	Hiatus
D12	B <i>Tribrachiatius orthostylus</i>	Calcareous nannofossil		54.37	121.90	19.97	2.73	0.73	
D13	T <i>Fasciculithus</i> spp.	Calcareous nannofossil		55.64	121.90	0.00	1.27	0.00	Hiatus
D14	B <i>Discoaster multiradiatus</i>	Calcareous nannofossil	NP9	57.21	132.18	5.75	1.57	0.37	
D15	T <i>Anthocyrtis mespilus</i>	Radiolarian	RP6a	62.00	177.25	49.68	4.79	1.04	
D16	B <i>Cruciplacolithus intermedius</i>	Calcareous nannofossil		65.47	186.70	9.40	3.47	0.27	
D17	T <i>Micula murus</i> , other Cretaceous nannofossils	Calcareous nannofossil		66.04	186.70	0.00	0.57	0.00	
D18	B <i>Ceratolithoides kampfneri</i>	Calcareous nannofossil		67.84	190.01	0.99	1.80	0.05	
D19	B <i>Lithraphidites quadratus</i>	Calcareous nannofossil	UC20	69.18	190.01	0.00	1.34	0.00	Condensed; average rate = 0.11 cm/k.y.
D20	T <i>Reinhardtites levii</i>	Calcareous nannofossil	UC19	70.14	190.01	4.73	0.96	0.49	
D21	T <i>Eiffellithus eximius</i>	Calcareous nannofossil		75.93	190.01	0.00	5.79	0.00	
D22	B <i>Broinsonia parca constricta</i>	Calcareous nannofossil		81.38	197.35	3.58	5.45	0.07	
D23	B <i>Lithastrinus grillii</i>	Calcareous nannofossil		86.50	205.72	8.87	5.12	0.17	
D24	B <i>Micula stauropora</i>	Calcareous nannofossil		89.77	215.21	1.75	3.27	0.05	
D25	B <i>Lithastrinus septenarius</i> senso lato	Calcareous nannofossil		91.78	226.05	17.23	2.01	0.86	
D26	B <i>Eiffellithus eximius</i>	Calcareous nannofossil		92.99	226.05	0.00	1.21	0.00	
D27	B <i>Erolithus moratus</i>	Calcareous nannofossil		93.73	226.05	4.50	0.74	0.61	Average rate = 0.46 cm/k.y.
D28	T <i>Helenea chiastia</i>	Calcareous nannofossil		93.9	232.89	5.10	0.17	3.00	
D29	B <i>Lithraphidites acutus</i>	Calcareous nannofossil		96.16	245.35	10.45	2.26	0.46	
D30	B <i>Eiffellithus turriseiffelii</i>	Calcareous nannofossil		103.13	269.01	24.75	6.97	0.36	

* = from Agnini et al. (2006) recalibrated to GTS2012. LSR = linear sedimentation rate. T = top, B = base, Ba = base of acme.

Table T17. Carbonate content and accumulation rates, Site U1407. (Continued on next eight pages.)

Age (Ma)	LSR (cm/k.y.)	Dry density (g/cm³)	CaCO ₃ (wt%)	MAR (g/cm²/k.y.)	CAR (g/cm²/k.y.)	nCAR (g/cm²/k.y.)
0.8	0.05	1.25	34.99	0.07	0.02	0.04
1.0	0.05	1.22	34.15	0.06	0.02	0.04
1.2	0.05	1.19	33.31	0.06	0.02	0.04
1.4	0.05	1.15	32.48	0.06	0.02	0.04
1.6	0.05	1.12	31.64	0.06	0.02	0.04
1.8	0.05	1.09	30.81	0.06	0.02	0.04
2.0	0.05	1.06	29.97	0.06	0.02	0.04
2.2	0.05	1.03	29.13	0.05	0.02	0.04
2.4	0.05	1.00	28.30	0.05	0.01	0.04
2.6	0.05	0.97	27.46	0.05	0.01	0.04
2.8	0.05	0.93	26.62	0.05	0.01	0.04
3.0	0.05	0.90	25.79	0.05	0.01	0.03
3.2	0.05	0.87	24.95	0.05	0.01	0.03
3.4	0.05	0.84	24.12	0.04	0.01	0.03
3.6	0.05	0.81	23.57	0.04	0.01	0.03
3.8	0.05	0.81	25.69	0.04	0.01	0.03
4.0	0.05	0.82	28.43	0.04	0.01	0.03
4.2	0.05	0.82	31.17	0.04	0.01	0.03
4.4	0.05	0.83	33.91	0.04	0.01	0.03
4.6	0.05	0.84	36.66	0.04	0.02	0.03
4.8	0.05	0.85	39.40	0.04	0.02	0.03
5.0	0.05	0.85	42.14	0.04	0.02	0.03
5.2	0.05	0.86	44.89	0.04	0.02	0.02
5.4	0.05	0.87	47.63	0.05	0.02	0.02
5.6	0.05	0.87	50.37	0.05	0.02	0.02

Table T17 (continued). (Continued on next page.)

Age (Ma)	LSR (cm/k.y.)	Dry density (g/cm ³)	CaCO ₃ (wt%)	MAR (g/cm ² /k.y.)	CAR (g/cm ² /k.y.)	nCAR (g/cm ² /k.y.)
5.8	0.05	0.88	53.12	0.05	0.02	0.02
6.0	0.05	0.89	55.86	0.05	0.03	0.02
6.2	0.05	0.89	58.60	0.05	0.03	0.02
6.4	0.05	0.90	61.35	0.05	0.03	0.02
6.6	0.05	0.92	61.73	0.05	0.03	0.02
6.8	0.05	0.96	59.78	0.05	0.03	0.02
7.0	0.05	1.00	57.84	0.05	0.03	0.02
7.2	0.05	1.03	55.89	0.05	0.03	0.02
7.4	0.05	1.07	53.95	0.06	0.03	0.03
7.6	0.05	1.11	52.00	0.06	0.03	0.03
7.8	0.05	1.15	50.05	0.06	0.03	0.03
8.0	0.05	1.18	48.11	0.06	0.03	0.03
8.2	0.05	1.22	46.16	0.06	0.03	0.03
8.4	0.05	1.26	44.22	0.07	0.03	0.04
8.6	0.05	1.30	42.27	0.07	0.03	0.04
8.8	0.05	1.33	40.33	0.07	0.03	0.04
9.0	0.05	1.37	38.38	0.07	0.03	0.04
9.2	0.05	1.41	36.43	0.07	0.03	0.05
9.4	0.05	1.43	35.09	0.07	0.03	0.05
9.6	0.05	1.39	35.51	0.07	0.03	0.05
9.8	0.05	1.34	36.04	0.07	0.03	0.04
10.0	0.05	1.29	36.57	0.07	0.02	0.04
10.2	0.05	1.24	37.10	0.06	0.02	0.04
10.4	0.05	1.19	37.63	0.06	0.02	0.04
10.6	0.05	1.14	38.16	0.06	0.02	0.04
10.8	0.05	1.09	38.69	0.06	0.02	0.03
11.0	0.05	1.04	39.22	0.05	0.02	0.03
11.2	0.05	0.99	39.75	0.05	0.02	0.03
11.4	0.05	0.95	40.28	0.05	0.02	0.03
11.6	0.05	0.90	40.81	0.05	0.02	0.03
11.8	0.05	0.85	41.33	0.04	0.02	0.03
12.0	0.05	0.83	40.59	0.04	0.02	0.03
12.2	0.05	0.85	38.69	0.04	0.02	0.03
12.4	0.05	0.87	36.79	0.05	0.02	0.03
12.6	0.05	0.89	34.88	0.05	0.02	0.03
12.8	0.05	0.91	32.98	0.05	0.02	0.03
13.0	0.05	0.93	31.08	0.05	0.02	0.03
13.2	0.05	0.96	29.17	0.05	0.01	0.04
13.4	0.05	0.98	27.27	0.05	0.01	0.04
13.6	0.05	1.00	25.37	0.05	0.01	0.04
13.8	0.05	1.01	23.60	0.05	0.01	0.04
14.0	0.05	0.99	22.01	0.05	0.01	0.04
14.2	0.05	0.97	20.44	0.05	0.01	0.04
14.4	0.05	0.95	18.86	0.05	0.01	0.04
14.6	0.05	0.93	17.28	0.05	0.01	0.04
14.8	0.05	0.91	15.70	0.05	0.01	0.04
15.0	0.05	0.89	14.12	0.05	0.01	0.04
15.2	0.05	0.87	12.54	0.05	0.01	0.04
15.4	0.05	0.85	10.96	0.04	0.00	0.04
15.6	0.05	0.83	9.38	0.04	0.00	0.04
15.8	0.05	0.81	7.80	0.04	0.00	0.04
16.0	0.05	0.79	6.22	0.04	0.00	0.04
16.2	0.05	0.77	4.64	0.04	0.00	0.04
16.4	0.05	0.75	3.06	0.04	0.00	0.04
16.6	0.05	0.73	1.48	0.04	0.00	0.04
16.8	0.05	0.72	0.44	0.04	0.00	0.04
17.0	0.05	0.73	0.42	0.04	0.00	0.04
17.2	0.05	0.74	0.42	0.04	0.00	0.04
17.4	0.05	0.76	0.43	0.04	0.00	0.04
17.6	0.05	0.77	0.43	0.04	0.00	0.04
17.8	0.05	0.78	0.43	0.04	0.00	0.04
18.0	0.05	0.79	0.43	0.04	0.00	0.04
18.2	0.05	0.81	0.43	0.04	0.00	0.04
18.4	0.05	0.82	0.43	0.04	0.00	0.04
18.6	0.05	0.83	0.44	0.04	0.00	0.04
18.8	0.05	0.84	0.44	0.04	0.00	0.04
19.0	0.05	0.85	0.44	0.04	0.00	0.04
19.2	0.05	0.87	0.44	0.05	0.00	0.04



Table T17 (continued). (Continued on next page.)

Age (Ma)	LSR (cm/k.y.)	Dry density (g/cm ³)	CaCO ₃ (wt%)	MAR (g/cm ² /k.y.)	CAR (g/cm ² /k.y.)	nCAR (g/cm ² /k.y.)
19.4	0.05	0.87	0.45	0.05	0.00	0.05
19.6	0.05	0.87	0.47	0.05	0.00	0.04
19.8	0.05	0.87	0.49	0.05	0.00	0.04
20.0	0.05	0.86	0.51	0.05	0.00	0.04
20.2	0.05	0.86	0.53	0.04	0.00	0.04
20.4	0.05	0.86	0.55	0.04	0.00	0.04
20.6	0.05	0.86	0.57	0.04	0.00	0.04
20.8	0.05	0.86	0.58	0.04	0.00	0.04
21.0	0.05	0.86	0.60	0.04	0.00	0.04
21.2	0.05	0.85	0.62	0.04	0.00	0.04
21.4	0.05	0.85	0.64	0.04	0.00	0.04
21.6	0.05	0.85	0.77	0.04	0.00	0.04
21.8	0.05	0.84	1.76	0.04	0.00	0.04
22.0	0.05	0.83	2.93	0.04	0.00	0.04
22.2	0.05	0.82	4.10	0.04	0.00	0.04
22.4	0.05	0.81	5.27	0.04	0.00	0.04
22.6	0.05	0.80	6.44	0.04	0.00	0.04
22.8	0.05	0.79	7.68	0.04	0.00	0.04
23.0	0.05	0.80	9.05	0.04	0.00	0.04
23.2	0.05	0.80	10.43	0.04	0.00	0.04
23.4	0.05	0.81	11.80	0.04	0.00	0.04
23.6	0.05	0.81	13.17	0.04	0.01	0.04
23.8	0.05	0.82	14.54	0.04	0.01	0.04
24.0	0.05	0.82	15.91	0.04	0.01	0.04
24.2	0.05	0.82	17.28	0.04	0.01	0.04
24.4	0.05	0.83	18.66	0.04	0.01	0.04
24.6	0.05	0.83	20.03	0.04	0.01	0.03
24.8	0.05	0.84	21.40	0.04	0.01	0.03
25.0	0.05	0.84	22.77	0.04	0.01	0.03
25.2	0.05	0.85	24.14	0.04	0.01	0.03
25.4	0.05	0.85	25.51	0.04	0.01	0.03
25.6	0.05	0.85	26.89	0.04	0.01	0.03
25.8	0.05	0.86	27.64	0.04	0.01	0.03
26.0	0.05	0.86	27.09	0.04	0.01	0.03
26.2	0.05	0.85	26.51	0.04	0.01	0.03
26.4	0.05	0.85	25.93	0.04	0.01	0.03
26.6	0.05	0.85	25.34	0.04	0.01	0.03
26.8	0.05	0.85	24.76	0.04	0.01	0.03
27.0	0.05	0.85	24.18	0.04	0.01	0.03
27.2	0.05	0.85	23.59	0.04	0.01	0.03
27.4	0.05	0.85	23.01	0.04	0.01	0.03
27.6	0.05	0.84	22.43	0.04	0.01	0.03
27.8	0.05	0.84	21.85	0.04	0.01	0.03
28.0	0.05	0.84	21.26	0.04	0.01	0.03
28.2	0.05	0.84	20.68	0.04	0.01	0.03
28.4	0.05	0.84	20.10	0.04	0.01	0.03
28.6	0.05	0.84	19.53	0.04	0.01	0.04
28.8	0.05	0.84	19.67	0.04	0.01	0.04
29.0	0.05	0.84	20.14	0.04	0.01	0.03
29.2	0.05	0.84	20.61	0.04	0.01	0.03
29.4	0.05	0.84	21.08	0.04	0.01	0.03
29.6	0.05	0.84	21.55	0.04	0.01	0.03
29.8	0.05	0.84	22.02	0.04	0.01	0.03
30.0	0.05	0.84	22.49	0.04	0.01	0.03
30.2	0.05	0.84	22.96	0.04	0.01	0.03
30.4	0.05	0.84	23.43	0.04	0.01	0.03
30.6	0.05	0.84	23.91	0.04	0.01	0.03
30.8	0.05	0.85	24.38	0.04	0.01	0.03
31.0	0.05	0.85	24.85	0.04	0.01	0.03
31.2	0.05	0.85	25.32	0.04	0.01	0.03
31.4	0.05	0.85	25.79	0.04	0.01	0.03
31.6	0.05	0.85	26.26	0.04	0.01	0.03
31.8	0.05	0.85	26.73	0.04	0.01	0.03
32.0	0.05	0.85	27.20	0.04	0.01	0.03
32.2	0.00	0.85	27.67	0.00	0.00	0.00
32.4	0.00	0.85	28.14	0.00	0.00	0.00
32.6	0.00	0.85	28.61	0.00	0.00	0.00
32.8	0.00	0.85	29.08	0.00	0.00	0.00



Table T17 (continued). (Continued on next page.)

Age (Ma)	LSR (cm/k.y.)	Dry density (g/cm ³)	CaCO ₃ (wt%)	MAR (g/cm ² /k.y.)	CAR (g/cm ² /k.y.)	nCAR (g/cm ² /k.y.)
33.0	0.00	0.85	29.55	0.00	0.00	0.00
33.2	0.00	0.85	30.02	0.00	0.00	0.00
33.4	0.00	0.86	30.49	0.00	0.00	0.00
33.6	0.00	0.86	30.96	0.00	0.00	0.00
33.8	0.00	0.86	31.43	0.00	0.00	0.00
34.0	0.00	0.86	31.91	0.00	0.00	0.00
34.2	0.00	0.86	32.38	0.00	0.00	0.00
34.4	0.00	0.86	32.84	0.00	0.00	0.00
34.6	0.46	0.86	33.17	0.40	0.13	0.27
34.8	0.00	0.86	33.41	0.00	0.00	0.00
35.0	0.00	0.86	33.64	0.00	0.00	0.00
35.2	0.00	0.85	33.88	0.00	0.00	0.00
35.4	0.00	0.85	34.12	0.00	0.00	0.00
35.6	0.00	0.85	34.36	0.00	0.00	0.00
35.8	0.00	0.85	34.60	0.00	0.00	0.00
36.0	0.00	0.85	34.84	0.00	0.00	0.00
36.2	0.00	0.84	35.08	0.00	0.00	0.00
36.4	0.00	0.84	35.32	0.00	0.00	0.00
36.6	0.00	0.84	35.55	0.00	0.00	0.00
36.8	0.00	0.84	35.79	0.00	0.00	0.00
37.0	0.00	0.84	36.03	0.00	0.00	0.00
37.2	0.00	0.84	36.27	0.00	0.00	0.00
37.4	0.00	0.83	36.51	0.00	0.00	0.00
37.6	0.00	0.83	36.75	0.00	0.00	0.00
37.8	0.00	0.83	36.99	0.00	0.00	0.00
38.0	0.00	0.83	37.23	0.00	0.00	0.00
38.2	0.00	0.83	37.46	0.00	0.00	0.00
38.4	0.00	0.83	37.70	0.00	0.00	0.00
38.6	0.00	0.82	37.94	0.00	0.00	0.00
38.8	0.00	0.82	38.18	0.00	0.00	0.00
39.0	0.00	0.82	38.42	0.00	0.00	0.00
39.2	0.00	0.82	38.66	0.00	0.00	0.00
39.4	0.00	0.82	38.90	0.00	0.00	0.00
39.6	0.00	0.82	39.14	0.00	0.00	0.00
39.8	0.00	0.81	39.38	0.00	0.00	0.00
40.0	0.00	0.81	39.61	0.00	0.00	0.00
40.2	0.00	0.81	39.85	0.00	0.00	0.00
40.4	0.00	0.81	40.09	0.00	0.00	0.00
40.6	0.00	0.81	40.33	0.00	0.00	0.00
40.8	0.00	0.80	40.57	0.00	0.00	0.00
41.0	0.00	0.80	40.81	0.00	0.00	0.00
41.2	0.00	0.80	41.05	0.00	0.00	0.00
41.4	0.00	0.80	41.29	0.00	0.00	0.00
41.6	0.00	0.80	41.52	0.00	0.00	0.00
41.8	0.00	0.80	41.76	0.00	0.00	0.00
42.0	0.00	0.79	42.00	0.00	0.00	0.00
42.2	0.00	0.79	42.24	0.00	0.00	0.00
42.4	0.00	0.79	42.48	0.00	0.00	0.00
42.6	0.00	0.79	42.72	0.00	0.00	0.00
42.8	0.00	0.79	42.96	0.00	0.00	0.00
43.0	0.00	0.79	43.20	0.00	0.00	0.00
43.2	0.00	0.78	43.43	0.00	0.00	0.00
43.4	0.00	0.78	43.67	0.00	0.00	0.00
43.6	0.00	0.78	43.91	0.00	0.00	0.00
43.8	0.00	0.78	44.15	0.00	0.00	0.00
44.0	0.00	0.78	44.39	0.00	0.00	0.00
44.2	1.80	0.82	47.28	1.47	0.70	0.78
44.4	1.80	0.83	45.17	1.49	0.67	0.82
44.6	1.80	0.77	47.29	1.39	0.66	0.73
44.8	1.80	0.79	45.60	1.43	0.65	0.78
45.0	1.80	0.78	40.22	1.41	0.57	0.84
45.2	1.80	0.80	45.00	1.44	0.65	0.79
45.4	1.80	0.82	46.35	1.48	0.68	0.79
45.6	1.80	0.80	43.90	1.44	0.63	0.81
45.8	2.22	0.82	47.68	1.81	0.86	0.95
46.0	2.22	0.85	46.42	1.88	0.87	1.01
46.2	2.22	0.91	53.12	2.01	1.07	0.94
46.4	2.22	0.91	47.14	2.03	0.96	1.07



Table T17 (continued). (Continued on next page.)

Age (Ma)	LSR (cm/k.y.)	Dry density (g/cm ³)	CaCO ₃ (wt%)	MAR (g/cm ² /k.y.)	CAR (g/cm ² /k.y.)	nCAR (g/cm ² /k.y.)
46.6	2.22	0.89	40.76	1.97	0.80	1.16
46.8	2.22	0.89	35.15	1.97	0.69	1.28
47.0	2.22	0.91	43.25	2.03	0.88	1.15
47.2	2.22	0.97	49.19	2.14	1.06	1.09
47.4	0.20	0.96	67.83	0.19	0.13	0.06
47.6	0.20	1.02	86.43	0.21	0.18	0.03
47.8	0.20	1.03	86.40	0.21	0.18	0.03
48.0	0.20	1.04	86.37	0.21	0.18	0.03
48.2	0.20	1.05	86.44	0.21	0.18	0.03
48.4	0.20	1.02	87.01	0.21	0.18	0.03
48.6	0.67	0.99	87.63	0.67	0.58	0.08
48.8	0.67	0.96	86.73	0.65	0.56	0.09
49.0	0.67	0.98	85.63	0.66	0.56	0.09
49.2	0.67	1.00	86.02	0.68	0.58	0.09
49.4	8.70	1.05	87.68	9.16	8.03	1.13
49.6	0.00	1.09	89.01	0.00	0.00	0.00
49.8	0.00	1.09	89.06	0.00	0.00	0.00
50.0	0.00	1.10	89.10	0.00	0.00	0.00
50.2	0.00	1.10	89.14	0.00	0.00	0.00
50.4	0.00	1.11	89.19	0.00	0.00	0.00
50.6	0.00	1.11	89.23	0.00	0.00	0.00
50.8	0.00	1.12	89.28	0.00	0.00	0.00
51.0	0.00	1.12	89.32	0.00	0.00	0.00
51.2	0.00	1.13	89.36	0.00	0.00	0.00
51.4	0.00	1.13	89.41	0.00	0.00	0.00
51.6	0.00	1.14	89.45	0.00	0.00	0.00
51.8	0.73	1.14	88.36	0.83	0.74	0.10
52.0	0.73	1.14	86.34	0.83	0.72	0.11
52.2	0.73	1.14	84.31	0.83	0.70	0.13
52.4	0.73	1.14	82.28	0.83	0.69	0.15
52.6	0.73	1.14	80.26	0.83	0.67	0.16
52.8	0.73	1.14	78.23	0.83	0.65	0.18
53.0	0.73	1.14	76.21	0.83	0.63	0.20
53.2	0.73	1.14	74.18	0.83	0.62	0.21
53.4	0.73	1.14	72.15	0.83	0.60	0.23
53.6	0.73	1.13	70.13	0.83	0.58	0.25
53.8	0.73	1.13	68.10	0.83	0.57	0.26
54.0	0.73	1.13	66.08	0.83	0.55	0.28
54.2	0.73	1.13	64.05	0.83	0.53	0.30
54.4	0.00	1.13	62.02	0.00	0.00	0.00
54.6	0.00	1.13	60.00	0.00	0.00	0.00
54.8	0.00	1.13	57.97	0.00	0.00	0.00
55.0	0.00	1.13	55.95	0.00	0.00	0.00
55.2	0.00	1.13	53.92	0.00	0.00	0.00
55.4	0.00	1.13	51.89	0.00	0.00	0.00
55.6	0.00	1.13	49.87	0.00	0.00	0.00
55.8	0.37	1.12	52.29	0.41	0.21	0.20
56.0	0.37	1.09	66.51	0.40	0.26	0.13
56.2	0.37	1.06	80.37	0.39	0.31	0.08
56.4	0.37	1.04	83.10	0.38	0.32	0.06
56.6	0.37	1.03	82.72	0.38	0.31	0.06
56.8	0.37	1.01	82.34	0.37	0.31	0.07
57.0	0.37	1.00	81.84	0.37	0.30	0.07
57.2	0.37	0.97	80.68	0.35	0.29	0.07
57.4	1.04	0.94	79.41	0.97	0.77	0.20
57.6	1.04	0.90	78.14	0.94	0.73	0.21
57.8	1.04	0.87	76.87	0.90	0.70	0.21
58.0	1.04	0.84	75.60	0.88	0.66	0.21
58.2	1.04	0.87	74.68	0.90	0.67	0.23
58.4	1.04	0.86	78.04	0.90	0.70	0.20
58.6	1.04	0.90	78.23	0.93	0.73	0.20
58.8	1.04	0.89	78.66	0.92	0.73	0.20
59.0	1.04	0.93	79.43	0.96	0.76	0.20
59.2	1.04	1.00	78.99	1.04	0.82	0.22
59.4	1.04	0.96	79.27	1.00	0.79	0.21
59.6	1.04	0.93	76.08	0.96	0.73	0.23
59.8	1.04	0.89	72.89	0.92	0.67	0.25
60.0	1.04	0.96	79.47	1.00	0.79	0.21



Table T17 (continued). (Continued on next page.)

Age (Ma)	LSR (cm/k.y.)	Dry density (g/cm ³)	CaCO ₃ (wt%)	MAR (g/cm ² /k.y.)	CAR (g/cm ² /k.y.)	nCAR (g/cm ² /k.y.)
60.2	1.04	1.03	84.35	1.07	0.90	0.17
60.4	1.04	1.01	83.35	1.05	0.87	0.17
60.6	1.04	1.00	80.81	1.04	0.84	0.20
60.8	1.04	0.95	78.68	0.99	0.78	0.21
61.0	1.04	0.93	78.24	0.96	0.75	0.21
61.2	1.04	0.89	79.64	0.92	0.74	0.19
61.4	1.04	1.04	79.53	1.08	0.86	0.22
61.6	1.04	1.13	72.10	1.18	0.85	0.33
61.8	1.04	1.25	65.15	1.30	0.85	0.45
62.0	0.27	1.25	63.29	0.34	0.21	0.12
62.2	0.27	1.16	62.30	0.31	0.20	0.12
62.4	0.27	1.18	61.69	0.32	0.20	0.12
62.6	0.27	1.20	61.09	0.32	0.20	0.13
62.8	0.27	1.21	59.98	0.33	0.20	0.13
63.0	0.27	1.23	57.73	0.33	0.19	0.14
63.2	0.27	1.24	55.43	0.34	0.19	0.15
63.4	0.27	1.24	55.20	0.34	0.19	0.15
63.6	0.27	1.22	59.25	0.33	0.20	0.13
63.8	0.27	1.19	63.42	0.32	0.20	0.12
64.0	0.27	1.17	67.59	0.32	0.21	0.10
64.2	0.27	1.14	71.76	0.31	0.22	0.09
64.4	0.27	1.12	75.94	0.30	0.23	0.07
64.6	0.27	1.10	80.11	0.30	0.24	0.06
64.8	0.27	1.08	82.97	0.29	0.24	0.05
65.0	0.27	1.08	81.97	0.29	0.24	0.05
65.2	0.27	1.08	80.87	0.29	0.24	0.06
65.4	0.27	1.10	81.19	0.30	0.24	0.06
65.6	0.00	1.12	81.86	0.00	0.00	0.00
65.8	0.00	1.14	82.52	0.00	0.00	0.00
66.0	0.00	1.16	83.19	0.00	0.00	0.00
66.2	0.06	1.19	83.85	0.07	0.05	0.01
66.4	0.06	1.21	84.51	0.07	0.06	0.01
66.6	0.06	1.23	85.18	0.07	0.06	0.01
66.8	0.06	1.25	85.84	0.07	0.06	0.01
67.0	0.06	1.27	86.51	0.07	0.06	0.01
67.2	0.06	1.30	87.17	0.07	0.06	0.01
67.4	0.06	1.32	87.83	0.07	0.06	0.01
67.6	0.06	1.32	88.31	0.07	0.06	0.01
67.8	0.06	1.30	88.67	0.07	0.06	0.01
68.0	0.00	1.28	89.03	0.00	0.00	0.00
68.2	0.00	1.27	89.39	0.00	0.00	0.00
68.4	0.00	1.25	89.75	0.00	0.00	0.00
68.6	0.00	1.23	90.11	0.00	0.00	0.00
68.8	0.00	1.22	90.47	0.00	0.00	0.00
69.0	0.00	1.20	90.83	0.00	0.00	0.00
69.2	0.49	1.18	91.19	0.58	0.53	0.05
69.4	0.49	1.17	91.41	0.57	0.53	0.05
69.6	0.49	1.18	90.72	0.58	0.53	0.05
69.8	0.49	1.19	89.82	0.59	0.53	0.06
70.0	0.49	1.21	88.67	0.60	0.53	0.07
70.2	0.00	1.22	88.38	0.00	0.00	0.00
70.4	0.00	1.22	88.31	0.00	0.00	0.00
70.6	0.00	1.22	88.24	0.00	0.00	0.00
70.8	0.00	1.22	88.17	0.00	0.00	0.00
71.0	0.00	1.22	88.10	0.00	0.00	0.00
71.2	0.00	1.22	88.03	0.00	0.00	0.00
71.4	0.00	1.22	87.96	0.00	0.00	0.00
71.6	0.00	1.22	87.89	0.00	0.00	0.00
71.8	0.00	1.22	87.82	0.00	0.00	0.00
72.0	0.00	1.22	87.75	0.00	0.00	0.00
72.2	0.00	1.22	87.68	0.00	0.00	0.00
72.4	0.00	1.22	87.61	0.00	0.00	0.00
72.6	0.00	1.22	87.54	0.00	0.00	0.00
72.8	0.00	1.22	87.47	0.00	0.00	0.00
73.0	0.00	1.22	87.40	0.00	0.00	0.00
73.2	0.00	1.22	87.33	0.00	0.00	0.00
73.4	0.00	1.22	87.26	0.00	0.00	0.00
73.6	0.00	1.22	87.19	0.00	0.00	0.00



Table T17 (continued). (Continued on next page.)

Age (Ma)	LSR (cm/k.y.)	Dry density (g/cm ³)	CaCO ₃ (wt%)	MAR (g/cm ² /k.y.)	CAR (g/cm ² /k.y.)	nCAR (g/cm ² /k.y.)
73.8	0.00	1.22	87.12	0.00	0.00	0.00
74.0	0.00	1.22	87.05	0.00	0.00	0.00
74.2	0.00	1.22	86.98	0.00	0.00	0.00
74.4	0.00	1.22	86.91	0.00	0.00	0.00
74.6	0.00	1.22	86.83	0.00	0.00	0.00
74.8	0.00	1.22	86.76	0.00	0.00	0.00
75.0	0.00	1.22	86.69	0.00	0.00	0.00
75.2	0.00	1.22	86.62	0.00	0.00	0.00
75.4	0.00	1.22	86.55	0.00	0.00	0.00
75.6	0.00	1.22	86.48	0.00	0.00	0.00
75.8	0.00	1.22	86.41	0.00	0.00	0.00
76.0	0.07	1.22	86.34	0.08	0.07	0.01
76.2	0.07	1.22	86.27	0.08	0.07	0.01
76.4	0.07	1.22	86.20	0.08	0.07	0.01
76.6	0.07	1.23	86.13	0.08	0.07	0.01
76.8	0.07	1.23	86.06	0.08	0.07	0.01
77.0	0.07	1.23	85.99	0.08	0.07	0.01
77.2	0.07	1.23	85.92	0.08	0.07	0.01
77.4	0.07	1.23	85.85	0.08	0.07	0.01
77.6	0.07	1.23	85.78	0.08	0.07	0.01
77.8	0.07	1.23	85.71	0.08	0.07	0.01
78.0	0.07	1.23	85.64	0.08	0.07	0.01
78.2	0.07	1.23	85.56	0.08	0.07	0.01
78.4	0.07	1.23	85.46	0.08	0.07	0.01
78.6	0.07	1.23	85.36	0.08	0.07	0.01
78.8	0.07	1.23	85.25	0.08	0.07	0.01
79.0	0.07	1.23	85.15	0.08	0.07	0.01
79.2	0.07	1.24	85.05	0.08	0.07	0.01
79.4	0.07	1.24	84.95	0.08	0.07	0.01
79.6	0.07	1.24	84.84	0.08	0.07	0.01
79.8	0.07	1.24	84.74	0.08	0.07	0.01
80.0	0.07	1.24	84.64	0.08	0.07	0.01
80.2	0.07	1.24	84.54	0.08	0.07	0.01
80.4	0.07	1.25	84.46	0.08	0.07	0.01
80.6	0.07	1.27	84.45	0.08	0.07	0.01
80.8	0.07	1.28	84.45	0.08	0.07	0.01
81.0	0.07	1.30	84.45	0.09	0.07	0.01
81.2	0.07	1.31	84.45	0.09	0.07	0.01
81.4	0.17	1.33	84.45	0.23	0.19	0.04
81.6	0.17	1.35	84.45	0.23	0.20	0.04
81.8	0.17	1.36	84.45	0.24	0.20	0.04
82.0	0.17	1.39	83.70	0.24	0.20	0.04
82.2	0.17	1.42	81.22	0.25	0.20	0.05
82.4	0.17	1.45	78.68	0.25	0.20	0.05
82.6	0.17	1.49	76.15	0.26	0.20	0.06
82.8	0.17	1.51	74.92	0.26	0.20	0.07
83.0	0.17	1.50	75.77	0.26	0.20	0.06
83.2	0.17	1.49	76.65	0.26	0.20	0.06
83.4	0.17	1.48	77.53	0.26	0.20	0.06
83.6	0.17	1.47	78.41	0.25	0.20	0.06
83.8	0.17	1.46	79.29	0.25	0.20	0.05
84.0	0.17	1.45	80.17	0.25	0.20	0.05
84.2	0.17	1.44	81.05	0.25	0.20	0.05
84.4	0.17	1.43	81.93	0.25	0.20	0.04
84.6	0.17	1.43	82.81	0.25	0.20	0.04
84.8	0.17	1.42	83.69	0.25	0.21	0.04
85.0	0.17	1.41	84.57	0.24	0.21	0.04
85.2	0.17	1.40	85.45	0.24	0.21	0.04
85.4	0.17	1.39	86.32	0.24	0.21	0.03
85.6	0.17	1.38	87.20	0.24	0.21	0.03
85.8	0.17	1.37	88.08	0.24	0.21	0.03
86.0	0.17	1.34	88.89	0.23	0.21	0.03
86.2	0.17	1.31	89.67	0.23	0.20	0.02
86.4	0.17	1.27	90.46	0.22	0.20	0.02
86.6	0.05	1.24	91.24	0.07	0.06	0.01
86.8	0.05	1.20	92.00	0.06	0.06	0.01
87.0	0.05	1.19	92.13	0.06	0.06	0.00
87.2	0.05	1.19	91.98	0.06	0.06	0.01



Table T17 (continued). (Continued on next page.)

Age (Ma)	LSR (cm/k.y.)	Dry density (g/cm ³)	CaCO ₃ (wt%)	MAR (g/cm ² /k.y.)	CAR (g/cm ² /k.y.)	nCAR (g/cm ² /k.y.)
87.4	0.05	1.19	91.84	0.06	0.06	0.01
87.6	0.05	1.20	91.69	0.06	0.06	0.01
87.8	0.05	1.20	91.54	0.06	0.06	0.01
88.0	0.05	1.21	91.39	0.06	0.06	0.01
88.2	0.05	1.21	91.24	0.06	0.06	0.01
88.4	0.05	1.21	91.09	0.06	0.06	0.01
88.6	0.05	1.22	90.94	0.07	0.06	0.01
88.8	0.05	1.22	90.79	0.07	0.06	0.01
89.0	0.05	1.23	90.64	0.07	0.06	0.01
89.2	0.05	1.23	90.49	0.07	0.06	0.01
89.4	0.05	1.23	90.36	0.07	0.06	0.01
89.6	0.05	1.22	90.27	0.07	0.06	0.01
89.8	0.86	1.21	90.18	1.04	0.93	0.10
90.0	0.86	1.20	90.08	1.03	0.92	0.10
90.2	0.86	1.18	89.99	1.02	0.91	0.10
90.4	0.86	1.17	89.90	1.00	0.90	0.10
90.6	0.86	1.16	89.81	0.99	0.89	0.10
90.8	0.86	1.15	89.72	0.98	0.88	0.10
91.0	0.86	1.14	89.62	0.97	0.87	0.10
91.2	0.86	1.12	89.53	0.96	0.86	0.10
91.4	0.86	1.11	89.44	0.95	0.85	0.10
91.6	0.86	1.10	89.35	0.94	0.84	0.10
91.8	0.00	1.08	89.41	0.00	0.00	0.00
92.0	0.00	1.06	89.62	0.00	0.00	0.00
92.2	0.00	1.03	89.82	0.00	0.00	0.00
92.4	0.00	1.00	90.02	0.00	0.00	0.00
92.6	0.00	0.98	90.23	0.00	0.00	0.00
92.8	0.00	0.95	90.43	0.00	0.00	0.00
93.0	0.61	0.93	90.63	0.56	0.51	0.05
93.2	0.61	1.01	89.32	0.62	0.55	0.07
93.4	0.61	1.26	86.43	0.77	0.66	0.10
93.6	0.61	1.28	87.60	0.78	0.68	0.10
93.8	3.00	1.31	67.55	3.93	2.66	1.28
94.0	0.46	1.26	84.98	0.58	0.49	0.09
94.2	0.46	1.32	82.79	0.61	0.51	0.11
94.4	0.46	1.34	82.75	0.62	0.51	0.11
94.6	0.46	1.26	83.88	0.58	0.49	0.09
94.8	0.46	1.29	82.96	0.60	0.49	0.10
95.0	0.46	1.39	81.48	0.64	0.52	0.12
95.2	0.46	1.53	83.94	0.71	0.59	0.11
95.4	0.46	1.50	82.61	0.69	0.57	0.12
95.6	0.46	1.44	80.65	0.66	0.54	0.13
95.8	0.46	1.40	80.54	0.65	0.52	0.13
96.0	0.46	1.43	85.34	0.66	0.56	0.10
96.2	0.36	1.44	85.28	0.51	0.43	0.08
96.4	0.36	1.43	81.68	0.51	0.41	0.09
96.6	0.36	1.44	80.35	0.51	0.41	0.10
96.8	0.36	1.49	81.01	0.53	0.43	0.10
97.0	0.36	1.51	78.45	0.54	0.42	0.12
97.2	0.36	1.52	74.68	0.54	0.40	0.14
97.4	0.36	1.53	74.95	0.54	0.41	0.14
97.6	0.36	1.52	77.63	0.54	0.42	0.12
97.8	0.36	1.52	80.32	0.54	0.43	0.11
98.0	0.36	1.51	83.00	0.54	0.45	0.09
98.2	0.36	1.51	85.69	0.54	0.46	0.08
98.4	0.36	1.51	86.53	0.54	0.47	0.07
98.6	0.36	1.53	85.17	0.55	0.46	0.08
98.8	0.36	1.56	83.82	0.55	0.46	0.09
99.0	0.36	1.50	83.74	0.53	0.45	0.09
99.2	0.36	1.40	83.38	0.50	0.41	0.08
99.4	0.36	1.49	78.57	0.53	0.42	0.11
99.6	0.36	1.57	74.87	0.56	0.42	0.14
99.8	0.36	1.58	76.07	0.56	0.43	0.13
100.0	0.36	1.57	76.59	0.56	0.43	0.13
100.2	0.36	1.50	74.45	0.53	0.40	0.14
100.4	0.36	1.48	73.32	0.52	0.38	0.14
100.6	0.36	1.49	73.07	0.53	0.39	0.14
100.8	0.36	1.51	72.82	0.54	0.39	0.15
101.0	0.36	1.52	72.59	0.54	0.39	0.15



Table T17 (continued).

Age (Ma)	LSR (cm/k.y.)	Dry density (g/cm ³)	CaCO ₃ (wt%)	MAR (g/cm ² /k.y.)	CAR (g/cm ² /k.y.)	nCAR (g/cm ² /k.y.)
101.2	0.36	1.54	72.44	0.55	0.40	0.15
101.4	0.36	1.57	72.47	0.56	0.40	0.15
101.6	0.36	1.62	75.92	0.57	0.44	0.14
101.8	0.36	1.67	80.46	0.59	0.48	0.12
102.0	0.36	1.67	80.52	0.59	0.48	0.12
102.2	0.36	1.64	78.77	0.58	0.46	0.12
102.4	0.36		76.27	0.00	0.00	0.00
102.6	0.36		73.34	0.00	0.00	0.00
102.8	0.36		73.10	0.00	0.00	0.00

LSR = linear sedimentation rate, MAR = mass accumulation rate, CAR = carbonate accumulation rate, nCAR = noncarbonate accumulation rate.

Table T18. Geochemistry of headspace gas samples, Hole U1407A.

Core, section, interval (cm)	Depth (mbsf)	Methane (ppmv)
342-U1407A-		
1H-5, 0–5	6.00	1.56
2H-4, 0–5	11.10	1.41
3H-7, 0–5	24.80	2.08
4H-7, 0–5	34.50	1.86
5H-7, 0–5	44.30	2.01
6H-7, 0–5	53.80	2.05
7H-7, 0–5	63.30	2.03
8H-7, 0–5	72.80	2.62
9H-7, 0–5	82.30	2.51
10H-7, 0–5	91.50	2.30
11H-7, 0–5	101.30	2.32
16X-2, 0–5	123.40	4.12
17X-1, 0–5	126.30	2.34
18X-3, 0–5	138.90	3.17
19X-3, 0–5	148.31	3.38
20X-7, 0–5	163.90	2.89
21X-5, 0–5	170.70	2.85
22X-5, 0–5	180.30	2.25
23X-6, 0–5	191.40	2.96
24X-4, 0–5	198.00	2.49
25X-3, 0–5	205.66	2.81
27X-6, 0–5	229.80	1.86
28X-6, 0–5	239.00	1.84
29X-6, 0–5	249.00	2.09
30X-6, 0–5	258.09	1.90
31X-5, 0–5	266.70	1.81



Table T19. Interstitial water constituents, Hole U1407A.

Core, section, interval (cm)	Depth (mbsf)	pH	Alkalinity (mM)	Ammonium (μM)	Salinity	Cl^- (mM)	Fe^{2+} (μM)	Na^+ (mM)	SO_4^{2-} (mM)	HPO_4^{2-} (μM)	Mn^{2+} (μM)	B (μM)	Ca^{2+} (mM)	Mg^{2+} (mM)	K^+ (mM)	Mg/Ca
342-U1407A-																
1H-4, 145–150	5.95	7.359	3.084	0	37	559.053	BDL	472.752	28.581	BDL	4.4	415.587	10.924	52.625	12.543	4.8
2H-3, 125–130	11.05	7.412	3.132	32	37	559.161	BDL	472.577	29.069	BDL	BDL	505.115	11.112	53.257	12.618	4.8
3H-6, 95–100	24.75	7.357	3.022	71	37	563.286	BDL	475.702	28.278	BDL	0.09	568.365	11.086	52.847	12.906	4.8
4H-6, 115–120	34.45	7.366	2.991	0	37	557.867	BDL	470.831	27.457	BDL	1.581	482.646	11.257	52.504	12.047	4.7
5H-6, 145–150	44.25	7.379	3.01	0	38	560.719	BDL	475.965	27.77	BDL	1.214	553.437	11.564	52.696	12.658	4.6
6H-6, 145–150	53.75	7.383	3.102	0	37	563.458	BDL	478.314	27.568	BDL	2.002	500.902	11.786	52.953	12.933	4.5
7H-6, 145–150	63.25	7.319	3.078	102	37	569.81	BDL	484.064	27.027	BDL	2.684	478.51	12.144	53.381	13.271	4.4
8H-6, 145–150	72.75	7.393	3.15	0	37	567.435	BDL	477.765	26.695	BDL	2.997	436.228	12.299	52.806	13.048	4.3
9H-6, 145–150	82.25	7.023	3.145	0	37	563.199	BDL	469.515	26.722	BDL	3.083	399.082	12.255	51.683	13.278	4.2
10H-6, 115–120	91.45	7.283	3.226	0	38	566.774	1.791	477.13	26.73	BDL	3.077	361.224	12.567	52.416	12.609	4.2
11H-6, 145–150	101.25	7.376	3.268	5	38	564.106	BDL	474.826	27.179	BDL	3.226	356.588	12.71	52.365	13.129	4.1
16X-1, 140–150	123.30	7.251	3.677	0	37	553.882	BDL	473.096	25.393	BDL	8.375	331.561	13.807	49.492	11.597	3.6
18X-2, 140–150	138.80	7.264	3.58	38	37	559.971	BDL	477.839	26.187	BDL	9.37	322.02	14.156	50.427	11.439	3.6
22X-4, 140–150	180.20	7.275	2.935	0	37	560.183	BDL	472.78	25.56	BDL	9.669	436.17	13.806	49.845	12.518	3.6
23X-5, 140–150	191.30	7.222	3.379	28	37	562.393	BDL	480.293	26.338	BDL	11.807	364.013	14.115	50.461	11.589	3.6
24X-3, 140–150	197.90	7.304	3.272	6	37	567.693	BDL	483.335	26.325	BDL	15.088	358.339	14.01	51.153	11.161	3.7
27X-5, 140–150	229.7	7.364	2.605	0	37	559.111	BDL	475.138	26.44	BDL	6.349	323.982	13.513	50.767	11.26	3.8
29X-5, 140–150	248.90	7.393	2.724	0	37	557.676	BDL	477.928	26.276	BDL	0.923	356.857	13.673	51.572	12.489	3.8
30X-5, 109–119	257.99	7.403	2.693	25	37	560.665	BDL	480.728	25.74	BDL	BDL	429.399	13.541	51.204	10.476	3.8
31X-4, 140–150	266.60	7.42	2.429	0	37	565.579	BDL	483.399	26.571	BDL	0.064	402.679	13.466	52.223	10.08	3.9

BDL = below detection limit ($\text{HPO}_4^{2-} = 0.2 \mu\text{M}$, $\text{Mn}^{2+} = 0.1 \mu\text{M}$, $\text{Fe}^{2+} = 0.6 \mu\text{M}$), calculated as two times the standard deviation of multiple measures of a blank.



Table T20. Sedimentary sample and bulk elemental geochemistry, Hole U1407A. (Continued on next two pages.)

Core, section, interval (cm)	Depth (mbstf)	CaCO ₃ (wt%)	IC (wt%)	TC (wt%)	TN (wt%)	TOC (wt%)
342-U1407A-						
1H-1, 39–40	0.39	35.245	4.226	4.46	0.03	0.23
1H-2, 39–40	1.89	22.833	2.738	2.95	0.05	0.21
1H-2, 39–40	1.89	23.569	2.826			
1H-3, 39–40	3.39	63.497	7.613	7.42	0.02	-0.19
1H-3, 39–40	3.39	61.919	7.424			
1H-4, 38–39	4.88	34.873	4.181	4.35	0.03	0.17
1H-5, 20–21	6.20	41.588	4.986	5.50	0.03	0.51
2H-1, 35–36	7.15	24.229	2.905	2.91	0.05	0.01
2H-2, 42–43	8.72	0.420	0.050	0.12	0.04	0.07
2H-3, 23–24	10.03	0.441	0.053	0.07	0.05	0.02
2H-4, 16–17	11.26	0.659	0.079	0.16	0.05	0.08
2H-5, 17–18	11.84	7.174	0.860	0.86	0.06	0.00
2H-6, 24–25	13.41	27.850	3.339	2.96	0.05	-0.38
2H-7, 26–27	14.93	19.339	2.319	2.35	0.06	0.03
3H-1, 52–53	16.82	33.012	3.958	4.00	0.06	0.04
3H-2, 39–40	18.19	44.535	5.340	5.30	0.05	-0.04
3H-3, 39–40	19.69	48.150	5.773	5.86	0.04	0.09
3H-4, 38–39	21.18	49.233	5.903	5.89	0.05	-0.01
3H-5, 42–43	22.72	45.402	5.444	5.41	0.04	-0.03
3H-6, 23–24	24.03	41.384	4.962	5.13	0.68	0.17
3H-7, 14–15	24.94	48.234	5.783	5.85	0.05	0.07
4H-1, 44–45	26.24	48.045	5.760	5.97	0.05	0.21
4H-2, 38–39	27.68	46.000	5.515	5.58	0.04	0.06
4H-3, 38–39	29.18	47.862	5.739	5.73	0.05	-0.01
4H-4, 38–39	30.68	46.791	5.610	5.60	0.05	-0.01
4H-5, 38–39	32.18	39.404	4.724	4.79	0.06	0.07
4H-6, 25–26	33.55	41.339	4.956	5.02	0.05	0.06
5H-1, 39–40	35.69	38.990	4.675	4.82	0.07	0.15
5H-2, 39–40	37.19	44.824	5.374	5.42	0.05	0.05
5H-3, 39–40	38.69	47.842	5.736	5.81	0.06	0.07
5H-4, 39–40	40.19	49.720	5.961	6.03	0.05	0.07
5H-5, 39–40	41.69	43.354	5.198	5.32	0.05	0.12
5H-6, 39–40	43.19	45.535	5.459	5.45	0.05	-0.01
5H-7, 13–14	44.43	40.033	4.800	4.80	0.06	0.00
6H-1, 38–39	45.18	44.948	5.389	5.68	0.06	0.29
6H-2, 38–39	46.68	46.012	5.517	5.56	0.05	0.04
6H-3, 38–39	48.18	49.121	5.889	6.00	0.06	0.11
6H-4, 38–39	49.68	47.701	5.719	5.73	0.06	0.01
6H-5, 30–31	51.10	46.430	5.567	5.58	0.04	0.01
6H-6, 25–26	52.55	39.721	4.762	4.79	0.05	0.03
7H-1, 40–41	54.70	53.818	6.453	6.47	0.05	0.02
7H-2, 39–40	56.19	50.236	6.023	6.05	0.04	0.03
7H-3, 39–40	57.69	42.333	5.076	5.22	0.06	0.14
7H-4, 10–11	58.90	70.645	8.470	8.57	0.03	0.10
7H-4, 30–31	59.10	53.181	6.376	6.38	0.05	0.00
7H-4, 46–47	59.26	79.466	9.528	9.81	0.02	0.28
7H-4, 87–88	59.67	47.769	5.727	5.74	0.05	0.01
7H-5, 39–40	60.69	50.144	6.012	6.14	0.05	0.13
7H-6, 38–39	62.18	45.140	5.412	5.49	0.05	0.08
7H-7, 22–23	63.52	44.356	5.318	5.41	0.06	0.09
8H-1, 38–39	64.18	52.089	6.245	6.20	0.04	-0.05
8H-2, 38–39	65.68	41.495	4.975	4.98	0.06	0.00
8H-3, 38–39	67.18	37.727	4.523	4.59	0.06	0.07
8H-4, 38–39	68.68	33.124	3.971	4.44	0.05	0.47
8H-5, 38–39	70.18	31.505	3.777	4.77	0.29	0.99
8H-6, 38–39	71.68	38.333	4.596	4.66	0.06	0.06
8H-7, 16–17	72.96	38.923	4.667	4.69	0.05	0.02
9H-1, 38–39	73.68	42.371	5.080	5.03	0.04	-0.05
9H-2, 38–39	75.18	42.934	5.148	5.77	0.03	0.62
9H-3, 38–39	76.68	45.781	5.489	5.63	0.04	0.14
9H-4, 38–39	78.18	39.993	4.795	5.11	0.04	0.31
9H-5, 38–39	79.68	44.507	5.336	5.36	0.05	0.02
9H-6, 38–39	81.18	66.308	7.950	7.98	0.02	0.03
9H-6, 38–39	81.18	65.320	7.832			
9H-7, 15–16	82.45	41.439	4.968	4.98	0.05	0.01
9H-7, 15–16	82.45	42.000	5.036			

Table T20 (continued). (Continued on next page.)

Core, section, interval (cm)	Depth (mbsf)	CaCO ₃ (wt%)	IC (wt%)	TC (wt%)	TN (wt%)	TOC (wt%)
10H-1, 38–39	83.18	86.459	10.366	10.43	0.00	0.06
10H-2, 38–39	84.68	86.334	10.351	10.84	0.01	0.49
10H-3, 38–39	86.18	87.888	10.538	10.51	0.01	-0.03
10H-4, 38–39	87.68	85.824	10.290	10.37	0.00	0.08
10H-5, 38–39	89.18	85.400	10.239	10.53	0.01	0.29
10H-6, 38–39	90.68	87.116	10.445	10.42	0.00	-0.02
10H-7, 20–21	91.70	90.091	10.802	10.87	0.00	0.07
11H-1, 38–39	92.68	84.764	10.163	11.13	0.00	0.97
11H-2, 38–39	94.18	90.404	10.839	10.97	-0.02	0.13
11H-3, 38–39	95.68	89.852	10.773	10.79	0.00	0.02
11H-4, 38–39	97.18	88.061	10.558	10.79	0.01	0.23
11H-5, 38–39	98.68	89.756	10.761	10.89	0.03	0.13
11H-6, 38–39	100.18	79.600	9.544	10.93	0.00	1.39
11H-7, 20–21	101.50	88.984	10.669	10.91	0.01	0.24
12H-1, 40–41	102.20	89.472	10.727	10.96	0.00	0.23
16X-1, 34–35	122.24	47.571	5.704	5.75	0.01	0.05
16X-1, 34–35	122.24	49.030	5.879			
16X-2, 57–58	123.97	83.429	10.003	10.24	0.00	0.24
17X-1, 49–50	126.79	81.961	9.827	9.89	0.00	0.06
18X-1, 30–31	136.20	75.319	9.031	9.36	0.00	0.33
18X-2, 40–41	137.80	74.495	8.932	9.00	0.00	0.07
18X-3, 54–55	139.44	74.826	8.971	8.62	0.02	-0.35
18X-4, 29–30	140.69	82.692	9.914	10.18	0.01	0.27
18X-5, 25–26	142.15	76.520	9.175	9.24	0.02	0.07
19X-1, 75–76	146.25	81.150	9.730	9.86	0.03	0.13
19X-2, 28–29	147.28	74.161	8.892	8.42	0.00	-0.47
19X-3, 22–23	148.53	81.946	9.825	9.77	0.01	-0.06
20X-1, 58–59	155.68	70.954	8.507	8.32	0.02	-0.19
20X-2, 65–66	157.25	87.534	10.495	10.47	0.03	-0.02
20X-3, 59–60	158.69	83.551	10.017	10.22	0.01	0.20
20X-4, 34–35	159.94	83.036	9.956	9.90	0.02	-0.06
20X-5, 34–35	161.44	83.737	10.040	9.93	0.01	-0.11
20X-6, 50–51	163.10	79.447	9.525	9.79	0.04	0.26
20X-7, 12–13	164.02	80.450	9.646	9.95	0.02	0.30
21X-1, 50–51	165.20	77.372	9.277	9.49	0.01	0.21
21X-2, 28–29	166.48	78.218	9.378	8.99	0.02	-0.39
21X-3, 52–53	168.22	78.527	9.415	9.43	0.02	0.01
21X-4, 58–59	169.78	80.905	9.700	9.59	0.02	-0.11
21X-5, 76–77	171.46	79.474	9.529	9.72	0.02	0.19
22X-1, 15–16	174.45	66.029	7.917	7.84	0.00	-0.08
22X-2, 11–12	175.91	64.073	7.682	7.84	0.01	0.16
22X-3, 29–30	177.59	62.524	7.496	7.58	0.01	0.08
22X-4, 47–48	179.27	60.646	7.271	7.43	0.02	0.16
22X-5, 58–59	180.88	53.746	6.444	6.41	0.03	-0.03
22X-5, 58–59	180.88	53.902	6.463			
23X-1, 83–84	184.73	83.473	10.008	10.25	0.02	0.24
23X-2, 57–58	185.97	80.593	9.663	9.89	0.01	0.23
23X-3, 54–55	187.44	88.088	10.561	10.43	0.01	-0.13
23X-4, 34–35	188.74	91.556	10.977	11.00	0.00	0.02
23X-5, 84–85	190.74	88.572	10.619	11.01	0.01	0.39
23X-5, 84–85	190.74	91.086	10.921			
23X-6, 37–38	191.77	88.441	10.604	10.65	0.03	0.05
24X-1, 32–33	193.82	85.595	10.263	10.11	0.00	-0.15
24X-2, 28–29	195.28	84.454	10.126	10.21	0.06	0.08
24X-3, 43–44	196.93	84.452	10.126	10.22	0.01	0.09
24X-4, 28–29	198.28	74.559	8.939	9.04	0.01	0.10
25X-1, 59–60	203.69	88.294	10.586	10.54	0.01	-0.05
25X-2, 66–67	205.01	92.242	11.060	10.53	0.04	-0.53
25X-3, 68–69	206.34	90.386	10.837	11.16	0.00	0.32
27X-1, 77–78	223.07	89.306	10.708	10.95	0.00	0.24
27X-2, 93–94	224.73	90.779	10.884	11.04	0.02	0.16
27X-3, 73–74	226.03	85.740	10.280	10.55	0.00	0.27
27X-4, 70–71	227.50	88.086	10.561	10.72	0.00	0.16
27X-5, 100–101	229.30	86.457	10.366	10.32	0.02	-0.05
27X-6, 18–19	229.98	86.209	10.336	10.64	0.03	0.30
28X-1, 32–33	232.22	1.248	0.150	1.39	0.16	1.24
28X-1, 32–33	232.22	2.473	0.297			
28X-1, 45–46	232.35	4.366	0.523	10.70	1.15	10.18
28X-1, 48–49	232.38	66.464	7.969	19.60	1.88	11.63

Table T20 (continued).

Core, section, interval (cm)	Depth (mbsf)	CaCO ₃ (wt%)	IC (wt%)	TC (wt%)	TN (wt%)	TOC (wt%)
28X-1, 136–137	233.26	90.318	10.829	11.01	0.00	0.18
28X-2, 34–35	233.74	84.156	10.090	10.18	0.01	0.09
28X-3, 36–37	235.26	82.167	9.852	10.58	0.01	0.73
28X-4, 54–55	236.94	84.319	10.110	10.30	0.00	0.19
28X-5, 68–69	238.58	80.739	9.680	9.51	0.02	-0.17
28X-6, 35–36	239.35	84.697	10.155	10.15	0.02	0.00
29X-1, 48–49	241.98	79.126	9.487	9.45	0.02	-0.04
29X-2, 48–49	243.48	87.430	10.483	10.27	0.00	-0.21
29X-3, 55–56	245.05	79.926	9.583	9.62	0.00	0.04
29X-4, 29–30	246.29	81.369	9.756	9.76	0.02	0.00
29X-5, 30–31	247.80	73.237	8.781	8.69	0.02	-0.09
30X-1, 38–39	251.48	87.148	10.449	10.68	0.00	0.23
30X-2, 108–109	253.68	82.949	9.945	10.06	0.01	0.11
30X-3, 31–32	254.41	85.104	10.204	10.43	0.00	0.23
30X-4, 39–40	255.99	74.175	8.893	8.79	0.01	-0.10
30X-5, 39–40	257.29	77.313	9.270	9.51	0.01	0.24
30X-6, 42–43	258.51	73.452	8.807	8.93	0.01	0.12
31X-1, 31–32	261.01	72.588	8.703	8.89	0.03	0.19
31X-2, 42–43	262.62	72.259	8.664	8.73	0.02	0.07
31X-3, 35–36	264.05	81.835	9.812	10.03	0.01	0.22
31X-4, 35–36	265.55	78.160	9.371	9.54	0.02	0.17
31X-5, 48–49	267.18	71.431	8.564	8.77	0.03	0.21
31X-6, 18–19	267.98	76.530	9.176	9.29	0.02	0.11
342-U1407B-						
7H-6, 10–11	57.00	46.393	5.562			
7H-6, 50–51	57.40	46.478	5.573			
7H-6, 90–91	57.80	58.249	6.984			
7H-6, 130–131	58.20	46.340	5.556			
7H-7, 20–21	58.60	49.733	5.963			
7H-7, 60–61	59.00	46.404	5.564			
10H-4, 10–11	82.50	46.407	5.564			
10H-4, 50–51	82.90	65.243	7.822			
10H-4, 141–142	83.81	69.025	8.276			
10H-5, 21–22	84.11	44.417	5.325			
10H-5, 50–51	84.40	67.990	8.152			
10H-5, 100–101	84.90	42.323	5.074			
10H-5, 145–146	85.35	64.440	7.726			
10H-6, 5–6	85.45	56.922	6.825			
10H-6, 11–12	85.51	82.612	9.905			
10H-6, 40–41	85.80	89.844	10.772			

IC = inorganic carbon, TC = total carbon, TN = total nitrogen, TOC = total organic carbon.



Table T21. Core top and composite depth, Site U1407. (Continued on next page.)

Core	Depth		Offset (m)	Cumulative offset (m)	Comment
	(mbsf)	(m CCSF)			
342-U1407A-					
1H	0.00	0.00	0.00	0.00	
2H	6.80	7.35	0.55	0.55	
3H	16.30	18.85	2.00	2.55	
4H	25.80	28.35	0.00	2.55	Tentative
5H	35.30	38.62	0.77	3.32	Tentative
6H	44.80	53.19	5.07	8.39	
7H	54.30	63.04	0.35	8.74	
8H	63.80	73.23	0.69	9.43	
9H	73.30	85.10	2.37	11.80	
10H	82.80	94.99	0.39	12.19	
11H	92.30	106.42	1.93	14.12	
12H	101.80	116.11	0.19	14.31	
13H	102.80	117.11	0.00	14.31	
14H	112.30	126.61	0.00	14.31	
15H	121.80	136.11	0.00	14.31	
16X	121.90	137.40	1.19	15.50	
17X	126.30	141.80	0.00	15.50	
18X	135.90	158.43	7.03	22.53	
19X	145.50	166.98	-1.05	21.48	
20X	155.10	185.60	9.02	30.50	
21X	164.70	195.12	-0.08	30.42	
22X	174.30	204.45	-0.27	30.15	
23X	183.90	212.93	-1.12	29.03	
24X	193.50	227.12	4.59	33.62	Tentative
25X	203.10	238.78	2.06	35.68	
26X	212.70	249.04	0.66	36.34	
27X	222.30	259.89	1.25	37.59	Tentative
28X	231.90	268.85	-0.64	36.95	
29X	241.50	286.73	8.28	45.23	Large offset
30X	251.10	298.61	2.28	47.51	
31X	260.70	307.66	-0.55	46.96	
32X	270.30	317.26	0.00	46.96	
33X	279.90	326.86	0.00	46.96	
34X	289.50	336.46	0.00	46.96	
35X	299.10	346.06	0.00	46.96	
342-U1407B-					
1H	0.00	0.10	0.10	0.10	
2H	8.40	8.85	0.35	0.45	
3H	17.90	18.85	0.50	0.95	
4H	27.40	28.35	0.00	0.95	Drilling advance
5H	30.40	29.85	-1.50	-0.55	
6H	39.90	44.13	4.78	4.23	Tentative
7H	49.40	54.97	1.34	5.57	
8H	58.90	65.72	1.25	6.82	
9H	68.40	76.47	1.25	8.07	
10H	77.90	87.30	1.33	9.40	
11H	87.40	99.99	3.19	12.59	
12H	95.00	107.59	0.00	12.59	Drilling advance
13X	127.00	154.57	14.98	27.57	Large offset
14X	136.60	164.28	0.11	27.68	
15X	146.20	174.08	0.20	27.88	
16X	155.80	183.74	0.06	27.94	
17X	165.40	195.30	1.96	29.90	
18X	175.00	205.32	0.42	30.32	
19X	184.60	212.50	-2.42	27.90	
20X	192.60	224.04	3.54	31.44	
21X	200.60	233.22	1.18	32.62	
22X	209.10	244.37	2.65	35.27	
23X	218.70	253.81	-0.16	35.11	
24X	228.30	265.24	1.83	36.94	
25X	237.90	278.38	3.54	40.48	
26X	247.50	289.74	1.76	42.24	
27X	257.10	304.53	5.19	47.43	
28X	266.70	313.46	-0.67	46.76	
342-U1407C-					
1H	0.00	0.10	0.10	0.10	
2H	7.70	7.80	0.00	0.10	Drilling advance



Table T21 (continued).

Core	Depth		Offset (m)	Cumulative offset (m)	Comment
	(mbsf)	(m CCSF)			
3H	10.70	10.79	-0.01	0.09	
4H	20.20	18.55	-1.74	-1.65	Tentative
5H	29.70	31.35	3.30	1.65	Tentative
6H	39.20	45.08	4.23	5.88	Tentative
7H	48.70	66.97	12.39	18.27	Large offset
8H	58.20	77.78	1.31	19.58	
9H	67.70	86.83	-0.45	19.13	
10H	77.20	96.58	0.25	19.38	
11H	86.70	106.40	0.32	19.70	
12H	96.00	115.70	0.00	19.70	Drilling advance
13X	117.00	136.70	0.00	19.70	
14X	122.00	145.77	4.07	23.77	Offset to remove overlap
15X	131.60	155.58	0.21	23.98	
16X	141.20	165.98	0.80	24.78	
17X	150.80	176.74	1.16	25.94	
18X	160.40	186.43	0.09	26.03	
19X	170.00	198.37	2.34	28.37	
20X	175.00	208.38	5.01	33.38	
21X	184.60	219.92	1.94	35.32	Tentative
22X	193.10	228.90	0.48	35.80	
23X	202.70	240.41	1.91	37.71	
24X	209.20	248.34	1.43	39.14	
25X	216.20	254.86	-0.48	38.66	
26X	223.20	262.35	0.49	39.15	
27X	232.80	271.07	-0.88	38.27	
28X	242.40	291.10	10.43	48.70	Large offset
29X	252.00	300.45	-0.25	48.45	

Table T22. Splice tie points, Site U1407.

Hole, core, section, interval (cm)	Depth		Hole, core, section, interval (cm)	Depth		Comment
	(mbsf)	(m CCSF)		(mbsf)	(m CCSF)	
342-			342-			
U1407A-1H-1, 120	1.20	1.20	Tie to	U1407A-1H-1, 0	0.00	0.00
U1407B-1H-6, 20	7.70	7.80	Tie to	U1407A-2H-1, 45	1.10	1.20
U1407A-2H-2, 30	8.60	9.15	Tie to	U1407B-2H-1, 30	7.25	7.80
U1407B-2H-5, 44	14.84	15.29	Tie to	U1407C-3H-3, 150	8.70	9.15
U1407C-3H-CC, 21	18.54	18.63	Append to	U1407C-4H-1, 0	15.20	15.29
U1408C-4H-CC, 24	29.97	28.32	Append to	U1407A-4H-1, 34	20.20	18.55
U1407A-4H-3, 50	29.30	31.85	Tie to	U1407C-5H-1, 50	26.14	28.69
U1407C-5H-6, 122	38.42	40.07	Tie to	U1407A-5H-1, 145	30.20	31.85
U1407A-5H-6, 108	43.88	47.20	Tie to	U1407C-6H-2, 62	36.75	40.07
U1407C-6H-7, 30	47.81	53.69	Tie to	U1407A-6H-1, 50	41.32	47.20
U1407A-6H-5, 90	51.70	60.09	Tie to	U1407B-7H-4, 62	45.30	53.69
U1407B-7H-6, 90	57.80	63.37	Tie to	U1407A-7H-1, 33	54.52	60.09
U1407A-7H-4, 23	59.03	67.77	Tie to	U1407B-8H-2, 55	54.63	Tentative
U1407B-8H-6, 6	66.46	73.28	Tie to	U1407C-7H-5, 31	60.95	63.37
U1407C-7H-5, 141	56.11	73.48	Tie to	U1407A-8H-1, 115	73.28	Unclear physical properties
U1407A-8H-3, 87	67.67	77.10	Tie to	U1407B-9H-1, 63	64.95	74.38
U1407B-9H-6, 29	76.19	84.26	Tie to	U1407C-8H-5, 48	69.03	77.10
U1407C-8H-6, 122	66.92	86.50	Tie to	U1407A-9H-1, 140	64.68	84.26
U1407A-9H-7, 12	82.42	94.22	Tie to	U1407B-10H-5, 92	74.70	86.50
U1407B-10H-6, 119	86.59	95.99	Tie to	U1407A-10H-1, 100	84.82	95.99
U1407A-10H-2, 34	84.64	96.83	Tie to	U1407C-10H-1, 25	83.80	96.83
U1407C-10H-3, 84	81.04	100.42	Tie to	U1407B-11H-1, 43	77.45	100.42
U1407B-11H-5, 121	94.61	107.20	Tie to	U1407C-11H-1, 80	87.83	107.20
U1407C-11H-CC, 10	96.05	115.75	Append to	U1407C-13X-1, 0	117.00	136.70
U1407C-13X-CC, 7	126.06	145.76	Append to	U1407C-14X-1, 0	122.00	145.77
U1407C-14X-CC, 23	131.80	155.57	Append to	U1407C-15X-1, 0	131.60	155.58
U1407C-15X-7, 0	140.60	164.58	Tie to	U1407B-14X-1, 30	136.90	164.58
U1407B-14X-3, 60	140.20	167.88	Tie to	U1407C-16X-2, 40	143.10	164.58
U1407C-16X-6, 133	150.03	174.81	Tie to	U1407B-15X-1, 73	146.93	174.81
U1407B-15X-4, 41	151.11	178.99	Tie to	U1407C-17X-2, 75	153.05	178.99
U1407C-17X-6, 80	159.10	185.04	Tie to	U1407B-16X-1, 130	157.10	Tentative
U1407B-16X-5, 77	162.57	190.51	Tie to	U1407C-18X-3, 108	185.04	185.04
U1407C-18X-7, 21	169.42	195.45	Tie to	U1407A-21X-1, 33	164.48	Small overlap
U1407A-21X-4, 124	170.44	200.86	Tie to	U1407B-17X-4, 106	165.03	200.86
U1407B-17X-7, 40	174.55	204.45	Tie to	U1407A-22X-1, 73	170.96	204.45
U1407A-22X-5, 63	180.93	211.08	Tie to	U1407C-22X-3, 44	174.30	211.08
U1407C-20X-5, 120	182.20	215.58	Tie to	U1407B-20X-2, 120	194.24	215.58
U1407B-19X-6, 122	193.32	221.22	Tie to	U1407C-21X-1, 130	196.54	221.22
U1407C-21X-4, 126	190.36	225.68	Tie to	U1407B-20X-2, 14	202.88	225.68
U1407B-20X-6, 80	200.90	232.34	Tie to	U1407C-22X-3, 68	208.88	232.34
U1407C-22X-5, 60	199.70	235.50	Tie to	U1407B-21X-2, 68	213.50	235.50
U1407B-21X-7, 48	209.94	242.56	Tie to	U1407C-23X-2, 65	202.88	242.56
U1407C-23X-6, 14	210.15	247.86	Tie to	U1407B-22X-3, 49	204.85	247.86
U1407B-22X-6, 68	216.79	252.06	Tie to	U1407C-24X-3, 72	212.59	252.06
U1407C-24X-4, 130	215.00	254.14	Tie to	U1407B-23X-1, 33	212.92	254.14
U1407B-23X-3, 98	222.68	257.79	Tie to	U1407C-25X-2, 143	219.03	257.79
U1407C-25X-5, 60	222.80	261.46	Tie to	U1407B-27X-2, 7	219.13	257.79
U1407A-27X-3, 36	225.66	263.25	Tie to	U1407A-27X-2, 7	223.87	261.46
U1407C-26X-5, 91	230.11	269.26	Tie to	U1407C-26X-1, 90	224.10	263.25
U1407A-28X-3, 55	235.45	272.40	Tie to	U1407C-28X-1, 41	224.50	269.26
U1407C-27X-6, 130	241.41	279.68	Tie to	U1407A-28X-1, 133	232.31	Tentative
U1407B-25X-7, 10	246.81	287.29	Tie to	U1407B-25X-1, 130	234.13	279.68
U1407A-29X-5, 74	248.24	293.47	Tie to	U1407A-29X-1, 56	242.06	287.29
U1407B-26X-5, 27	253.77	296.01	Tie to	U1407B-26X-3, 73	251.23	293.47
U1407C-28X-7, 10	251.31	300.01	Tie to	U1407C-28X-4, 41	247.31	296.01
U1407A-30X-3, 144	255.54	303.05	Tie to	U1407A-30X-1, 140	252.50	300.01
U1407C-29X-5, 35	258.35	306.80	Tie to	U1407C-29X-2, 110	254.60	303.05
U1407B-27X-5, 18	263.28	310.71	Tie to	U1407B-27X-2, 77	259.37	306.80
U1407A-31X-6, 5	267.85	314.81	Tie to	U1407A-31X-3, 5	263.75	310.71
U1407B-28X-CC, 49	269.82	316.58	Tie to	U1407B-28X-1, 135	268.05	Tentative